**AFRICA CENTER OF EXCELLENCE FOR WATER MANAGEMENT**

**ADDIS ABABA UNIVERSITY**

**SHOOL OF GRADUATE STUDIES**

**COLLEGE OF NATURAL AND COMPUTATIONAL SCIENCES**

# Enhanced removal of pharmaceutical contaminants from water using electrochemical oxidation coupled with adsorption process

**Wondimu Kebede Wakejo**

A PhD dissertation submitted to the Africa Center of Excellence for Water Management, the School of Graduate Studies of Addis Ababa University in partial fulfillment of the requirements for the **Degree of Doctor of Philosophy in Water Management (Water Science and Technology)**

**Addis Ababa University**

**Addis Ababa, Ethiopia**

**May, 2024**

**AFRICA CENTER OF EXCELLENCE FOR WATER MANAGEMENT**

**ADDIS ABABA UNIVERSITY SHOOL OF GRADUATE STUDIES**

# Enhanced removal of pharmaceutical contaminants from water using electrochemical oxidation coupled with adsorption process

**By**

**Wondimu Kebede Wakejo**

A PhD dissertation submitted to Africa Center of Excellence for Water Management, the School of Graduate Studies of Addis Ababa University in partial fulfillment of the requirements for the Degree of Doctor of Philosophy in Water Management (Water Science and Technology)

# Declaration

I, Wondimu Kebede Wakejo (GSR 2240/12), hereby declare that this thesis, "**Enhanced removal of pharmaceutical contaminants from water using electrochemical oxidation coupled with adsorption process''** has been developed by me and has not been submitted to any other institution for award of any academic qualification. The content of the dissertation has not been plagiarized and where works of other researchers have been used, they have been properly cited.

| **PhD Candidate Name** | **Signature** | **Date** |
|---|---|---|
| ……. | …….. | …… |

**AFRICA CENTER OF EXCELLENCE FOR WATER MANAGEMENT**

**ADDIS ABABA UNIVERSITY**

# Enhanced removal of pharmaceutical contaminants from water using electrochemical oxidation coupled with adsorption process


**By:**

**Wondimu Kebede Wakejo**


**A PhD DISSERTATION SUBMITTED**

**TO**

**AFRICA CENTER OF EXCELLENCE FOR WATER MANAGEMENT**

**ADDIS ABABA UNIVERSITY**

**APPROVED BY BOARD OF EXAMINERS**

This is to certify that we have read this PhD research dissertation and that in our opinion; it is fully adequate, in scope and quality, as a PhD dissertation for The Degree of Doctor of Philosophy in Water Management (Water Science and Technology).

Advisor

Name: Prof. Joon Wun Kang Signature___ 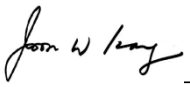 Date___06/07/2024____

Co-Advisor
Name: Dr. Beteley Tekola Signature_____ Date_____

External Examiner
Name: Dr. Yeojoon Yoon Signature  Date __05/07/2024____

Internal Examiner
Name: Prof. Nigus Gabbiye Signature  Date__03/07/2024____

Chairperson
Name: Prof. Yonas Chebude Signature_____ Date_____

# ACKNOWLEDGEMENT

After being admitted to the Africa Center of Excellence for Water Management (ACEWM) for a Ph.D. study, I faced a car accident that led to a severe brain injury, which persisted for three years. This situation became devastating and my greatest personal challenge of all time, and there were many instances where I contemplated quitting the Ph.D. study. However, my Almighty God, Jesus Christ, a miracle worker and promise keeper, changed everything at some point. Afterwards, my health was fully restored, and I resumed my pursuit of studies. Words cannot fully explain this situation, but I simply want to express my gratitude, Lord, for your mercy and love upon me and for the Holy Spirit that provided me strength and peace throughout my entire journey. Therefore, I must genuinely say that Jesus Christ is a savior!!

A final Ph.D. dissertation is not merely the output of a single person but the result of contributions from many individuals and institutions. It is crucial to acknowledge that this work represents a collective output involving the support and collaboration of various people and organizations, extending beyond the sole efforts of the Ph.D. candidate.

Accordingly, I would like to extend my genuine appreciation and gratitude to my advisors, Prof. Joon Wun Kang and Dr. Beteley Tekola (Associate Prof.). You have granted me intellectual freedom in this work and introduced new ideas demanding high quality work. Your crucial guidance throughout this dissertation has been instrumental in shaping the outcome. I wholeheartedly appreciate your support, encouragement and guidance throughout your supervision of this work. I am well aware of your generous efforts and everything you have done for me.

I am also profoundly grateful to the Africa Center of Excellence for Water Management (ACEWM) under the World Bank ACEII project for funding this research work. My sincere and special thanks extend to Prof. Feleke Zewge, the Director of ACEWM, and Dr. Beteley Tekola, the Deputy Director of ACEWM, for their facilitation and support in creating the essential ground for this work. Additionally, I am deeply indebted to Wachemo University for sponsoring this study.

I express my deepest gratitude to the ACEWM-Water Science and Technology (WST) track supervisory committee (Prof. Feleke Zewge, Prof. Dr. Ing. Esayas Alemayehu, Prof. Yonas Chebude, Prof. Nigus Gabbiye, Dr. Adey Feleke, and Dr. Andualem Mekonnen) for their invaluable input during the progress report presentation. This work would have been inconceivable without their critical guidance and scientific support.

Furthermore, my heartfelt gratitude extends to all the ACEWM staff members who provided direct and indirect assistance throughout this work. I would like to give special recognition to Mr. Netsanet Assefa for his excellent coordination during this study and to Ms. Eden Eritrea for her support during the experimental work in the ACEWM-core laboratory. The Cadila Pharmaceuticals (Addis Ababa, Ethiopia) and EPHARM (Addis Ababa, Ethiopia) are greatly acknowledged for providing me with pharmaceutical standards.

Of utmost importance, I express my sincere appreciation to the Finnish National Agency for Education (EDUFI Fellowship) for the grant I received to complete this dissertation. In this context, my earnest gratitude goes to Prof. Amit Bhatnagar for the EDUFI Fellowship funding acquisition, providing his laboratory facilities, office, and supervision during my stay at LUT University, Finland. Your unwavering support and encouragement have been invaluable to me, and I truly appreciate your exceptional assistance. Additionally, I thank Dr. Ali Maged for his mentorship at LUT University and Dr. Abayneh Getachew for his technical and moral support.

Finally, I would like to express my warmest gratitude to my entire family, including my father, mother, brothers, sisters, and close friends, for their unwavering love, encouragement and support in many ways throughout the challenging period.

Wondimu Kebede Wakejo

ACEWM, AAU, 2024

# Bio-Data

I graduated with a B.Sc. in Chemical Engineering from Bahir Dar University, Ethiopia. Following graduation, I worked as a trainee Process Engineer in Finchaa Sugar Factory (Ethiopia) and later worked as a Process Engineer in Tendaho Sugar Factory (Afar, Ethiopia). Afterwards, I joined Wachemo University, Ethiopia in 2016. The following year, I joined the Addis Ababa Institute of Technology, Ethiopia and graduated with an MSc in Process Engineering in 2018. Returning to Wachemo University, I worked as a lecturer for 1 year. Following the ACEWM call for a Ph.D. study, I joined the ACEWM Ph.D. in Water Management program (specialization in Water Science and Technology) in 2019. In 2023, I received a Finnish National Agency for Education (EDUFI) fellowship grant and conducted part of my dissertation work at LUT University in Finland. The same year, I was appointed as a consulting Editor in an Elsevier journal, "Advances in bamboo science". The following articles are published by the candidate or are under review after joining the Ph.D. program, whereby the first article is from the coursework while others are from the dissertation titled "**Enhanced removal of pharmaceutical contaminants from water using electrochemical oxidation coupled with adsorption process**".

**1] Wondimu Kebede Wakejo**, Beteley Tekola Meshesha, Nigus Gabbiye Habtu, Yilkal Gebeyehu Mekonnen. Anthropogenic nitrate contamination of water resources in Ethiopia: an overview. Water Supply 1 November 2022; 22 (11): 8157–8172.
doi: https://doi.org/10.2166/ws.2022.377.

**2] Wondimu K. Wakejo**, Beteley T. Meshesha, Joon W. Kang, Yonas Chebude. Enhanced Ciprofloxacin Removal from Aqueous Solution Using a Chemically Modified Biochar Derived from Bamboo Sawdust: Adsorption Process Optimization with Response Surface Methodology, Adsorption Science & Technology, vol. 2022, Article ID 2699530, 23 pages, 2022. https://doi.org/10.1155/2022/2699530.

**3] Wondimu Kebede Wakejo**, Beteley Tekola Meshesha, Joon Wun Kang, Abayneh Getachew Demesa. Bamboo sawdust-derived high surface area activated carbon for remarkable removal of paracetamol from aqueous solution: sorption kinetics, isotherm,

thermodynamics, and regeneration studies. Water Practice and Technology 1 June 2023; 18 (6): 1366–1388. doi: https://doi.org/10.2166/wpt.2023.094.

**4] Wondimu K. Wakejo**, Ali Maged, Beteley T. Meshesha, Joon W. Kang, Abayneh G. Demesa, Sandip Chakrabarti, Thallada Bhaskar, Ashok Kumar Gupta, Amit Bhatnagar. Tuneable functionalized biochar for simultaneous removal of pharmaceuticals from binary mixture, Colloids and Surfaces A: Physicochemical and Engineering Aspects, 681, 2024,132718, https://doi.org/10.1016/j.colsurfa.2023.132718.

**5] Wondimu K. Wakejo**, Beteley T. Meshesha, Ali Maged, Joon W. Kang, Eden E. Dessalegn, Abayneh G. Demesa, Ashok Kumar Gupta, Amit Bhatnagar. Integrated electrochemical-adsorption for simultaneous removal of pharmaceuticals from water: Process optimization and synergistic insights (manuscript under review).

# Table of contents

**Contents**

Declaration ..... ii

Acknowledgement ..... iv

Bio-data ..... vi

Table of contents ..... viii

List of Tables ..... xiv

List of Figures ..... xvi

Acronyms ..... xxi

Abstract ..... xxiii

CHAPTER ONE ..... 1

1. INTRODUCTION ..... 1

1.1. Statement of the problem ..... 5

1.2. Objective of the Study ..... 8

1.2.1. General objective ..... 8

1.2.2. Specific objectives ..... 8

1.3. Research questions ..... 8

1.4. Significance of the study ..... 9

1.5. Scope of the study ..... 10

1.6. Outline of the dissertation ..... 11

CHAPTER TWO ..... 13

2. LITERATURE REVIEW ..... 13

2.1. Pharmaceutical contaminants ..... 13

2.1.1. Categories of pharmaceuticals ..... 14

2.1.2. Sources of pharmaceutical contaminants ..... 18
2.1.3. Occurrences of pharmaceuticals in water environment ..... 19
2.1.4. Effects of pharmaceutical contaminants ..... 21
2.2. Physical/chemical pharmaceuticals removal technologies ..... 22
2.2.1. Adsorption process ..... 22
2.3. Advanced oxidation processes (AOPs) for pharmaceuticals removal ..... 30
2.3.1. Electrochemical oxidation ..... 31
2.3.2. Ozonation ..... 34
2.3.3. UV/Chlorine process ..... 35
2.3.4. UV/$H_2O_2$ ..... 35
2.3.5. Heterogeneous photo-catalysis ..... 36
2.4. Coupled treatment processes for pharmaceuticals removal ..... 36
2.4.1. Adsorption-based coupled processes ..... 37
2.4.2. Membrane-based coupled technologies ..... 38
2.4.3. Biological-based coupled processes ..... 39
2.4.4. Advanced oxidation-based coupled processes ..... 39
2.5. Research design and statistical modeling ..... 40
CHAPTER THREE ..... 42
3. MATERIALS AND METHODS ..... 42
3.1. The experimental workflow design of the dissertation ..... 42
3.2. Materials/equipment and chemicals used ..... 44
3.2.1. Materials used ..... 44
3.2.2. Equipment/instruments used ..... 44
3.2.3. Chemicals and reagents ..... 44
3.3. Synthesis of the adsorbent ..... 45

3.4. Water matrices ..... 47
3.5. Adsorbent characterization ..... 48
3.5.1. The pH of point of zero charge determination ($pH_{pzc}$) ..... 48
3.5.2. Fourier Transform Infra-red Spectroscopy (FTIR) ..... 48
3.5.3. Scanning Electron Microscopy/Energy-Dispersive Spectroscopy (SEM/EDS) ..... 49
3.5.4. Surface area analysis ..... 49
3.5.5. Raman spectroscopy ..... 49
3.6. Batch adsorption studies (single component) ..... 50
3.6.1. Modeling of adsorption kinetics ..... 51
3.6.2. Modeling of single component adsorption isotherm ..... 53
3.6.3. Regeneration study ..... 54
3.7. Batch adsorption studies (binary component) ..... 55
3.7.1. Modeling of binary component adsorption isotherm ..... 55
3.8. Flow mode (fixed-bed) adsorption studies ..... 57
3.9. Electrochemical oxidation (EO) experiment ..... 59
3.10. Coupled process (EO+adsorption) ..... 60
3.11. Analysis of pharmaceutical contaminants ..... 61
3.11.1. Chromatographic Analysis ..... 61
3.11.2. Total organic carbon (TOC) Analysis ..... 62
3.11.3. Chemical oxygen demand (COD) determination ..... 62
3.12. Experimental design and statistical analysis ..... 62
3.13. Energy consumption ..... 65
CHAPTER FOUR ..... 66
4. Results and discussion ..... 66
4.1. Adsorbent characterization results ..... 66

4.1.1. FTIR analysis ..... 68
4.1.2. SEM/EDS analysis ..... 70
4.1.3. BET surface area ..... 74
4.1.4. XRD analysis ..... 75
4.1.5. Raman analysis ..... 76
4.1.6. The pH of the point of zero charge ($pH_{pzc}$) ..... 77
4.2. Batch adsorption (CIP removal) results ..... 78
4.2.1. Model fitting and analysis of variance (ANOVA) using CCD ..... 78
4.2.2. Effect of main process variables ..... 81
4.2.3. Effect of interaction variables ..... 83
4.2.4. Process optimization of CIP sorption ..... 86
4.2.5. Regeneration of CAC after single CIP adsorption ..... 87
4.3. Batch adsorption (ACM removal) results ..... 88
4.3.1. Regeneration of CAC after single ACM adsorption ..... 90
4.4. Batch adsorption (single and binary component removal) ..... 91
4.4.1. Kinetic modelling of single and binary sorption ..... 99
4.4.2. Single component isotherm analysis ..... 101
4.4.3. Binary component isotherm analysis ..... 105
4.5. Adsorption Mechanism ..... 107
4.6. Column adsorption results ..... 110
4.6.1. Influence of adsorbent loading ..... 111
4.6.2. Influence of initial concentration of ACM and CIP ..... 112
4.6.3. Influence of inlet flow rate ..... 113
4.7. Electrochemical oxidation results ..... 117
4.7.1. Cyclic voltammetry (CV) analysis ..... 117

4.7.2. EO process optimization using RSM ..... 119
4.7.3. Kinetics of EO process ..... 131
4.7.4. Effect of water matrix on EO process ..... 132
4.7.5. Effect of scavenger on EO process ..... 134
4.7.6. TOC and COD removal ..... 135
4.7.7. Application of EO in multiple contaminants removal ..... 136
4.8. Coupled process (EO+adsorption) optimization ..... 137
4.8.1. Main process factors affecting the coupled process ..... 142
4.8.2. Interaction factors affecting the coupled process ..... 145
4.8.3. Validation of the coupled process optimization ..... 145
4.8.4. TOC removal by coupled process ..... 148
4.8.5. Effect of water matrix on the coupled process ..... 149
4.8.6. COD removal using coupled process ..... 151
4.8.7. Application of coupled process in multiple pharmaceuticals removal ..... 152
4.9. Performance evaluation of single and coupled processes ..... 153
4.9.1. COD removal ..... 153
4.9.2. TOC removal ..... 154
4.9.3. Binary contaminant (ACM+CIP) removal ..... 156
4.9.4. Multiple pharmaceuticals removal ..... 157
4.9.5. Effect of water matrix on removal efficiency ..... 159
4.10. Electrical energy consumption ..... 161
5. Conclusions ..... 162
6. Recommendations ..... 165
7. References ..... 167
Appendices ..... 207

Appendix A: Characterization ..... 207
Appendix B: Adsorption (single process) ..... 209
Appendix C: Electrochemical oxidation (EO) (single process) ..... 218
Appendix D: Coupled process (EO+adsorption) ..... 228
Appendix E: Publications ..... 232
Appendix F: Conference presentations ..... 236

# List of Tables

Table 2.1. The concentrations, sources, and countries where the target pharmaceuticals were detected in water resources. ..... 19
Table 2.2. Adsorptive capacities of various adsorbents in the removal of pharmaceutical contaminants from water..... 24
Table 3.1. The optimization of adsorbent synthesis and chemical activation processes. ..... 46
Table 3.2. Adsorption kinetic models used in this study (linear and non-linear forms)..... 52
Table 3.3. The single component adsorption isotherm models employed in ACM and CIP removal from water..... 53
Table 3.4. Column adsorption factors and their levels. ..... 58
Table 3.6. The independent variables and their levels of the CCD experimental design for the ACM+CIP degradation using the EO process. ..... 64
Table 4.1. The ACM and CIP removal efficiencies of bamboo sawdust derived adsorbents. ..... 68
Table 4.2. Specific surface area and pore size of the bamboo based adsorbents..... 74
Table 4.3. ANOVA results of the CIP adsorption onto CAC..... 79
Table 4.4. Effect of the particle size on the removal of ACM and CIP from water using CAC. . 95
Table 4.5. Non-linear kinetic and isotherm model parameters for ACM and CIP removal in single and binary component sorption systems. ..... 104
Table 4.6. Langmuir and competitive Langmuir isotherm model constants for single and binary component sorption of ACM and CIP onto CAC, respectively..... 107
Table 4.7. Breakthrough parameters at different initial ACM and CIP concentrations ($C_0$), CAC amounts (M), flow rates (Q), breakthrough times ($t_b$), total operation time ($t_{total}$), total adsorbed quantities ($q_{total}$), experimental maximum sorption capacities ($q_{bed}$), total amount of adsorbate delivered to the column system ($m_{total}$), total removal efficiencies of the column (RE%), treated volume of effluent ($V_{eff}$) and unadsorbed adsorbate concentrations at equilibrium ($C_{eq}$)..... 115
Table 4.8. ANOVA for ACM and CIP degradation using the EO process. ..... 120
Table 4.9. ANOVA for ACM and CIP removal using the coupled process (EO+adsorption).. 139
Table A.1. The secondary WWTPs effluent characteristics..... 207
Table B.1. CCD experimental design of CIP adsorption using CAC..... 209

Table B.2. Linear kinetic and isotherm model parameters for single sorption of ACM and CIP onto CAC. ..... 216
Table B.3. Calibration curve equations and $R^2$ values for the quantification of pharmaceuticals using UV-Vis spectrophotometer in single and simultaneous adsorption systems. ..... 217
Table C.1. The CCD experimental design of the EO process in ACM/CIP degradation. ..... 218
Table C. 2. Experimental results of BBD for the coupled process. ..... 219
Table C.3. The HPLC method employed for the quantification of the pharmaceuticals for the performance evaluation of adsorption, EO and EO+adsorption processes. ..... 223

# List of Figures

Figure 2.1. Chemical structure of ACM. ..... 16
Figure 2.2. Chemical structure of CIP. ..... 16
Figure 2.3. Chemical structure of AMX. ..... 17
Figure 2.4. Chemical structure of ATN. ..... 18
Figure 3.1. Conceptual framework of the dissertation. ..... 43
Figure 3.2. Synthesis procedure for the bamboo sawdust derived adsorbents. ..... 47
Figure 3.3. Experimental setup of the column/fixed-bed adsorption. ..... 59
Figure 3.4. The electrochemical oxidation setup used in this study. ..... 60
Figure 3.5. The experimental setup of the EO process coupled with the adsorption. ..... 61
Figure 4.1. FTIR spectra of pristine bamboo sawdust carbon (BSC), chemically activated carbon (CAC), CAC after ACM adsorption (CAC-ACM), CAC after adsorption of ciprofloxacin (CAC-CIP) and CAC after simultaneous adsorption of ACM and CIP (CAC-ACM+CIP). ..... 70
Figure 4.2. SEM images of (a) pristine bamboo sawdust, (b) bamboo sawdust carbon (BSC), (c) CAC before adsorption and (d) CAC after adsorption of ACM and CIP (CACA). ..... 72
Figure 4.3. The elemental composition of CAC (a) and EDS mapping for CAC. ..... 73
..... 75
Figure 4.4. The XRD patterns of BSC, CAC and CACA after sorption of ACM and CIP (CAC-ACM+CIP). ..... 75
Figure 4.5. Raman spectra of the pristine BSC, CAC and CAC after binary adsorption (CAC-ACM+CIP). ..... 77
Figure 4.6. $pH_{pzc}$ of the CAC adsorbent. ..... 78
Figure 4.7. The influence of main effects on CIP removal using CAC (a) CIP initial concentration, (b) adsorbent dose, (c) pH and (d) contact time. ..... 85
Figure 4.8. Interaction effects (a) adsorbent dose versus CIP initial concentration (b) contact time versus adsorbent dose (c) contact time versus pH. ..... 86
Figure 4.9. The CIP removal efficiency of CAC per each adsorption cycle. ..... 87
Figure 4.10. The effect of pH (a), contact time (b), ACM initial concentration (c) and CAC dose (d) on the single component adsorption of ACM from water. ..... 90
Figure 4.11. The ACM removal efficiency of CAC per each adsorption cycle. ..... 91

Figure 4.12. Influence of pH on single and binary sorption of ACM and CIP (experimental conditions: ACM/CIP concentration = 20 mg/L, CAC dose = 0.5 g/L, contact time = 120 min).93
Figure 4.13. Influence of CAC dose on the single and binary sorption of ACM and CIP (experimental conditions: ACM/CIP concentration = 20 mg/L, pH = 6.8, contact time = 120 min). ..... 94
Figure 4.14. Influence of ionic strength on the single and binary sorption of ACM and CIP (experimental conditions: ACM/CIP concentration = 20 mg/L, CAC dose = 0.5 g/L, pH = 6.8, contact time = 120 min). ..... 97
Figure 4.15. Influence of water matrix on ACM and CIP removal (a) single component sorption and (b) binary component sorption (experimental conditions: ACM/CIP concentration = 20 mg/L, pH = 6.8, contact time = 120 min). ..... 98
Figure 4.16. Non-linear kinetic models employed for ACM and CIP removal from water in single and binary component adsorption systems. (a) Single sorption ACM kinetics; (b) binary sorption ACM kinetics; (c) single sorption CIP kinetics; (d) binary sorption CIP kinetics (experimental conditions: ACM/CIP concentration = 20 mg/L, pH = 6.8, CAC dose = 0.5 g/L). ..... 101
Figure 4.17. Non-linear isotherm model plots (a) single sorption ACM (b) single sorption of CIP isotherm (experimental conditions: pH = 6.8, CAC dose = 0.5 g/L, contact time = 120 min)... 103
Figure 4.18. The dimensionless separation factor for the single component sorption of ACM and CIP onto CAC. ..... 103
Figure 4.19. Binary component sorption isotherm for ACM (a) and CIP (b) (experimental conditions: pH = 6.8, CAC dose = 0.5 g/L and contact time = 120 min). ..... 107
Figure 4.20. Mechanism of simultaneous removal of ACM and CIP from water using CAC... 110
Figure 4.21. Breakthrough curves of CIP and ACM sorption onto CAC in (a-d) Run 1-4 for the binary component solution and (e-h) Run 1-4 for the single component solution. ..... 116
Figure 4.22. Cyclic voltammograms of 0.05 M NaCl solution in the presence/absence of the 20 mg/L of ACM and CIP on I $rO_2$/Ti electrode at 25 ℃ (Scan rate = 10 mV/s and pH = 5.5). .... 118
Figure 4.23. Pareto analysis for ACM (a) and CIP (b) degradation using EO. ..... 123
Figure 4.24. Effect of NaCl concentration on simultaneous degradation of (a) ACM and (b) CIP. ..... 125
Figure 4.25. The 3D surface plots for the interaction factors of ACM degradation using EO... 129

Figure 4.26. The 3D surface plots for the interaction factors of CIP degradation using EO..... 130
Figure 4.27. Kinetics of EO process (a-b) pseudo-first-order and pseudo-second-order models for ACM and (c-d) pseudo-first-order and pseudo-second-order models for CIP, respectively..... 132
Figure 4.28. Effect of water matrix on the degradation of ACM and CIP using EO (pH = 5.5, EO time = 80 min and initial ACM/CIP = 20 mg/L). ..... 134
Figure 4.29. Effect of water matrix on the degradation of ACM and CIP using EO (current density = 44 mA/cm$^2$, pH = 5.5, and initial ACM/CIP = 20 mg/L). ..... 135
Figure 4.30. The TOC (a) and COD (b) removal efficiencies of the EO process at varying EO times (current density = 44 mA/cm$^2$, pH = 5.5, EO time = 80 min)..... 136
Figure 4.31. Degradation of multiple pharmaceutical contaminants using EO (current density = 44 mA/cm$^2$, pH = 5.5, EO time = 80 min and initial ACM/CIP/ATN/AMX = 20 mg/L)..... 137
Figure 4.32. The 3D response plots of the coupled process for ACM and CIP removal. ..... 146
Figure 4.33. The contour plots of the coupled process for ACM and CIP removal. ..... 147
Figure 4.34. TOC removal using the coupled process (current density = 22 mA/cm$^2$, pH = 5.5, adsorbent dose = 0.1 g/L and adsorption time = 60 min). ..... 149
Figure 4.35. Effect of water matrix on simultaneous removal of ACM and CIP from water using the coupled process (pH = 5.5, EO time = 40 min, adsorbent dose = 0.1 g/L and adsorption time = 60 min)..... 150
Figure 4.36. The COD removal efficiency of the coupled process (current density = 22 mA/cm$^2$, pH = 5.5, adsorbent dose = 0.1 g/L and adsorption time = 60 min). ..... 152
Figure 4.37. The removal of multiple pharmaceuticals from water using the coupled process (current density = 22 mA/cm$^2$, pH = 5.5, EO time = 40 min and adsorption time = 60 min).... 153
Figure 4.38. Performance evaluation of the single and coupled process in COD removal from water: EO process (current density = 44 mA/cm$^2$, pH = 5.5, $C_o$ = 20 mg/L) and coupled process (current density = 22 mA/cm$^2$, pH = 5.5, adsorption time = 60 min and adsorbent dose = 0.1 g/L) varying the EO process time (10-240 min)..... 154
Figure 4.39**.** Performance evaluation of single and coupled process in TOC removal from water (EO process: current density = 44 mA/cm$^2$, pH = 5.5 and coupled process: current density = 22 mA/cm$^2$, pH = 5.5, adsorption time = 60 min and adsorbent dose = 0.1 g/L)..... 156
Figure 4.40. Performance evaluation of the single and coupled process in ACM+CIP removal from water (sole EO optimal conditions: pH = 5.5, ACM+CIP initial concentration = 20 mg/L,

current density = 44 mA/cm$^2$ and NaCl = 0.05M and oxidation time = 80 min; sole adsorption process optimal conditions: adsorbent dose = 0.5 g/L, pH = 6.8, contact time = 120 min and ACM/CIP concentration = 20 mg/L; coupled process optimal conditions: current density = 22 mA/cm$^2$, EO time = 40 min, NaCl = 0.05 M, adsorbent dose = 0.1 g/L, pH = 5.5, ACM/CIP initial concentration = 20 mg/L and adsorption time = 60 min). ..... 157
Figure 4.41. Performance evaluation of single and coupled process in multiple pharmaceuticals removal from water (EO optimal conditions: pH = 5.5, ACM/CIP initial concentration = 20 mg/L, current density = 44 mA/cm$^2$ and NaCl = 0.05M and oxidation time = 80 min; adsorption process optimal conditions: adsorbent dose = 0.5 g/L, pH = 6.8, contact time = 120 min and ACM/CIP concentration = 20 mg/L; coupled process optimal conditions: current density = 22 mA/cm$^2$, EO time = 40 min, NaCl = 0.02 M, adsorbent dose = 0.1 g/L, pH = 5.5, ACM/CIP initial concentration = 20 mg/L and adsorption time = 60 min). ..... 159
Figure 4.42. Effect of water matrix on ACM and CIP removal using single and coupled process (EO optimal conditions: pH = 5.5, ACM/CIP initial concentration = 20 mg/L, current density = 44 mA/cm$^2$ and NaCl = 0.05M and oxidation time = 80 min; adsorption process optimal conditions: adsorbent dose = 0.5 g/L, pH = 6.8, contact time = 120 min and ACM/CIP concentration = 20 mg/L; coupled process optimal conditions: current density = 22 mA/cm$^2$, EO time = 40 min, NaCl = 0.02 M, adsorbent dose = 0.1 g/L, pH = 5.5, ACM/CIP initial concentration = 20 mg/L and adsorption time = 60 min). ..... 161
Figure A.1. FTIR spectra of ACM and CIP compounds. ..... 207
Figure B.1. Diagnostic plots of the quadratic model for CIP removal: a) Normal probability versus externally studentized residuals; (b) externally studentized residuals againist predicted (c) predicted againist actulal..... 210
Figure B.3. The plot of CAC adsorbent capacity for single sorption of CIP with time. ..... 211
Figure B.4. Linear kinetic models employed for CIP single sorption onto CAC (a) Pseudo-first-order model, (b) Pseudo-second-order model, (c) Elovich and (d) intra-particle models. ..... 212
Figure B.5. Linear kinetic models of ACM single sorption onto CAC (a) Pseudo-first-order, (b) Pseudo-second-order, (c) Elovich and (d) intra-particle model. ..... 213
Figure B.6. Linear isotherm model plots for CIP single sorption onto CAC (a) Langmuir, (b) Freundlich, (c) Temkin and (d) Dubinin-Radushkevich. ..... 214

Figure B.7. Linear isotherm model plots for ACM single sorption onto CAC (a) Langmuir, (b) Freundlich, (c) Redlich-Peterson, (d) Dubinin-Radushkevich. ..... 215
Figure C.1. Chromatograms of ACM and CIP for binary contaminant system (a) before EO and (b) after EO (EO time = 80 min, pH = 5, current density = 44 mA/cm$^2$) and (c) after EO+adsorption (EO time = 40 min, current density = 22 mA/cm$^2$, adsorbent dose = 0.1 g/L and adsorption time = 60 min)..... 221
Figure C.2. Chromatograms of ACM, CIP, AMX and ATN (a) before EO and (b) after EO (EO time = 80 min, pH = 5, current density = 44 mA/cm$^2$) and (c) after EO+adsorption (EO time = 40 min, current density = 22 mA/cm$^2$, adsorbent dose = 0.1 g/L and adsorption time = 60 min)... 222
Figure C.3. The influence of main EO process factors on ACM degradation (a) EO time (min), (b) pH, (c) Current density (mA/cm$^2$), (d) Initial pollutant concentration (mg/L). ..... 224
Figure C.4. The influence of main EO process factors on CIP degradation (a) EO time (min), (b) pH, (c) Current density (mA/cm$^2$), (d) Initial pollutant concentration (mg/L)..... 225
Figure C.5. Diagnostic plots for the ACM degradation quadratic model: a) Normal probability versus externally studentized residuals; (b) Residual vs. Predicted (c) residual vs. Run (d) Predicted vs. Actual (e) Residual vs. EO time (min) (f) DFFITS vs. Run. ..... 226
Figure C.6. Diagnostic plots for the CIP degradation quadratic model: a) Normal probability versus externally studentized residuals; (b) Residual vs. Predicted (c) residual vs. Run (d) Predicted vs. Actual (e) Residual vs. EO time (min) (f) DFFITS vs. Run. ..... 227
Figure D.1. One factor effect analysis for ACM removal using the coupled process. ..... 228
Figure D.3. Diagnostic analysis for ACM removal using the coupled process. ..... 230
Figure D.4. Diagnostic analysis for CIP removal using the coupled process. ..... 231

# Acronyms

AC: Activated Carbon

ACEWM: Africa Center of Excellence for Water Management

ACM: Acetaminophen

AMX: Amoxicillin

AOPs: Advanced Oxidation Processes

ATN: Atenolol

BET: Brunauer-Emmett-Teller

BBD: Box-Behnken Design

BOD: Biological Oxygen Demand

CAC: Chemically activated carbon

CAS: Conventional Activated Sludge

CCD: Central Composite Design

CIP: Ciprofloxacin

COD: Chemical Oxygen Demand

EO: Electrochemical oxidation

FTIR: Fourier Transform Infra-red Spectroscopy

GAC: Granular Activated Carbon

HPLC: High Performance Liquid Chromatography

LC-MS: Liquid Chromatography-Mass Spectrometry

μGAC: Micro-grain Activated Carbon

MBR: Membrane Bioreactor

NSAIDs: Non-steroidal and Anti-inflammatory Drugs

OMPs: Organic Contaminants

PAC: Powdered Activated Carbon

$pH_{pzc}$: pH of the point of zero charge

RSM: Response Surface Methodology

SEM/EDS: Scanning Electron Microscopy with Energy Disperive Spectroscopy.

SDGs: Sustainable Development Goals

TOC: Total Organic Carbon

UK: United Kingdom

WWTPs: Wastewater Treatment Plants

XRD: X-ray Diffraction

Note: A list of publications is provided in bio-data. The acronyms used in publication II (MBC) and in publication IV (FBC) refer to the same adsorbent material synthesized through chemical modification of bamboo sawdust, which is identical to the acronym used in publication III (CAC). The names Paracetamol (PCT) and Acetaminophen (ACM) refer to the same pharmaceutical compound and are hence used interchangeably.

# Abstract

Pharmaceutical contaminants are emerging water contaminants that have become a growing global concern. These contaminants have been frequently detected in surface water, wastewater and drinking water at trace concentrations. Among the pharmaceuticals, acetaminophen (ACM) and ciprofloxacin (CIP) are extensively consumed as analgesics and antibiotics, respectively, and thus ubiquitously detected in the environment. These contaminants are associated with negative effects on human health and aquatic life. In response to this problem, treatment processes such as electrochemical oxidation (EO) and adsorption have previously been attempted as single treatment systems to remove these pharmaceuticals from water. However, these single treatment systems are highly sensitive to water matrix, and their efficiency is limited when employed in multiple pharmaceuticals removal from complex water matrices. Therefore, this study aimed to elucidate the performance of individual (EO and adsorption) and coupled processes (EO+adsorption) in the removal of these pharmaceuticals from water to investigate the benefit of coupling both processes. The individual EO and adsorption processes were independently optimized and then compared with the EO+adsorption process. The adsorption process was conducted using a chemically activated carbon (CAC) synthesized from bamboo sawdust. The comprehensive CAC characterization results, such as BET surface area, SEM, FTIR, Raman spectroscopy and $pH_{pzc,}$ showcased its remarkable adsorptive properties (high surface area, plentiful functional groups and high porosity). More specifically, the employed chemical activation technique significantly increased the surface area from 565.09 $m^2/g$ for raw bamboo sawdust carbon (BSC) to 1158.05 $m^2/g$ for CAC.

In the batch CIP adsorption system, CAC showed excellent CIP removal efficiency (96%) compared to BSC efficiency (45%). The parameters of CIP adsorption process, such as initial CIP concentration, pH, adsorbent dose, and contact time, were studied and found to have a significant effect on CIP removal from water. The optimal CIP removal (96%) was obtained at CAC dose (0.5 g/L), CIP initial concentration (20 mg/L), pH (7.5), and contact time (46 min). The kinetic data of single component CIP adsorption was well described by the pseudo-second-order model ($R^2$ = 0.999), and both Langmuir ($R^2$ = 0.994) and Freundlich ($R^2$ = 0.972) models

provided the best fit for the isotherm data. On the other hand, the single component batch adsorption of ACM resulted in 99.6% ACM removal from water using CAC under optimal conditions of ACM (20 mg/L), CAC (0.5 g/L), contact time (90 min), and pH (8). In this case, the kinetic study revealed that the ACM adsorption process followed the pseudo-second-order kinetic model ($R^2$ = 0.999). On the other hand, the isotherm experimental data were best described by the Langmuir ($R^2$ = 0.987) and Freundlich ($R^2$ = 0.968) models. These results suggest that the adsorption of single component ACM and CIP was mainly controlled by chemisorption process. Moreover, the single component removal of ACM and CIP isotherm analysis revealed that ACM and CIP adsorption onto the CAC was monolayer adsorption onto the heterogeneous surface. The reusability study depicted that CAC can be successfully reused for five consecutive adsorption-desorption cycles in the batch adsorption of single component ACM and CIP.

The single component ACM and CIP adsorption study exhibited a greater removal capacity for ACM (192.43 mg/g) than CIP (70.95 mg/g), as predicted by the non-linear Langmuir isotherm model. The competitive Langmuir isotherm model, employed for the simultaneous adsorption of ACM and CIP, predicted a maximum adsorption capacity of 125.31 mg/g for ACM and 65.44 mg/g for CIP. In this regard, the adsorption capacity ratio ($q_{m,\ binary}/q_{m,\ single} < 1$) suggests an antagonistic behavior of these pollutants when they co-exist in the same water matrix. On the other hand, the binary component adsorption of ACM and CIP was best described by the pseudo-second-order kinetic model, indicating that the chemisorption process mainly controlled the adsorption process. Under optimal conditions (inlet ACM/CIP concentration = 10 mg/L, flow rate = 1.5 mL/min and adsorbent loading = 100 mg), the fixed-bed column study showcased the maximum bed capacity of ACM (172.48 mg/g) and CIP (147.67 mg/g), with the highest respective removal efficiency of 44.23% and 37.86% in the binary component adsorption system in . However, the single component column adsorption system achieved a higher removal efficiency of 65.83% (ACM) and 42.59% (CIP).

The EO process was also employed for the simultaneous degradation of ACM and CIP in the water. The central composite design (CCD) was employed for optimizing the EO process, and optimal conditions for current density (44 $mA/cm^2$), pH (5.5), contact time (80 min) and initial

pollutant concentration (20 mg/L) were obtained. Under these conditions, a removal of 94.5% for ACM and 92.7% for CIP was achieved. The EO process resulted in 65% total organic carbon (TOC) and 90.4% chemical oxygen demand (COD) removal at 240 min under optimal conditions. The EO kinetic study revealed that the degradation of ACM and CIP followed pseudo-first-order kinetics.

The coupled process (EO+adsorption) optimization using the Box-Behnken Design (BBD) of the response surface methodology (RSM) technique provided optimal operating conditions for current density (22 $mA/cm^2$), pH (5.5), EO time (40 min), adsorbent dose (0.1g/L) and adsorption time (60 min). Under these conditions, remarkable removal of pharmaceuticals (> 99.9%) and > 99% of TOC and COD were achieved when the EO time was extended to 120 min. Furthermore, the coupled process was employed for the simultaneous removal of multiple pharmaceuticals (20 mg/L of ACM+CIP+ATN (atenolol)+AMX (amoxicillin)) from water under optimal conditions. On top of that, the effect of water matrix on the target pharmaceuticals removal performances of EO, adsorption and EO+adsorption was investigated. These results show that the single processes (EO and adsorption) are highly sensitive to the water matrix compared to the coupled (EO+adsorption) process. Consequently, coupling the EO process with adsorption proved to be effective in addressing the influence of the water matrix, which substantially affected the removal efficiencies of the single processes. Overall, the coupled process demonstrated remarkable performances in single (ACM or CIP), binary (ACM+CIP), multiple pharmaceuticals (ACM+CIP+ATN+AMX), and oxidation by-products removal from diverse water matrices. Therefore, the EO+adsorption can serve as a promising treatment technique for the remediation of recalcitrant and ubiquitously detected pharmaceutical contaminants, such as ACM, CIP, ATN, and AMX from water.

# CHAPTER ONE

## 1. INTRODUCTION

The extensive consumption of pharmaceuticals, such as ACM and CIP has led to their continuous discharge into the environment (Huang et al., 2023). As a result, these compounds are frequently detected in both surface water and groundwater at trace concentrations (ng/L-µg/L) (Gong et al., 2023). Due to the uncontrolled discharges, the concentration of these recalcitrant compounds is rising with time. Consequently, these contaminants have become a point of environmental concern among the public due to their potential toxicity and environmental persistence (Huang et al., 2023). In this context, the environmental accumulation of pharmaceuticals such as antibiotics has resulted in emergence of antibiotic resistant bacteria and antibiotic resistance genes. In light of this, the treatment of life-threatening bacterial infections is becoming complicated (Duarte et al., 2022; Haenni et al., 2022). On top of that, the recent COVID-19 pandemic has triggered vast pharmaceutical consumption, likely increasing their concentration in the environment (Vieira et al., 2023). Hence, it is hypothesized that without significant intervention, this anthropogenic issue may pose imminent challenges to ensuring safe living conditions in the foreseeable future. The United Nations has launched the fundamental sustainable development goals (SDGs) to achieve better living conditions. Therefore, addressing the water contamination issue aligns with SDG goal 6 (clean water and sanitation).

Among pharmaceuticals, antibiotics like CIP are widely consumed to treat bacterial infections, while analgesics such as ACM are commonly consumed to relieve pain (Anjali & Shanthakumar, 2022). ACM, alternatively known as paracetamol, is a widely used over-the-counter medication which is affordable, accessible and can be used without a prescription. After consumption, approximately 58–68% of ACM is excreted from the human body (Santhosh et al., 2021). Once released, it accumulates in the environment owing to its high solubility and hydrophilicity (Jakóbczyk et al., 2022). Water contamination with ACM can result in several harmful effects on human health, including hepatotoxicity, mutagenesis, endocrine disruption, and cancer in humans (Chen et al., 2021; Q. Zhang et al., 2020). On the other hand, CIP is a quinolone

antibiotic that has been widely consumed, and about 70% of the consumed CIP can be excreted through urine and faeces due to its poor metabolism (Alexsandro et al., 2022; Montenegro-ayo et al., 2023). The reported health risks due to water contamination with CIP include excessive production of liver enzymes, thrombocytopenia, renal impairment, leukopenia, and antibiotic resistance (Alexsandro et al., 2022; Antonelli et al., 2022; Aseman-bashiz et al., 2021; Ma et al., 2022; Palomares-reyna et al., 2022; C. Wang et al., 2022). Therefore, ACM and CIP are considered top-priority pharmaceutical contaminants (Antonelli et al., 2022; Aseman-bashiz et al., 2021), demanding efficient and cost-effective removal technology.

The conventional wastewater treatment plants (WWTPs) are inefficient in removing water-soluble, hydrophilic and non-biodegradable pharmaceutical compounds (ACM and CIP), and hence, these pharmaceuticals are constantly released into the aquatic environment (Östman et al., 2019). In an attempt to effectively remove ACM and CIP from water, various treatment techniques, including ozonation (He et al., 2020), electro-Fenton (Orimolade et al., 2020), electrochemical oxidation (EO) (Montenegro-ayo et al., 2023b), photo-catalysis (X. Hu et al., 2020), sonolysis (Stucchi et al., 2020), adsorption (Abdul et al., 2021), UV/chlorine (Pai & Wang, 2022) were investigated. Among these, the EO process is one the advanced oxidation processes (AOPs) that has been widely used in practical water applications due to its high efficiency, simplicity, environmental compatibility, and flexibility (Montenegro-ayo et al., 2023). The AOPs are defined in a broad sense as chemical treatment methods designed to remove organic substances in water and wastewater by oxidation through reactions with hydroxyl radical ($OH^{\bullet}$) (Glaze et al., 1998). The addition of electrolytes such as sodium chloride (NaCl) and sodium sulphate ($Na_2SO_4$) is required to effectively degrade pollutants in the EO process. Among these, NaCl provided faster degradation of organic compounds in the EO process (Carneiro et al., 2020). This can be ascribed to the involvement of electro-generated active chlorine species such as $Cl_2$, HOCl, and $OCl^-$ in the EO process (Lan et al., 2017).

Despite the high degradation of these compounds in the EO process, attaining complete mineralization has become very challenging (Ganthavee & Trzcinski, 2023). As a result, the parent pharmaceuticals (ACM and CIP) are transformed into several transformation by-products after oxidation, which are even more recalcitrant to oxidation (Kermani et al., 2019). This phenomenon can be corroborated by noting TOC and COD after the EO process. It is reported

that achieving TOC and COD removal below permissible levels using the EO process is very challenging due to the formation of electrochemically non-degradable toxic by-products such as organic halogens and toxic ions after EO treatment (Ganesan et al., 2019). In this regard, degradation of pharmaceuticals (> 90%), TOC (< 65%), and COD removal (< 70%) were mostly reported in the EO process, especially at lower oxidation times (< 90 min) (Alexsandro et al., 2022; Antonelli et al., 2022; Duan et al., 2020; Hu et al., 2020; Ojo et al., 2023; Periyasamy & Muthuchamy, 2018). These results indicate that the EO process only partially eliminated pharmaceuticals while converting some into toxic by-products. Therefore, achieving the complete removal of pharmaceuticals and their transformation by-products from water demands high energy consumption due to the requirement of longer oxidation time, which makes the treatment process economically unfeasible. This is a significant limitation of EO, particularly when removing pharmaceuticals from complex water matrices that contain several interfering constituents.

On the other hand, the adsorption process is easy to operate and highly effective, especially for single contaminant removal from the water without incurring significant costs (Ganthavee & Trzcinski, 2023). However, removing multiple pharmaceuticals from a complex water matrix requires a high adsorbent dose. Therefore, the efficiency of single treatment processes like EO and adsorption greatly depends on the water matrix and the multitude of pollutants to be treated. Coupling EO and adsorption can provide the economic and environmental sustainability, especially in full-scale wastewater treatment processes (Ganthavee & Trzcinski, 2023). To fully grasp the benefit of coupling EO with the adsorption process, other classes of pharmaceuticals, including ATN (a beta blocker commonly used as an anti-hypertensive), and AMX (a penicillin antibiotic used to treat bacterial infections), were also considered. ATN and AMX are characterized by low bio-degradability and their frequent occurrence in water bodies (García-rosero et al., 2022; Laksaci et al., 2023).

The target pharmaceuticals considered in this study include pharmaceutical compounds from four pharmaceutical classes: analgesic (acetaminophen (ACM) alternatively known as paracetamol (PCT)), flouroquinolones anti-biotic (ciprofloxacin: CIP), penicillin anti-biotic (amoxicillin: AMX), beta-blocker (atenolol: ATN) drugs. This research is mainly based on the removal of single and binary component pharmaceutical mixtures of ACM and CIP from water

using the adsorption process, EO, and EO+adsorption. These processes were also applied to the multi-component pharmaceutical contaminant mixtures (ACM+CIP+AMX+ATN) removal from water under optimal operating conditions. The selection of these model compounds was based on several factors: their high global consumption, relevance during the COVID-19 pandemic, frequent detection in water resources, representative characteristics within their respective classes, and the potential health risks they pose to both humans and ecosystems. Furthermore, these pharmaceuticals have been identified as top-priority compounds in previous studies.

In this study, a chemically activated carbon (CAC) was synthesized from the bamboo sawdust through carbonation at 700 ºC under a limited oxygen environment. Besides, the process parameters of EO such as EO time (min), initial pharmaceutical concentration (mg/L), current density ($mA/cm^2$), electrolyte concentration (M) and pH; and the adsorption process parameters such as initial target pharmaceutical concentration (mg/L), adsorbent dose (g/L), contact time (min) and pH have a significant impact on the removal efficiency of ACM and CIP from water in the single and coupled processes. Furthermore, water matrices, including pure water, tap water and secondary wastewater treatment plant (WWTPs) effluent were investigated to evaluate the performances of the EO, adsorption and EO+adsorption in removing target pharmaceuticals from diverse water matrices.

The individual processes were first thoroughly studied and optimized in batch (adsorption and EO) and flow (adsorption) mode operations. Adsorption studies were conducted for single pharmaceutical (ACM or CIP) and binary mixture of pharmaceuticals (ACM+CIP) removal from water in batch and column studies. In EO studies, simultaneous degradation of ACM+CIP was considered. To this end, the coupled process was examined in batch mode operation utilizing some of the data obtained from the optimization of the single processes. The EO process was sequentially coupled with the adsorption to overcome the limitations of the individual processes through synergy for enhanced removal of ACM, CIP, ACM+CIP, ACM+CIP+AMX+ATN, and organic compounds (after EO treatment) from water. Moreover, the coupled process parameters of EO (pH, current density, and oxidation time) and adsorption (adsorption time and adsorbent dose) were optimized using the BBD. The BBD has been successfully employed in optimizing the individual EO and adsorption processes in previous studies (Chaabani et al., 2022; Gilpavas et al., 2020; Jawad, 2020; Sözüdoğru et al., 2023). Herein, an integrated optimization technique

was used for the coupled process optimization to fully understand the mutual inter-dependence among the EO and adsorption process parameters. To the best of our knowledge, this study is the first investigation for the simultaneous removal of the aforementioned pharmaceuticals employing bamboo-based adsorbent, and $IrO_2$/Ti electrodes in EO process. Besides, it is the first study to apply the coupled process in simultaneous removal of the target pharmaceuticals (ACM+CIP and ACM+CIP+AMX+ATN) along with the removal of organic compounds (EO-treated water), complemented by the integrated process optimization employed for the removal of ACM+CIP from water. Moreover, a comparative evaluation of the single and coupled process was performed under their respective optimal operating conditions on pharmaceuticals (binary or multiple pharmaceuticals), TOC, COD removal from diverse water matrices.

## 1.1. Statement of the problem

Advancements in pharmaceutical development for treating various human and animal diseases are increasing alongside technological innovations. The consumption of pharmaceuticals such as ACM and CIP has risen dramatically in the past years and is believed to increase even more with the world population growth (Anjali & Shanthakumar, 2022). Moreover, the recent global pandemic (COVID-19) has likely increased the environmental concentration of pharmaceuticals associated with COVID-19 symptom treatment, including antibiotics (CIP and AMX), analgesics (ACM) and anti-hypertensive (ATN) (Bagheri et al., 2024; Ortiz et al., 2024; Petromelidou et al., 2024). As a result, these contaminants are ubiquitously detected in water environment such as wastewater, surface water, groundwater and even in drinking water, with a concentration ranging from ng/L to µg/L (Anjali & Shanthakumar, 2022, 2023; Rosas-ramírez et al., 2022; Serna-galvis et al., 2019; Singh & Suthar, 2021). Water contamination with pharmaceuticals (ACM, CIP, AMX and ATN) can cause serious environmental and health impacts on humans and other organisms as they are designed to have a physiological effect on humans and animals in trace concentrations (Klavarioti et al., 2009). At even minimal concentration (< 1 µg/L), these contaminants can result in the alteration of organisms behaviour, physiology and physico-chemical processes, such as disruption of metabolic processes, possessing hormone receptors, mimicking natural hormones, reproductive problems, cancer, mutagenic effects and endocrine disruption (Chen et al., 2021; Ma et al., 2022; Q. Zhang et al., 2020). On the other hand, these contaminants are characterized by their refractory (recalcitrant) behavior for the conventional

wastewater treatment methods and are hence frequently released into the water bodies (Ortiz et al., 2024). Consequently, these contaminants disseminate through the point sources (hospital effluents, pharmaceutical industry effluents, domestic wastewater, and sewage effluents) and non-point sources (contaminated sludge disposals, hazardous waste disposal sites, landfill leachates, and urban runoffs) into the environment (Singh & Suthar, 2021). Source control of these contaminants is challenging as they are continuously being consumed and released into the environment from diverse sources (Kim & Zoh, 2016).

Numerous previous studies (Adeleye et al., 2022; Hawash et al., 2023; Jameel et al., 2020; Waleng & Nomngongo, 2022; Mheidli et al., 2022; Rodríguez-rodríguez et al., 2023) have reported the occurrence of the pharmaceuticals (ACM, CIP, AMX and ATN) in the water environment. It was also reported that the conventional treatment plants (employing coagulation, filtration, flocculation, sedimentation, and biological degradation) are unable to sufficiently remove these compounds from water due to their non-biodegradability and hdrophilicity nature. Subsequently, these pharmaceuticals are being introduced into the environment without detection (Gogoi et al., 2018), and thus; this issue become a major environmental and human health concern (Rocha et al., 2020). Moreover, the ongoing increase in pharmaceutical drug consumption and improper disposal into the environment may develop antibiotic-resistant organisms (bacteria genes/strains) and affect the drug effectiveness against bacteria. Therefore, efficient, sustainable and economically viable technologies are required to remove these contaminants from water.

In response to water contamination with these pharmaceuticals, various treatment techniques such as adsorption (Firdaus et al., 2024), EO (Fu et al., 2023), UV/chlorine (Kwon et al., 2018), ozonation (Sohn et al., 2024), photo-Fenton (Sohn et al., 2024), sonolysis (Gasmi et al., 2023), and photo-catalysis (Gasmi et al., 2023), biodegradation (Mantovani et al., 2024), membrane filtration (Alqadhi et al., 2024) and their combinations have been employed. However, this problem has not been fully addressed due to the lack of the safe, efficient, cost-effective and sustainable water treatment techniques to effectively remove these pharmaceuticals from water. Therefore, wide application of the proposed treatment techniques in common practices is still limited (Szabová et al., 2020). In this regard, the scientific pursuit of economical, efficient and sustainable processes has continued.

Among the employed technologies, EO (Ortiz et al., 2024) and adsorption (Demircan et al., 2024) have received increased attention. The current attention to the EO process for water treatment is due to its operational simplicity and high efficiency (Hamadeen & Elkhatib, 2022). On the other hand, adsorption offers the advantage of low-cost, easy implementation/operation, flexibility, and no toxic by-product formation. Adsorbents such as activated carbon (Firdaus et al., 2024), activated bentonite (Maged, 2020), and biochar (Ripanda et al., 2024), metal organic framework (Luo et al., 2024), aerogel (Han et al., 2022), and montmorillonite (Shi et al., 2021), and silica microsphere (Natarajan et al., 2021) have been employed to remove ACM, CIP, ATN and AMX from water. Nevertheless, the efficiency of the single treatment techniques such as EO and adsorption is limited in removing pharmaceuticals from complex water matrices. The effective removal of pharmaceuticals from complex water matrices demands high electric current and oxidation time for EO, and high adsorbent dose for the adsorption process, making the treatment process economically unviable. In light of this, coupling EO with adsorption can provide higher pharmaceuticals, TOC and COD removal from various water matrices with low supplied electric current, shorter oxidation time for EO and a low adsorbent dose for adsorption. In doing so, effective removal of oxidation by-products can be achieved from the EO pre-treated water. Previous studies typically only investigated the efficiencies of the single treatment techniques, mostly in removing single pharmaceutical contaminant from simple water matrix. However, Ganesan et al. (2019) indicated the benefit of coupling EO with the adsorption process, considering the removal of only a single pharmaceutical contaminant (CIP) from water (Ganesan et al., 2019).

However, detailed optimization of the coupled process (EO+adsorption) and comparative evaluation of the single and coupled processes have not been reported for simultaneous removal of diverse pharmaceuticals from water. Moreover, the influence of the water matrix on the removal of pharmaceuticals from various water matrices using the coupled (EO+adsorption) process has not been fully investigated. Therefore, this work conducted detailed optimization for the EO (ACM+CIP removal) and adsorption (ACM, CIP, and ACM+CIP removal) and EO+adsorption (ACM+CIP removal) processes. The adsorption study was conducted using an adsorbent derived from the bamboo sawdust, named CAC. Furthermore, an integrated optimization technique was employed in the coupled process optimization for ACM+CIP removal, considering the main parameters of EO (current density ($mA/cm^2$), EO time (min), pH)

and adsorption (adsorbent dose (g/L) and adsorption time (min)) using the BBD of the RSM framework. The comparative evaluation of the single and coupled process is provided for ACM+CIP, ACM+CIP+AMX+ATN, TOC and COD removal from diverse water matrices.

## 1.2. Objective of the Study

### 1.2.1. General objective

Enhanced removal of pharmaceutical contaminants from water using electrochemical oxidation coupled with adsorption process.

### 1.2.2. Specific objectives

- To synthesize and characterize chemically activated carbon (CAC) from bamboo sawdust.
- To optimize the adsorption of CIP onto the CAC employing the central composite design (CCD).
- To evaluate the performance of CAC on adsorptive removal of ACM (or paracetamol) from water.
- To investigate the removal of ACM, CIP and ACM+CIP in batch and column adsorption studies using the CAC adsorbent.
- To optimize the simultaneous degradation of ACM and CIP in the EO process.
- To evaluate the performance of EO+adsorpion for the removal of pharmaceuticals (ACM+CIP and ACM+CIP+AMX+ATN), TOC and COD from diverse water matrices.

## 1.3. Research questions

The valuable research questions addressed in this study are:

- How efficient are the adsorption, EO and EO+adsorption in pharmaceuticals (ACM, CIP, ACM+CIP and ACM+CIP+AMX+ATN) removal from water?

- How does the water matrix affect the single and coupled process performances in removing ACM+CIP from water?
- What are the main factors (parameters) that significantly affect the efficiency of the EO, adsorption and EO+adsorption in removing ACM, CIP and ACM+CIP from the water?
- What are the optimum operational conditions for effective removal of ACM, CIP and ACM+CIP from water using the EO, adsorption and coupled processes?
- What are the benefits of coupling EO with adsorption for the removal of ACM+CIP, ACM+CIP+AMX+ATN, TOC and COD from water?

## 1.4. Significance of the study

The target pharmaceuticals (ACM, CIP, AMX and CIP) are ubiquitously detected in different water bodies. The environmental accumulation of these contaminants intensifies with the expanding global population, driven by increased consumption. On the other hand, the potential health hazards associated with these contaminants on aquatic life and humans are repeatedly reported. As a result, water contamination with these pharmaceuticals has become a significant threat to human health, gaining a global concern. Effective control of the dissemination of these compounds requires advanced removal technologies.

The EO and adsorption processes are efficient water treatment techniques mostly employed independently for removing pharmaceuticals from water. However, EO and adsorption have limitations, such as limited removal efficiency in multiple pharmaceuticals removal from complex water matrices and the formation of oxidation by-products (EO process) when employed individually. In this study, the single process (EO and adsorption) parameters were optimized to enhance the removal efficiency of pharmaceuticals from water. In addition, this work elucidated the benefit of integrating EO with adsorption considering the removal of binary pharmaceuticals (ACM+CIP), multiple pharmaceuticals (ACM+CIP+AMX+CIP), TOC, COD removal from diverse water matrices. Integrating EO with adsorption process demonstrated remarkable removal of the target pharmaceuticals from water and high mineralization at relatively low current density, shorter EO time and low adsorbent dose. The successful removal of these pharmaceuticals from water is a crucial achievement for wastewater reuse; hence, it can be considered a good solution for the upcoming safe water scarcity. Besides, the effective

removal of these compounds from water minimizes the chance of antibiotic resistant bacteria and antibiotic resistant genes development, which often results from the spread of these pharmaceuticals in the environment. This study presented the performance of EO, adsorption and EO+adsorption by assessing different operational conditions. Herein, the knowledge generated on the coupled process is highly valuable for considering the integrated process as an additional treatment step to the existing wastewater treatment plants for complete removal of pharmaceutical contaminants from water. Moreover, this study presented the benefit of integrating EO with adsorption, paving the way for future investigations into the potential scale-up of the proposed coupled process.

### 1.5. Scope of the study

This work aimed to investigate the performances of EO, adsorption, and EO+adsorption processes in removing ACM, CIP, ACM+CIP, and ACM+CIP+AMX+ATN from water. Adsorbents employed in this study were synthesized from bamboo sawdust via chemical activation ($FeCl_3.6H_2O$ and KOH). The synthesized adsorbents were then tested on the removal of ACM, CIP and ACM+CIP from water. Afterward, the best-performing adsorbent was exhaustively characterized using x-ray diffraction (XRD), Fourier transform infra-red spectroscopy (FTIR), Brunauer-Emmett-Teller surface area (BET), Raman spectroscopy, scanning electron microscopy with energy dispersive spectroscopy (SEM/EDS) and pH of point of zero charge ($pH_{pzc}$), and it was used throughout the adsorption studies. Primarily, the target pharmaceuticals considered in this study can be categorized under two major classes, namely non-steroidal anti-inflammatory drug (ACM) and quinolone antibiotic (CIP). However, other classes of pharmaceuticals such as beta-blocker (ATN) and penicillin antibiotic (AMX) were also used to fully investigate the performance of EO, adsorption and EO+adsorption processes over diverse pharmaceuticals removal from water. The process parameters of the single and coupled processes were optimized in removing the target pharmaceuticals from water. The coupled process (EO+adsorption) was optimized by systematically considering the significant factors of each process, aiming to explore their inter-dependence. In the coupled process, EO and adsorption were sequentially integrated to address electro-generated by-products in the adsorption step. Water matrices such as pure water, tap water, and real wastewater (secondary

treatment plant effluent) were employed to evaluate the performances of the single and coupled processes in removing the target pharmaceuticals from simple and complex water matrices.

## 1.6. Outline of the dissertation

This dissertation includes six chapters:

**Chapter One**

This chapter provides a comprehensive overview of the current research work. It encompasses the research background, problem statement, main and specific objectives, research questions, significance of the study, scope of the study, and the outline of the dissertation.

**Chapter Two**

This chapter offers an extensive literature review to provide a thorough understanding of the current research work. It covers various aspects, including types of pharmaceutical contaminants, categories of pharmaceuticals, sources of pharmaceutical contaminants, occurrences of pharmaceutical contaminants in water environments, and effects of pharmaceutical contaminants. Moreover, it provides detailed explanations on the pharmaceutical contaminants removal technologies, such as adsorption, advanced oxidation processes (electrochemical oxidation, ozonation, UV/chlorine, UV/$H_2O_2$, heterogeneous photo-catalysis), and coupled/hybrid water treatment processes.

**Chapter Three**

Chapter three outlines the materials and methods employed in this research. It provides comprehensive descriptions of all the materials, chemicals, equipment and details on the experimental setup and methods employed in this study.

**Chapter Four**

This chapter presents detailed discussions of all the experimental results generated in this research work. The results associated with each specific objective are briefly explained in this chapter.

## Chapter five

Chapter five, the concluding section of this dissertation, summarizes the key findings and offers recommendations for further research endeavors. This dissertation is built upon three published papers, with an additional manuscript currently under review.

# CHAPTER TWO

## 2. LITERATURE REVIEW

### 2.1. Pharmaceutical contaminants

Thousands of pharmaceutical compounds have been developed, and their numbers continue to increase because of their growing demand. The European Union (EU) market has registered around 3000 commonly used pharmaceuticals, with their usage still increasing (Kumar et al., 2023). Pharmaceutical contaminants are categorized as emerging contaminants in water. The United States Environmental Protection Agency (U.S. EPA) defined "emerging " as compounds or materials which were previously not listed for routine monitoring, characterized by a perceived potential or real threat to the health of humans and environments and lack published health standards, environmental protection laws and regulations (Oluwole et al., 2020). These are mainly uncontrolled anthropogenic compounds present in the air, soil, water, food, and human/animal tissues in trace concentrations ng/L to µg/L. Other emerging contaminants include personal care products, disinfection by-products, endocrine disrupting chemicals, polycyclic aromatic hydrocarbons, pesticides, detergents, illicit drugs, flame-retardants, plasticizers, phthalates, micro-plastics, nanoparticles, and per-fluoroalkylated substances (Menya et al., 2023).

Tiwari et al. (2016) reported a two-fold increase in the daily dosage of anti-hypertensive, cholesterol-lowering, anti-diabetic and anti-depressant drugs in Organization for Economic Co-operation and Development (OECD) member countries in the last 13 years (2000-2013) (Tiwari et al., 2016). Among these compounds, pharmaceuticals that become environmental concerns include antibiotics, legal and illicit drugs, analgesics, steroids and beta-blockers (Gogoi et al., 2018). These contaminants have a therapeutic effect on the human body, even at low concentrations. Due to the inefficient removal of these contaminants by conventional wastewater plants (WWTPs), they have been detected in the aquatic environment.

Antibiotics are the leading pharmaceutical pollutants, followed by non-steroidal anti-inflammatory drugs (NSAIDs), antidepressants, lipid regulators, β-blockers and hormones

(Ouyang et al., 2020). Pharmaceutical residues remain active after being released into the environment and degrade water quality, adversely impacting the ecosystem and human health, such as joint diseases, nephropathy, endocrine disruption, and central nervous system failure (Li et al., 2023). They are typically complex molecules with diverse properties. Due to their resistance to the WWTPs, these contaminants are continuously discharged into water bodies such as rivers, streams and lakes (Miarov et al., 2020). In the last decade, the occurrence and fate of antibiotics in environmental matrices have received increased attention since antibiotics are persistent and refractory to biodegradation. As a result, these compounds accumulate in the environment and become a potential risk to aquatic and terrestrial organisms (Tan et al., 2017).

Water demand increases, whereas the quality and quantity of freshwater are continuously declining due to several anthropogenic activities (Afrouz Bagheri et al., 2019). The continuous discharge of pharmaceuticals into the environment in the past few decades resulted in the contamination of water bodies (Ouyang et al., 2020). These days, it is becoming more evident that pharmaceutical drugs are ceaselessly released into the water because of high consumption and ineffective removal in the WWTPs (Dubey et al., 2023). As a result, these contaminants and their metabolites are ubiquitously detected in wastewater, sewage, surface water, groundwater, and even drinking water. In this regard, significant research activities are in progress to map pharmaceuticals worldwide, aided by the development of modern analytical methods like liquid chromatography coupled with mass spectroscopy (LC-MS) for multi-target compound detection (Chinnaiyan et al., 2018).

### 2.1.1. Categories of pharmaceuticals

There are various categories of pharmaceuticals based on therapeutic uses, chemical structure, mechanism of action, and route of administration. Among these, pharmaceuticals being used for different therapeutic uses exhibiting distinct chemical structure are employed in this study. These include antibiotics, NSAIDs, analgesics, antifungal, anticonvulsants, antidepressants, beta-blockers, lipid-regulating drugs, steroidal hormones, x-ray contrast media, UV filters, stimulants, anti-itching drugs, insect repellents, plasticizers, etc. Antibiotics and NSAIDs are the foremost commonly prescribed drugs. The environmental existence of pharmaceuticals under these categories has been widely reported (Oluwole et al., 2020; Tang et al., 2020; Pham, 2018; Wilt et

al., 2018). Based on the volume of prescriptions, toxicity, and their occurrence in the environment, therapeutic drugs such as antibiotics, hormones, NSAIDs, beta-blockers, blood lipid regulators, anti-epileptics, analgesics and antidepressants are the widely studied classes of pharmaceutical (Miarov et al., 2020). Some classes of pharmaceuticals, like NSAIDs, are even more abused because of their anti-inflammatory and analgesic effect (Wei et al., 2020). Among all classes of pharmaceuticals, antibiotics, analgesic and anti-hypertensive drugs such as ACM, CIP, AMX and ATN are ranked as highly consumed drugs worldwide. This is because they can easily be purchased with or without a prescription and are mostly used for highly prevalent diseases and symptoms among the population (Goh & Ismail, 2020). Detailed explanations about these pharmaceuticals are presented below.

### i) Acetaminophen (ACM)/Paracetamol (PCT)

Acetaminophen ($C_8H_9NO_2$) also known as paracetamol (PCT), is a common anti-inflammatory/analgesic pharmaceutical widely used without prescription to treat headaches, migraine, neuralgia, backache and rheumatic pain (Ziylan-yavas & Ince, 2018). Moreover, ACM has been widely used in anti-influenza drugs around the world (Skwarczynska-wojsa, 2024). It is commonly used in Latin America, Africa and the Middle East (Islam et al., 2019). After consumption, ACM is not fully metabolized in the human body, and thus released into the environment via urine and faeces in both metabolized and unmetabolized forms (Skwarczynska-wojsa, 2024). It is reported that around 58-68% of the consumed ACM is excreted in the unmetabolized form (Natarajan et al., 2021). Due to its wide production and extensive consumption, it has been ubiquitously detected in various water bodies, including influents and effluents of conventional WWTPs, hospital effluents, groundwater, and surface water ranging from 10 to 134,000 ng/L (Goh & Ismail, 2020; Yun et al., 2019). In the aquatic environment, ACM readily accumulates due to its high solubility and hydrophilicity (Jakóbczyk et al., 2022). A notable significance lies in addressing the higher concentration of ACM detected in the aquatic environment compared to other drugs within the same family. There is a pressing need to address and manage the water contamination with ACM for environmental well-being. The secondary WWTP effluents have been recognized as the primary source for ACM pollution of water resources (Goh & Ismail, 2020). Even though removing ACM from water is paramount, commonly used water and wastewater treatment systems seem impotent for effectively

eliminating ACM from water due to its high solubility, high hydrophilicity and resistance to bio-degradation (Yun et al., 2019). Therefore, new treatment systems are required to effectively remove ACM from water. The chemical structure of the ACM is shown in Figure 2.1.

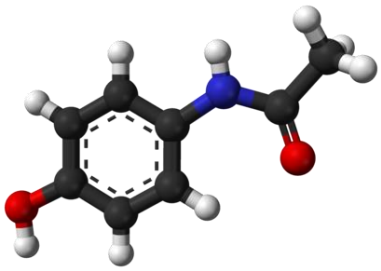

Figure 2.1. Chemical structure of ACM.

**ii) Ciprofloxacin (CIP)**

CIP ($C_{17}H_{18}FN_3O_3$) is an antibiotic in the quinolone group that was first introduced in 1987. It is now the most commonly used drug among the second-generation quinolones, accounting for over 20 million prescriptions in 2010, making it the 35$^{th}$ widely prescribed generic drug and the 5$^{th}$ most frequently used antibacterial drug in the U.S. for bone and joint infections, urinary tract infections, eye irritations. Recently, COVID-19 patients have been treated with CIP (Amar et al., 2024). Concentrations of CIP in the environment vary from ng/L to mg/L (Amar et al., 2024). The high concentration of this antibiotic in the effluents leads to the development of antibiotic resistant bacteria and antibiotic resistant genes through prolonged exposure to CIP. Thus, effective removal mechanisms are needed to protect the environment against CIP. The molecular structure of the CIP is presented in Figure 2.2.

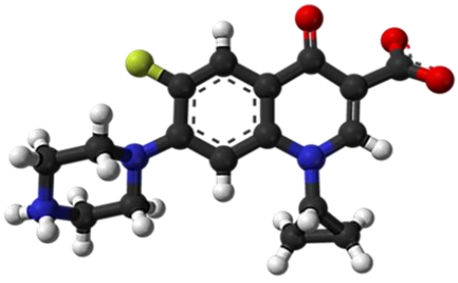

Figure 2.2. Chemical structure of CIP.

iii) **Amoxicillin (AMX)**

AMX ($C_{16}H_{19}N_3O_5S$) is an antibiotic in the beta-lactam group and is often used for human and animal bacterial infection treatments (Anastopoulos et al., 2020; Yaghmaeian et al., 2014). AMX has amphoteric properties due to three main functional groups: $NH_2$, –COOH and –OH. Single-dose therapy with 500 mg of AMX in the human body results in an excretion rate of up to 86 ± 8% within 2 hrs of ingestion (Anastopoulos et al., 2020). Moreover, AMX is resistant to bio-degradation (Karimi-maleh et al., 2021), and its existence in surface water, domestic and industrial wastewater is related to the potential environmental risks (Anastopoulos et al., 2020). It was detected in surface water, such as river, in the concentration range of 7.11–7.81 ng/L (Shi et al., 2020). Based on the available reports, a maximum concentration of AMX reaching up to 79.6 ng/L was recorded in the water environment. Therefore, efficient treatment of water containing AMX is imperative to safeguard human health and the environment (Yaghmaeian et al., 2014). Figure 2.3 shows the chemical structure of AMX.

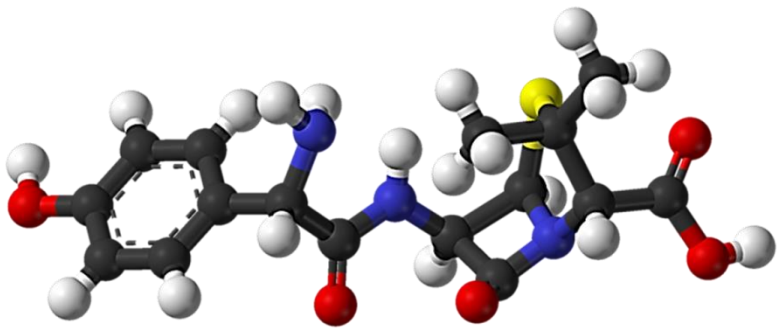

Figure 2.3. Chemical structure of AMX.

**iv) Atenolol (ATN)**

Atenolol ($C_{14}H_{22}N_2O_3$) is a β-blocker commonly used for treating high blood pressure and heart-related conditions. Atenolol has been detected in river water and exhibited a significant persistence with concentration ranging from 0.16 to 1.18 µg/L (Jennifer et al., 2017). Also, it has been detected in the wastewater treatment plant effluents (García-rosero et al., 2022). It has a low biodegradability and high presence in rivers and wastewater (García-rosero et al., 2022). After consumption, ATN undergoes partial metabolism and is ultimately excreted via urine in non-

metabolized forms (>85%) (Iancu et al., 2020). These reports provide evidence of the need to implement an effective technology for the removal of ATN from surface water and wastewater. The chemical structure of ATN is presented in Figure 2.4.

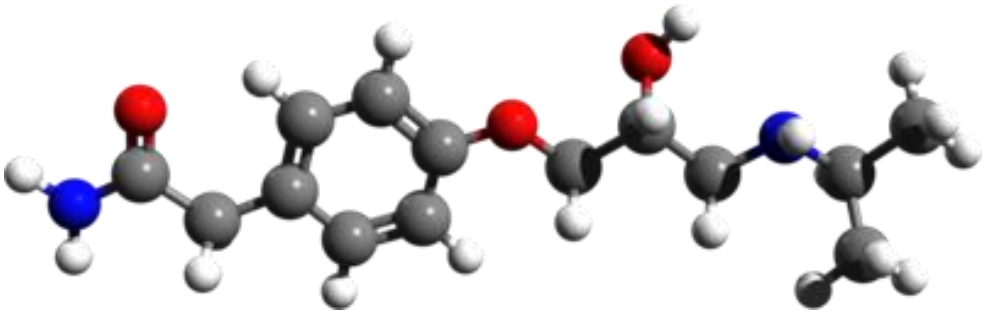

Figure 2.4. Chemical structure of ATN.

### 2.1.2. Sources of pharmaceutical contaminants

The intensive consumption of pharmaceutical products since the 1960s significantly increased their presence within various environments such as wastewater, river water, sediments and seawaters (Thiebault, 2019). Pharmaceutical residues identified in wastewater can be categorized under human and veterinary antibiotics, prescription and non-prescription drugs, and some sex and steroid hormones (Gogoi et al., 2018). These contaminants are introduced into the environment via different sources, including hospital wastewater, landfill leachates, sewer leakage, manure or sludge application in agricultural activities, industrial waste (especially pharmaceutical factory effluents), surface runoff from urban or agricultural areas, domestic wastewater containing human/animal urine and faeces, research activities utilizing these compounds, disposal of unused and expired drugs (Al-juboori et al., 2024; Dubey et al., 2023; Qian et al., 2023; Yu et al., 2024). Conventional WWTPs only partially eliminate the initial load of pharmaceutical contaminants. Despite their efforts, a significant portion of pharmaceutical contaminants, typically 20% to 65%, remain in the treated effluents that are eventually discharged into receiving streams, rivers, or coastal areas (Castaño-Ortiz et al., 2024). These pharmaceutical contaminants in wastewater effluents and aquatic environments may find their way into drinking water intended for human consumption (Thiebault, 2019). There is a growing awareness of the impacts of these contaminants in various parts of the ecosystem, such as water,

sediments, and biota, reaching concentration levels that can pose a threat to aquatic organisms (Rocha et al., 2020).

### 2.1.3. Occurrences of pharmaceuticals in water environment

Pharmaceutical residues from various sources enter the water environment and have become a global concern (Nguyen et al., 2023). The increased consumption of several pharmaceuticals such as ACM, and AMX during the COVID-19 pandemic caused the release of these contaminants into the environment from hospitals, medical and quarantine centers (Castaño-Ortiz et al., 2024; Nguyen et al., 2023). In this regard, advancements in analytical equipment like High Performance Liquid Chromatography coupled with Mass Spectroscopy (HPLC–MS), have enabled the detection of pharmaceuticals in water bodies at trace concentrations (ng/L) (Kock et al., 2023). Based on the review of current reports, occurrences of certain pharmaceuticals in water resources are presented in Table 2.1.

Table 2.1. The concentrations, sources, and countries where the target pharmaceuticals were detected in water resources.

| Pharmaceuticals | Concentration (µg/L) | Sources | Country | References |
|---|---|---|---|---|
| Acetaminophen (ACM) or paracetamol (PCT) | 260.49 | WWTP influent | France | (Guillossou et al., 2019) |
| | 2.62 | WWTP effluent | France | (Guillossou et al., 2019) |
| | 108.38–246 .64 | WWTP influent | South Wales, UK | (Kasprzyk-hordern et al., 2009) |
| | <0.08–1.57 | WWTP effluent | South Wales, UK | (Kasprzyk-hordern et al., 2009) |
| | 5.760 | WWTP influent | Kwazulu-Natal, South Africa | (Oluwole et al., 2020) |

Table 2.1. Continued.

| Pharmaceuticals | Concentration (µg/L) | Sources | Country | References |
|---|---|---|---|---|
| ACM | 28.58 | WWTP influent | Republic of Korea | (Son et al., 2023) |
| | 0.38 | Groundwater | USA | (Nguyen et al., 2023) |
| | 62.25 | Hospital effluent | Taiwan | (Nguyen et al., 2023) |
| CIP | 6,500 | Surface water | India | (Kovalakova et al., 2020) |
| | 1.21 – 3.85 | WWTP influent | Spain | (Gracia-lor et al., 2012) |
| | 0.52 – 1.8 | WWTP effluent | Spain | (Gracia-lor et al., 2012) |
| | 160- 13, 625 | WWTP influent | Spain | (Rosal et al., 2010) |
| | <LOQ- 5, 692 | WWTP effluent | Spain | (Rosal et al., 2010) |
| | 0.12 – 0.2 | WWTP influent | South Africa | (Mzukisi et al., 2020) |
| | 0.8 – 1.4 | WWTP effluent | South Africa | (Mzukisi et al., 2020) |
| | 830 | WWTP effluent | Ethiopia | (Gezahegn et al., 2019) |
| | 0.76-1.53 | Hospital wastewater | Ethiopia | (Gadisa et al., 2024) |
| Amoxicillin (AMX) | <LOQ –0.021 | Surface water | Egypt | (Mzukisi et al., 2020) |
| | <LOQ – 4.66 | WWTP effluent | Egypt | (Mzukisi et al., 2020) |
| | 0.0027 | Surface water | Nigeria | (Mzukisi et al., 2020) |
| Atenolol (ATN) | 0.5–13.2 | Surface water | Argentina | (Puri et al., 2023) |

Note: WWTP: wastewater treatment plant, LOQ: limit of quantification of the method employed in the cited reference.

### 2.1.4. Effects of pharmaceutical contaminants

Pharmaceuticals are designed to target specific cell, metabolic or enzymatic signals to achieve the desired therapeutic effects. Therefore, they are biologically active even at trace doses (Kock et al., 2023). They exhibit the same bioactivity upon reappearing as contaminants, potentially causing severe health effects. Pharmaceuticals in the aquatic environment are associated with various negative effects on humans and the environment, including short and long-term toxicity, endocrine disruption and the development of antibiotic-resistant microorganisms (Kim & Zoh, 2016). Consuming water or food contaminated with antibiotic residues may lead to various adverse health effects on humans, such as allergic hypersensitivity reactions, toxic effects, hepatotoxicity, nephropathy, endocrine disruption, mutagenicity, carcinogenicity (Miarov et al., 2020). Another adverse health effects of these include hindering metabolic processes, possessing hormone receptors, mimicking natural hormones, and inducing development and reproductive problems (Shin et al., 2020). Reports have also indicated several disorders among fauna, such as fish or bacteria at field-relevant concentrations (Thiebault, 2019). More specifically, trace amounts of CIP present in drinking water can result in symptoms such as nausea, headaches, diarrhea, vomiting, and tremors. Conversely, elevated levels of CIP often lead to thrombocytopenia, excessive liver enzyme levels, and acute renal failure (Kamal et al., 2024). Other reported adverse effects of CIP on the aquatic ecosystems include disruption of plant photosynthesis, abnormalities in plant and alteration of algal structure (Kamal et al., 2024). On the other hand, water contamination with ACM can result in several harmful effects on human health, including hepatotoxicity, mutagenesis, endocrine disruption, and cancer in humans (Chen et al., 2021; Q. Zhang et al., 2020).

The health impacts of the pharmaceutical contaminants have been investigated using biomarkers such as daphnia magna, Dreissena polymorph, Danio rerio, and Gammarus pulex in various studies. These species were used due to their important physiological characteristics. In this regard, considering these simple species to assess physiological parameters allows the estimation of the health effects of these contaminants on more complex organisms (Arias, 2019). Another primary concern regarding the release of pharmaceuticals such as CIP and AMX into the environment is the development of antibiotic-resistant genes and bacteria that

can reduce the therapeutic potential of antibiotics against human and animal pathogens (Han et al., 2018). The occurrence and persistence of pharmaceutical contaminants, alone or in mixtures, will have irreparable harmful effects, presumably leading to the extinction of some ecosystems. There is a knowledge gap in health impact assessment of pharmaceutical contaminants such as death rate of humans due to exposure to these contaminants. Therefore, it is crucial to set stricter discharge limits for pharmaceuticals, investigate detailed health impact analysis and develop advanced technologies to address this environmental problem (Rout et al., 2021).

## 2.2. Physical/chemical pharmaceuticals removal technologies

### 2.2.1. Adsorption process

Adsorption is a widely used separation method for contaminant removal in water and wastewater treatment. It is the adherence/binding of atoms, molecules, or ions of gas, liquid, or solid onto the material surface (Sulyman et al., 2017). An adsorbent is a porous material that can adsorb substances onto its surface by intermolecular forces. Adsorbents can be synthesized from several materials, such as silica, clay, zeolites, biomass (industrial by-products, agricultural wastes), and polymeric materials with or without modification. Numerous adsorbents, including biochar (Alshakhs et al., 2024), activated carbon (Thanh et al., 2020), clay (Chauhan et al., 2020), magnetic nanomaterial (Loc et al., 2023), metal-organic framework (Yılmaz et al., 2021), iron nanoparticles with a freshwater microalga (Kumar et al., 2021), chitosan magnetic nano-biosorbent (Natarajan et al., 2022) microalgae ( Pereira et al., 2023), groundnut shell (Malesic-eleftheriadou et al., 2021) have been used to remove pharmaceuticals contaminants from water. The adsorption process is techno-economically more attractive due to its inexpensiveness, universality and environmental friendliness (Ali et al., 2020). It has been widely applied in both lab-scale and large-scale industrial applications.

Carbon-based adsorbents are one of the most effective adsorbents widely utilized for the remediation of organic and inorganic contaminants from water. The broad-spectrum, uncharged and non-polar contaminants can be effectively removed from wastewater by adsorption onto carbon materials. This phenomenon may be linked to the porous structure of carbon, which offers an ample surface area for effective adsorption. Furthermore, the surface chemistry and

pore size distribution of adsorbents play pivotal roles in determining the degree of pharmaceutical contaminants removal (Peres et al., 2017). The utilization of materials like activated carbon (AC), biochar (BC), and hydrochar (HC) for the removal of pharmaceutical contaminants from water has received increased attention among researchers. This is attributed to the simplicity, cost-effectiveness, and high performance associated with these materials (Rocha et al., 2020).

Choosing an appropriate adsorbent for a particular adsorption process constitutes a primary objective in adsorption studies. The crucial factors to investigate during an adsorbent selection include high adsorption capacity, adsorption rate, efficiency in removing various target pollutants, selectivity for different substances, surface area, physical strength, kinetics, non-toxicity, regenerability, tolerance for a diverse water matrix, and cost-effectiveness. Carbon-based adsorbents have drawn significant attention because of their chemical inertness, biocompatibility and thermal stabilities (Ali et al., 2020). Activated carbon is one of the carbon-based adsorbents commonly employed to remove organic contaminants from water and wastewater.

In lab and full-scale operations, the adsorption process can be operated in batch and continuous (flow) modes. In the batch adsorption process, the binding of the adsorbate molecule onto the adsorbent occurs physically or chemically for a certain period after charging the adsorbent and the aqueous solution containing the adsorbate. The efficiency of adsorptive removal is influenced by several factors, including the type of adsorbent, its physicochemical properties (such as pore volume, size, diameter, and surface area), pH levels, initial pollutant concentration, temperature, contact time, and the dosage of the adsorbent. In contrast, the continuous adsorptive process consists of a column containing a fixed adsorbent material through which water or an aqueous solution containing the target adsorbate flows through the column. Fixed-bed columns are widely used for adsorption in flow mode. In the flow mode operation, mass transfer is favourable by a gradient concentration, which is the driving force of the adsorption process. The flow mode adsorption process is often characterized by the breakthrough curves, which show the change in pollutant concentration (effluent) with time. As a result, the breakthrough curve serves as an indicator, signalling the optimal time for regenerating the adsorbent. In a flow mode adsorption

process, factors such as bed height (adsorbent weight), flow rate, initial pollutant concentration in the feed and pH of the solution affect the performance of column adsorption.

In addition, the physico-chemical properties of the adsorbent, such as the adsorbent porosity, surface area of the adsorbent, point of zero charge and the dissociation constant (pKa) value, affect the adsorption process (Juela, 2020). Similarly, the nature of the adsorbate molecule (size, charge and hydrophobicity) and the water background matrix influence the performance of the adsorption process (Guillossou et al., 2020). There are two types of adsorption processes: single component sorption and simultaneous sorption of contaminants. These sorption processes are explained in the following sections. Adsorbents applied in the removal of pharmaceutical contaminants from water are presented in Table 2.2.

Table 2.2. Adsorptive capacities of various adsorbents in the removal of pharmaceutical contaminants from water.

| Adsorbent type | Properties of adsorbent | Pharmaceutical contaminant | Type of water matrix | Operating conditions | Adsorbent capacity (mg/g) | References |
|---|---|---|---|---|---|---|
| **Batch adsorption** | | | | | | |
| Biochar | $S_{BET}$: 134.1671 $m^2/g$, pore size = 4.5 nm, pore diameter = 5.4 nm, pore volume = 0.15 $m^3/g$ | CIP | Deionized water | $C_o$ = 60 mg/L, time = 180 min, pH = 4, rpm = 150 and temperature = 21ºC. | 27.97 | (Lu & Zhao, 2024) |
| Modified thermal kaolin | $S_{BET}$ = 25 $m^2/g$, pore size = 25.1 nm, pore volume = 0.16 $m^3/g$ | CIP | Deionized water | adsorbent dose = 0.75 g/L, pH= 5, and time = 100 min. | 31.85 | (Yuxuan Yang et al., 2022) |
| Graphene-boron nitride composite aerogel | $S_{BET}$ = 91.3 $m^2/g$ | CIP | Deionized water | $C_o$ = 10.5 mg/L, pH = 7, adsorbent = 0.25 g/L | 185 | (Han et al., 2022) |
| Cross-linked electrospun mats | - | ATN | Deionized water | $C_o$ = 10 mg/L, adsorbent = 1 g/L, pH =7 | 7.31 | (Cecone et al., 2024) |

Table 2.2. Continued.

| Adsorbent type | Properties of adsorbent | Pharmaceutical contaminant | Type of water matrix | Operating conditions | Adsorbent capacity (mg/g) | References |
|---|---|---|---|---|---|---|
| Alginate/activated hydrochar composite beads | $S_{BET}$ = 533.42 $m^2$/g, pore diameter = 2.12 nm and pore volume = 0.28 $m^3$/g | ACM | Deionized water | $C_o$ = 100 mg/L, adsorbent = 1 g/L, pH = 6.5. | 165.94 | (Peixoto et al., 2022) |
| $CoFe_2O_4$-modified biochar | $S_{BET}$ = 25.69 $m^2$/g, pore volume = 0.025 $m^3$/g, pore volume = 3.92 nm | AMX | Deionized water | $C_0$ = 50 mg/L, pH = 7, contact time = 60 min, and adsorbent = 0.5 g/L. | 136.83 | (Chakhtouna et al., 2021) |
| **Continuous adsorption** | | | | | | |
| Biochar | $S_{BET}$ = 308.6 m²/g, pore diameter = 2.8 nm | ACM | Deionized water | $C_o$ = 100 mg/L, pH = 5.7 and flow rates = 2.5 mL/min and 5.0 mL/min, adsorbent loading (0.38 and 0.75 g) | 27.65 | (Luiz et al., 2023) |
| Diatomaceous earth | - | CIP | Deionized water | pH = 2.0 | 105.1 | (García-alonso et al., 2019) |
| Acid activated bentonite | $S_{BET}$ = 29.59 $m^2$/g, pore volume = 0.09 $m^3$/g, pore diameter = 11.37 nm | CIP | Deionized water | pH = 5-6.1 | 97.12 | (Maged et al., 2020) |
| Date pits activated carbons | $S_{BET}$ =1055 $m^2$/g, micro pore-volume: 0.36 $m^3$/g | AMX | synthetic wastewater | pH < 6.0 | 424 | (Belhachemi & Djelaila, 2017) |

### i) Single sorption of contaminants

The adsorption process has been widely applied to remove a single contaminant at a time. The commonly employed isotherm models (Langmuir and Freundlich) were developed for single sorption systems. In recent studies, pharmaceuticals including ACM (Hyun et al., 2023), CIP (Pal et al., 2024), ATN (García-rosero et al., 2022), AMX (Laksaci et al., 2023), tetracycline (Li et al., 2024; Yang et al., 2024), and carbamazepine (Mehmood et al., 2024), diclofenac (França et al., 2019) were removed from single component contaminant systems. In single component sorption systems, there is no competition for adsorbent active sites if the adsorption is conducted in a pure water matrix. In real-world scenarios, however, single contaminants do not exist alone; instead, there is typically a combination of contaminants. Therefore, considering more than one component in the adsorption process offers practical advantages.

### ii) Simultaneous sorption of contaminants

Simultaneous sorption of contaminants involves adsorption of more than one component at a time. In this sorption system, adsorbate molecules compete for the active sites of the adsorbent. Therefore, simultaneous sorption provides an adsorbent capacity closer to real-world applications, as the adsorption process of environmental samples involves the adsorption of multiple components. Simultaneous sorption such as sorption of ACM and nimesulide (NMS) (ACM+NMS) (Pauletto et al., 2024), atenolol (ATN) with propranolol (PPL), sulfasalazine (SFS) and sulfamethazine (SMZ) (ATN+PPL+SFS+SMZ) (Kim et al., 2024), ofloxacin (OFX) oxytetracycline (OXT), ciprofloxacin (CIP), and sulfamethoxazole (SMT) (OFX+OXT+CIP+SMT) (Zafar et al., 2023), tetracycline (TC) and ciprofloxacin (CIP) (TC+CIP) (Tong et al., 2023) and amoxicillin (AMX) and metronidazole (MTZ) (AMX+MTZ) (El et al., 2023) were studied. The simultaneous sorption process data should be described using the multi-component isotherm models such as competitive/extended Langmuir model, non-modified Langmuir model, extended Freundlich model, Modified Redlich-Peterson model, Jian and Snoeyink modified Langmuir model and p-factor models. The study of the simultaneous adsorption process helps to understand the potential of the adsorbent over multiple contaminants, adsorbate-adsorbate interactions (synergistic or antagonist effects) and the adsorbent-adsorbate interactions. In simultaneous adsorption systems, the adsorption process can be non-interactive,

antagonistic, and synergistic when it fulfills conditions as shown in Eq. (2.1), Eq. (2.2), and Eq. (2.3) (Tovar-gómez et al., 2014), respectively.

$$\frac{q_{m\,binary}}{q_{m\,single}} = 1 \tag{2.1}$$

$$\frac{q_{m\,binary}}{q_{m\,single}} < 1 \tag{2.2}$$

$$\frac{q_{m\,binary}}{q_{m\,single}} > 1 \tag{2.3}$$

$q_{m\ binary}$ and $q_{m\ single}$ refer to the maximum adsorption capacity in binary and single component adsorption systems, respectively.

**iii. Mechanism of the adsorption process**

The adsorption process is generally classified as physical adsorption (physi-sorption) or chemical adsorption (chemisorption). Physi-sorption is carried out by Van der Waals forces, dipole interactions, and hydrogen bonding (Sulyman et al., 2017). In this process, there is no electron exchange between the adsorbent and adsorbate molecules. In physi-sorption, equilibrium is rapidly achieved, and the process requires low activation energy for physical adsorption. It is characterized by its non-specific and reversible nature. However, chemisorption results from the chemical bonding between adsorbent and adsorbate molecules, making it a specific and irreversible process. This type of adsorption alters both the chemical and electronic properties of the adsorbent during the chemisorption process.

The binding of adsorbent and adsorbate by the covalent bond is called weak chemical adsorption, whereas the binding between adsorbent and adsorbate by an ionic bond is termed strong chemical adsorption (Sulyman et al., 2017). The adsorbent-adsorbate interaction mechanisms include electrostatic attraction, π-π interaction, hydrogen bonding, pore filling, functional groups complexation, n-π interaction and Lewis-acid base interaction. These adsorption mechanisms are explained as follows:

### a) Electrostatic interaction

The electrostatic interaction is one of the most investigated mechanisms of adsorption. The electrostatic interaction can be electrostatic attraction or electrostatic repulsion. This mechanism can be explained by noting the pH of the point of zero charge of the adsorbent ($pH_{pzc}$) and the dissociation constants (pKa) of the pharmaceuticals. Typically, the surface charge of the pharmaceuticals becomes positive at solution pH values less than their pKa value and vice versa. On the other hand, the surface charge of the adsorbent becomes positive for the solution pH values less than $pH_{pzc}$ and negative for solution pH values higher than $pH_{pzc}$. Electrostatic attraction occurs when the adsorbent and pharmaceuticals exhibit different charges (positive and negative). In contrast, electrostatic repulsion occurs when they have similar charges (either positive or negative). Electrostatic interaction mechanism has been reported for ACM and CIP adsorption (Al et al., 2021; Grimm et al., 2024).

### b) π-π interactions

The π-π interactions occur between the aromatic groups of adsorbent and adsorbate molecules. In most cases, π-π interactions most likely happen during the adsorption of pharmaceuticals, as pharmaceutical contaminants typically contain at least one aromatic ring. The π–electron-deficient regions (**π** –electron acceptor) on pharmaceuticals interact with π–electron-rich regions (**π** –electron donor) of the adsorbent surfaces (Bose et al., 2023). Studies pointed out that aromatic rings of ACM and CIP interact with the aromatic ring of the biochar, exhibiting π-π interaction (Grisales-cifuentes et al., 2021; Yang et al., 2022).

### c) Hydrogen bonding

The hydrogen bonding mechanism is prevalent in the adsorption process with carbon-based adsorbents. It is an inter-molecular or intra-molecular interaction between hydrogen atoms and oxygen, fluorine, nitrogen and other atoms (Qiu et al., 2022). In CIP adsorption, hydrogen bonding takes place between the –OH group of the adsorbent (hydrogen bonding acceptor) and the $F^-$ group of CIP (hydrogen bonding donor) (Yang et al., 2022). Similarly, hydrogen bonding occurs between ACM (N–H and O–H groups) and carbonyl groups of the adsorbent (Grimm et al., 2024). The availability of oxygen-containing functional groups in the biochar promotes the adsorption of organic compounds through hydrogen bonding (Qiu et al., 2022).

### d) Pore filling

The pore-filling effect is one of the adsorption mechanisms between biochar and pollutants (Cheng et al., 2021). The pore-filling mechanism of ACM adsorption onto commercial activated carbon occurs primarily at high adsorbate concentrations (> 300 mg/L) (H. Nguyen et al., 2020). ACM molecules diffuse through the solution and enter the pores of the CAC. Once get inside the pores, the molecules are adsorbed onto the internal surface of the pores due to hydrogen bonding and π-π interaction. Therefore, pore-filling mechanism contributes to the efficient adsorption of ACM (Grimm et al., 2024). Moreover, the pore-filling mechanism depends on the molecular size of the adsorbed molecules and the pore size of the biochar (Cheng et al., 2021).

### e) Complexation reaction

Complexation reaction is classified as outer and inner layer complexation. It involves the formation of complexes with specific metal-ligand interactions (Nie et al., 2021). Metal and metal oxide modification of adsorbents such as biochar promotes the adsorption of antibiotics through complexation (Rajapaksha et al., 2019). This process occurs between oxygen-containing functional groups on adsorbents (biochar or activated carbon) and metal ions (Nie et al., 2021) or vice versa. The complexation between Fe-O species on biochar and CIP zwitterions (ketone or carboxylate functional groups) is an important adsorption mechanism in the adsorption of CIP from water (Li et al., 2021).

### f) Lewis-acid base reaction

Lewis acid-base reactions occur between amino groups of the sorbates (donor of pair of electrons: Lewis base) and oxygen-containing functional groups of the carbonaceous adsorbents (acceptor of pair of electrons: Lewis acid) (Kah et al., 2017). Lewis acid-base reactions are also possible between iron species on the adsorbent as Lewis acid and nitrogen/oxygen sites in ACM as Lewis base (Yılmaz et al., 2021). Moreover, Lewis acid-base interactions are possible between phenols (sorbate) and the amino moieties of the biochar (Kah et al., 2017). It was also reported that the Lewis-acid base interactions between the sulfonyl group of the sorbent and –NH-/–$NH_2$ of sulfamethoxazole (Ma et al., 2024). Therefore, Lewis-acid base reactions are essential adsorption mechanisms during the adsorption of pharmaceuticals from water.

## 2.3. Advanced oxidation processes (AOPs) for pharmaceuticals removal

In a broad sense, advanced oxidation processes (AOPs) are chemical treatment methods designed to remove organic substances in water and wastewater by oxidation through reactions with hydroxyl radical (•OH). AOPs generally overcome the limitations of other treatment processes, although they may not result in the complete mineralization of the organic pollutants at short oxidation time. Moreover, AOPs are regarded as a highly competitive technology for removing bio-recalcitrant, persistent and chemically stable organic contaminants from water and the inactivation of pathogenic microorganisms not treatable by conventional techniques (Garrido-cardenas & Agüera, 2020; Nyankson & Kumar, 2019). AOPs involve the in-situ generation of non-selective and highly reactive oxygen species (ROS) such as hydroxyl radicals (•OH), $H_2O_2$, $O_3$ and superoxide anion radicals ($O^{\bullet}_2^-$) for mineralization of organic compounds to $CO_2$, $H_2O$ and inorganic ions or acids (Kanakaraju et al., 2018; Kwon et al., 2018; Yin & Shang, 2020). The AOPs can be operated at ambient conditions of temperature and pressure and are considered promising for the remediation of groundwater, surface water, and wastewater containing non-biodegradable organic pollutants such as pharmaceuticals, pesticides, and aromatics (Kaur et al., 2019).

AOPs can be photochemical and non-photochemical oxidation processes. Photochemical processes include UV oxidation (Kwon et al., 2019), UV/ $H_2O_2$, UV/$O_3$, UV/$H_2O_2$/$O_3$, UV/Ultrasound, photo-Fenton, photo-catalysis, sono-photo-catalysis, vacuum UV, and microwave. Whereas, the non-photochemical processes include ozonation, ultrasound (US), US/$H_2O_2$, US/$O_3$, US/Fenton, electro-chemical oxidation, supercritical water oxidation, ionization radiation, photo-catalysis, sonolysis, electron-beam irradiation, wet-air oxidation (Kanakaraju et al., 2018; Oluwole et al., 2020). The efficiency of AOPs in removing pharmaceuticals from water depends on the type of AOPs employed, operating conditions, and the nature of pharmaceuticals in the water. However, these processes require higher operational costs mainly due to increased energy demands or consumption of chemicals. They can oxidize pharmaceuticals, which could lead to their removal or the formation of intermediates that are more amendable to biodegradation, depending on the type of advanced oxidation process

employed (Sipma et al., 2010). Some of the AOPs commonly used in removing pharmaceuticals such as ACM, CIP, AMX and ATN from water and wastewater are explained below.

### 2.3.1. Electrochemical oxidation

Electrochemical oxidation (EO) is one of the AOPs widely employed in remediating pharmaceutical contamination from water due to the generation of $^{\bullet}OH$ radicals, powerful and non-selective oxidizing agents (Ortiz et al., 2024). Nonetheless, the literature presents studies in which oxidation of the pharmaceutical compounds using EO can lead to unintentional formation of intermediate by-products, resulting from the incomplete mineralization of the parent compounds (Ortiz et al., 2024). In the EO process, anode materials, including iridium dioxide ($IrO_2$), iron, conducting polymers, and boron-doped diamond (BDD) electrodes, degrade pharmaceuticals during water treatment. The main benefits of adopting EO include avoiding redox chemicals, close control of the desired reactions and onsite treatment (Nuguse et al., 2023). Two main mechanisms are involved during the EO process: (i) direct oxidation at the anodic electrode surface through an anodic electron transfer reaction and (ii) indirect oxidation through a mediator (electro-generated oxidants) (Yoon et al., 2015). Both of these oxidation mechanisms may co-exist during the EO treatment of the aqueous solutions (Gilpavas et al., 2020). Direct oxidation involves electron transfer to the anode and degradation of contaminants adsorbed on the anode surface. It is theoretically possible at more negative potentials than those needed for water splitting and oxygen evolution. However, this process result in electrode fouling, thereby declining the electrode efficiency (Feng et al., 2016). The indirect EO occurs via $\bullet OH$ radical and other electro-generated oxidants. In the EO process, chlorine is formed by the oxidation of chloride at the anode. Moreover, the presence of chloride in the wastewater is crucial for the EO process, as it generates active chlorine, enhancing the degradation efficiency. Other electro-generated oxidants involved during the EO process include $H_2O_2$, $O_3$, $^{\bullet}Cl$, $^{\bullet}SO_4^-$, which vary according to the electrolyte composition and electrode material (Onur, 2023). During the EO process, the pharmaceutical contaminant (R) present in the water can be oxidized via various ways when the applied current corresponds to the anode (M) potential within the range of oxygen evolution (Giraldo et al., 2015; Panizza & Martinez-huitle, 2013; Weng & Yu, 2019). These include:

(i) Pharmaceuticals reaction with physi-sorbed •OH radicals (electro-generated at the metal oxide anode from the water discharge) (Eqs. 2.4-2.5). This process is heterogeneous and the anode surface absorbs the electro-generated •OH radicals.

$$M + H_2O \rightarrow M(^{\bullet}OH)_{ads} + H^+ + e^- \quad (2.4)$$

$$M(^{\bullet}OH)_{ads} + R \rightarrow M + CO_2 + H_2O \quad (2.5)$$

The physi-sorbed •OH radicals induce non-selective oxidation of pharmaceuticals, leading to their complete combustion.

(ii) Pharmaceuticals reaction with chemi-sorbed active oxygen, which is electro-generated by the transition of oxygen from the adsorbed •OH radicals to the lattice of the oxide anode, resulting in the formation of higher oxide (Eqs. (2.6) and (2.7)).

$$M(^{\bullet}OH)_{ads} \rightarrow MO + H^+ + e^- \quad (2.6)$$

$$MO + R \rightarrow M + RO \quad (2.7)$$

The higher oxide usually gives only selective and partial oxidation with the formation of organic intermediates (RO).

(iii) For EO process employing NaCl as an electrolyte or for wastewater containing chloride ions, indirect oxidation of pharmaceuticals with active chlorine species (gaseous chlorine, hypochlorous acid or hypochlorite) electro-generated from the oxidation of chloride ions is presented in (Eqs. (2.8), (2.9) and (2.10)):

$$2Cl^- \rightarrow Cl_2 + 2e^- \quad (2.8)$$

$$Cl_2 + H_2O \rightarrow HOCl^- + H^+ + Cl^- \quad (2.9)$$

$$HOCl + R \rightarrow CO_2 + H_2O + H^+ + Cl^- \quad (2.10)$$

Higher electro-active chlorine oxidizing species can be generated at higher NaCl concentrations during the EO process (Onur, 2023). The reactions that take place during EO at the anode, cathode and within the bulk solution is provided in Eqs. (2.11-2.21).

Anodic reactions:

$$2Cl^- \rightarrow Cl_2 + 2e^- \quad (2.11)$$

$$6HOCl + 3H_2O \rightarrow 2ClO_3^- + 4Cl^- + 12H^+ + 1.5O_2 + 6e^- \quad (2.12)$$

$$2H_2O \rightarrow O_2 + 4H^+ + 6e^- \quad (2.13)$$

Cathodic reactions:

$$2H_2O + 2e^- \rightarrow 2OH^- + H_2 \quad (2.14)$$

$$OCl^- + 2H_2O + 2e^- \rightarrow Cl^- + 2OH^- + H_2O \quad (2.15)$$

$$6ClO^- + 3H_2O \rightarrow 2ClO_3^- + 4Cl^- + 6H^+ + \frac{3}{2}O_2 + 6e^- \quad (2.16)$$

$$ClO_3^- + H_2O \rightarrow ClO_4^- + 2H + 2e^- \quad (2.17)$$

Solution reactions:

$$Cl_2 + H_2O \rightarrow HOCl + H^+ + Cl^- \quad (2.18)$$

$$HOCl \leftrightarrow H^+ + OCl^- \quad (2.19)$$

Indirect oxidation through •OH in bulk solution

$$2H_2O \rightarrow O_2 + 4H^+ + 4e^- \quad (2.20)$$

$$R + \bullet OH \rightarrow RO + CO_2 + H_2O \quad (2.21)$$

R = pharmaceuticals (ACM/CIP)

**a) Types of electrodes**

The electrode material type is recognised to significantly affect the effectiveness, selectivity, and robustness of the EO system (Ogundele et al., 2023). Therefore, it is crucial to identify electrode types employed in the EO process. There are two widely utilized types of electrodes in the EO process. These are active and inactive anode electrodes. The active electrode involves changes

on the electrode surface that affect the EO process. These include Ti/$IrO_2$, Ti/$RuO_2$, Ti/$RuO_2$–$IrO_2$, Ti/$IrO_2$–$Ta_2O_5$ and Pt. In active anodes, oxygen atoms are covalently bound to the anode surface (Fu et al., 2023), and these types of electrodes exhibit notable electro-catalytic activity. Active electrodes have demonstrated remarkable efficiency in removing organic contaminants and disinfecting wastewater (Jung et al., 2015; Ogundele et al., 2023).

The surface does not change in non-active electrodes and only acts as an electron sink. The non-active electrodes serve as active electron concentration sites but cannot be involved in the anodic oxidation process. These electrodes include boron-doped diamond (BDD), $PbO_2$ and $Ti_4O_7$ and are the most efficient anodes due to their high potential for generating large quantities of •OH and different secondary oxidants. On non-active anodes, the oxygen atoms of •OH are not covalently bound to the surface of the anode but mineralize the contaminants directly (Fu et al., 2023).

### 2.3.2. Ozonation

Ozone is a powerful electrophile oxidant that reacts rapidly and selectively with electron-rich moieties such as alkenes, amines and aromatic rings (Guillossou et al., 2020; Guo et al., 2020). It is a very powerful oxidizing agent (E° = 2.07V) able to degrade a wide range of organic and inorganic compounds. During ozonation, the degradation of organic substances occurs via two main mechanisms: direct oxidation with dissolved ozone or indirect oxidation through hydroxyl radical. In direct ozone oxidation, molecular ozone reacts selectively with electron-rich moieties such as phenols, activated aromatics, non-protonated amines and olefins, with kinetics constants ranging from 1 to $10^7$ $M^{-1}$ $s^{-1}$. In contrast, the generated •OH reacts unselectively with almost all organic molecules (whose reaction constants ($k_{\bullet HO}$) are in the order of $10^9$ – $10^{10}$ $M^{-1}s^{-1}$) in the indirect oxidation reaction (Prada-vásquez et al., 2020). The contribution of each mechanism is strongly dependent on the pH of the solution. In acidic solutions (pH < 3), significant ozone decomposition does not occur, and essentially, only the direct pathway takes place, while at basic pH, the rates of radicals generation increase significantly, and the indirect reaction becomes predominant (Prada-vásquez et al., 2020). Ozonation can generally remove micro-pollutants while inactivating bacteria and viruses at even lower ozone doses, such as 0.5 g $O_3$/g of dissolved organic carbon (DOC)), corresponds to 2.6 mg $O_3$/L. In ozone degradation of

pharmaceuticals, knowledge of the specific ozone dose (g $O_3$/g DOC) and the kinetic constants for ozone and •OH reactions enable the prediction of the efficiency of ozonation reaction during municipal wastewater treatment (Gomes et al., 2017). Ozonation has been widely used in drinking water production and has recently been transferred to advanced wastewater treatment systems (Guillossou et a., 2020).

### 2.3.3. UV/Chlorine process

The UV/chlorine is an effective AOP for the elimination of pharmaceuticals from water using the in-situ generated •OH radicals and reactive chlorine species (RCS) ($Cl^{\bullet}$, $Cl_2^{\bullet-}$, and $ClO^{\bullet}$). This approach benefits from the non- selectivity of •OH radical as well as the selectivity of RCS in reacting with organic pollutants such as pharmaceuticals (Ghanbari et al., 2021). In a particular study (Y. Zhang et al., 2020), electrically driven UV/$Cl_2$ was employed as a beneficial approach for the elimination of pharmaceuticals, including CIP, by combining UV irradiation with in-situ electro-generated $Cl_2$. The electrically driven UV/$Cl_2$ effectively eliminated CIP from the water (Y. Zhang et al., 2020). On the other hand, the UV/chlorine process, when compared with the UV/$H_2O_2$ process, demonstrated significant savings in energy consumption ranging from 3.5% to 98% for the degradation of pharmaceuticals in natural water. However, it is essential to note that there are considerations related to toxicity. The acute toxicity was found to be substantially influenced by the UV/chlorine process, primarily due to the formation of chloro-products. Initially, acute toxicity was significantly increased during the initial reaction time, followed by a subsequent decrease due to reduced chloro-product formation over time. This suggests a dynamic impact on toxicity levels throughout the UV/chlorine degradation (Guo et al., 2020).

### 2.3.4. UV/$H_2O_2$

The UV-based processes that produce radicals include UV/$H_2O_2$, UV/Chlorine, UV photolysis and UV/$TiO_2$. The UV/$H_2O_2$ is a traditional AOP that generates •OH through the UV photolysis of the -O-O- peroxidic bond in $H_2O_2$ (Ahn et al., 2017; Guo et al., 2019). The formation rate of •OH in the UV/$H_2O_2$ process depends on the quantum yield and the absorbance coefficient of $H_2O_2$ at the specific wavelength. In the UV/$H_2O_2$ process, the quantum yield is reported to be 0.5 for the production of •OH at relatively high UV light intensity at 254 nm and low peroxide

concentrations. $H_2O_2$ has a maximum absorbance at 210-230 nm, and its UV absorbance coefficient at 254 nm is 19.6 $M^{-1}$ $cm^{-1}$ (Guo et al., 2020). The amount of •OH in UV/$H_2O_2$ depends on its production and consumption. Increasing the concentration of $H_2O_2$ promotes the generation of •OH during the UV/$H_2O_2$ process. However, this enhancement becomes limited at high concentrations of $H_2O_2$, resulting from the important scavenging effect of $H_2O_2$ on •OH at $2.7\times10^7$ $M^{-1}$ $s^{-1}$ (Guo et al., 2020).

### 2.3.5. Heterogeneous photo-catalysis

The UV/$TiO_2$ is considered one of the widely studied heterogeneous photo-catalytic AOP processes. It is one of the AOPs that integrate low-energy UV light with semi-conductors acting as photo-catalysts. In this treatment technique, pharmaceuticals degradation occur using atmospheric oxygen as an oxidant, resulting in the mineralization of the pharmaceuticals to harmless organic products and low molecular weight acids that are more biodegradable. Pharmaceuticals containing carbon will be oxidized to carbon dioxide while the other elements bonded to the organic compounds get converted to anions such as nitrates, sulphates, or chloride. The $TiO_2$ photo-catalysts absorbs UV radiation holes and electrons, producing •OH (Kaur et al., 2019). The produced •OH is responsible for the degradation of the pharmaceuticals.

## 2.4. Coupled treatment processes for pharmaceuticals removal

The aforementioned water treatment technologies have some sort of limitations in removing pharmaceutical contaminants from water when employed individually. AOPs may lead to the formation of toxic intermediate products, necessitating additional treatment steps or higher oxidation times. Additionally, application of AOPs alone in a large-scale water treatment systems require high energy consumption (Ganiyu et al., 2015). On the other hand, adsorption process is a low-cost water treatment process which provides high removal of single contaminant from simple water matrix. However, its efficiency is limited when removing multiple contaminants from complex water matrices. In contrast, coupled treatment systems offer a considerable advantage by addressing the limitations of the individual processes, and thus remarkable removal efficiencies have been reported using the coupled technologies. Nevertheless, each category of the coupled technology offers unique advantages and challenges,

and the selection of a specific technology depends on the particular water treatment needs and characteristics of the water matrix.

### 2.4.1. Adsorption-based coupled processes

The adsorption process can be coupled with various water treatment techniques, including AOPs and biological processes. Coupling adsorption with AOPs is considered a promising research direction that can solve the problems associated with the stand-alone processes. This process can be operated sequentially (oxidation followed by adsorption or vice versa) or simultaneously (oxidation-adsorption). Adsorption can be integrated with EO, UV/$Cl_2$ and ozonation. In most cases, adsorption comes after oxidation to handle the toxic by-products generated during oxidation since complete mineralization is very challenging, especially when considering complex water matrices. Moreover, during AOPs-based oxidation, several reactions occur other than the •OH-mediated reactions, which contribute to incomplete mineralization when applying AOPs in water treatment. Therefore, coupling adsorption with EO is a beneficial approach in water treatment. In a particular study (Ganesan et al., 2019), adsorption was coupled with EO to effectively eliminate CIP from water. Meanwhile, the EO+adsorption successfully removed sulfate, fluoride ions and toxic by-products generated during the EO process. In the same study, an absolute removal of CIP from water was reported using the EO+adsorption. Also, the conducted toxicity assessment revealed that EO treated water had a significant toxicity which was remarkably reduced after the adsorption process (Ganesan et al., 2019). Therefore, the EO+adsorption has been proven to be effective in eliminating pharmaceuticals and associated toxicity from water. Coupling EO with adsorption can enhance techno-economic feasibility and environmental viability, particularly in industrial-scale pharmaceutical wastewater treatment (Ganthavee & Trzcinski, 2023). The effectiveness of the EO coupled with the adsorption process depends on the individual process parameters such as current density, initial solution pH, oxidation time, initial pollutant concentration, adsorbent dose and adsorption time. Therefore, coupled process optimization is one of the crucial strategies to maximize the contaminant removal efficiency of the coupled process. Adsorption can also be coupled with ozonation process. More specifically, Guillossou et al. (2020) coupled adsorption with ozonation (activated carbon) to remove pharmaceuticals from wastewater. The two processes (ozonation and

adsorption) appeared complementary as organic pharmaceuticals with a low reactivity toward ozone were well absorbed onto the powdered activated carbon and pharmaceuticals refractory to adsorption were well eliminated by ozone oxidation (Guillossou, et al., 2020).

### 2.4.2. Membrane-based coupled technologies

The utilization of membrane filtration technologies, often combined with other treatment mechanisms, such as adsorption or AOPs, was evaluated for their effectiveness in removing pharmaceutical contaminants from water. The membrane-based hybrid process includes EO-membrane separation (Wei et al., 2020), membrane bioreactor (MBR) (Alfonso-Muniozguren et al., 2021), MBR-activated carbon adsorption (García et al., 2021), membrane separation-photo-catalytic process (Papac Zjačić et al., 2022) and membrane filtration-ozonation/chlorination (Acero et al., 2015).

Integrating EO with membrane separation is considered an efficient approach for treating industrial wastewater, as it offers advantages such as achieving standard limits for wastewater discharge for potential reuse and economic benefits. This integrated process is considered the best technology due to its ability to simultaneously separate and degrade organic pollutants with high efficiency and low energy consumption, thanks to enhanced mass transfer and electro-active area, longer service life, and easy regeneration procedure (Wei et al., 2020). Several studies have employed MBR treatment to remove micro-pollutants effectively. It is particularly effective for moderately removable compounds through conventional activated sludge (CAS) treatments, achieving additional 20-50% reductions in micro-pollutant concentrations. However, for compounds already highly degraded by CAS processes or recalcitrant compounds, MBRs may not yield significant improvements in removal efficiency (Grandclément et al., 2017). Including powdered activated carbon in a MBR system has been shown to enhance the removal of pharmaceutical contaminants, with improvements ranging from 10% to 80%. For biodegradable pharmaceuticals, the removal efficiency can reach as high as 80-100% when powdered activated carbon is used in the MBR reactor (García et al., 2021). It is reported that using a combination of NF and granular activated carbon resulted in 98% cyclophosphamide removal, even with a short empty bed contact time of 3 minutes (Gouveia et al., 2022).

### 2.4.3. Biological-based coupled processes

The biological process is known to be effective in dealing with conventional contaminants. However, sufficient removal cannot be achieved using only biological processes to remove pharmaceutical contaminants. The rationale is due to the less biodegradability and persistence of pharmaceutical contaminants. However, better results can be achieved by integrating biological processes with other processes, such as membrane filtration, adsorption and AOPs. In a particular study, a biological process (anaerobic bacteria) was coupled with EO for removing the 17α-ethynylestradiol (EE2) from wastewater. The biodegradation of EE2 with individual microorganisms was found to have poor efficiency, ranging from 10.3% to 45.8% in 120 hours. However, after combining with EO, it can reach up to 81.9% after 90 minutes (He et al., 2017). This shows the benefit of coupling biological processes with the EO process. Moreover, the biological process can be coupled with ultrasound to remove pharmaceutical contaminants from water. The ultrasound can be used as pre-treatment to a biological system to the biological process (Alfonso-Muniozguren et al., 2021).

### 2.4.4. Advanced oxidation-based coupled processes

The AOPs-based coupled treatment systems include AOPs-AOPs, AOPs-adsorption, AOPs-biodegradation, AOPs-membrane bioreactor and AOPs-membrane separation. Due to the diverse nature of the pharmaceutical contaminants, it is difficult to achieve complete removal of multiple pharmaceuticals from complex water matrices using a single treatment technology (Hong et al., 2020). Moreover, the complex nature of the environmental water matrix makes the single treatment technologies unreliable for effective removal of multiple pharmaceutical contaminants from wastewater. Generally, AOPs treatment of organic compounds results in the formation of biodegradable and simpler compounds. Several studies have highlighted the formation of more toxic by-products following the AOPs process, necessitating either process optimization or an additional treatment step to act as a barrier (Ganesan et al., 2019; Ghazal et al., 2022; Hong et al., 2020; Poelmans et al., 2020; Roy et al., 2023;Tang et al., 2019). Therefore, AOPs are mostly employed as pre-treatment steps to adsorption and biodegradation. In particular, AOPs followed by the adsorption process have advantages such as high pharmaceuticals and toxicity removal

when compared to the individual treatment processes. In general, reported AOPs-based coupled processes showed enhanced mineralization (Aboudalle et al., 2021), degradation (Aboudalle et al., 2021) and lower toxicity (Jaén-gil et al., 2021) compared to the single treatment processes. However, the coupled treatment processes and their optimization have not been fully studied for removing pharmaceutical contaminants from water. It should be noted that there is an apparent research demand on the mechanism, process design and application of hybrid technologies for removing pharmaceutical contaminants from water. In this regard, research works need to focus on developing efficient coupled technologies as the single technologies cannot sufficiently remove pharmaceutical contaminants from environmental water matrices. In addition, the operating conditions of the coupled processes need to be optimized to achieve better results.

## 2.5. Research design and statistical modeling

Various statistical methods such as Taguchi, heuristic search technique, iterative mathematical search technique, genetic algorithm, tabu search, simulated annealing artificial neural network modeling, factorial design and response surface methodology (RSM) have been used for the analysis of data. Factorial design, RSM and Taguchi methods are now widely employed in place of the one-variable-at-a-time experimental approach, which is time-consuming and costly (Nesßeli et al., 2011). RSM was introduced in 1951 by Box and Wilson, who suggested using a second-degree polynomial model. It comprises a set of mathematical and statistical techniques employed for modelling and analyzing problems where a response of interest is influenced by numerous variables to optimize this response. It is an efficient statistical method for modeling and optimizing various variables to predict the best performance conditions with a minimum number of experiments.

RSM offers several advantages compared to classical experimental or optimization methods that employ the one-variable-at-a-time technique. Firstly, it provides a considerable amount of information from a small number of experiments. Indeed, classical methods are time-consuming, and a large number of experiments are needed to explain the behavior of a system. Secondly, it is possible to observe the interaction effect of the independent parameters on the response. The interaction effect of the process parameters, such as synergism, antagonism and addition, would be more critical. The model equation easily clarifies these effects for binary combinations of the

independent parameters. In addition, the empirical model that related the response to the independent variables is used to obtain information about the process. Therefore, we can say that RSM is a useful tool for optimizing chemical and biochemical processes (Bas, 2007). RSM has been successfully used for material and process optimization in wastewater treatment processes (Kamyab et al., 2022; Sharma et al., 2023; Yang et al., 2022).

# CHAPTER THREE

## 3. MATERIALS AND METHODS

This chapter describes all the methods used in this study to prepare solutions, samples, experimental setups, experimental analysis, parameter optimization and data analysis. In this study, treatment technologies such as adsorption and EO processes were employed individually and in combination (EO+adsorption). The main aim was to effectively remove target pharmaceutical contaminants (ACM, CIP, AMX and ATN) from water in single, binary, and multiple contaminant systems. The EO followed by the adsorption process was employed as a coupled process for the removal of pharmaceutical contaminants from water.

### 3.1. The experimental workflow design of the dissertation

The framework of the experimental work conducted to accomplish the objectives of the dissertation is presented in Figure 3.1. This research work consists of four major tasks: adsorbent synthesis, EO process, adsorption process, and the EO+adsorption for the removal of pharmaceutical contaminants from single, binary, and multi-contaminant systems employing diverse water matrices. The adsorption process was conducted in batch and fixed-bed column operation modes considering the single and binary pharmaceutical mixtures. The influence of the water matrix on the adsorption process was examined for single and binary component mixtures of pharmaceutical contaminants in batch adsorption studies.

Bamboo sawdust was chemically treated using ferric chloride ($FeCl_3.6H_2O$) and potassium hydroxide (KOH) to produce a chemically activated carbon. The chemical activation process was optimized to obtain a high-capacity activated carbon. Accordingly, various activated carbon adsorbents were synthesized via different chemical modification approaches. Among the activated carbons synthesized via different chemical modifications techniques (single and dual chemical modifications), the best-performing adsorbent was selected and used throughout the adsorption studies. The as-synthesized adsorbent was characterized using Fourier Transform Infrared Spectroscopy (FTIR), Scanning Electron Microscopy with Energy-Dispersive Spectroscopy (SEM/EDS), Brunauer-Emmett-Teller (BET) surface area, X-ray Diffraction

(XRD), Raman Spectroscopy and pH of the point of zero charge ($pH_{pzc}$) characterization techniques. The process parameters of EO, adsorption, and the EO+adsorption were optimized. Moreover, important aspects of the adsorption process, such as isotherm, and kinetics were investigated. The key aspects of the EO process, including reaction kinetics, cyclic voltammetry, the effect of the electrolyte concentration and radical scavenging tests, were studied in addition to the EO process parameter optimization. Central composite design (CCD) of the response surface methodology (RSM) was employed to optimize the adsorption, EO and the EO+adsorption parameters. The residual concentrations of the pharmaceutical contaminants were quantified using a UV-Vis spectrophotometer, and High Performance Liquid Chromatography (HPLC). Moreover, the total organic carbon (TOC) and chemical oxidation demand (COD) of the aqueous solutions were analysed using TOC analyzer and spectrophotometer, respectively. The conceptual framework of the dissertation is provided in Figure 3.1.

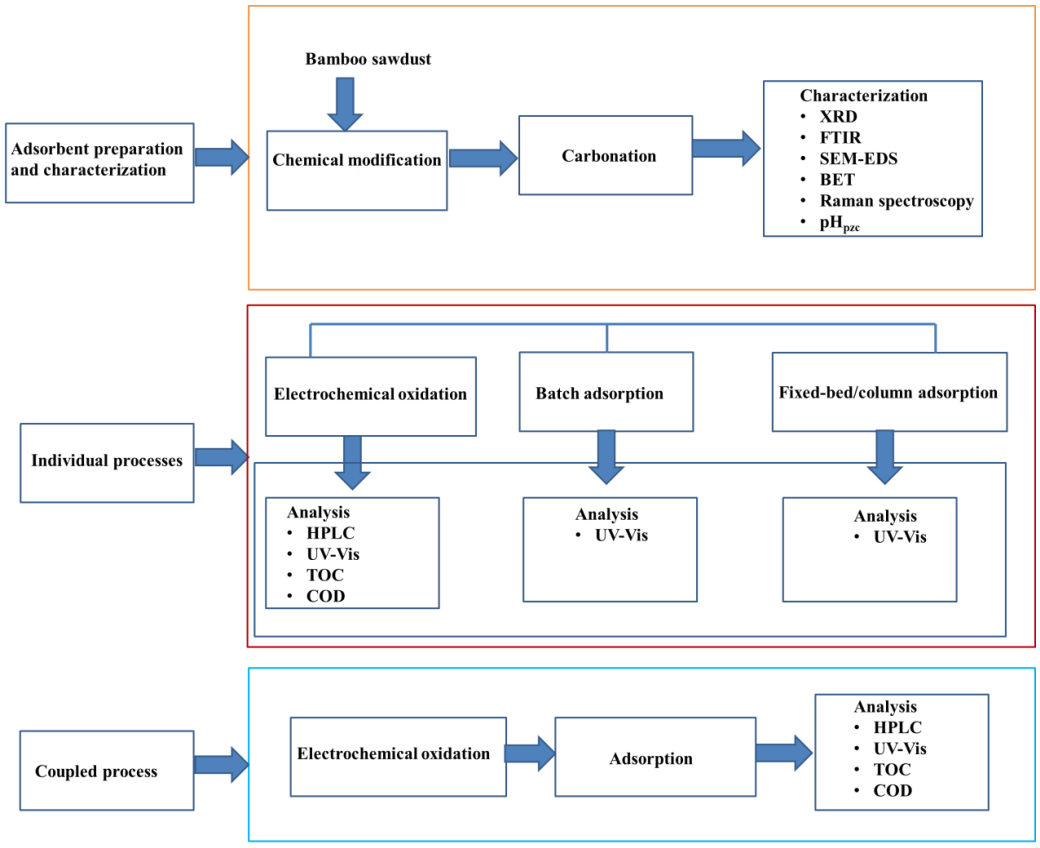


Figure 3.1. Conceptual framework of the dissertation.

## 3.2. Materials/equipment and chemicals used

### 3.2.1. Materials used

The materials used during this research work include bamboo sawdust, filter paper (Whatman:0.45μm), glass and plastic bottles, sample bags (plastic), volumetric flasks, beakers, burettes, test tubes, micro-pipettes, syringe filters, magnetic rods, $IrO_2$/Ti mesh electrode, plastic cups, measuring cylinder, aluminum foil, electronic pipettes, quartz cuvettes, crucibles, wash bottles, towels, glass thermometer, lab-scale glass column, etc.

### 3.2.2. Equipment/instruments used

The laboratory equipment or instruments used in this study include mesh screen (for particle size screening), distiller (to produce distilled water), TOC analyser (to measure TOC), vacuum filter (to separate adsorbent from solution), centrifuge (to separate liquid and solid), carbolite carbonizer (to carbonize bamboo sawdust), analytical balance (to weigh samples), UV-Vis spectrophotometer (to measure absorbance), water bath shaker (to conduct adsorption), lab scale sample grinder (to reduce size of samples), HPLC (to quantify pharmaceuticals), FTIR analyser (to identify functional group), SEM analysis instrument (to evaluate morphology of samples), XRD analyser (to identify crystalline phases), BET analyser (to measure surface area), Raman Spectroscopy (to identify degree of graphitization), vortex mixer (for mixing), spectrophotometer (Hatch) (to measure BOD), pH meter (to measure pH of the samples), auto-lab (to conduct cyclic voltammetry analysis), magnetic stirrer (for mixing), DC power supply (to conduct EO experiment), oven (to dry samples), peristaltic pumps (to feed sample to the adsorption column) and glassware dryer (to dry glassware) etc.

### 3.2.3. Chemicals and reagents

Model pharmaceutical contaminants such as acetaminophen ($C_8H_9NO_2$), ciprofloxacin ($C_{17}H_{18}FN_3O_3$), atenolol ($C_{14}H_{22}N_2O_3$) and amoxicillin ($C_{16}H_{19}N_3O_5S$) were obtained from Cadila Pharmaceuticals (Ethiopia), EPHARM (Ethiopia), and Sigma-Aldrich Suomi Oy (Finland). The stock solutions of these pharmaceuticals were prepared using acetaminophen purity grade (≥ 99%) and ciprofloxacin hydrochloride ($C_{17}H_{19}ClFN_3O_3$) (purity grade ≥ 99.50%),

amoxicillin (purity grade ≥ 99%)), atenolol (purity grade ≥ 99%). Analytical grade chemicals such as $FeCl_3.6H_2O$, KOH, HCl, NaOH, and NaCl were purchased from Rankem chemical supplier (Ethiopia) and used in the chemical modification of the bamboo sawdust and other experimental works. Other chemicals used in this study include methanol (HPLC grade), phosphate buffer and formic acid (HPLC grade), HCl, $HNO_3$, $H_3PO_4$, NaOH, $H_2SO_4$, ultra-pure water, potassium dihydrogen phosphate. These analytical-grade chemicals were used without further purification.

### 3.3. Synthesis of the adsorbent

Bamboo sawdust was collected from local areas, processing bamboo for various applications. The collected bamboo sawdust was washed and dried at 120 ºC to synthesize adsorbents using the single and dual chemical activation techniques. The dried bamboo sawdust was then ground to a powder with a particle size of less than 850 μm. The bamboo sawdust powder was chemically activated using a single chemical ($FeCl_3.6H_2O$ or KOH) and dual chemical activation ($FeCl_3.6H_2O$+KOH), and the ratio of the activating agents to the bamboo sawdust was optimized as presented in Table 3.1. The chemical modification was carried out at 80 ºC with continuous stirring at 600 rpm for 120 min. The impregnated bamboo sawdust mixture was then dried at 60 ºC in a vacuum oven for 24 hrs. Next, the dried and chemically treated bamboo sawdust was ground to a particle size of less than 450 μm before being carbonized at 700 ºC for 60 min at a heating ramp rate of 10 ºC/min in an oxygen-limited carbolite furnace. The chemically activated and carbonized bamboo sawdust was washed with ultrapure water until the filtrate pH became 7 and dried at 120 ºC overnight to get a chemically activated carbon (CAC). The CAC was then ground to a particle size of less than 150 μm and stored in air-tight polyethylene bags for adsorption studies. Furthermore, pristine bamboo sawdust (BS), bamboo sawdust carbon (BSC), bamboo sawdust activated solely with ferric chloride (AC-Fe), and bamboo sawdust activated solely with potassium hydroxide (AC-KOH) were also prepared using a similar synthesis procedure to evaluate the effect of different chemical modifications.

The dual chemical activation was carried out by varying iron ratios (AC-0.5Fe and AC-1.5Fe) and KOH concentrations (AC-0.5KOH and AC-1.5KOH). The pristine bamboo sawdust and adsorbents synthesized through carbonation with varying chemical activating agents (ratios and

concentrations) were employed in pharmaceutical removal from water to assess the performance of the carbonation and activation processes. All chemically activated adsorbents derived from bamboo sawdust were synthesized using a procedure outlined in Figure 3.2, with variations made in the Fe ratio and KOH concentration.

Table 3.1. The optimization of adsorbent synthesis and chemical activation processes.

| **Adsorbents without chemical activation** | | |
|---|---|---|
| As-synthesized adsorbents | Bamboo sawdust to KOH ratio (W/V) | Bamboo sawdust to $FeCl_3.6H_2O$ ratio (W/W) |
| BS | 0 | 0 |
| BSC | 0 | 0 |
| **Adsorbents with single chemical activation** | | |
| As-synthesized adsorbents | Bamboo sawdust to $FeCl_3.6H_2O$ ratio (W/W) | Bamboo sawdust to KOH (1M) ratio (W/V) |
| AC-KOH | 0 | 1:5 |
| AC-Fe | 5:1 | 0 |
| **Adsorbents with dual chemical activation (changing Fe ratio)** | | |
| As-synthesized adsorbents | Bamboo sawdust to $FeCl_3.6H_2O$ ratio (W/W) | Bamboo sawdust to KOH (1M) ratio (W/V) |
| CAC | 5:1 | 1:5 |
| CAC-0.5Fe | 5:0.5 | 1:5 |
| CAC-1.5Fe | 5:1.5 | 1:5 |
| **Adsorbents with dual chemical activation (changing KOH concentration)** | | |
| As-synthesized adsorbents | Bamboo sawdust to $FeCl_3.6H_2O$ ratio (W/W) | Bamboo sawdust to KOH ratio (W/V) |
| CAC-0.5KOH | 5:1 | 1:5 w/v (at 0.5 M KOH) |
| CAC-1.5KOH | 5:1 | 1:5 w/v (at 2.5 M KOH) |

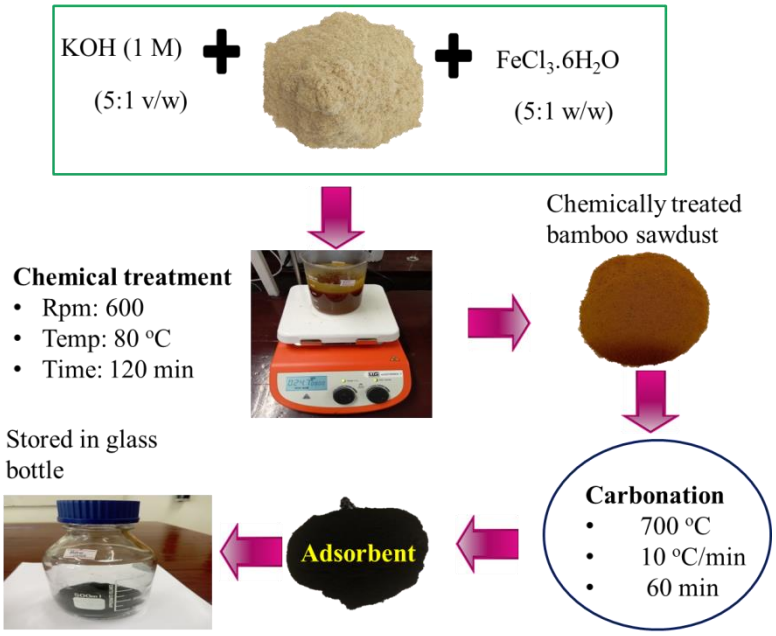


Figure 3.2. Synthesis procedure for the bamboo sawdust derived adsorbents.

## 3.4. Water matrices

In this study, various water matrices were used to investigate the performance of the EO, adsorption and EO+adsorption. The main model pharmaceutical compounds (ACM and CIP) were spiked into ultrapure water, tap water and secondary treatment plant effluent (real wastewater) to examine the effect of the water matrix on the removal of pharmaceuticals from diverse water matrices using single and coupled processes. The tested real wastewater samples were taken from the Akaki Kality secondary wastewater treatment plant effluent (Addis Ababa, Ethiopia) and employed in single and simultaneous ACM and CIP adsorption process. Also, real wastewater sample was taken from Mikkeli wastewater treatment plant effluent (Mikkeli, Finland) and used in single EO, coupled process and comparative evaluation of single and coupled processes. The collected real wastewater samples were kept at 4°C before analysis.

## 3.5. Adsorbent characterization

The as-synthesized adsorbents were characterized using an FTIR (Spectrum 65 PerkinElmer), XRD (Rigaku MiniFlex 600 Benchtop), BET surface area analyzer (micrometrics TriStar II Plus, USA), $pH_{pzc}$, SEM with energy-dispersive spectroscopy (SEM/EDS: JEOL JSM-7900F) and Raman imaging microscope (thermo scientific: DXR3xi). The FTIR spectra analyses of the adsorbents were conducted for a wavenumber range of 500-4000 $cm^{-1}$. The X-ray diffraction (XRD) studies were conducted for $2\theta^o$ from $0^o$ to $40^o$ to understand the crystal structure of the adsorbents. Moreover, the BET surface areas of the as-synthesized adsorbents were analyzed using a multi-point BET surface area analyzer equipped with a sample degassing system (micrometrics, VacPrep 061, USA) employing nitrogen adsorption and desorption. The SEM/EDS analysis was conducted using a voltage of 20 kV, capturing images at magnifications ranging from 500 to 100,000. Also, the Raman spectroscopy analysis was conducted to determine the degree of graphitization of the synthesized adsorbents.

### 3.5.1. The pH of point of zero charge determination ($pH_{pzc}$)

The pH of the point zero charge of the adsorbent (CAC) was determined by a pH titration procedure using the method used by Gallouze and his co-workers (Gallouze et al., 2020). In brief, 50 mL of 0.01M NaCl solution was taken into several Erlenmeyer flasks. The initial pH ($pH_{initial}$) values of the NaCl solutions in each flask were adjusted to the desired values between 2 and 12 by adding 0.1 M HCl or 0.1 M NaOH. Aliquots of 50 mL of these solutions were placed in an Erlenmeyer flask and mixed with 0.1 g of the CAC sample. Next, these samples were shaken at 200 rpm for 24 hrs. Afterwards, the final pH values of these solutions were recorded. The initial pH values were plotted against the change in pH values between the initial and final values. The initial pH value at which y-axis = 0 denotes the $pH_{pzc}$ value of the adsorbent.

### 3.5.2. Fourier Transform Infra-red Spectroscopy (FTIR)

The functional groups of the adsorbent samples were determined using the FTIR characterization technique (Mary et al., 2016). The FTIR spectra analysis was conducted using the conventional KBr technique. In this method, adsorbent samples were mixed with a dry KBr pellet at a ratio of 1:100. This method is used to qualitatively assess the formation of functional groups on the

surface of the material. The spectra were collected at a resolution of 4 $cm^{-1}$ and a scan speed of 1.2 kHz over a wavenumber range of 4000-500 $cm^{-1}$ on a PerkinElmer Spectrum.

### 3.5.3. Scanning Electron Microscopy/Energy-Dispersive Spectroscopy (SEM/EDS)

Morphological structures and elemental compositions of adsorbent samples were traced using SEM (SEM: JEOL JSM-7900F) with energy dispersive spectroscopy (EDS) detector (Thermo Scientific Ultra-Dry). In principle, an electron microscope produces images of a sample by scanning the surface with a focused beam of electrons. The electrons interact with atoms in the sample, producing various signals that contain information about the surface topography and composition of the sample. The electron beam is scanned in a raster scan pattern, and the position of the beam is combined with the intensity of the detected signal to produce an image. Specimens were observed in a high vacuum SEM analyser, in low vacuum or wet conditions in a variable pressure or environmental SEM and at a wide range of cryogenic or elevated temperatures.

### 3.5.4. Surface area analysis

The BET specific surface area of the as-synthesized adsorbent samples were measured using a multi-point BET analysis employing nitrogen adsorption and desorption with a micrometrics (TriStar II Plus, USA) surface area analyzer. The surface area analyzer is equipped with a gas degassing system (micrometrics, VacPrep 061, USA). Initially, the samples were degassed overnight at 120 °C. The measured data was processed by the BET isotherm in the range of relative pressure ($p/p^o$ = 0.05–0.35) to obtain the value of specific surface area (Sg) (Lengauer et al., 2018). The specific surface areas of the adsorbent samples were determined by the physical adsorption of a gas on the surface of the solid and by calculating the amount of adsorbate gas corresponding to a monomolecular layer on the surface.

### 3.5.5. Raman spectroscopy

Raman spectroscopy was used to elucidate the vibrational modes of adsorbent molecules, thereby enabling a detailed analysis of the degree of graphitization of the synthesized adsorbent. A Raman imaging microscope was employed to collect Raman images for the adsorbent samples

(chemically modified and unmodified). Based on the collected Raman images, the effect of chemical activation on the degree of graphitization of the adsorbent samples was evaluated.

### 3.6. Batch adsorption studies (single component)

Preliminary batch adsorption experiments were undertaken to investigate the adsorptive potential of all the bamboo sawdust-derived adsorbents listed in Table 3.1. Based on the preliminary adsorbents screening test, CAC exhibited superior ACM and CIP removal performance and was used throughout the adsorption studies. The successfully synthesized CAC adsorbent was first tested on single component removal of CIP from water in batch adsorption experiment, and the process was optimized with the CCD framework of RSM. Demonstrating a remarkable adsorption capacity for CIP removal, CAC was also applied in ACM removal from water in a batch study. Batch adsorption experiments were conducted in a water bath shaker under a controlled temperature (at 25 ºC) and shaking speed (200 rpm). The CIP stock solution was prepared by dissolving 1000 mg of CIP in one litre of ultra-pure water, and solutions of desired CIP concentrations were prepared by spiking the required amount of the CIP stock solution. The single component CIP removal equilibrium time was determined at pH of 7.0, CIP initial concentration of 20 mg/L, and adsorbent dosage of 0.5 g/L considering contact time of 10, 30, 50, 70, 90, 110, and 130 min. The single component CIP removal process parameters such as initial concentration (5–50 mg/L), pH (2-12), contact time (5–60 min), and adsorbents dose (0.25–1.25 g/L) were optimized. These parameter ranges were selected based on preliminary adsorption experiments (including equilibrium studies, determination of the pH of the point of zero charge, and preliminary tests), while also taking into account the commonly reported operational conditions for CIP removal in the literature.

The single component ACM removal process parameters were optimized using a one-factor-at-a-time approach. This approach was followed as the ACM removal mechanism with the CAC adsorbent is not well understood, and thus, this approach provides a full understating of the trends of each factor on the ACM removal from water. The pH of the ACM solution was adjusted using 0.1M HCl and 0.1M NaOH. All adsorption studies were conducted in 100 ml conical flasks using a shaker water bath at 200 rpm and 25 ºC. Before residual pharmaceuticals (ACM and CIP) analysis, the adsorption solution was centrifuged at 4000 rpm for 10 minutes

and filtered through a 0.45μm syringe filter. Adsorption experiments of kinetics, and isotherms were carried out in triplicate, and the mean values were considered. Moreover, the UV-Vis spectrophotometer (Cary Series UV-Vis-NIR Spectrophotometer G9825A, Agilent Technologies) was used to measure the concentrations of ACM and CIP in aqueous solutions, with measurements taken at 250 nm and 273 nm, respectively. These wavelength ranges were obtained by conducting a wavelength scan (200-800 nm) for ACM and CIP. The pharmaceutical residues (ACM and CIP) were evaluated at their respective wavelengths. All single pollutant sorption experiments were conducted in triplicate, and mean values were used to plot the graphs. The adsorption capacity and percentage removal were calculated employing Eq. (3.1) and Eq. (3.2), respectively (Falyouna et al., 2022).

$$q_e = \frac{C_o - C_e}{m} \times V \tag{3.1}$$

$$R\ (\%) = \frac{C_o - C_e}{C_i} \times 100 \tag{3.2}$$

Where $q_e$ (mg/g), $C_o$ (mg/L), $C_e$ (mg/L), m (g), V (L) and R (%) denote equilibrium adsorption capacity, initial pharmaceutical concentration, equilibrium pharmaceutical concentration, the mass of adsorbent, volume of the solution and removal (%) of pharmaceuticals from water, respectively.

### 3.6.1. Modeling of adsorption kinetics

The adsorption kinetic study is very useful in evaluating the time profile of the contaminant removal from the aqueous solution, which is valuable in designing and operating the adsorption process for practical applications. Some well-known kinetic models were applied to the experimental data to evaluate the single and binary sorption rate and mechanism of ACM and CIP adsorption. Data were fitted to both linear (**case I**: single pollutant removal using Origin 2022 software) and non-linear forms (**case II**: simultaneous removal (binary component removal) using MATLAB R2023a software*)* of these models, namely, pseudo-first-order (PFO; Eq. (3.3); (Lagergren, 1898)), pseudo-second-order (PSO; Eq. (3.4); (Ho & McKay, 1999)), Avrami kinetic model (AV) (Avrami, 1939); Eq. (3.5), Elovich model (Elovich et al., 1962) (Eq. 3.6) and intra–particle kinetic models (Weber and Morris, 1963) (Eq. 3.7) as provided in Table

3.2. The adsorption kinetic studies were conducted under the optimal conditions of adsorption process. The kinetic model equations employed in this study are presented in Table 3.2.

Table 3.2. Adsorption kinetic models used in this study (linear and non-linear forms).

| Kinetic models | Model equations | | Eq. no. |
|---|---|---|---|
| | Non-linear form | Linear form | |
| Pseudo-first-order model (PFO) (Lagergren, 1898) | $q_t = q_e(1 - e^{-k_1 t})$ | $\ln(q_e - q_t) = lnq_e - k_1 t$ | (3.3) |
| Pseudo-second-order model (PSO) (Ho & McKay, 1999) | $q_t = \frac{k_2 q_e^2 t}{1 + k_2 q_e t}$ | $\frac{1}{q_t} = \frac{1}{k_2^2 q_e^2} + \frac{t}{q_e}$ | (3.4) |
| Avrami (Avrami, 1939) | $q_t = q_e(1 - e^{(-(k_{Av}t)^{n_{AV}})})$ | - | (3.5) |
| Elovich (Elovich et al., 1962) | - | $q_t = \frac{1}{\beta}\ln(\alpha\beta) + \frac{1}{\beta} lnt$ | (3.6) |
| Intra-particle (Weber and Morris, 1963) | - | $q_t = K_{id} t^{1/2} + K_o$ | (3.7) |

where, $q_e$(mg/g) and $q_t$ (mg/g) are the adsorption capacity at equilibrium and at time t (min), respectively, $k_1$ (1/min) is the rate constant of PFO, $k_2$ (g/ mg.min) is the rate constant of PSO, and $K_{id}$ (mg/g $min^{0.5}$) is the rate constant of the intra-particle diffusion model. In the Avrami model, $k_{Av}$ is the constant of AV (mg/g.min), and $n_{AV}$ is a fractional adsorption order related to the adsorption mechanism. In the Elovich model, α (mg/g. min) indicates the initial adsorption rate, β (g/mg) represents the activation energy rate change with surface coverage, and $K_o$ represents the thickness of the boundary layer.

### 3.6.2. Modeling of single component adsorption isotherm

The adsorption isotherm model analysis is essential for investigating the interactions between contaminants and adsorbent, aiding in understanding the adsorption mechanism (Gilpavas et al., 2020; Balarak et al., 2021). This study utilized well-known isotherm models, such as Langmuir, Freundlich, Sips, Temkin, and Dubinin–Radushkevich (D–R), depicted in Eqs. 3.8-3.13, for the single component adsorption study. The isotherm study was conducted under optimal operating conditions. The employed single component isotherm model equations for ACM and CIP removal from water are provided in Table 3.3.

Table 3.3. The single component adsorption isotherm models employed in ACM and CIP removal from water.

| Isotherm models | Model equations | | |
|---|---|---|---|
| | Non-linear | Linear | Eq. no |
| Langmuir model (Langmuir, 1918) | $q_e = \frac{q_m K_L C_e}{1 + K_L C_e}$ | $\frac{C_e}{q_e} = \frac{1}{q_m b} + \frac{C_e}{q_m}$ | 3.8 |
| Freundlich model (Freundlich, 1924) | $q_e = K_F C_e^{1/n}$ | $lnq_e = lnK_F + \frac{lnC_e}{n}$ | 3.9 |
| Sips (Sips, 1948) | $q_e = \frac{K_s (C_e)^{\beta_s}}{(1 + \alpha (C_e)^{\beta_s})}$ | - | 3.10 |
| Temkin (Temkin and Payzhev, 1940) | - | $\mathrm{lnq_e} = \beta \mathrm{lnK_T} + \beta \mathrm{lnC_e}$ | 3.11 |
| Dubinin–Radushkevich (D–R) (Dubinin and Radusshkevich, 1947) | - | $\mathrm{lnq_e} = \mathrm{lnq_m} - K_D \varepsilon^2$ | 3.12 |
| Redlich-Peterson | - | $\ln(C_e / q_e) = \beta \ln C_e - \ln A$ | 3.13 |

where, $q_e$ (mg/g) is the adsorption capacity of CAC at the equilibrium time, $C_e$ is the equilibrium concentration (mg/L), $q_m$ (mg/g) is the Langmuir constant associated with adsorption capacity at its maximum adsorption capacity (mg/g), $K_L$ is the constant of Langmuir (L/mg), $K_F$ is the constant of Freundlich (mg/g) $(L/mg)^{1/n}$, $n$ is the exponent of Freundlich related to adsorption intensity. In the Sips model, $K_s$ ((mg/g)($L^{\beta}$. $mg^{-\beta}$)) refers to Sips adsorption intensity, α ($L^{\beta}$. $mg^{-\beta}$) and $\beta_s$ are the Sips constant and exponent, respectively. The correlation coefficient ($R^2$) was used to designate the best fit of the experimental data with the models. $R^2$ and root mean square error (RMSE) were used to compare the performance of isotherm models. The lower RMSE value for the applied model indicates that the model provides a more accurate representation of the experimental data. The Temkin model constants, β and $K_T$ (L/mg) are related to the heat of adsorption and maximum binding energy, respectively. In the D-R model, $K_D$ ($mol^2/KJ^2$) stands for adsorption energy constant, $q_m$ represents the theoretical saturation capacity (mg/g), and ε (kJ/mol) is the Polanyi potential, calculated from Eq. (3.14). Also, β (L/mg) and A (L/g) are the Redlich-Peterson model constants. Based on the Langmuir equation, an essential parameter of adsorption ($R_L$) is expressed in Eq. (3.14).

$$R_L = \frac{1}{(1+bC_o)} \tag{3.14}$$

The $C_0$ (mg/L) and b (L/mg) are the initial CIP concentration and Langmuir constant, respectively. The calculated value of $R_L$ can characterize the type of the isotherm and its nature: (i) irreversible isotherm ($R_L$=0); (ii) favorable isotherm (0<$R_L$<1); (iii) linear isotherm ($R_L$=1); unfavorable isotherm ($R_L$>1) (J. Li et al., 2018; Stylianou et al., 2021). The above D-R model (Eq. 3.12) can be evaluated after evaluating ε using Eq. (3.15).

$$\varepsilon = RTln(1 + \frac{1}{C_e}) \tag{3.15}$$

The constant $K_D$ is expressed by the slope of the plot of $lnq_e$ vs. $\varepsilon^2$, and the adsorption capacity, $q_m$ (mg/g), can be obtained from the intercept.

### 3.6.3. Regeneration study

The regeneration studies are crucial for the economic evaluation of the synthesized adsorbent materials. The regeneration studies were performed for single component adsorption of ACM

and CIP under optimal process conditions. Desorption solvents such as dilute HCl, 3% NaOH+methanol, and NaOH were used in the previous studies (Al et al., 2021; Balasubramani et al., 2020; Ghadiri et al., 2020). These desorbing solvents were tested for the desorption of the ACM and CIP from the CAC. Among these solvents, 0.3 M HCl provided the highest desorption efficiency for ACM and CIP removal from CAC. Hence, 0.3 M HCl was used as an eluent for ACM and CIP desorption in this study.

## 3.7. Batch adsorption studies (binary component)

In the environmental water matrix, a single contaminant cannot exist alone; instead, mixtures of pollutants co-exist in environmental samples. Therefore, considering the removal of more than one pollutant at a time has a greater environmental relevance. The effect of a pharmaceuticals mixture (single or binary component) on the adsorption process was thoroughly studied to provide insight into the potential of the synthesized adsorbent over multiple pharmaceuticals removal from water. Detailed adsorption studies were conducted to reveal the behaviour of ACM and CIP adsorption (simultaneous) onto the CAC in a batch and fixed-bed adsorption process. The in-depth adsorption studies conducted on the single and binary component pharmaceutical mixture helped to understand the whole adsorption nature of pharmaceutical contaminants removal. The competitive adsorption of the binary component system was carried out using five different binary concentration ratios (10:160 mg/L, 40:120 mg/L, 80:80 mg/L, 120:40 mg/L, and 160:10 mg/L) interchangeably used for ACM to CIP and CIP to ACM in aqueous solution. The residual concentrations of ACM and CIP were quantified using a UV-Vis spectrophotometer (Cary Series UV-Vis-NIR Spectrophotometer G9825A, Agilent Technologies) with measurements taken at 250 nm and 273 nm, respectively.

### 3.7.1. Modeling of binary component adsorption isotherm

The conventional isotherm models (as mentioned in section 3.6.2) were developed for the single component adsorption processes and cannot accurately describe the adsorption systems involving binary or multiple contaminants. The competitive Langmuir multi-component isotherm model (Eq. 3.16) was employed to analyze the binary component mixture data (components i and j)

(Yadav et al., 2022). All binary sorption experiments were conducted in triplicate, and mean values were used to plot the graphs with the error bars.

$$q_{e,i} = \frac{q_m K_{L,i} C_{e,i}}{1 + K_{L,i} C_{e,i} + K_{L,j} C_{e,j}} \quad (3.16)$$

where $q_m$, $K_{L,i}$, $K_{L,j}$, $C_{e,i}$, $C_{e,j}$, and $q_{e,i}$ denote maximum sorption capacity, competitive Langmuir constants of i and j, equilibrium concentrations of i and j, and equilibrium adsorption capacity of component i in the binary mixture, respectively. For a solution containing ACM and CIP, the non-linear form of the model is expressed in Eqs. (3.17-3.18) for ACM and CIP, respectively, while the linearized forms of the model for each pharmaceutical are provided in Eqs. (3.19-3.20) (Yadav et al., 2022).

$$q_{e,ACM} = \frac{q_{m,ACM} K_{L,ACM} C_{e,ACM}}{1 + K_{L,ACM} C_{e,ACM} + K_{L,CIP} C_{e,CIP}} \quad (3.17)$$

$$q_{e,CIP} = \frac{q_{m,CIP} K_{L,CIP} C_{e,CIP}}{1 + K_{L,CIP} C_{e,CIP} + K_{L,ACM} C_{e,ACM}} \quad (3.18)$$

$$\frac{1}{q_{e,ACM}} = \frac{1}{q_{m,ACM}} + \frac{1}{q_{m,ACM} K_{L,ACM}} \left[\frac{1 + K_{L,CIP} C_{e,CIP}}{C_{e,ACM}}\right] \quad (3.19)$$

$$\frac{1}{q_{e,CIP}} = \frac{1}{q_{m,CIP}} + \frac{1}{q_{m,CIP} K_{L,CIP}} \left[\frac{1 + K_{L,ACM} C_{e,ACM}}{C_{e,CIP}}\right] \quad (3.20)$$

A linear plot of $\left[\frac{1 + K_{L,CIP} C_{e,CIP}}{C_{e,ACM}}\right]$ vs $\left[\frac{1}{q_{e,ACM}}\right]$ was drawn by employing binary component adsorption data. Here, $C_e$ and $q_e$ values of ACM and $C_e$ value of CIP obtained in the binary component adsorption were substituted in the competitive Langmuir isotherm model to estimate the binary component adsorption capacity. The $K_{L,ACM}$ and $K_{L,CIP}$ obtained from the single component Langmuir isotherm analysis were used to evaluate the binary component adsorption capacity. Next, the slope $\left[\frac{1}{q_{m,ACM} K_{L,ACM}}\right]$ and intercept $\left[\frac{1}{q_{m,ACM}}\right]$ were used to evaluate the maximum adsorption capacity of ACM ($q_{m,\ ACM}$) in the binary component water matrix. Similarly, the maximum adsorption capacity of CIP ($q_{m,\ CIP}$) was evaluated using Eq. (3.20). The binary component competitive adsorption Langmuir isotherm constants ($K_{L,ACM}$ and $K_{L,CIP}$) were determined from the slope of Eq. (3.19) and Eq. (3.20), respectively.

## 3.8. Flow mode (fixed-bed) adsorption studies

Flow mode sorption experiments were conducted using a fixed-bed column to evaluate the adsorbent potential for up-scaling the sorption process. The glass column (7 mm internal diameter and 100 mm length) was packed by loading CAC between two glass wool layers to prevent adsorbent entrainment and ensure uniform flow, as depicted in Figure 3.3. The column was then continuously fed with an aqueous solution containing ACM and CIP using a peristaltic pump at desired flow rates. The performance of the column was evaluated for single and binary component systems by varying operational parameters such as adsorbent mass (M), initial pollutant concentration ($C_o$), and adsorbate solution flow rate (Q) as shown in Table 3.4. The column experiment was conducted at four experimental conditions ($R_1$-$R_4$) with the designations $R_1$ (M = 50 mg, $C_o$ = 5 mg/L, and Q = 1.5 mL/min), $R_2$ (M = 50 mg, $C_o$ = 10 mg/L, and Q = 1.5 mL/min), $R_3$ (M = 100 mg, $C_o$ = 10 mg/L, and Q = 3 mL/min), and $R_4$ (M = 100 mg, $C_o$ = 10 mg/L, and Q = 1.5 mL/min). The experiments for all runs were duplicated under uniform conditions, and the performance of the column was evaluated by plotting breakthrough curves (time vs. $C_t/C_o$). Accordingly, the ACM and CIP removal column data was generated using CAC. As a result, the column performance indicators parameters such as breakthrough time ($t_b$), column exhaustion time ($t_e$), total effluent treated ($V_{eff}$, mL) and the total amount of pollutant adsorbed ($q_{tot}$, mg), maximum experimental uptake capacity ($q_{bed}$, mg/g) were evaluated. The column breakthrough point is when the effluent concentration ratio ($C_t/C_o$) exceeds 0.05 of the initial pollutant concentration ($C_o$). On the other hand, the column exhaustion ($t_e$) point is a condition when the effluent concentration reaches 95% of the initial concentration, and no significant variation in $C_t/C_o$ occurs. The $V_{eff,}$ $q_{total}$ and $q_{bed}$ can be calculated using Eqs. (3.21-3.23), respectively.

$$V_{eff} = Q \times t_{total} \tag{3.21}$$

$$q_{total} = \frac{Q}{1000}\int_{t=0}^{t=total} C_{ad}\,dt \tag{3.22}$$

$$q_{bed} = \frac{q_{total}}{m} \tag{3.23}$$

where $Q$ is the flow rate (mL/min), $t_{total}$ is total flow time (min), and $C_{ad}$ is the adsorbed ACM or CIP concentration (mg/L), and $m$ is CAC dry mass (g). The total amount of ACM and CIP

molecules passed through the column system $m_{total}$ (mg) is calculated using Eq. (3.24). The removal percentage (RE, %) of ACM and CIP molecules can be calculated from Eq. (3.25). At equilibrium, the residual ACM and CIP concentration $C_{eq}$ (mg/L) during the column adsorption process can be obtained using Eq. (3.26).

$$m_{total} = \frac{C_o Q t_{total}}{1000} \tag{3.24}$$

$$RE(\%) = \frac{q_{total}}{m_{total}} \times 100 \tag{3.25}$$

$$C_{eq} = \frac{m_{total} - q_{total}}{V_{eff}} \times 1000 \tag{3.26}$$

Table 3.4. Column adsorption factors and their levels.

| Parameters | Levels | |
|---|---|---|
| | Low | High |
| Flow rate (mL/min) | 1.5 | 3 |
| Adsorbent loading (mg) | 50 | 100 |
| Initial concentration (ACM+CIP: mg/L) | 5 | 10 |

In this study, three independent column studies were conducted: adsorption of single ACM, adsorption of single CIP, and simultaneous adsorption of ACM+CIP onto the CAC fixed-bed. Performing a column study for even a single contaminant is known to be a very time-consuming task. Herein, three column studies (ACM removal, CIP removal, and ACM+CIP removal) were performed in duplicate. Therefore, generating quality data by performing duplicate analyses was prioritized over increasing the number of levels for each factor. Moreover, considering two levels of factors for a column study is a common trend, especially when performing independent full fixed-bed studies for the removal of more than one contaminant from water.

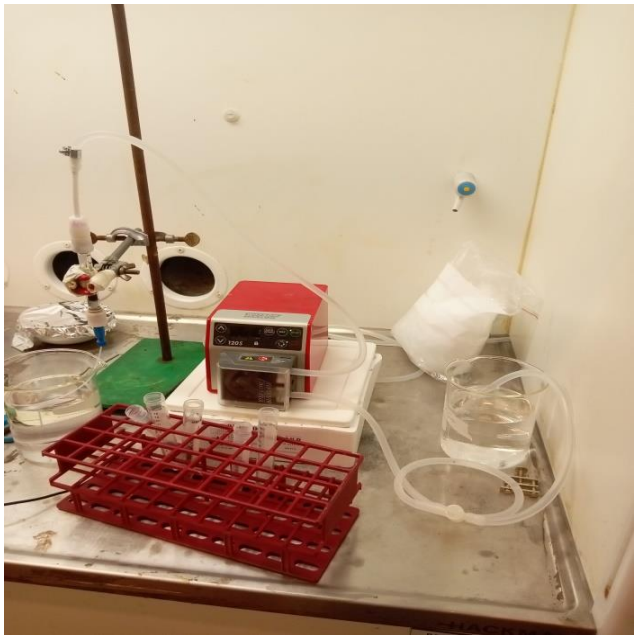

Figure 3.3. Experimental setup of the column/fixed-bed adsorption.

### 3.9. Electrochemical oxidation (EO) experiment

The EO experiment was conducted using an $IrO_2$/Ti electrode (2 cm×7 cm and 1 mm thickness) as anode and cathode in a 500 mL glass beaker containing 20 mg/L of each pharmaceutical (ACM+CIP) in an aqueous solution. The EO experiment was conducted using a programmable power supply (GWINSTEK, PSP-405, Taiwan). The inter-distance between the anode and cathode electrode was 2 cm, and the EO reaction was conducted under continuous stirring (250 rpm) at room temperature (25 ℃). The effect of EO operational parameters on ACM/CIP degradation, such as initial pharmaceutical concentration, EO time, solution pH, and current density, were studied using the RSM optimization technique at a constant NaCl (electrolyte) concentration of 0.05M. The employed 0.05 M NaCl concentration was based the preliminary study conducted to ascertain a suitable concentration of NaCl that would provide sufficient current to the reactor (Wulan et al., 2020). An aliquot of 50 mL target pharmaceutical solution was periodically taken to evaluate the EO degradation efficiency. All the EO experiments were triplicated, and the error bars were provided except for the RSM optimization process. The EO setup used in this study is presented in Figure 3.4.

Figure 3.4. The electrochemical oxidation setup used in this study.

### 3.10. Coupled process (EO+adsorption)

The EO+adsorption process experiment was carried out sequentially (EO followed by adsorption). The individual processes (EO and adsorption) are studied in detail, considering all the operational aspects (process parameters effect, single and binary contaminant removal, kinetics, and water matrix effect, etc.). Despite their higher removal efficiency in ACM and CIP removal from simple water matrix (pure water), the TOC and COD removal efficiencies from complex water matrices is limited. Therefore, coupling both processes would offer a significant advantage in removing the pharmaceutical contaminants from single and multi-component pollutant mixtures. The same experimental EO setup utilized in the EO process was adopted for the coupled process, as the coupled process is a sequential combination of the EO and adsorption processes. The EO and adsorption processes were individually optimized to obtain the best operating conditions for the removal of target pharmaceuticals from water. Moreover, the coupled process was optimized by employing a coupled process optimization technique. This approach helps to understand the mutual inter-dependence between EO and adsorption process parameters. In the coupled process optimization, some of the parameters of EO and adsorption were kept at optimized conditions obtained from the individual processes. Coupled process parameters such as current density, EO time, initial pH, adsorption time, and adsorbent dose

were optimized using a Box-Behnken Design of the RSM optimization technique. The experimental setup of the coupled process used in this study is provided in Figure 3.5.

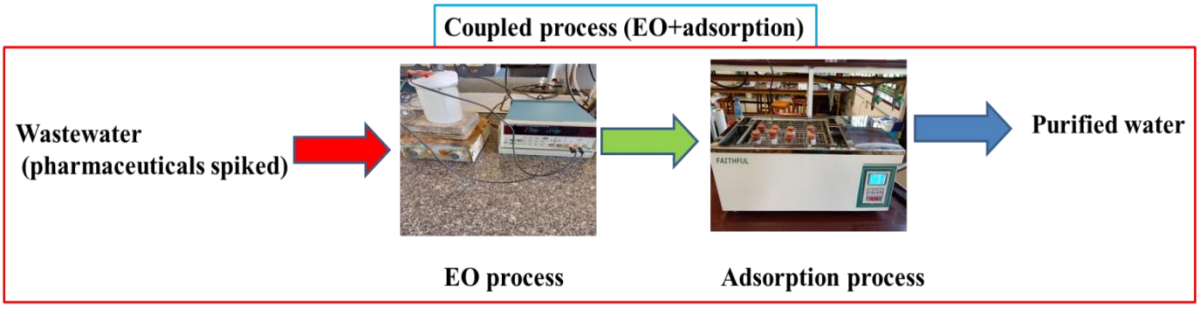


Figure 3.5. The experimental setup of the EO process coupled with the adsorption.

## 3.11. Analysis of pharmaceutical contaminants

### 3.11.1. Chromatographic Analysis

The residual concentrations of ACM and CIP were quantified using High Performance Liquid Chromatography (Shimadzu HPLC, Germany) equipped with a UV-visible detector. All the samples were filtered using a 0.45 µm Sartorius syringe filter before analysis. The chromatographic separation was conducted using a kinetex® 5 µm EVO C18 (dimension: 150 × 6 mm) column at 30 ℃. Different mobile phases such as 1% acetic acid in ultrapure water (eluent A) and methanol (eluent B), as well as 1% formic acid in ultrapure water (eluent A) and methanol (eluent B), were employed to select the optimal mobile phase for quantifying the target pharmaceuticals using the specified column. The methanol and ultrapure water with 1% formic acid exhibited the best results and were used throughout the pharmaceutical quantification analysis. Again, the ratio of mobile phase (1% formic acid in ultra-pure water (eluent A) to 1% formic acid in methanol (eluent B)) was optimized to be 55:45 V/V at a 1 mL/min flow rate. The HPLC was operated in isocratic mode at a constant oven temperature (30 ℃) using 3 µL sample injection volume. The isocratic separation was carried out at two wavelength channels (254 and 280 nm) for a total separation time of 10 min to ensure proper detection of each pharmaceutical. The removal efficiency of EO degradation of the ACM and CIP was calculated using Eq. 3.27 (Delgado-vargas et al., 2023).

$$\text{Removal } \% = \frac{C_o - C_t}{C_o} \quad (3.27)$$

where $C_o$ and $C_t$ refer to the initial and final concentration of pharmaceuticals.

### 3.11.2. Total organic carbon (TOC) Analysis

The TOC was analyzed to evaluate the mineralization efficiency of the treatment processes. TOC was analyzed using a multi N/C (analytikajena, 2100 s) TOC analyzer. The TOC removal calculation was performed employing Eq. 3.28.

$$\text{Mineralization } \% = \frac{\text{TOC}_\text{o} - \text{TOC}_\text{t}}{\text{TOC}_\text{o}} \quad (3.28)$$

where $TOC_o$ and $TOC_t$ refer to the initial and final TOC values.

### 3.11.3. Chemical oxygen demand (COD) determination

The COD of aqueous solutions were determined with a spectrophotometer (DR 3900, Hach Lange GmbH, Germany) employing a spectroquant 400 COD reagents using a spectrophotometer. COD removal calculations were performed using Eq. 3.29.

$$\text{COD removal } \% = \frac{\text{COD}_\text{o} - \text{COD}_\text{t}}{\text{COD}_\text{o}} \quad (3.29)$$

where $COD_o$ and $COD_t$ refer to the initial and final TOC values.

## 3.12. Experimental design and statistical analysis

The CCD is one of the frameworks of RSM often employed to analyze experimental data statistically. Design expert software (Trial version: 11.0) was used to analyze experimental data of adsorption, EO, and the coupled process. In this approach, responses are affected by various process variables. In the adsorption process, the main process variables, such as pH, adsorbent dose, contact time, and initial concentration were combined to give 30 experiments for ACM and CIP removal from water. In the case of the EO process, main process parameters such as current density, EO time, initial pH and initial pharmaceutical concentration were considered to optimize the electrochemical degradation of the target pharmaceutical contaminants. Similar to the

adsorption process, the EO process was optimized using the CCD framework of the RSM. However, the coupled process was optimized using a coupled process parameters optimization technique, which integrates crucial parameters of EO and the adsorption process. In EO optimization, all the other factors, such as electrolyte concentration (0.05 M NaCl), string speed (250 rpm), temperature (25 ℃) and distance between the anode and cathode electrodes (2cm), were kept constant during the EO process. Each variable's low, middle, and high levels were designated by the rotatable CCD as −1, −0.5, 0, 0.5, and +1, respectively. In the coupled process optimization, the most influential parameters of EO (current density, pH and EO time) and adsorption process (adsorbent dose and adsorption time) were considered and optimized with Box-Behnken design (BBD). For the optimization and statistical analysis, the levels of each factor were set based on the preliminary experimental data. The CCD experimental design of adsorption (CIP removal), EO (ACM+CIP removal), and BBD of the coupled processes (ACM+CIP removal) are presented in Tables 3.5, 3.6, and 3.7, respectively. The relationship between the coded and actual values is presented in Eq. (3.30) (Najafpoor et al., 2019).

$$x_i = \frac{X_i - X_o}{\Delta X} \tag{3.30}$$

Where $x_i$ refers to dimensionless coded values of the $i^{th}$ independent variable, $X_i$ is the actual value of the independent variable, $X_o$ is the central point of actual value, and $\Delta X$ is the step change value of the variable. In this regard, RSM was employed to derive a quadratic polynomial model for evaluating the effects of the independent variables on the response. The quadratic equation of the optimal model can be represented using Eq. (3.31) (Gholami et al., 2022).

$$Y = \beta_o + \sum_{i=1}^{n=4} \beta_i X_i + \sum_{i=0}^{4} \sum_{j=1}^{4} \beta_{ij} X_i X_j + \sum_{i=1}^{4} \beta_{ii} X_j{}^2 + \varepsilon \tag{3.31}$$

where Y is the model predicted response, $\beta_0$ is the coefficient of the model (constant), $X_i$ (i =1 to 4) represents the independent variables, and $\beta_i$, $\beta_{ii}$, and $\beta_{ij}$ (i and j =1–4) indicate the linear, quadratic and second-order interaction coefficients, and ε is the corresponding error. Analysis of variance (ANOVA) was employed to statistically evaluate the suitability of the developed polynomial model for predicting the experimental results.

Table 3.5. The independent variables and their levels in the CCD experimental design for the CIP adsorption process.

| Factors | | Levels | | | Star points | |
|---|---|---|---|---|---|---|
| Actual | Coded | Low (-1) | Central (0) | High (+) | -α | +α |
| CIP initial concentration (mg/L) | A | 20 | 30 | 40 | 10 | 50 |
| Adsorbent dosage (g/L) | B | 0.5 | 0.75 | 1.00 | 0.125 | 1.25 |
| pH | C | 5.25 | 7.5 | 9.75 | 3 | 12 |
| Contact time (min) | D | 18.75 | 30.00 | 46.25 | 5 | 60 |

Table 3.6. The independent variables and their levels of the CCD experimental design for the ACM+CIP degradation using the EO process.

| Factors | | Levels | | | Star points | |
|---|---|---|---|---|---|---|
| Actual | Coded | Low (-) | Central (0) | High (+) | -α | +α |
| EO oxidation time (min) | A | 40 | 60 | 80 | 20 | 100 |
| pH | B | 4 | 6.5 | 9 | 1.5 | 11.5 |
| Current density ($mA/cm^2$) | C | 23.21 | 42.85 | 62.5 | 3.56 | 82.14 |
| ACM+CIP initial concentration (mg/L) | D | 15 | 20 | 25 | 10 | 30 |

Table 3.7. The independent variables and their levels in the BBD experimental design for the ACM+CIP removal using the EO+adsorption process.

| Factors | | Levels | | |
|---|---|---|---|---|
| Actual | Coded | Low (-) | Central (0) | High (+) |
| EO time (min) | A | 10 | 35 | 60 |
| pH | B | 9 | 6 | 9 |
| Current density (mA/cm$^2$) | C | 15 | 20 | 25 |
| Adsorbent dose (g/L) | D | 0.08 | 0.1 | 0.12 |
| Adsorption time (min) | E | 20 | 50 | 80 |

## 3.13. Energy consumption

The assessment of the economic aspects of the electrochemical oxidation-based processes depends on the energy consumption of the intended process. The specific energy consumption ($EC_{sp}$: kWh/m$^3$) of the EO in EO alone and EO in coupled process was calculated using Eq. 3.32 (Abidi et al., 2022).

$$EC_{sp} = \frac{U_{cell}.I.t}{V \times 10^3} \quad (3.32)$$

Where, $U_{cell}$ is the cell potential (V), I is the applied current (A), t is the electrochemical oxidation time (h), and V is the volume of the solution (m$^3$).

# CHAPTER FOUR

## 4. Results and discussion

### 4.1. Adsorbent characterization results

Bamboo sawdust-derived adsorbents were characterized using FTIR, XRD, SEM/EDS, BET, Raman spectroscopy and $pH_{pzc}$ characterization techniques. These characterizations help to understand the nature of the adsorbents, which then elucidate the overall adsorption process. Moreover, characterization results (SEM and BET) were used to select the best adsorbent among the synthesized adsorbents such as pristine bamboo sawdust, bamboo sawdust carbon (BSC), adsorbents with single chemical activation (AC-KOH and AC-Fe) and dual chemical activation (CAC, AC-0.5KOH, AC-1.5KOH, AC-0.5Fe and AC-1.5Fe). Table 4.1 presents the removal efficiencies of bamboo sawdust-derived adsorbents in single and binary component adsorption of ACM and CIP from water. The effect of iron content on the adsorption of ACM and CIP from the single and binary component systems was investigated, keeping the bamboo sawdust to KOH ratio of (1:5 w/v for 1M KOH solution) constant. Therefore, the amount of iron in the chemical activation of the adsorbent was optimized by considering different ratios (1:5, 0.5:5, and 1.5:5 w/w) of iron to bamboo sawdust. Increasing the iron content in the ratio of iron to bamboo sawdust from 0.5:5 w/w to 1:5 w/w increased the removal of ACM and CIP from 92.56% and 89.94% to 99.8% and 96%, respectively, in single sorption studies. Similarly, the removal of ACM and CIP increased from 84.27% and 80.83% to 94.52% and 92.35%, respectively, in the binary component adsorption systems. This can be ascribed to the active involvement of more iron species (on the surface of activated carbon) during the adsorption of ACM and CIP via mechanisms explained in section 4.5. However, a further increase in the iron content in the ratio of iron to bamboo sawdust from 1:5w/w to 1.5:5w/w decreased the removal of ACM and CIP, as the surface area was decreased as shown in Table 4.2. The mechanism of iron involvement in the adsorption of ACM/CIP onto the CAC is explained in section 4.5. Herein, the adverse effect of the decrease in surface area outweighs the benefits obtained from incorporating iron in the adsorption process. On the other hand, increasing the iron ratio increases the cost of the adsorbent synthesis. Consequently, the optimal ratio of iron to bamboo sawdust (1:5 w/w) was utilized to synthesize activated carbon from bamboo sawdust.

The effect of KOH concentration on the removal of ACM and CIP by the adsorbents was explored, considering various concentrations of KOH (0.5M, 1M, and 1.5M). The iron-to-bamboo sawdust ratio was maintained at the optimal condition (1:5 w/w), and the bamboo sawdust-to-KOH ratio was kept constant at 1:5 w/v. In this regard, increasing the KOH concentration from 0.5M to 1 M (maintaining the same ratio of iron to bamboo sawdust) increased the removal of ACM and CIP from 93.46% and 91.82 to 99.8% and 96%, respectively, in single component adsorption. Likewise, the removal of ACM and CIP increased from 86.27% and 81.18% to 94.52% and 92.35%, respectively, in binary component adsorption. This trend shows that the pharmaceutical contaminants removal efficiency increases with the concentration of KOH applied during the adsorbent synthesis. It can also be ascribed to the increment of surface area (Table 4.2) with the concentration of the KOH. Further increase in KOH concentration from 1M to 1.5 M increased ACM and CIP removal from 99.8% and 96% to 99.95% and 97.05%, respectively, in the single component sorption process. However, the removal of ACM and CIP increased from 94.52% and 92.35% to 95.12% and 93.05%, respectively, in the binary component adsorption. In this case, enhancement of ACM and CIP removal in single and binary component adsorption is insignificant. The rationale is that maximum removal of ACM and CIP was already attained at a 1M KOH concentration, and any further enhancement proved negligible removal enhancement. Conversely, it increases the cost of adsorbent synthesis. Therefore, a KOH concentration of 1M, with a ratio of 1:5 w/v for the bamboo sawdust to KOH solution (1M), was considered the optimal concentration of KOH. Overall, CAC exhibited excellent removal efficiency for ACM and CIP removal with a reasonable amount of chemicals used for the activation. All the synthesized adsorbents were applied in the pharmaceutical adsorption process to evaluate their removal efficiencies, and the results are provided in Table 4.1.

Table 4.1. The ACM and CIP removal efficiencies of bamboo sawdust derived adsorbents.

| Adsorbent | Single component adsorption % | | Binary component adsorption % | | Remark |
|---|---|---|---|---|---|
| | ACM | CIP | ACM | CIP | |
| Bamboo sawdust powder (pristine) | 29.55 | 24.86 | 21.85 | 15.65 | Not selected |
| BSC | 48.52 | 45.01 | 40.86 | 35.06 | **Selected for comparison** |
| AC-0.5Fe | 92.56 | 89.94 | 84.27 | 80.83 | Not selected |
| AC-1.5Fe | 90.89 | 88.87 | 82.85 | 78.96 | Not selected |
| AC-0.5KOH | 93.46 | 91.82 | 86.27 | 81.18 | Not selected |
| AC-1.5KOH | 99.95 | 97.05 | 95.12 | 93.05 | Not selected |
| **CAC** | **99.8** | **96** | **94.52** | **92.35** | **Selected** |
| AC-Fe | 70.26 | 67.38 | 61.52 | 56.62 | Not selected |
| AC-KOH | 81.45 | 79.45 | 71.16 | 68.56 | Not selected |

### 4.1.1. FTIR analysis

The FTIR spectra of bamboo sawdust carbon (BSC), chemically activated carbon (CAC), and CAC after single sorption (CAC-ACM and CAC-CIP) and binary sorption (CAC-ACM+CIP) of ACM and CIP are depicted in Figure 4.1. Notable functional groups were not observed on the surface of unmodified BSC. However, several peaks observed in CAC at 3543, 2918, 1052 and 540 $cm^{-1}$ were assigned to the stretching vibrations of -OH in carbonyl and phenol groups (Ding & Liu, 2020), stretching vibrations of aliphatic C-H (Zhihao Chen et al., 2022), C-O stretching vibrations of esters and carboxylic acids (Wu et al., 2022) and Fe-O vibration bonds (Bedia et al., 2020), respectively. The stretching vibrations of aliphatic C-H observed at 2900 $cm^{-1}$ may indicate an incomplete carbonization of the bamboo sawdust (Xu et al., 2019). The surface chemistry of the CAC indicated that the activated carbon was successfully functionalized via dual chemical activation (KOH + $FeCl_3.6H_2O$).

Following the single and binary adsorption of ACM and CIP, the intensity and positions of the spectral peaks corresponding to the functional groups of CAC were changed. In this regard, the peak assigned to -OH stretching was shifted from 3543 $cm^{-1}$ – 3456 $cm^{-1}$ to 3402 $cm^{-1}$ (CAC-ACM), 3417 $cm^{-1}$ (CAC-CIP), and 3654 $cm^{-1}$ (CAC-ACM+CIP) after single and binary adsorption of ACM and CIP, respectively. Meanwhile, various new peaks appeared on the surface of CAC at 1657 $cm^{-1}$, 1390 $cm^{-1}$, and 661 $cm^{-1}$, attributed to the sorption of pharmaceuticals onto the adsorbent surface. The -OH stretching peak after the adsorption of ACM is more substantial compared to that of the CIP adsorption. This could indicate a more significant involvement of the -OH group in the single sorption of ACM (CAC-ACM) than CIP (CAC-CIP). In contrast, the peaks assigned to C-H stretching and O-H bending were more involved in CIP sorption (CAC-CIP) than ACM sorption. After the binary sorption of ACM and CIP (CAC-ACM+CIP), the peak assigned to -OH bending (shifted and broadened), C-O stretching (shifted and broadened), and Fe-O stretching vibration (strong) showed significant changes. Moreover, the peak intensity observed on CAC at 540 $cm^{-1}$ (Fe–O) significantly increased after the simultaneous adsorption of ACM and CIP (Zheng & Duan, 2022). This could be ascribed to the participation of the Fe-O group in the simultaneous adsorption of ACM and CIP, as evidenced by the presence of FTIR spectral peaks for ACM and CIP (as shown in appendix Figure A.1) at this spectral range. The presence of iron on the surface of the CAC was further confirmed by testing the magnetic properties of the CAC using a magnetic rod (CAC particles were collected by the magnet). The magnetic property of CAC is beneficial for easy separation of the material from aqueous solution (Jiang et al., 2023). The overall spectral changes observed on the CAC after adsorption confirmed the successful adsorption of ACM and CIP onto the CAC. This finding can be attributed to the involvement of various functional groups (-OH, C-H, C-O, and Fe-O) in removing ACM and CIP from the water via different adsorption mechanisms.

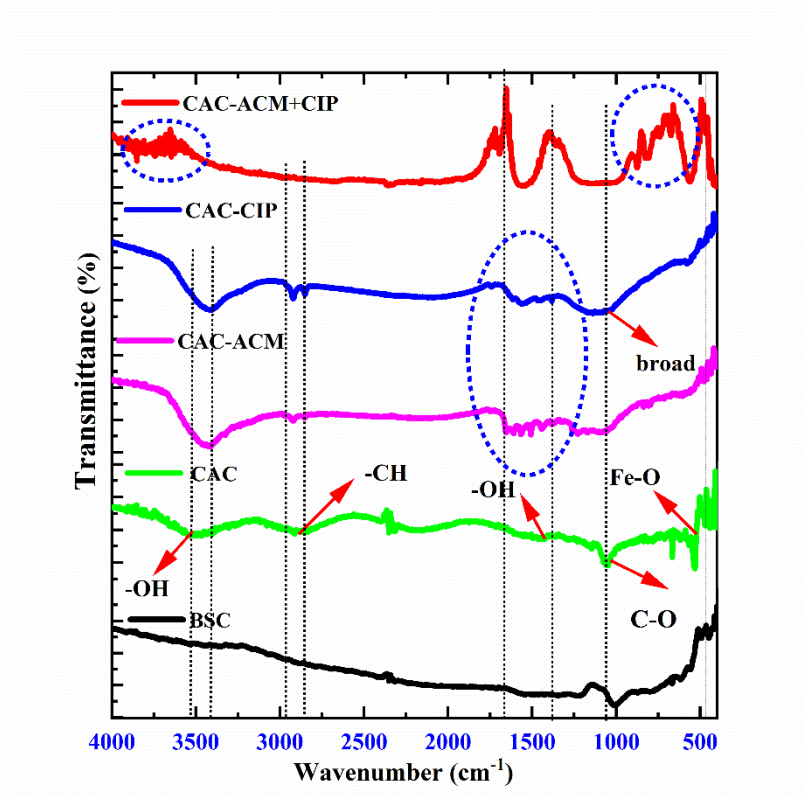


Figure 4.1. FTIR spectra of pristine bamboo sawdust carbon (BSC), chemically activated carbon (CAC), CAC after ACM adsorption (CAC-ACM), CAC after adsorption of ciprofloxacin (CAC-CIP) and CAC after simultaneous adsorption of ACM and CIP (CAC-ACM+CIP).

### 4.1.2. SEM/EDS analysis

Scanning electron microscopy with energy-dispersive spectroscopy (SEM/EDS) was used to examine the morphological differences and chemical composition of the pristine bamboo sawdust, BSC, CAC and CAC after adsorption. It can be seen from Figure 4.2 (a) that the bamboo sawdust has an irregular surface with no pores. Moreover, Figure 4.2 (b) reveals that the pristine bamboo carbon morphology has an irregular and tubular structure with no pores. However, Figure 4.2 (c) indicates that the CAC has a rough surface with several cavities, voids and pores distributed on the surface of the activated carbon. The SEM image demonstrated that chemical activation resulted in the formation of pores on the surface of the activated carbon. Moreover, the SEM image analysis result agrees with the BET result of the adsorbent, which presented a significant increment (565 $m^2/g$ to 1158 $m^2/g$) in surface areas after chemical activation. The SEM analysis result showed that the formation of pores on the adsorbent surface

after chemical activation is consistent with the previous report (Tunç et al., 2022). Moreover, the EDS analysis provided the compositions of elements on the surface of the CAC, such as carbon (62.88%), oxygen (23.62%), magnesium (0.11%), Al (0.12%), Si (0.37%), potassium (2.26%), iron (10.1%) and Ca (0.54%) as shown in Figure 4.3 (a). The Multi-elemental Mapping (MAP) analysis is presented in Figure 4.3 (b). The main elements observed on CAC, such as carbon (C), oxygen (O), potassium (K) and iron (Fe), are represented by purple, light green, red and blue colours in Figure 4.3 (b). The MAP analysis revealed that Fe is uniformly distributed on the surface of the CAC. Overall, the porous structure of the adsorbent shown by the SEM image, surface functional groups indicated by FTIR and the higher specific surface area (BET analysis) supported the experimental findings of the higher ACM and CIP removal obtained in the adsorption process.

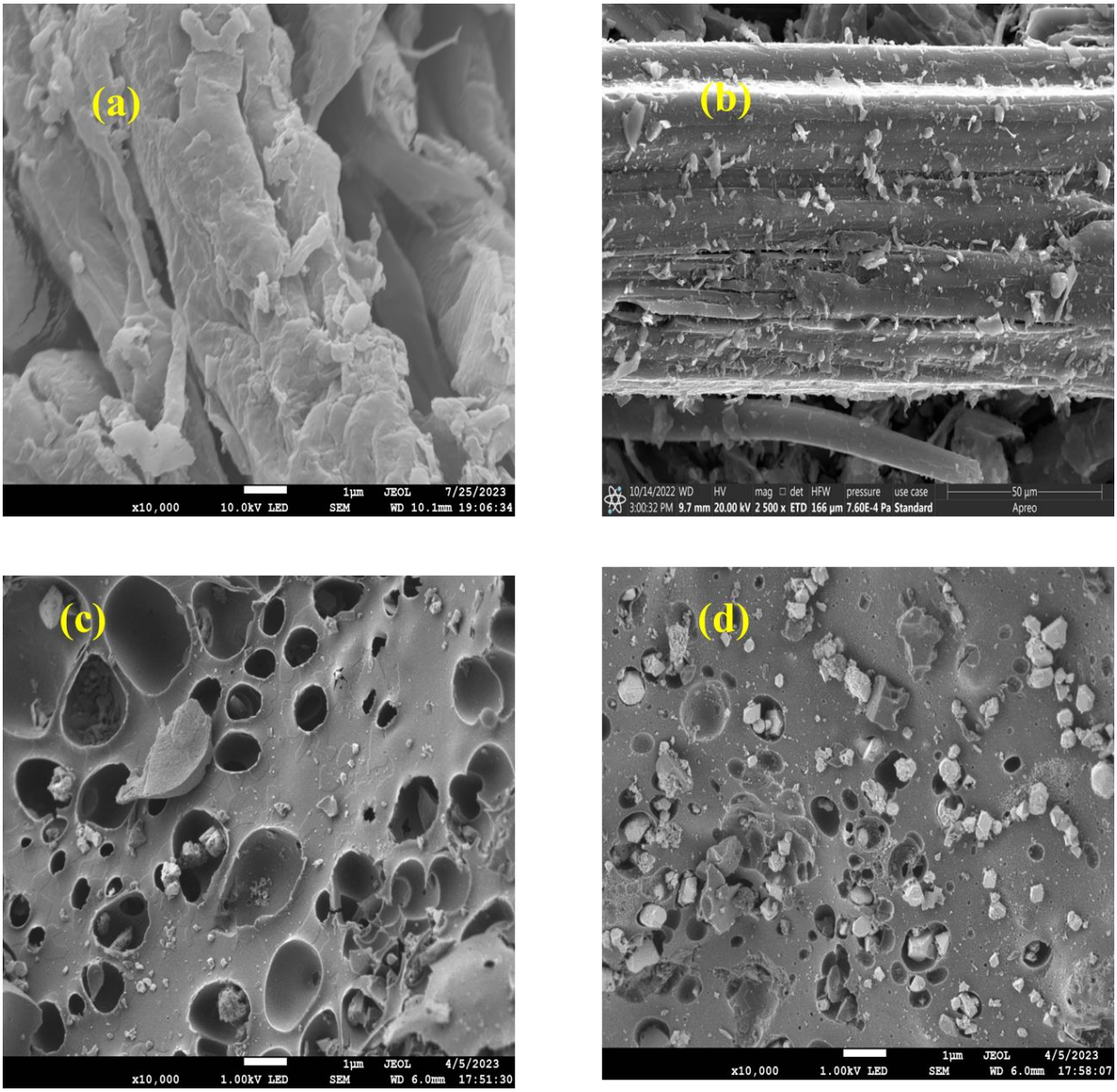


Figure 4.2. SEM images of (a) pristine bamboo sawdust, (b) bamboo sawdust carbon (BSC), (c) CAC before adsorption and (d) CAC after adsorption of ACM and CIP (CACA).

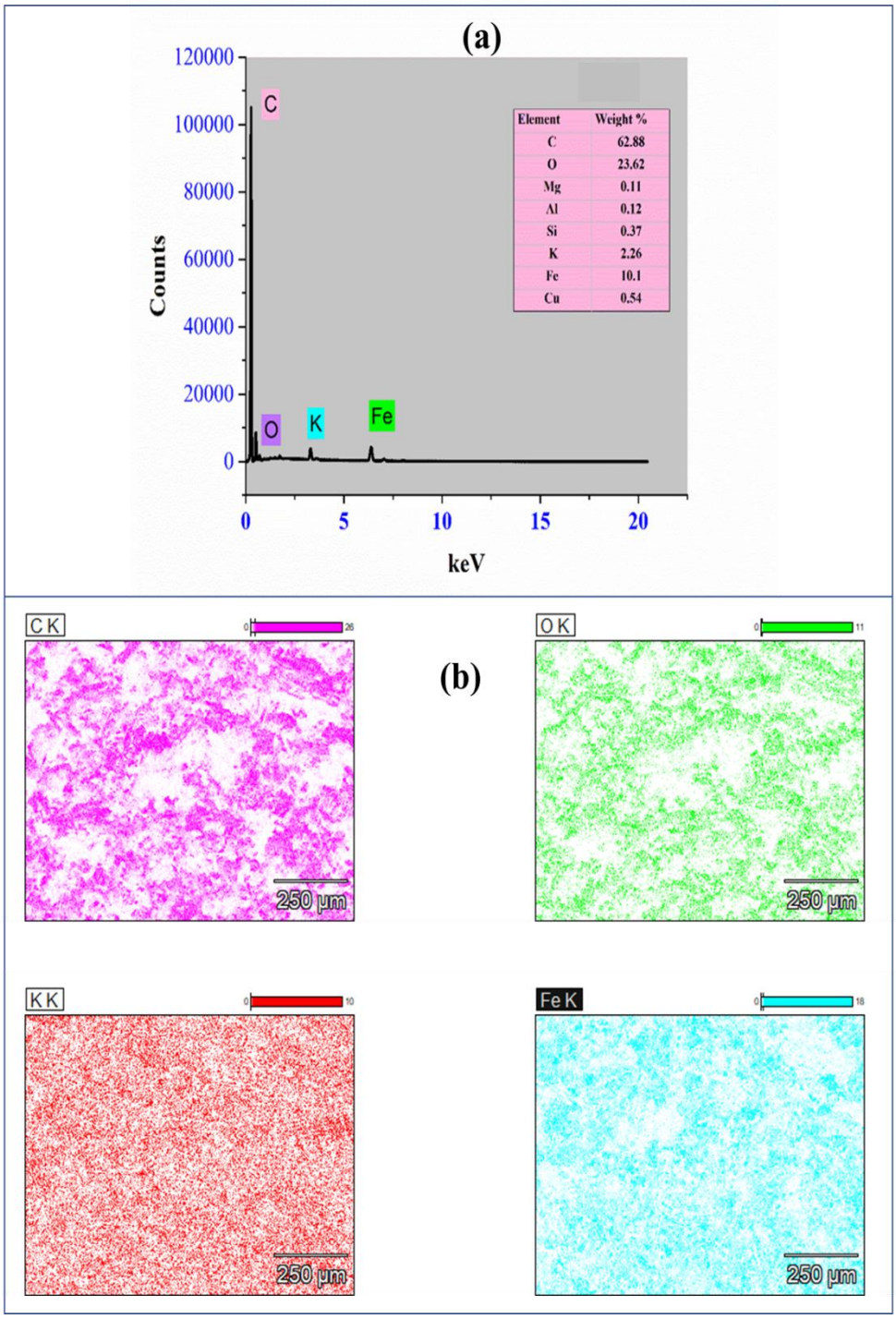


Figure 4.3. The elemental composition of CAC (a) and EDS mapping for CAC.

### 4.1.3. BET surface area

The BET surface area of CAC is significantly higher than that of raw bamboo sawdust carbon (BSC), as shown in Table 4.2. This result indicated that the simultaneous activation of bamboo sawdust with $FeCl_3.6H_2O$ and KOH enhanced the surface area of the activated carbon significantly. The increase in surface area may be attributed to the formation of new pores and the opening of initially inaccessible pores during the chemical activation process, which would help develop a more porous structure (Peng et al., 2018). The surface area is an important parameter that plays a significant role in physical adsorption. The higher surface area of the material leads to higher pollutant adsorption due to the availability of many adsorption sites for more organic pollutant removal (Peng et al., 2018). Among the synthesized adsorbents, AC-1.5 KOH exhibited the highest surface area (Table 4.2); however, the increased quantity of KOH employed in its preparation increases its cost compared to the CAC. Nevertheless, it led to a marginally superior removal of ACM and CIP from water compared to the removal efficiency achieved with the CAC. As a result, CAC was selected as an efficient adsorbent for the removal of ACM and CIP from water.

Table 4.2. Specific surface area and pore size of the bamboo based adsorbents.

| Adsorbents | BET surface area ($m^2/g$) | Pore volume ($cm^3/g$) | Pore radius (Å) | Remark |
|---|---|---|---|---|
| BSC | 565.09 | 1.897 | 13.24 | Not selected |
| **CAC** | **1158.05** | **0.435** | **9.234** | **Selected** |
| AC-0.5Fe | 1126.52 | 0.358 | 8.65 | Not selected |
| AC-1.5Fe | 850.56 | 0.287 | 7.59 | Not selected |
| AC-0.5KOH | 720.85 | 0.236 | 7.065 | Not selected |
| AC-1.5 KOH | 1206.57 | 0.438 | 10.45 | Not selected |

### 4.1.4. XRD analysis

The XRD was conducted to investigate the crystalline compositions of the bamboo sawdust-derived adsorbents. The XRD analysis result is shown in Figure 4.4. The peaks at 30.1, 35.6, 43.2, and 57.2º are assigned to magnetite (Peng et al., 2021), whereas the peak observed in CAC at 33.2º is assigned to hematite. The emergence of these peaks on the surface of CAC confirmed the presence of Fe-O in the structure of the activated carbon. Al et al. (2021) detected a peak at a similar angular degree for $Fe_3O_4$ cubic crystals on an adsorbent prepared from powdered activated carbon magnetized by iron (III) oxide magnetic nanoparticles (Al et al., 2021). Iron (Fe) was believed to be present on the surface of activated carbon as indicated by characteristic peaks of magnetite and hematite (Gong et al., 2016; He et al., 2018; Mian et al., 2018). The XRD result revealed that Fe was successfully loaded onto the CAC, which is consistent with the findings of the FTIR analysis. Therefore, the chemical modification of the adsorbent has desirable structural changes on the activated carbon, as evidenced by the XRD plot.

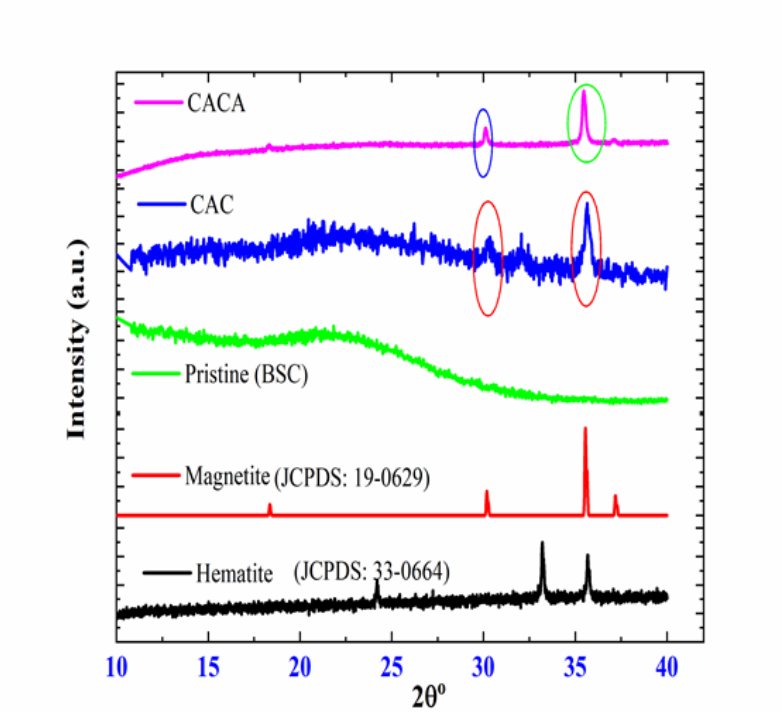


Figure 4.4. The XRD patterns of BSC, CAC and CACA after sorption of ACM and CIP (CAC-ACM+CIP).

### 4.1.5. Raman analysis

The Raman spectra of pristine BSC, CAC, and CAC after adsorption are presented in Figure 4.5. The D and G bands were detected at wavelengths 1350 $cm^{-1}$ and 1591 $cm^{-1}$ in Figure 4.5, respectively. The D band corresponds to the C atom with a hybrid arrangement ($sp^3$), whereas the G band corresponds to the C atom $sp^2$ hybrid configuration (Z. Li et al., 2020). The G band is primarily attributed to the presence of aromatic rings and graphite crystallites, while the D band is mainly caused by a disordered carbon lattice (Minaei et al., 2023). The peak intensity ratio of pristine BSC, CAC, and spent CAC (CAC-ACM+CIP) was 0.864, 0.941, and 0.860, respectively. The peak intensity ratio less than unity indicates a highly graphitic nature of the bamboo-based adsorbents (Maged et al., 2021). The graphitic nature of the biochar could facilitate the formation of π-π bonds between organic molecules during adsorption (Z. Li et al., 2020). These results show that chemical activation ($FeCl_3.6H_2O$ and KOH) increased the degree of biochar disordering by removing organic matter and loading Fe particles on the surface of FBC (Feng et al., 2021). The observed phenomenon could be due to the increased porosity of the material, which was confirmed by SEM analysis. The increase in peak intensity ratio (0.864 to 0.941) after chemical activation shows the formation of more functional groups on the biochar (Shirani et al., 2020). However, a reduction in the Raman band intensity ratio (0.941 to 0.860) after adsorption (CAC-ACM+CIP) reveals the involvement of observed functional groups (-OH, C-H, C-O and Fe-O) in the adsorption process.

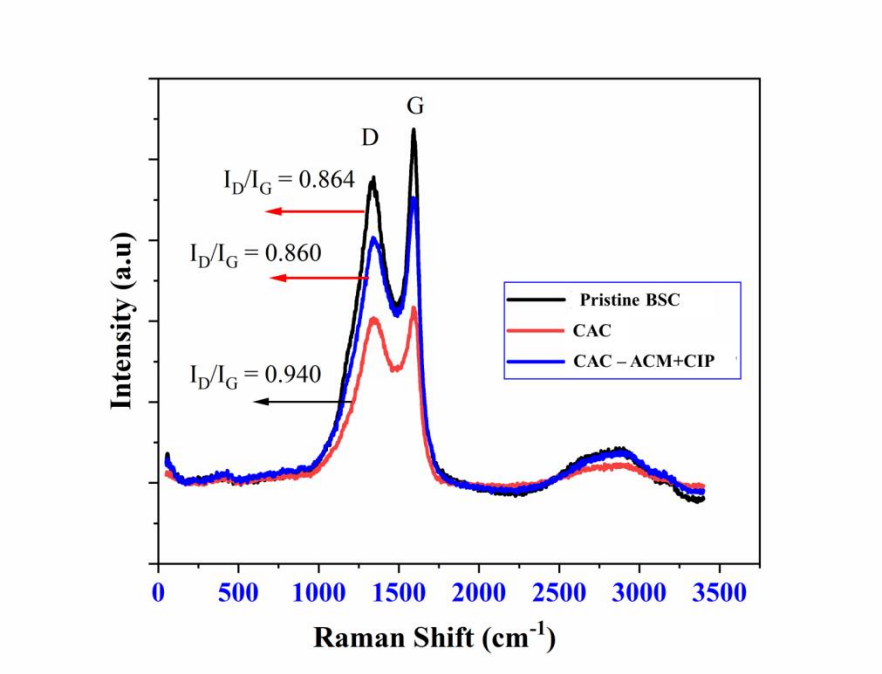


Figure 4.5. Raman spectra of the pristine BSC, CAC and CAC after binary adsorption (CAC-ACM+CIP).

### 4.1.6. The pH of the point of zero charge ($pH_{pzc}$)

Determining $pH_{pzc}$ is essential for the adsorption process study as the adsorption mechanism strongly depends on the solution pH. The pH of the point of zero charge of CAC is about 6.5, as shown in Figure 4.6. Based on the $pH_{pzc}$ result, the surface of CAC is positively charged when pH is below 6.5 and negatively charged when pH is above 6.5. On the other hand, at pH below 6.0, CIP is mainly present in its cationic form (Peng et al., 2018), and the surface of the CAC is positively charged. Hence, the adsorbent and CIP molecules repel each other, and thus CIP removal efficiency decreases. Increasing pH above 6.1 changes the CIP molecule from cationic to zwitterionic, leading to a gradual increase in CIP adsorption (Atugoda et al., 2021). Due to the strong electrostatic interaction between CAC and CIP zwitterion (pH 6.0-8.7), maximum adsorption was obtained. In contrast, at pH higher than 8.7, the adsorption process efficiency decreased as the repulsive force increased between the negatively charged CAC surface and anionic CIP molecules (Najafpoor et al., 2019). Similar results were obtained by (Najafpoor et al., 2019) in removing CIP from water using γ-$Al_2O_3$ nanoparticles. Similarly, another study by

Ji et al. (2021), reported consistent findings, identifying a pH range of 6–8 as the optimal condition for titanate nanotubes to effectively remove CIP molecules from water (Ji et al., 2021).

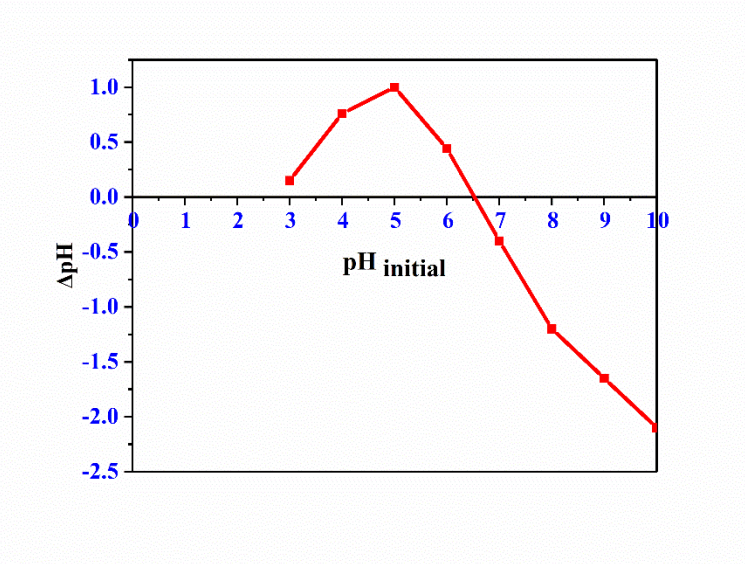


Figure 4.6. $pH_{pzc}$ of the CAC adsorbent.

## 4.2. Batch adsorption (CIP removal) results

### 4.2.1. Model fitting and analysis of variance (ANOVA) using CCD

The central composite design (CCD) was used to optimize the CIP adsorption process parameters. The CCD experimental design of CIP adsorption data is presented in appendix (Table B.1). The second-order polynomial model fitted the experimental data of CIP adsorption onto CAC ($R^2$ = 0.986). The suggested quadratic model's $R^2$ and adjusted $R^2$ were 0.990 and 0.986, respectively. ANOVA was used to assess the validity and adequacy of the model and determine the effect of main factors and possible interaction factors. ANOVA indicated that the suggested polynomial model was statistically significant. The result of the ANOVA analysis is presented in Table 4.3. As shown in Table 4.3, the F- and p-values of the model were 229.46 and < 0.0001, respectively. There is only a 0.01% chance that an F-value this large could occur due to noise. A, B, C, D, AB, BD, CD, $B^2$, and $C^2$ are significant model terms from the ANOVA. Hence, all the independent variables (initial CIP concentration, pH, contact time, and adsorbent dosage) significantly affected the CIP removal. Both Yousefi et al. (2021) and Najafpoor et al.

(2019) reported similar findings for the CIP removal using magnetization of functionalized multi-walled carbon nanotubes and γ-$Al_2O_3$ nanoparticles as an adsorbent, respectively (Najafpoor et al., 2019; Yousefi et al., 2021). In their studies, adsorption parameters, including initial CIP concentration, pH, contact duration, and adsorbent dose were significant in CIP removal from an aqueous solution.

Model terms with p-values less than 0.05 are significant, and those with p-values higher than 0.05 are insignificant. Relative to pure error, the Lack of Fit is not significant, as indicated by the Lack of Fit F-value of 1.74. There is a 28.06% chance that a Lack of Fit F-value this large could occur due to noise. As a result, a lack of fit that is not significant is desired since we want the model to fit the CIP experimental data well. Adeq precision measures the signal-to-noise ratio, and a value greater than 4 is desirable. In this design, the ratio of 56.59 indicates an adequate signal. This model can be used to navigate the design space successfully.

Table 4.3. ANOVA results of the CIP adsorption onto CAC.

| Source | Sum of Squares | df | Mean Square | F-value | p-value | |
|---|---|---|---|---|---|---|
| Model | 4671.16 | 9 | 519.02 | 229.46 | < 0.0001 | significant |
| A-Initial CIP Concentration | 787.42 | 1 | 787.42 | 348.12 | < 0.0001 | |
| B-Adsorbent dose | 2224.34 | 1 | 2224.34 | 983.38 | < 0.0001 | |
| C-pH | 144.01 | 1 | 144.01 | 63.67 | < 0.0001 | |
| D-Contact time | 691.76 | 1 | 691.76 | 305.83 | < 0.0001 | |
| AB | 326.80 | 1 | 326.80 | 144.48 | < 0.0001 | |
| BD | 129.79 | 1 | 129.79 | 57.38 | < 0.0001 | |
| CD | 138.47 | 1 | 138.47 | 61.22 | < 0.0001 | |
| $B^2$ | 150.60 | 1 | 150.60 | 66.58 | < 0.0001 | |
| $C^2$ | 102.79 | 1 | 102.79 | 45.45 | < 0.0001 | |
| Residual | 45.24 | 20 | 2.26 | | | |
| Lack of Fit | 37.98 | 15 | 2.53 | 1.74 | 0.2806 | not significant |
| Pure Error | 7.26 | 5 | 1.45 | | | |
| Cor Total | 4716.40 | 29 | | | | |

df: degree of freedom.

Based on the CCD statistical analysis, the final model equation in terms of the actual factors for CIP adsorption onto CAC is presented in Eq. (4.1), with significant factors (main and

interaction). In Eq. (4.1), A, B, C, and D are the coded values of initial CIP concentration, adsorbent dose, pH, and contact time, respectively. Whereas, AB, BD, and CD are the significant interaction parameters.

$$\text{CIP removal} = 89.49 - 5.73A + 9.63B - 2.45C + 5.37D + 4.52AB - 2.85BD + 2.94CD - 2.30B^2 - 1.90C^2 \quad (4.1)$$

The influence of each factor on the removal of CIP can be seen from their coefficients in Eq. 4.1. The coefficients of each factor are -5.98, 9.38, -2.70, and 5.12, respectively, confirming that A and C have a negative effect, whereas B and D have a positive effect on the CIP removal. The results displayed in Table 4.3 indicated that the influence of each parameter on the CIP removal followed the order: B > A > D > C, which is in agreement with the results described in Eq. 4.1. Notably, the adsorbent dose and the initial concentration of CIP had the most significant effect on the CIP removal process**.**

According to the model fit statistics, the regression parameters, such as the coefficient of determination ($R^2$), adjusted coefficient of determination, and predicted determination coefficients, are 0.987, 0.982, and 0.967, respectively. Thus, the model represents 98% of the variation in the CIP removal response. The values of model regression parameters indicate the proper fitness of the model ($R^2 > 0.96$). Using the CCD experimental design, Ashraf and his co-workers reported similar model fit statistics values ($R^2 = 0.96$) for the CIP adsorption ( Najafpoor et al., 2019b).

Diagnostic plots such as externally studentized residuals against predicted, predicted against actual, and the normal probability against externally studentized residuals were analyzed to assess the adequacy of the model. These results are presented in appendix (Figure B.1 (a-c)). The normal probability against the externally studentized residual plot shown in appendix (Figure B.1 (a)) indicated that all the points are close to the straight line, showing that the error was normally distributed. From the plot of predicted against actual shown in appendix (Figure B.1 (b)), it can be seen that the predicted values are well correlated with the actual (experimental) values, and the model predicted data were not significantly different from the experimental results. The highest residual (difference between actual and predicted) is 2.93 for the CIP removal of 88.35%. In a plot of externally studentized residuals against the predicted shown in Figure A1 (c), the

residuals were randomly distributed between +3.00 and −3.00, indicating that the CCD model successfully established the relationship between the independent variable and the CIP removal (Peng et al., 2021). Overall, the diagnostic plot results agree with the coefficient of determination values of the model. Thus, the quadratic model suggested by the CCD experimental design adequately described the experimental CIP adsorption data.

### 4.2.2. Effect of main process variables

#### i) Effect of CIP initial concentration

The effect of initial CIP concentration on the adsorption efficiency was investigated. Figure 4.7 (a)) depicted that increasing the CIP initial concentration from 10 to 40 mg/L decreased the CIP removal efficiency from 100 to 75.52% at pH (7.5), adsorbent dose (0.5 g/L), and contact time (46.25 min). In line with this result, Yousefi et al. (2021) reported that increasing the CIP concentration from 30 to 100 mg/L decreased CIP removal efficiency from 83% to 59% (Yousefi et al., 2021). On the other hand, Wang et al. investigated the effect of the initial CIP concentration (10–200 mg/L) at pH (6) and adsorbent dosage (135 mg/L) on the adsorption capacity. In their study, the adsorption capacity of the adsorbent for cationic CIP increased very quickly for CIP initial concentration of less than 50 mg/L and then decreased with the increase of CIP initial concentration above 50 mg/L (Wang et al., 2018). Hence, an increase in CIP initial concentration decreased the removal efficiency. The might be due the definite amount of active sites at a fixed adsorbent dose, such that increasing the initial concentration decreases the removal efficiency. In this study, unlike the case for CIP percentage removal, the CIP adsorption capacity increased from 20 mg/g to 60 mg/g by increasing the initial CIP concentration from 10 to 40 mg/L. The reason could be reduced resistance to CIP uptake from the aqueous solution. Moreover, the higher initial CIP concentration provides a driving force to overcome the mass transfer resistance of the CIP between the solid and aqueous phases (El-bendary et al., 2021).

#### ii) Effect of adsorbent dose on CIP sorption

The adsorbent dose has a significant effect on the CIP removal from an aqueous solution. As depicted in Figure 4.7 (b), using an adsorbent dose of 0.25g/L at pH 7.5, 30 mg/L initial CIP concentration and 46.25 min contact time resulted in 96.02 % CIP removal, whereas using an

adsorbent dose of 1.0 g/L at similar adsorption conditions almost completely removed CIP from the solution. A similar adsorption trend was observed by Gulen et al (2020) in the adsorption of CIP from water using a 2: 1 dioctahedral clay structure with the increase of CIP adsorption from 1.8% (0.034 g/L) to 99.2% (2 g/L) (Gulen & Demircivi, 2020). Moreover, Shang et al. reported a significant increase in the CIP removal efficiency from 36% to 100%, for an increase in adsorbent (herbal residue biochar) dosage from 0.025 to 0.5 g/L (Shang et al., 2016). The increase in the percentage of CIP removal with an increase in adsorbent dose is because of the increased available active sites, which enhanced the CIP uptake (Najafpoor et al., 2019b; Khoshnamvand et al., 2017).

### iii) Effect of pH on CIP sorption

The pH of the solution is an essential parameter of adsorption processes because it affects the surface nature of the adsorbent and adsorbate-adsorbent interactions (Najafpoor et al., 2019). At pH less than $pKa_1$ (6.1), the amine group in piperazine moiety receives a proton, and $CIP^+$ appears. However, for pH above $pKa_2$ (8.7), CIP occurs in anionic form ($CIP^-$) due to amine group deprotonation. At pH between $pKa_1$ and $pKa_2$ of CIP, the CIP molecule exists in zwitterionic form due to the charge balance of the amine and carboxylic groups (Yousefi et al., 2021; Zhang et al., 2017). Figure 4.7 (c) depicted that the CIP removal efficiency of CAC increased by increasing the pH of the solution from 5.25 to 7.5 and then decreased with any further increase in pH. Hence, increasing pH from 5.25 to 7.5 at fixed initial CIP concentration (20 mg/L), adsorbent dose (0.5 g/L), and contact time (46.25 min) increased the CIP removal from 93.62% to 96.02%. Further elevation of pH to 9.75 reduced the CIP removal to 94.61%. Thus, the optimal pH for CIP adsorption onto the CAC is 7.5. This pH level is important since CIP forms zwitterion, leading to the strong electrostatic attraction between CIP and negatively charged CAC ($pH_{pzc}$ of 6.5). Hence, maximum adsorption was obtained at this pH level. Dehghan et al. (2019) observed a similar adsorption trend for the CIP using a metal-organic framework (MOF). They reported that an increase in pH from 3 to 7.5 increased the adsorption of CIP onto MOF. However, at pH values above 7.5, CIP adsorption decreased. The reason for this adsorption behavior can be attributed to protonation–deprotonation reactions in groups of CIP molecules (Dehghan et al., 2019).

### iv) Effect of contact time on CIP sorption

Contact time is one of the significant factors in the adsorption of the CIP onto the CAC in this work. As shown in Figure 4.7 (d), adsorption at an adsorbent dose (0.5 g/L), pH (7.5), CIP initial concentration (20 mg/L), and the contact time (18.75 min) resulted in 79.58% of CIP removal. However, CIP removal efficiency increased to 96.02 % under similar adsorption conditions when the contact time increased to 46.25 min. Moreover, appendix (Figure B.3) showed that the adsorption rate was rapid in the first 30 minutes and moderate in 30-70 minutes. This may be attributed to the availability of abundant free active sites on CAC at the initial adsorption stage for CIP sorption. The rate slowed after 70 minutes, and no appreciable CIP removal was achieved. Hence, equilibrium was reached at about 70 min. The number of available active sites decreases with time, and eventually, the adsorbent becomes saturated (El-bendary et al., 2021). For CIP adsorption process optimization, adsorption experiments were conducted using the contact time range (less than 60 min), which was intentionally taken to investigate the effect of contact time and its interaction effects. Increasing the contact time allowed CIP molecules to reach the active sites of the adsorbent up to equilibrium time. Beyond the equilibrium time, no significant CIP uptake occurred, as depicted in appendix (Figure B.3).

## 4.2.3. Effect of interaction variables

RSM is a powerful tool with important features for evaluating the interactive effect of variables. In this study, 3D surface plots (Figure 4.8 (a-c)) were used to study the interaction effects on CIP removal. The significant interaction effects include initial CIP concentration-adsorbent dose, adsorbent dose-contact time, and pH-contact time.

### a) CIP initial concentration and adsorbent dose interaction effect

The interaction effect of CIP initial concentration and the adsorbent dose is shown in Figure 4.8 (a). The interaction effect of CIP initial concentration and the adsorbent dose was positively significant. The 3D plot shows that the CIP removal was highest at the initial CIP concentration range of 20-25mg/L and adsorbent dose range of 0.75–1.0 g/L. In this range of initial concentration (20-25 mg/L), increasing the adsorbent dose increases the removal efficiency.The

enhanced removal of CIP at the higher CAC dose was due to higher active sites for CIP adsorption (Bhattacharya et al., 2021).

**b) Adsorbent dose and contact time interaction effect**

The interaction effect of CAC dose and the contact time on CIP removal is displayed using a 3D plot in Figure 4.8 (b). The CIP removal was highest for the CAC dose of 0.75-1.0g/L and 40-46 min reaction time. This study revealed that CIP removal increased with contact time and adsorbent dose. This may be attributed to the availability of more active sites with adsorbent dose increment and enough contact time for CAC and CIP molecules to interact (Bhattacharya et al., 2021).

**c) pH and contact time interaction effect**

The interaction effect of pH and contact time on CIP removal is shown in Figure 4.8 (c). The percentage of CIP removal increased with an increase in contact time. A kinetics study showed that the adsorption rate was rapid in the first 30 minutes and became slow after 30 minutes. The CIP adsorption is strongly dependent on the pH of the solution. CIP exists in zwitterion form at pH between 6.1 and 8.7, and the electrostatic interaction between CIP and CAC is strong. The point of zero charge of CAC was 6.5, and for pH less than 6.1 and beyond 8.7, the repulsive forces became dominant, and less CIP removal was achieved. Thus, this pH range is an optimum pH level for the highest CIP removal. Figure 4.8 (c) depicted that when pH decreased from 9.75 to 5.25 with an increase in contact time from 18.75 to 46.25 min, the CIP removal increased from 71.88 to 93.62%. In contrast, an increase in pH and a decrease in contact time decreased CIP removal. The reverse of this condition decreased the CIP removal. This showed that contact time had a superior influence on CIP removal than pH for interaction effects. However, for an increase in pH and contact time from 5.25 min and 18.75 min to 9.75 and 46.25 min, CIP removal increased from 83.07% to 94.61%, respectively. Maximum CIP removal (96.02) was obtained at pH (7.5) and contact time (46.25 min) using CAC adsorbent.

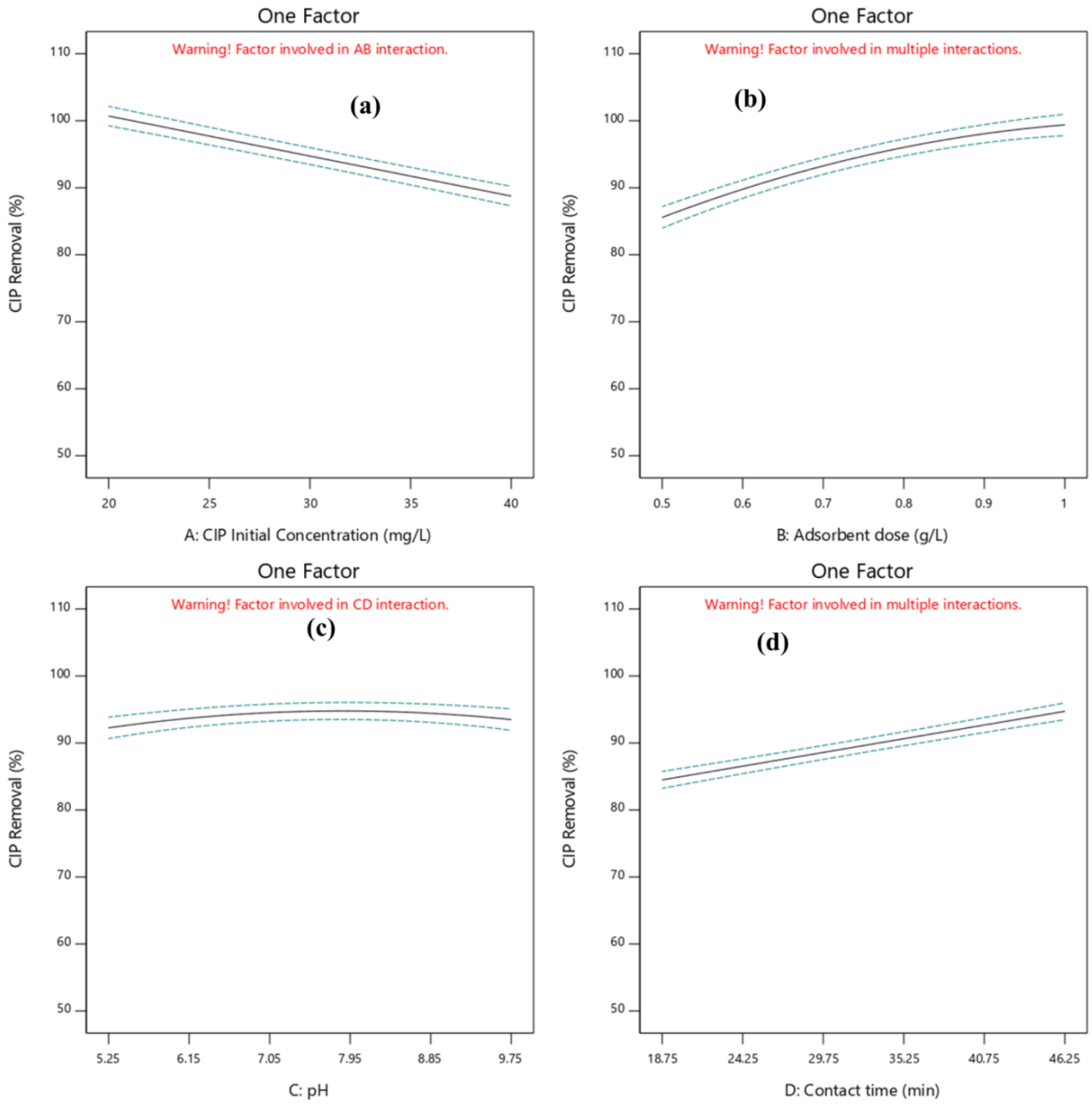


Figure 4.7. The influence of main effects on CIP removal using CAC (a) CIP initial concentration, (b) adsorbent dose, (c) pH and (d) contact time.

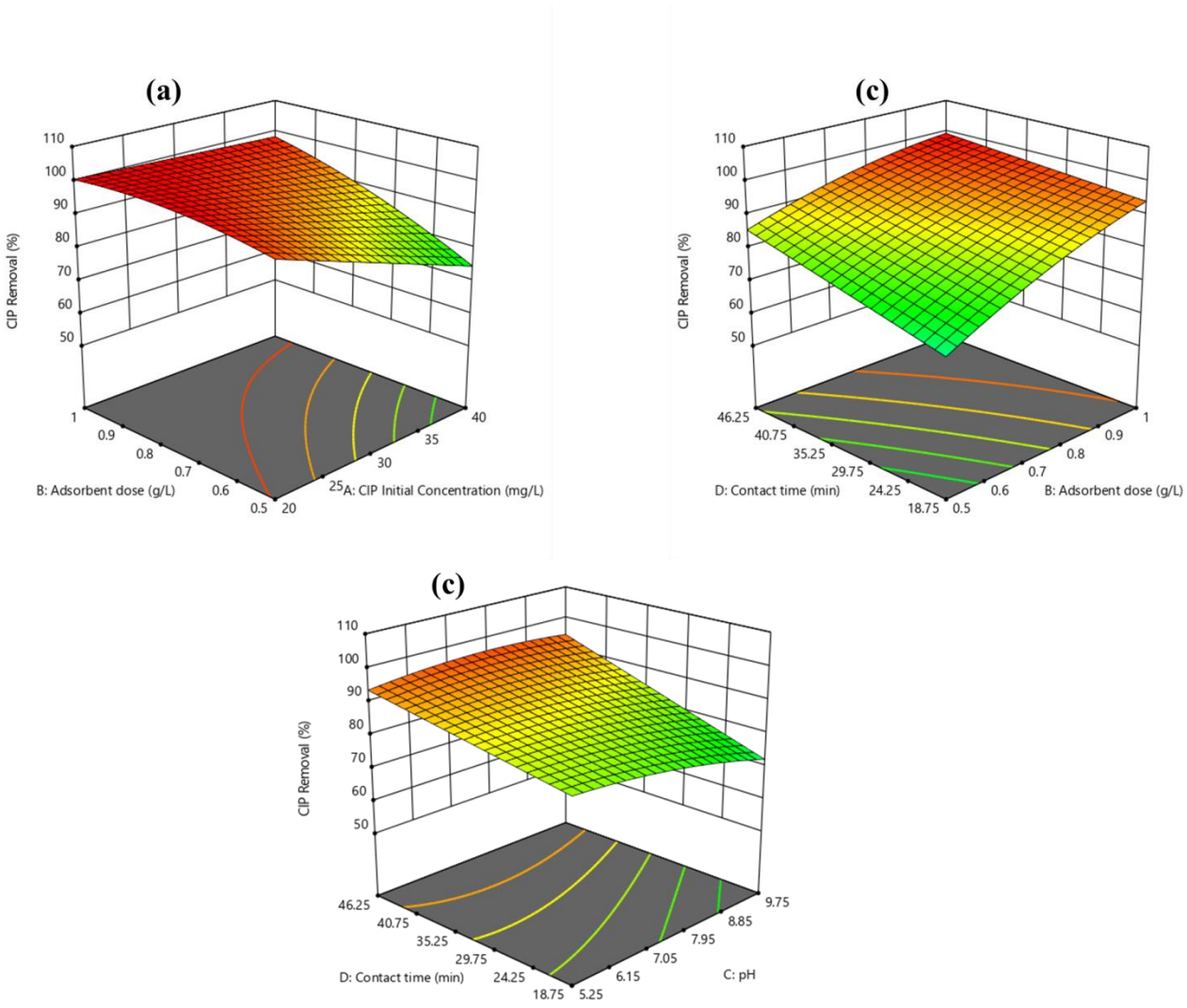


Figure 4.8. Interaction effects (a) adsorbent dose versus CIP initial concentration (b) contact time versus adsorbent dose (c) contact time versus pH.

### 4.2.4. Process optimization of CIP sorption

The optimization approach followed in CCD design to obtain the best operating conditions was through minimizing the adsorbent dosage, taking the initial CIP concentration, pH, and contact time in the range, and maximizing CIP removal. Based on this criterion, the optimal condition that gave maximum CIP removal efficiency (96.02%) using the CAC adsorbent was pH (7.5), adsorbent (0.5 g/L), contact time (46.25 min), and initial CIP concentration (20 mg/L) with a good desirability value of 0.97. Adsorption tests were conducted at these optimum conditions to

confirm the model's credibility. Accordingly, 95.7%, 96.42%, and 96.24% CIP removal values were obtained, and the mean value of these results is 96.11%. Thus, the model predicted CIP removal (96%), which was close to the experimental value obtained (96.11%), showing that the model is valid.

### 4.2.5. Regeneration of CAC after single CIP adsorption

The CIP removal efficiency of CAC after first cycle desorption with 0.3 M NaOH, Methanol, 3% NaOH + methanol, and 0.3M HCl was 72.7, 47.09, 67.96, and 93.56%, respectively. Hence, 0.3 M HCl was used as an eluent for CIP desorption throughout the regeneration study. After 5 sequential adsorption-desorption cycles, the removal of CIP by CAC varied from 95.68% to 88.13% (reduction of 7.55%) as shown in Figure 4.9. The reusability studies revealed that 88% of CIP can be removed even in the fifth cycle suggesting enhanced stability and reusability of CAC. The CIP is highly soluble in HCl and the concentration of HCl used (0.3 M) for regeneration is not strong enough to significantly damage the functional groups of the adsorbent (-OH, C-H, C-O and Fe-O) at first adsorption cycles. However, the observed gradual reduction of removal efficiency might be due to the loss of the functional groups of the CAC. The reusability of the CAC without significant loss in CIP removal is one of the benefits of this process regarding environmental concerns and economic feasibility.

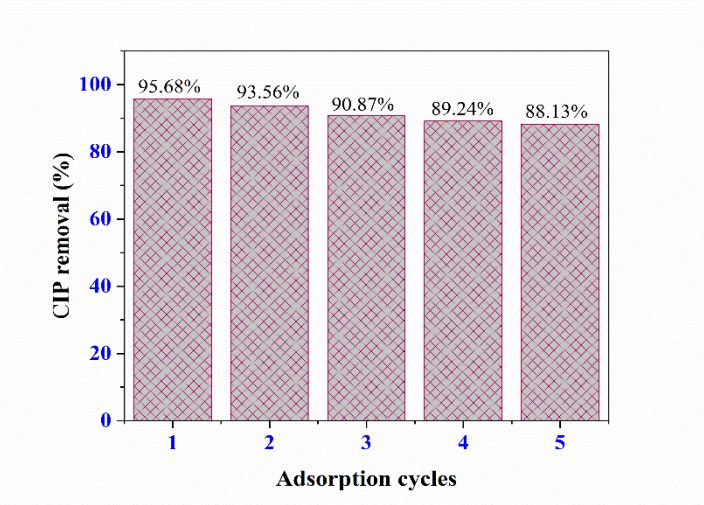


Figure 4.9. The CIP removal efficiency of CAC per each adsorption cycle.

## 4.3. Batch adsorption (ACM removal) results

### i) Effect of pH on ACM sorption

The influence of pH on the adsorptive removal of ACM by CAC is depicted in Figure 4.10 (a). ACM is a weak electrolyte that can exist in two forms, non-ionized (acid) and ionized (base) forms, depending on its pKa value (9.38) and the pH of the solution ( Igwegbe et al., 2021; Taylor et al., 2015). When the solution pH is less than the pKa value of ACM, it mainly exists in neutral and non-ionized forms (Moussavi et al., 2016). The pH values from 2 to 8 did not significantly affect ACM adsorption onto CAC. At this pH range, ACM molecules mainly exist in neutral or non-ionic forms (Moussavi et al., 2016), which leads to negligible electrostatic attraction. However, a further increase in pH from 8 to 12 notably decreased ACM removal from 99.7% to 93.85%. This can be explained by considering the pKa value of ACM (9.38) and the point of zero charge of CAC adsorbent (6.5). The surface of CAC is negatively charged above $pH_{pzc}$ (6.5). In contrast, it is positively charged below the solution pH of 6.5. Solution pH higher than the pKa value of ACM (9.38) did not favour the adsorption of ACM onto CAC due to electrostatic repulsion between the negatively charged adsorbent surface and anion of ACM (Kumar et al., 2021). In this regard, a solution of pH 8 was considered for ACM adsorption onto CAC. Other previous studies (Natarajan et al., 2021; Taylor et al., 2015) have also reported a similar trend for the influence of pH on the adsorption of ACM onto various adsorbents.

### ii) Effect of contact time on ACM sorption

The effect of contact time on ACM adsorption was studied for contact time ranging from 20 to 120 min at ACM (20 mg/L), CAC (0.5 g/L), and pH (8.0). As depicted in Figure 4.10 (b), ACM adsorption onto CAC was increased from 95.22% to 99.72% when contact time was increased from 20 to 90 min. The increase in ACM removal with time is related to the time the ACM molecules require to come in contact with the CAC. In this study, the synthesized CAC adsorbent material has a high surface area, providing higher adsorption active sites for the ACM molecule. Thus, ACM adsorption requires enough time for the adsorption until the CAC saturates. However, further contact time did not significantly increase ACM removal. This is because of the attainment of equilibrium (Natarajan et al., 2021). The equilibrium time

determined for the adsorption of ACM onto CAC was (90 min). Hence, contact time (90 min) was optimal for ACM adsorption onto CAC adsorbent.

### iii) Effect of ACM initial concentration

Adsorbate initial concentration plays a significant role in the adsorption process. Initial adsorbate concentration can be an important driving force in overcoming mass transfer resistance between aqueous and solid phases (Mondal et al., 2016). Figure 4.10 (c) represents the effect of ACM initial concentration over the ACM concentration range of 10 mg/L to 120 mg/L. The removal efficiency decreased from 99.97% to 77.7% when ACM increased from 10 mg/L to 120 mg/L. The decrease in ACM removal with ACM initial concentration is due to the limited adsorption sites and a decrease in intra-particle diffusion (Wong et al., 2018). Here, 20 mg/L ACM concentration was taken as an optimal ACM concentration for investigating CAC performance. Most of the previous works considered ACM concentration of 20 mg/L or less for evaluating the adsorptive capacity of various adsorbents (Marqués et al., 2015; Nafisur & Nasir, 2020; Yanyan et al., 2018). As ACM is present in trace quantity in surface water, a low concentration of ACM should give a high removal percentage (Natarajan et al., 2021).

### iv) Effect of adsorbent dose on ACM sorption

The effect of the adsorbent dose profile was studied by varying the CAC dose from 0.125 g/L to 1.6 g/L for 20 mg/L ACM concentration. As presented in Figure 4.10 (d), it was observed that ACM removal increased from 92.45% to 99.65% when the adsorbent dose increased from 0.125 g/L to 0.5 g/L. This is because an increase in mass results in more available sorptive surface area and, as a result, more active sorption sites (Mondal et al., 2016). As depicted in Figure 4.7 (d), an adsorbent dose of 0.5 g/L almost completely removed 20 mg/L of the ACM from water. Thus, increasing the CAC dose beyond 0.5 g/L has no significant increase or benefit. Besides, an increase in adsorbent dose is directly related to the operational cost (Shi et al., 2019). In the environment, ACM is present at the ppb level; hence, using a high quantity of the adsorbent will not increase adsorption capacity (Natarajan et al., 2021). Given these facts, a CAC dose of 0.5 g/L is considered optimal for ACM removal at pre-determined ACM initial concentration, contact time and pH values.

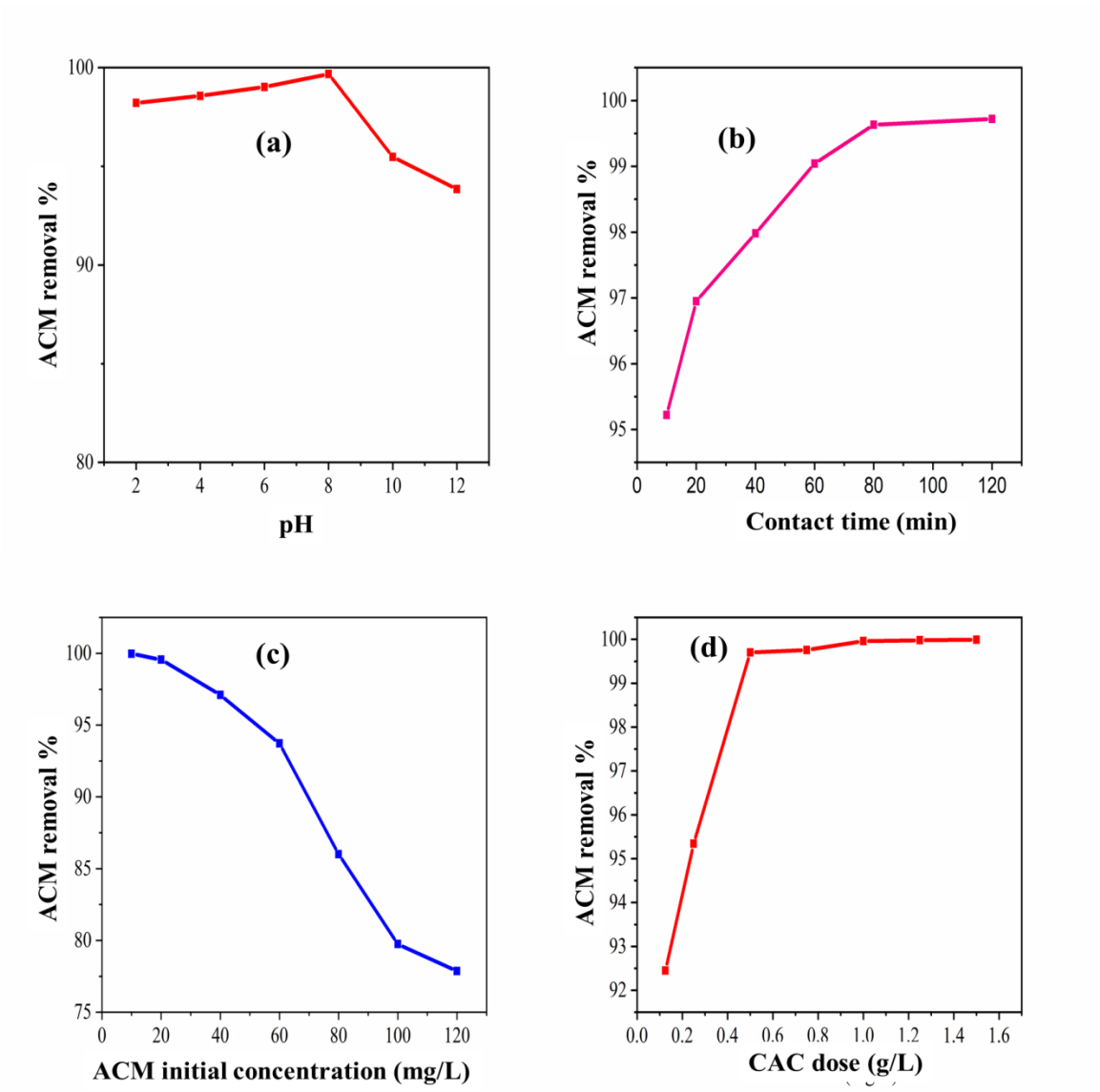


Figure 4.10. The effect of pH (a), contact time (b), ACM initial concentration (c) and CAC dose (d) on the single component adsorption of ACM from water.

### 4.3.1. Regeneration of CAC after single ACM adsorption

The ACM removal efficiency of CAC after the first adsorption-desorption cycle with 0.3 M NaOH, Methanol, 3% NaOH + methanol, and 0.3M HCl was 60.3%, 40.25%, 63.62%, and 90.24%, respectively. Consequently, 0.3 M HCl was used as a desorbing solution for ACM throughout the reuse study. The removal of ACM varied from 98.97% to 80.34% after five consecutive adsorption-desorption cycles, as shown in Figure 4.11. This result revealed that

CAC could be effectively employed for five consecutive adsorption cycles, capable of removing 80% of ACM from water at the fifth cycle. These regeneration study results indicated that the ACM removal efficiency of CAC was faintly diminished after each cycle and then nearly constant in the fifth cycle. Similar to the CAC reuse after CIP adsorption, the observed gradual reduction in ACM removal efficiency might be due to the gradual loss of functional groups of the CAC. Hence, the reusability of the CAC up to five consecutive cycles for ACM removal with higher removal efficiency shows the promising potential of the CAC for application in emerging contaminant (ACM) removal.

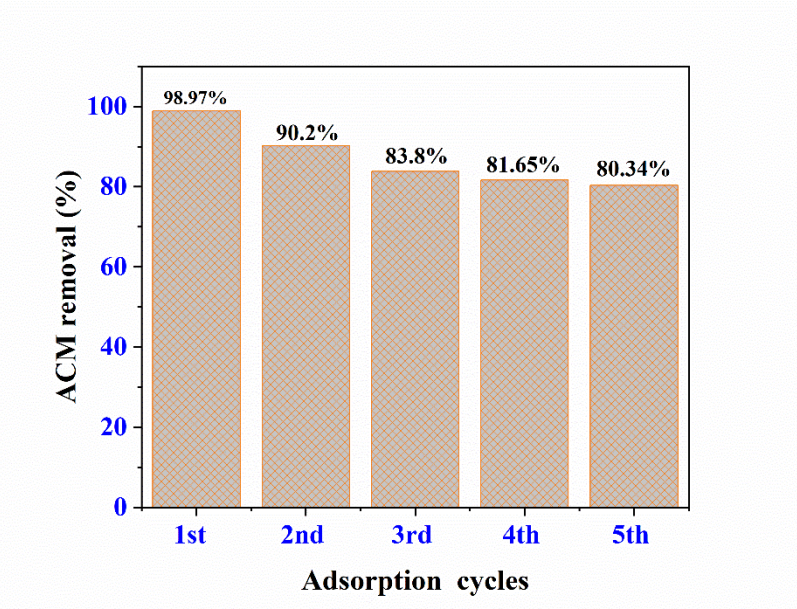


Figure 4.11. The ACM removal efficiency of CAC per each adsorption cycle.

## 4.4. Batch adsorption (single and binary component removal)

The single component sorption of ACM and CIP onto CAC was optimized in sections 4.2 and 4.3, respectively. Studies on the single component adsorption of ACM and CIP gave insights into the single component adsorptive characteristics of ACM and CIP, and the optimum operational conditions were determined. The optimized initial pharmaceutical contaminant dose (20 mg/L) was used in the subsequent simultaneous adsorption of ACM and CIP onto the CAC. The individual adsorption characteristics of ACM and CIP were further explored to facilitate a

comparative investigation with the binary component adsorption process. The calibration curve equations are provided in appendix (Table B.3).

### i) Influence of solution pH on single and binary component adsorption

The obtained experimental data demonstrated that the single and binary component adsorption exhibited a similar trend of solution pH influence on ACM and CIP removal (Figure 4.12). The removal efficiency increased as the solution pH increased; it reached its maximum at a pH of 6.8 and decreased beyond this pH. The decrease in ACM and CIP adsorption beyond solution pH 6.8 can be due to the effect of electrostatic repulsion. The point of zero charge ($pH_{pzc}$) of CAC was 6.5. Therefore, CAC is positively charged at a solution pH less than $pH_{pzc}$ (6.5) and negatively charged at a pH higher than $pH_{pzc}$ (Figure 4.12). In solution, CIP can be anionic (pH > 8.7), cationic (pH < 6.1), and zwitterionic (6.1 < pH < 8.7), depending on the solution pH. However, ACM predominantly exists in its neutral form for solution pH ranging from 2 to 8 and is less influenced by pH variation in this range (Georgin et al., 2021). Higher sorption performance was noted for ACM and CIP at pH values between 6.5 and 8.0, suggesting a higher electrostatic attraction between CAC and ACM/CIP in this range. However, significant electrostatic repulsion was observed in pH ranges (pH < 6.5 and pH > 8.7), as evidenced by the reduction in the uptake of ACM and CIP in single and binary pollutant sorption. According to the results, the optimum pH for both single and binary systems was found to be 6.8.

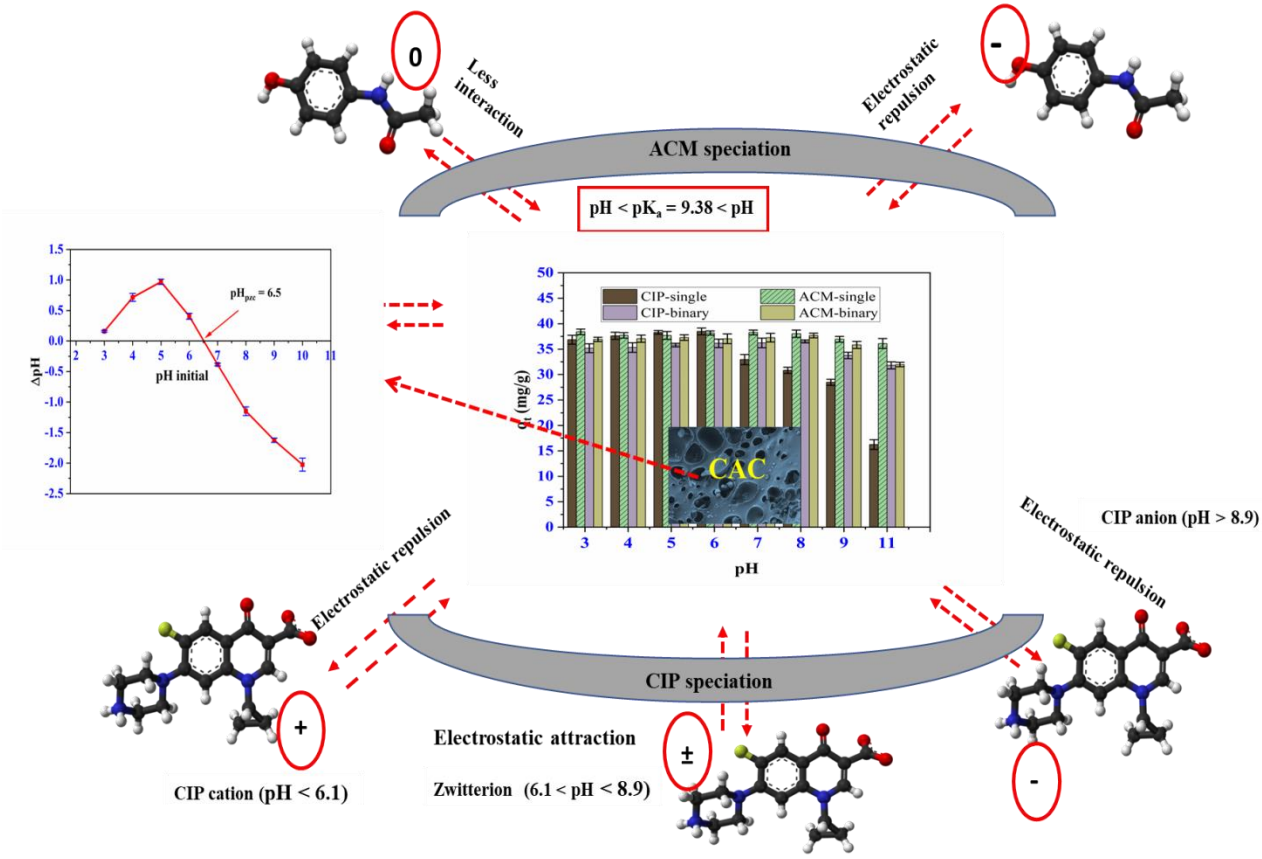


Figure 4.12. Influence of pH on single and binary sorption of ACM and CIP (experimental conditions: ACM/CIP concentration = 20 mg/L, CAC dose = 0.5 g/L, contact time = 120 min).

### ii) Influence of CAC dosage on single and binary component adsorption

The adsorbent dose directly affects the removal efficiency and economic aspects of the adsorbent in practical applications. Figure 4.13 presents the ACM and CIP removal efficiency as a function of CAC dose in single and binary component systems. The removal of ACM in a single component system increased from 89.95% to 99% when the CAC dose increased from 0.25 g/L to 0.5 g/L. Similarly, the removal of CIP increased from 79.6% to 95% for the same increment in the CAC dose. This result shows a higher affinity of CAC to ACM due to its molecular properties (smaller molecular size and relatively higher log $K_{ow}$). ACM has demonstrated no significant removal beyond 0.5 g/L, whereas CIP removal was increased from 95.1% to 99.36% when the CAC dose increased to 1.0 g/L. The increasing trend of removal efficiency with adsorbent dose is due to the higher number of adsorption sites at higher adsorbent doses

(Natarajan et al., 2022). In the binary system, ACM and CIP removal efficiency increased from 74.96% and 70.16% to 98.65% and 98.54%, respectively, when the CAC dose increased from 0.25 g/L to 1.0 g/L. Nearly complete removal was achieved when the CAC dose was further increased to 1.25 g/L in the single (> 99.3%) and binary component (> 99.05%) sorption systems for ACM and CIP. The CAC dose of 0.5 g/L was considered the optimum value for the comparative evaluation of these systems.

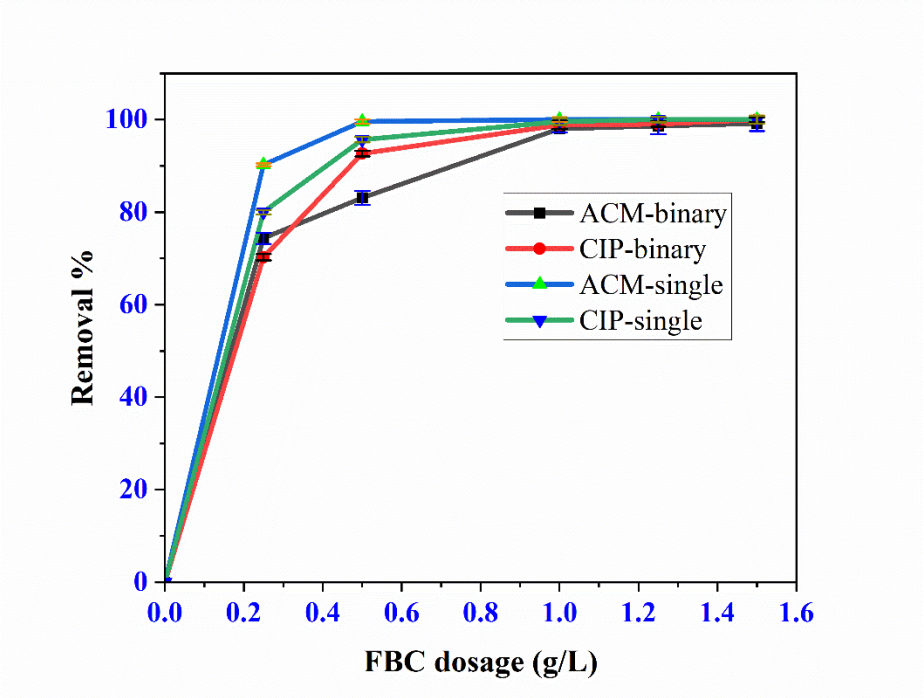


Figure 4.13. Influence of CAC dose on the single and binary sorption of ACM and CIP (experimental conditions: ACM/CIP concentration = 20 mg/L, pH = 6.8, contact time = 120 min).

**iii) Influence of particle size on single and binary component adsorption**

In the adsorption process, the particle size influences the adsorption of sorbate onto sorbent. Generally, removal efficiency decreases with increasing particle size of the adsorbent. This study investigated the influence of adsorbent particle size (<150, 150 - 425, 425 - 600, and 600 - 850 μm) on single and binary component sorption of ACM and CIP using CAC. Adsorbent surface area, pore volume and pore size are directly related to its particle size. Consequently, the removal efficiency is greatly influenced by variations in the adsorbent particle size. Table 4.4 presents the

effect of adsorbent particle size on the removal (%) of ACM and CIP in single and binary component adsorption. In a single component system, a significant decrease in CIP removal (95.4% to 27.84%) was observed when the CAC particle size increased from 150 µm to 800 µm, while ACM showed a reduction from 95.44% to 53.21%. Particle size had a more significant effect on ACM removal (%) in binary component adsorption, as its removal efficiency decreased significantly from 93.74% to 9.5% when the particle size increased from 150 µm to 800 µm.

In comparison, CIP exhibited a relatively lower reduction in removal efficiency (92.96% to 50.45%). The disparity in the influence of particle size on pollutant removal (%) for ACM and CIP can be attributed to the competition between these pollutants for available active sites. The simultaneous adsorption of ACM and CIP is highly dependent on the physico-chemical properties (pore volume, pore size and surface area) of the adsorbent due to their molecular size difference. As shown in Table 4.4, the difference in molecular size between ACM (smaller compound) and CIP (larger compound) resulted in a more pronounced suppressive effect on the removal of ACM (%) due to the pore blockage phenomenon caused by CIP. Similar research findings were reported regarding the effect of particle size on the removal of ACM and CIP (Patel et al., 2021). Table 4.4 presents the experimental results of the removal (%) of ACM and CIP from water using different CAC particle sizes.

Table 4.4. Effect of the particle size on the removal of ACM and CIP from water using CAC.

| Particle Size | Single component | | Binary component | |
|---|---|---|---|---|
| | ACM removal (%) | CIP removal (%) | ACM removal (%) | CIP removal (%) |
| <150 µm | 99.44 | 95.48 | 93.74 | 92.96 |
| 150-425 µm | 86.84 | 38.97 | 41.94 | 49.34 |
| 425-600 µm | 74.09 | 28.44 | 26.06 | 38.10 |
| 600-850 µm | 53.21 | 27.84 | 9.50 | 20.45 |

**iv) Influence of ionic strength on single and binary component adsorption**

The wastewater matrix contains a specific concentration of salt ions, and their presence in the solution considerably affects the adsorption behaviour of micro-pollutants (Maged et al., 2021). The simultaneous sorption of ACM and CIP onto CAC in an electrolyte (0.025-0.1 M NaCl) solution was investigated (Figure 4.14). Under optimum binary component adsorption conditions, the removal of ACM and CIP was 93.98% and 91.86%, respectively, in the control experiment (without NaCl). Increasing ionic strength (0 to 0.05M NaCl) increased the removal of ACM and CIP to 94.04% and 93.33%, respectively. On the contrary, a further increase in ionic strength (0.05 to 0.1 M NaCl) resulted in a significant reduction in the removal of ACM and CIP, with the respective removal efficiencies dropping to 65.05% and 60.75%. Similarly, ACM and CIP removal increased with increasing ionic strength (0 to 0.05 M NaCl) in the single sorption systems from 98.45 and 96.14% to 99.59 and 98.28%, respectively. However, the ACM and CIP removal efficiency dropped to 73.89 and 68%, respectively, with increasing the NaCl up to 0.1 M. It should be noted that CIP removal was highly influenced by the electrolyte compared to ACM. This could be attributed to the adsorption mechanism of CIP onto CAC, which strongly depends on the electrostatic attraction. The lesser impact of ionic strength on the sorption of ACM can be ascribed to its mild sensitivity to changes in pH (2-8) during the adsorption process. This can be explained by the significant dependence of the CIP sorption mechanism on the pH of the solution (electrostatic attraction). Previous studies have reported similar trends of enhanced pharmaceutical contaminants removal by increasing ionic strength to a certain extent using pristine and NaOH activated carbon derived from spent coffee (Shin et al., 2021). These findings suggest that carbon-based adsorbents undergo surface charge neutralization through double-layer compression, while the reduced solubility of pharmaceuticals can be attributed to the presence of $Na^+$ concentrations in the solution, resulting in salting-out effects (Shin et al., 2020). However, upon a further increase in ionic strength, a screening effect could occur between the carbonaceous adsorbent and the target pharmaceutical contaminant, thereby reducing the adsorption of the pharmaceutical contaminants (Zhao et al., 2016). As a result, the findings from the ionic strength study revealed that the adsorptive removal of pharmaceutical contaminants (ACM and CIP) is influenced by the characteristics of the water matrix, such as the ionic strength.

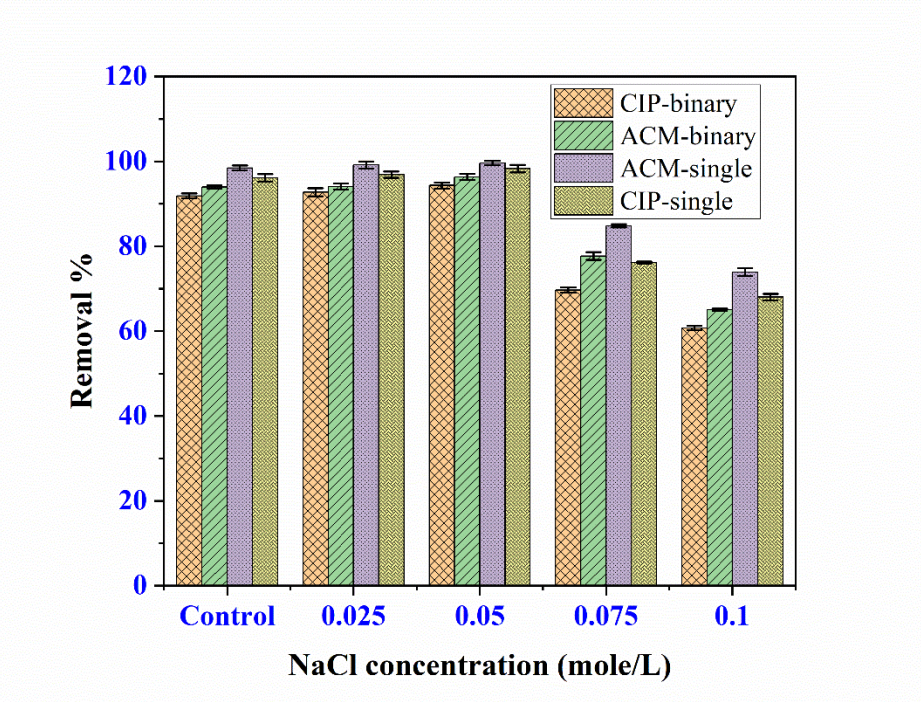


Figure 4.14. Influence of ionic strength on the single and binary sorption of ACM and CIP (experimental conditions: ACM/CIP concentration = 20 mg/L, CAC dose = 0.5 g/L, pH = 6.8, contact time = 120 min).

**ii) Influence of water matrix on single and binary component adsorption**

The water background matrix is an environmental factor that can affect the efficiency of water treatment processes. Therefore, this study assessed the influence of the water matrix (pure, tap water and real wastewater) on the sorption of ACM and CIP by the CAC adsorbent under the optimized conditions outlined earlier. The wastewater sample was collected from Akaki Kality wastewater treatment plant secondary effluent (Addis Ababa, Ethiopia). The characteristics of the wastewater are presented in appendix (Table A.1). In wastewater analysis, the dosage of CAC was varied to determine the amount required to completely remove pharmaceuticals. This investigation helps to understand the applicability of CAC in a real water matrix. Figure 4.15 (a) shows CIP removal (%) in different water matrices with CAC dose varying from 0.25 g/L to 1.5 g/L from the binary mixture. At a CAC dose of 0.5 g/L, more than 90% removal of ACM and CIP was achieved in pure water. However, removal (%) decreased to 61.64% for CIP when applied to real wastewater at a similar CAC dosage. In contrast, increasing the CAC dosage from

0.25 g/L to 1.5 g/L increased CIP removal (%) from 69.95% to 99.5%, 30.25% to 94.2%, and 19.82% to 86.06% in pure, tap, and real wastewater, respectively. Complete removal of CIP in binary component adsorption was achieved using CAC (1.5 g/L) in both pure water and tap water matrices. Increasing the adsorbent dosage provides more active sites, enhancing CIP adsorption. Similarly, an increase in CAC dose (Figure 4.15 (a)) from 0.25 g/L to 1.5 g/L increased the removal efficiency of ACM in the binary mixture from 75.1%, 35.5%, and 23.4% to 97.2%, 97.72% and 91.9 % in pure, tap and wastewater, respectively. The relatively lower removal efficiency observed for both pollutants in real wastewater is due to various organic and inorganic competing ions in the wastewater matrix. A similar water matrix effect on the sorption was observed in the single component adsorption of ACM and CIP using CAC (Figure 4.15 (b)). Interestingly, the CAC adsorbent exhibited substantial removal efficiencies for ACM and CIP in all water matrices tested. The superior removal efficiency observed in various water matrices can be related to high surface area (1158.05 $m^2/g$), plentiful pores (shown by SEM images), and essential functional groups (-OH, C-O, C-H and Fe-O) of CAC.

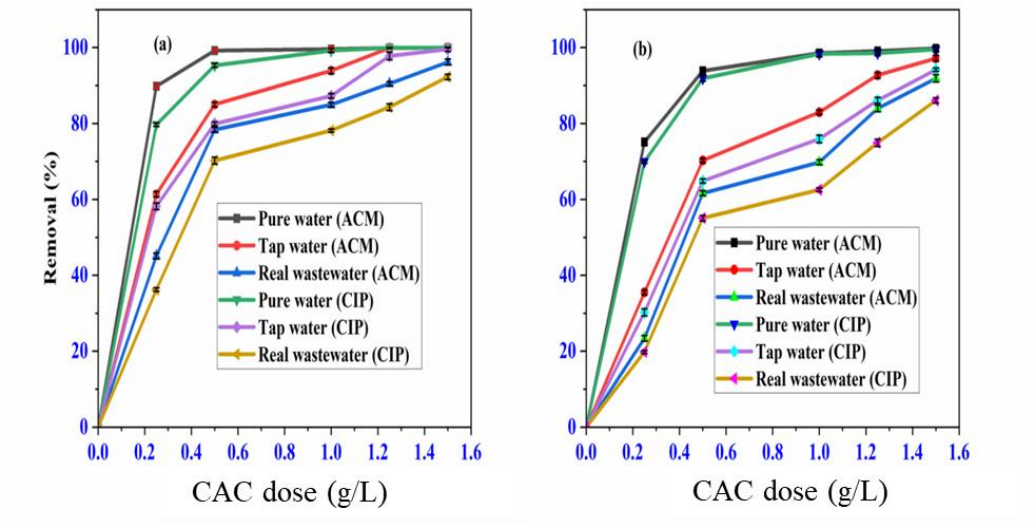


Figure 4.15. Influence of water matrix on ACM and CIP removal (a) single component sorption and (b) binary component sorption (experimental conditions: ACM/CIP concentration = 20 mg/L, pH = 6.8, contact time = 120 min).

### 4.4.1. Kinetic modelling of single and binary sorption

The kinetics of the individual sorption processes of CIP and ACM were initially analyzed using linear equations derived from the pseudo-first-order, pseudo-second-order, intra-particle, and Elovich models. This analysis provided crucial insights into the adsorption mechanisms of these contaminants. In both ACM and CIP single sorption, the linear form of the pseudo-second-order model provided the best fittings results (highest $R^2$ and experimental adsorption capacity ($q_{e,\ exp}$) close to calculated adsorption capacity ($q_{e,\ cal}$) as shown in appendix Figures (B.3-B.4) and Table 4.5. The kinetic modelling results of the single sorption of ACM and CIP were further confirmed by employing the non-linear forms of kinetic models such as the pseudo-first-order model (PFO) and pseudo-second-order (PSO) and Avrami (AV) models as depicted in Figure 4.16 (a and c) and Table 4.6. The findings from the kinetic investigation of the single sorption of ACM and CIP using non-linear models agree with the results obtained from the linear models, indicating the reliability of the pseudo-second-order (PSO) model. The non-linear forms of these models were also employed for the binary sorption of ACM and CIP, as shown in Figure 4.16 (b and d). The binary component adsorption kinetics shows the antagonistic behaviour of pollutants in a binary pollutant solution.

The experimental kinetic data were analyzed using non-linear forms of kinetic models such as the pseudo-first-order model (PFO), pseudo-second-order (PSO), and Avrami (AV) for ACM and CIP in single and binary sorption experiments (Figure 4.16 (a-d)). The experimental data illustrates that the equilibrium for the single component adsorption of CIP was achieved relatively fast at 70 min (Figure 4.16 (c)), which can be attributed to its large molecular weight. On the other hand, the single component adsorption of ACM (Figure 4.16 (a)), which has a smaller molecular weight, reached equilibrium more slowly, taking about 90 min. As shown in Figure 4.16 (b and d), the binary component adsorption (ACM and CIP) onto CAC was rapid in the initial 60 and 100 min, with removal efficiencies exceeding 95% and 90% in single and binary component adsorption, respectively. The rapid initial adsorption observed is due to the ample vacant active sites on CAC and an adequate concentration of pollutant molecules. After the initial rapid adsorption, the adsorption rate gradually slowed, with equilibrium achieved in less than 90 min for single component adsorption and around 120 min for binary pollutant adsorption. This observation indicates that the available active sites of CAC become occupied

(saturated), and the adsorption rate slows down. The employed kinetic models were evaluated based on the coefficient of determination ($R^2$), sum of squared error (SSE), root mean square error (RMSE), and closeness of experimental equilibrium capacity ($q_{e,\ exp}$) with the model predicted equilibrium capacity ($q_{e,\ cal}$). In all cases, PSO showed the lowest (SSE and RMSE), highest ($R^2$), and acceptable $q_e$ (values close to experimental $q_e$) values, as shown in Table 4.5. Additionally, the linear kinetic model analysis in appendix (Figure B.4- B.5) provided PSO model as a best model for single sorption of ACM/CIP. Therefore, the PSO model best described the kinetic behavior of single and binary sorption of ACM and CIP onto CAC. The PSO rate constant for binary sorption of ACM and CIP is lower than the PSO rate constant for ACM and CIP in the single sorption systems. This can be explained by the competitive effect of the pharmaceuticals in the binary mixture that reduced the adsorption rate, as confirmed by the longer equilibrium time compared to the single sorption systems. The kinetic study results suggest that the chemisorption mainly controlled the removal of ACM and CIP from water in single and binary component sorption systems. Furthermore, the FTIR and XRD results indicated that oxygen-containing functional groups were observed on the surface of CAC. The observed Fe-O on the surface of the CAC contributed to the complexation and Lewis-acid base reaction, which are indicative of the chemisorption behavior of the ACM/CIP adsorption onto the CAC in addition to the PSO kinetic model results. Moreover, the observed π-π interaction mechanism is likely represents the chemical sorption of ACM/CIP onto the CAC. Overall, these results indicated that the single and binary sorption of ACM/CIP onto the CAC was a chemisorption process.

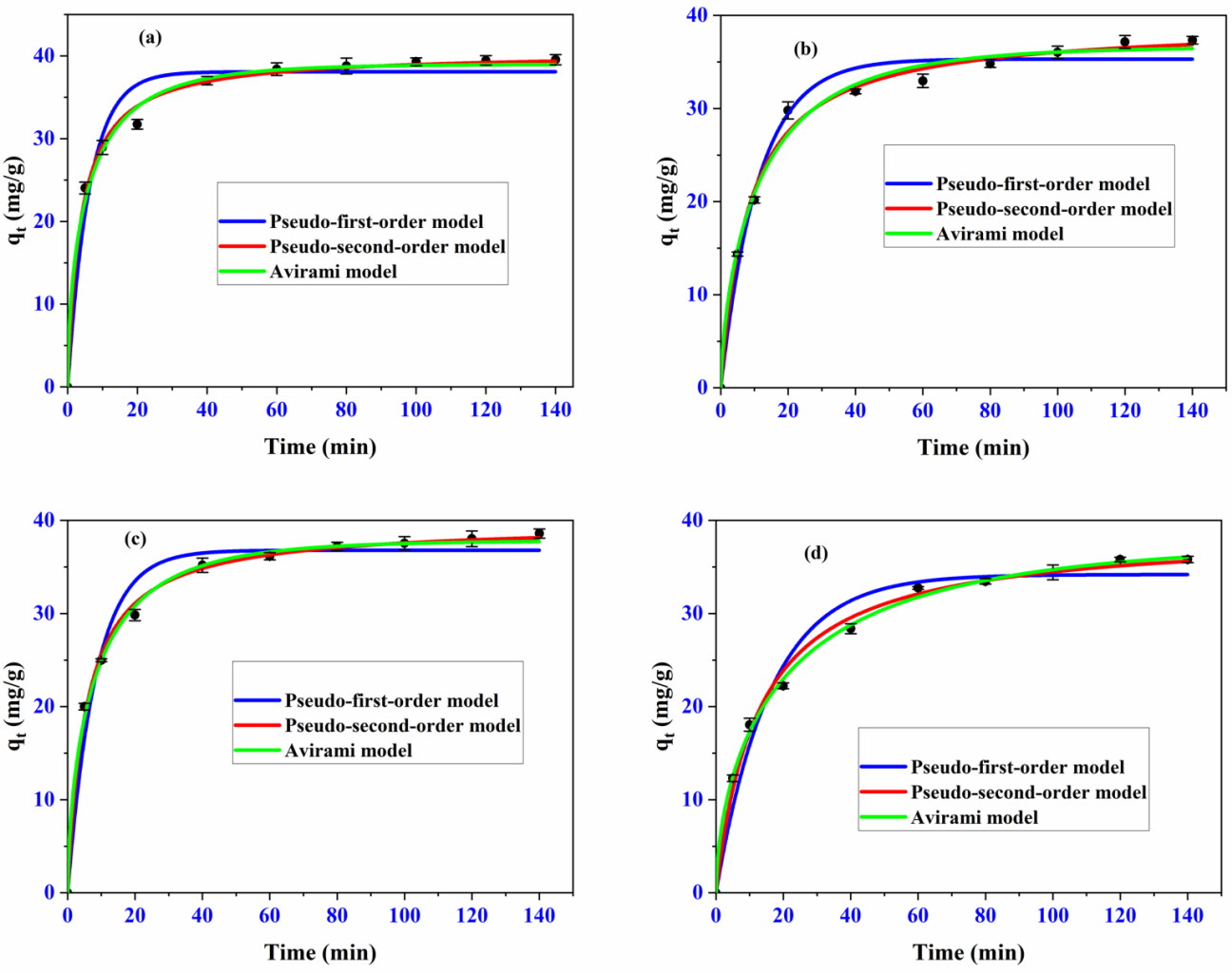


Figure 4.16. Non-linear kinetic models employed for ACM and CIP removal from water in single and binary component adsorption systems. (a) Single sorption ACM kinetics; (b) binary sorption ACM kinetics; (c) single sorption CIP kinetics; (d) binary sorption CIP kinetics (experimental conditions: ACM/CIP concentration = 20 mg/L, pH = 6.8, CAC dose = 0.5 g/L).

### 4.4.2. Single component isotherm analysis

The single component experimental isotherm data was evaluated using two-parameter adsorption isotherm models, namely Langmuir and Freundlich, as well as a three-parameter model (Sips). The non-linear isotherm models for single sorption of ACM/CIP are provided in Figures 4.17 (a-b). The linear isotherm models parameters are also provided in appendix (Figure B.6- Figure B.7) and Table B.2). The results indicated that the adsorption capacity of CAC increased as the

concentrations of ACM and CIP increased, eventually reaching saturation in single and binary sorption systems (Figure 4.17 (a-b)). The employed isotherm models were assessed based on the goodness of fit criteria ($R^2$, SSE, and RMSE) values (Table 4.5). Among the three models employed, the Sips model best described the experimental data of ACM and CIP sorption (single component systems). The Sips isotherm model is a combined form of the Langmuir and Freundlich isotherm models and applies to heterogeneous adsorption systems (Tzabar & Brake, 2016). The isotherm analysis result corroborates the multi-layer sorption of ACM and CIP onto the heterogeneous surface of CAC at lower sorbate concentrations and mono-layer sorption at higher sorbate concentrations (Maged et al., 2023). Based on the FTIR results before and after adsorption, there are various functional groups on the surface of CAC responsible for ACM/CIP removal. Therefore, the active sites are heterogeneous. The multilayer adsorption at low concentration indicates that the adsorbent active sites are not saturated, allowing the adsorbate to bind to various active sites and form a multilayer. However, at high concentrations, the adsorbate forms a monolayer due to the saturation of the active sites. In consonance, all the calculated values of the dimensionless separation factor ($R_L$) (Eq. 3.13) fall between 0 and 1 (Figure 4.18), indicating that the adsorption of ACM and CIP onto CAC is favorable.

As depicted in Table 4.5, the maximum Langmuir adsorption capacities obtained were 192.43 mg/g (ACM) and 70.95 mg/g (CIP) in a single component sorption system. The difference in the adsorptive capacity of CAC for ACM and CIP can be explained by noting the physico-chemical properties of the adsorbent and the molecular structure of the adsorbate (appendix Table A.2). In this regard, it can be noted that ACM has a smaller size, which makes it easier to diffuse into the micro-pores of the CAC. On top of that, ACM ($\log K_{ow} = 0.46$) is more hydrophobic than CIP ($\log K_{ow} = 0.28$), which favors the affinity of ACM to CAC. The higher hydrophobicity of ACM enhanced its affinity to CAC. On the other hand, CIP has a larger molecular size, so its diffusion into the micro-pores of the CAC is relatively limited. Also, the lower hydrophobicity of CIP could be another possible reason for its lower removal. The favorability of the sorption process can be assured by considering the dimensionless separation factor ($R_L$) value, as depicted in Figure 4.18.

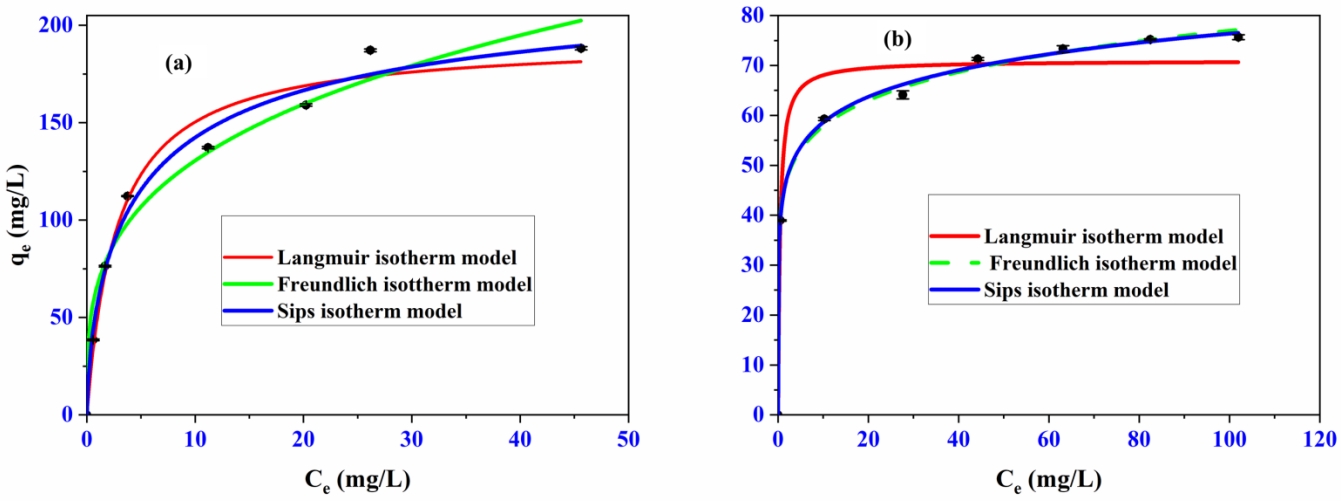


Figure 4.17. Non-linear isotherm model plots (a) single sorption ACM (b) single sorption of CIP isotherm (experimental conditions: pH = 6.8, CAC dose = 0.5 g/L, contact time = 120 min).

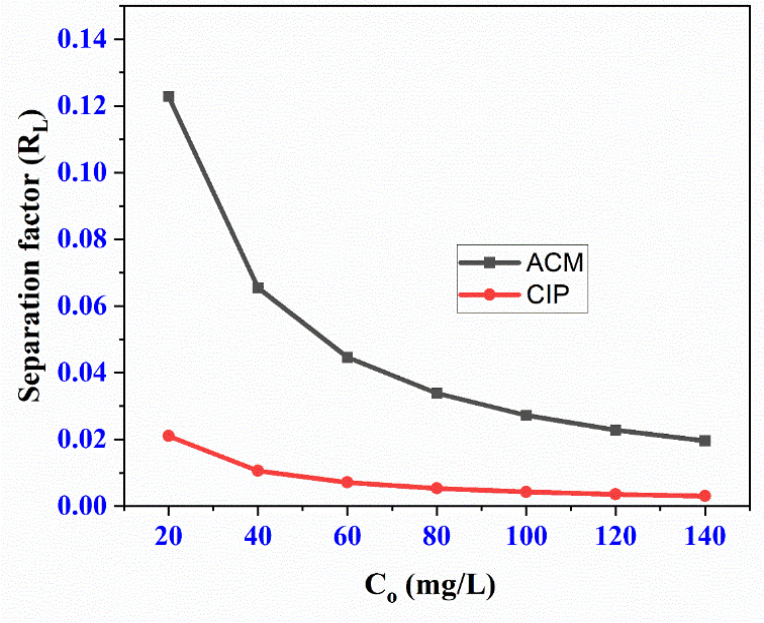


Figure 4.18. The dimensionless separation factor for the single component sorption of ACM and CIP onto CAC.

Table 4.5. Non-linear kinetic and isotherm model parameters for ACM and CIP removal in single and binary component sorption systems.

| Kinetic analysis | | | | | | Isotherm analysis | | | |
|---|---|---|---|---|---|---|---|---|---|
| Model | Model parameters | Single component | | Binary component | | Model | Model parameters | Single component | |
| | | ACM | CIP | ACM | CIP | | | ACM | CIP |
| PFO | $q_{e,cal}$ (mg/g) | 38.08 | 36.79 | 35.31 | 34.18 | Langmuir | $K_L$ (L/mg) | 0.36 | 2.33 |
| | $q_{e,exp}$ (mg/g) | 39.55 | 38.59 | 37.35 | 35.80 | | $q_m$ (mg/g) | 192.43 | 70.95 |
| | $k_1$(1/min) | 0.16 | 0.12 | 0.09 | 0.06 | | $R^2$ | 0.980 | 0.965 |
| | $R^2$ | 0.969 | 0.972 | 0.983 | 0.973 | | RMSE | 10.41 | 5.31 |
| | RMSE | 2.28 | 2.02 | 1.67 | 2.06 | | SSE | 650.07 | 168.91 |
| | SSE | 41.65 | 32.79 | 22.44 | 34.18 | Freundlich | $K_F$ (mg/g)(L/mg)$^{1/n}$ | 67.05 | 43.67 |
| PSO | $q_{e,exp}$ (mg/g) | 39.55 | 38.59 | 37.35 | 35.80 | | n | 3.45 | 8.06 |
| | $q_{e,cal}$ (mg/g) | 40.45 | 39.65 | 39.10 | 38.79 | | $R^2$ | 0.970 | 0.997 |
| | $k_2$ (g/mg.min) | 0.006 | 0.004 | 0.003 | 0.002 | | RMSE | 12.81 | 1.29 |
| | $R^2$ | 0.995 | 0.997 | 0.993 | 0.994 | | SSE | 984.81 | 10.05 |
| | RMSE | 0.91 | 0.67 | 1.07 | 0.94 | | $K_s$ ((mg/g)($L^{\beta}$. $mg^{-\beta}$)), | 76.88 | 56.63 |
| | SSE | 6.67 | 3.57 | 9.13 | 7.14 | | α ($L^{\beta}$. $mg^{-\beta}$) | 0.33 | 0.31 |

Table 4.5. Continued.

| Kinetic analysis | | | | | | Isotherm analysis | | | |
|---|---|---|---|---|---|---|---|---|---|
| AV | $q_e$ (mg/g) | 39.01 | 37.82 | 36.64 | 37.79 | Sips | $\beta_s$ | 0.68 | 0.18 |
| | $K_{av}$ (mg/g.min) | 0.16 | 0.11 | 0.08 | 0.04 | | $R^2$ | 0.988 | 0.998 |
| | $n_{av}$ (g/mg) | 0.62 | 0.65 | 0.69 | 0.61 | | RMSE | 8.89 | 1.27 |
| | $R^2$ | 0.995 | 0.9996 | 0.990 | 0.998 | | SSE | 395.52 | 8.06 |
| | RMSE | 2.51 | 2.12 | 1.88 | 2.25 | | | | |
| | SSE | 44.32 | 31.64 | 24.83 | 35.54 | | | | |

### 4.4.3. Binary component isotherm analysis

The competitive Langmuir isotherm model was used to evaluate the binary component sorption isotherm. The experimental equilibrium data plot for competitive isotherm analysis of ACM and CIP is displayed in Figure 4.19 (a and b). In the binary component adsorption, the adsorption capacity of CAC for ACM decreased to 125.31 mg/g, a value lower than the single component system (192.43 mg/g). Similarly, the adsorption of CIP was reduced to 65.44 mg/g in the binary component system, compared to 70.95 mg/g in the single component system. These findings suggest that the simultaneous removal of ACM and CIP from a binary mixture has an antagonistic nature. Besides, the employed competitive Langmuir isotherm model described the experimental binary component adsorption data ($R^2 > 0.98$), and the estimated binary component adsorption isotherm parameters are presented in Table 4.6. The adsorptive nature of pollutants in a binary system is predicted based on the following conditions (Eqs. (4.2-4.4)). In binary/multi-component systems, the adsorption process is regarded as non-interactive, antagonistic, and synergistic when it fulfils conditions as shown in Eq. (4.2), Eq. (4.3), and Eq. (4.4), respectively (Tovar-gómez et al., 2014).

$$\frac{q_{m\,binary}}{q_{m\,single}} = 1 \quad (4.2)$$

$$\frac{q_{m\,binary}}{q_{m\,single}} < 1 \quad (4.3)$$

$$\frac{q_{m\,binary}}{q_{m\,single}} > 1 \quad (4.4)$$

$q_{m\ binary}$ and $q_{m\ single}$ refer to the maximum adsorption capacity in binary and single component adsorption systems, respectively. The adsorption capacity of ACM decreased sharply (34.88%) in the presence of CIP. In contrast, CIP removal was reduced by 7.76% in the presence of ACM in the solution. Table 4.6 demonstrates that the ratio ($q_{m\ binary}/q_{m\ single}$) for ACM and CIP adsorption onto CAC is 0.65 and 0.92, respectively, satisfying the adsorption condition represented in Eq. (4.4). Therefore, the actual experimental findings (removal efficiency, adsorption capacity, and kinetics) of simultaneous removal, along with the ratio $\frac{q_{m,binary}}{q_{m,single}}$ show that the simultaneous adsorption of ACM+CIP onto the CAC exhibited an antagonistic nature. The main adsorption mechanisms reported for ACM include π-π interaction, hydrogen bonding, Lewis acid-base reaction, and pore filling. However, CIP removal mechanisms include electrostatic interaction, π-π interaction, hydrogen bonding, and complexation reaction. The FTIR results indicated that hydrogen bonding is more influential in the case of ACM than CIP during simultaneous removal. On the other hand, electrostatic attraction is more substantial in CIP adsorption than in ACM adsorption during the simultaneous adsorption of ACM+CIP onto the CAC. Also, π-π interaction is more influential in CIP adsorption than in ACM adsorption, as CIP is more aromatic than ACM. Moreover, ACM is a smaller molecule and more hydrophobic than CIP, which favors its affinity to CAC and diffusion into the micropores of the CAC. As a result, these mechanistic differences are responsible for the antagonistic interaction between the two pharmaceuticals (ACM/CIP) when they co-exist in the same water matrix.

Moreover, the presence of ACM had a minimal effect on CIP removal, while the adsorption of ACM was significantly affected by the presence of CIP. This could be due to the CIP (large molecular size), which potentially shields the adsorption sites and blocks the micro-pores of the adsorbent (Jung et al., 2015). Similar behaviour of adsorption was reported for the simultaneous removal of pharmaceutical contaminant (tetracycline (TCY)) from the binary component mixture of TCY and sulfadiazine (SDZ) using phosphoric acid activated carbon (PAC) (Yadav et al., 2022). Also, other studies reported the antagonistic/synergistic nature of the adsorption process for multi-component pollutant water matrix (Chandrasekaran et al., 2020; Manjunath & Kumar, 2018).

Table 4.6. Langmuir and competitive Langmuir isotherm model constants for single and binary component sorption of ACM and CIP onto CAC, respectively.

| Contaminant | Model parameters | Single component | Binary component | $\frac{q_{m\ binary}}{q_{m\ single}}$ | $R^2$ (binary component) |
|---|---|---|---|---|---|
| ACM | $q_m$ (mg/g) | 192.43 | 125.31 | 0.65 | 0.998 |
| | $K_{L,ACM}$ | 0.36 | 4.64 | | |
| CIP | $q_m$ (mg/g) | 70.95 | 65.44 | 0.92 | 0.985 |
| | $K_{L,CIP}$ | 2.33 | 8.88 | | |

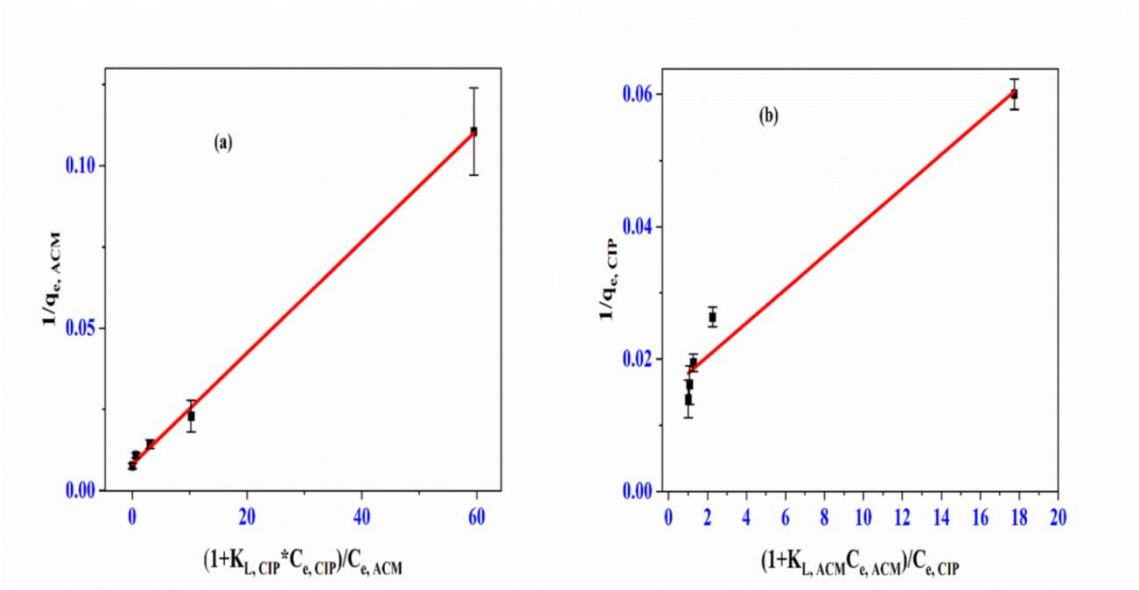


Figure 4.19. Binary component sorption isotherm for ACM (a) and CIP (b) (experimental conditions: pH = 6.8, CAC dose = 0.5 g/L and contact time = 120 min).

## 4.5. Adsorption Mechanism

The adsorption mechanism can be understood by investigating the characteristic nature and mutual interaction between the adsorbent and adsorbate. The characterization results elucidate the nature of the adsorbent, providing insights into the adsorption mechanism in single and binary component mixtures. In this regard, the analysis of FTIR, $pH_{pzc}$, SEM-EDX, and XRD

characterization results revealed that various adsorption mechanisms, including electrostatic interactions, complexation reactions, π-π electron donor-acceptor (EDA) interactions, hydrogen bonding and Lewis-acid base interactions were involved in the removal of ACM and CIP from water as shown in Figure 4.21. During CIP adsorption, π-π EDA interactions take place between the fluorine group on the CIP molecules (π-electron acceptor) and the aromatic rings on the CAC surface (π-electron donor) (Yang et al., 2022). Similarly, hydrogen bonding can take place between the –OH group of the CAC (hydrogen bonding acceptor) and the $F^-$ group of CIP (hydrogen bonding donor) (Rajapaksha et al., 2019). Another instrumental mechanism involved in the CIP adsorption onto the CAC was electrostatic interactions that rely on the surface charge of the CAC and speciation of CIP in the solution with pH variation and explained in sections 4.4 (i). The acid dissociation constant (pKa) values of CIP are 6.1 ($pKa_1$) and 8.7 ($PKa_2$) (Al et al., 2021).

The lower removal of ACM and CIP was observed at solution pH values less than 6.1 and greater than 8.7, indicating significant electrostatic repulsion at these pH ranges. Additionally, there was likely a complexation reaction or ligand exchange between the CIP zwitterions (ketone or carboxylate functional groups) and Fe-O species on the surface of the CAC. In this context, it has been reported that the oxygen atom in the carboxylic group of CIP zwitterions exhibits a stronger ligand capability for coordinating with iron on the CAC surface (Li et al., 2021).

In contrast, the electrostatic attraction may not be the primary driving mechanism for ACM sorption onto CAC, as the pH (2-8) was shown to have less influence on the removal of ACM in single and binary component adsorption as shown in Figure 20. However, some interactions such as hydrophobic interactions (which depend on the water/octanol partition coefficient of the adsorbent) (Pauletto et al., 2021a), π–π EDA interaction (between aromatic rings of ACM (amide group) and aromatic structure of CAC graphene layers) (Grisales-Cifuentes et al., 2021), n-π interaction (when the carbonyl oxygen groups (-COOH and –OH) on the surface of CAC acts as electron donor and aromatic rings of ACM acts as electron acceptor) (Igwegbe et al., 2021), hydrogen bonding between ACM (N–H and O–H groups) and carbonyl groups of CAC (Yılmaz et al., 2021) and Lewis-acid base interactions between iron metal in CAC as Lewis acid and nitrogen/oxygen sites in ACM as Lewis base (Igwegbe et al., 2021; Yılmaz et al., 2021) were

possible ACM removal mechanisms. Moreover, pore-filling is another possible mechanism for ACM removal using CAC.

In the single-component adsorption analysis, the removal of ACM was notably higher than that of CIP using CAC. On the other hand, the removal of ACM (smaller molecule) is more influenced than the removal of CIP in the binary system. This phenomenon can be ascribed to the fact that the pores are blocked by CIP molecules (larger molecules), which affects the pore-filling mechanism of ACM adsorption onto CAC (Grimm et al., 2022). The XRD analysis spectra confirmed that the peak intensity corresponds to Fe-O decreased and shifted after ACM and CIP adsorption, indicating that Fe-O played an essential role in adsorbing both pollutants from water, whether in single or binary component adsorption systems. Moreover, the corresponding peaks for -OH, C-O, and C-H on the surface of CAC were shifted, and their intensities changed after adsorption. More specifically, the FTIR spectra showed a decrease in the intensity of the C-O band (at 1052 $cm^{-1}$) after single and binary adsorption, indicating the possible involvement of n-π interaction in the ACM and CIP adsorption (Pauletto et al., 2021a). SEM analysis of CAC after adsorption revealed that the surface of CAC was covered with new particles (not seen on CAC before adsorption), confirming the successful sorption of ACM and CIP onto the surface of CAC.

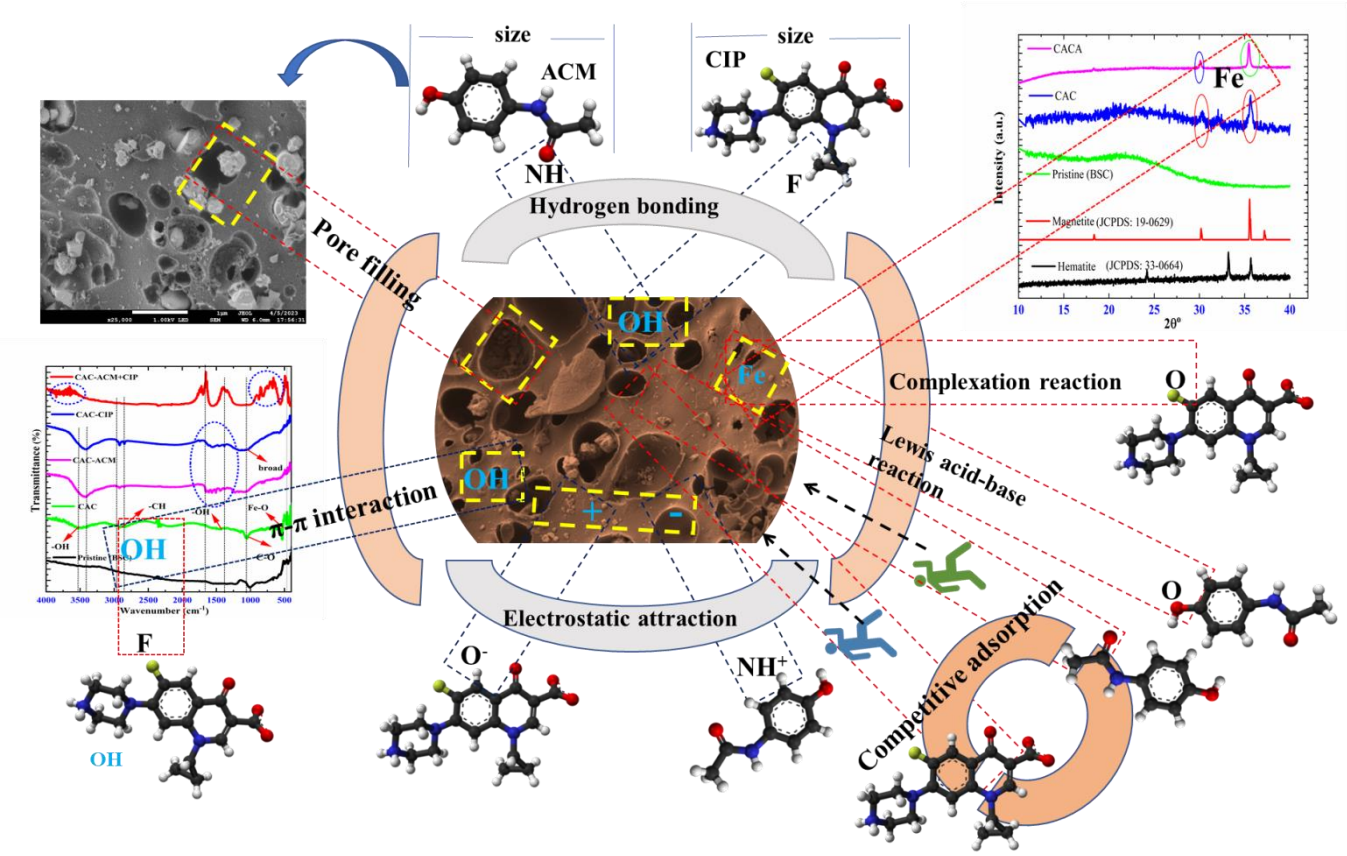


Figure 4.20. Mechanism of simultaneous removal of ACM and CIP from water using CAC.

## 4.6. Column adsorption results

Fixed-bed column experiments were conducted under the optimal condition (pH = 6.8) obtained from the batch study to evaluate the feasibility of CAC in removing pharmaceutical pollutants. The experiments involved a single pollutant (ACM or CIP) and a binary mixture of pollutants (ACM and CIP) in column adsorption. The breakthrough curves (Figure 4.21 (a-h)) for both single component and binary component mixtures were analyzed, and the experimental conditions and parameters are outlined in Table 4.7. The breakthrough time observed in binary component adsorption was between 5 min and 22 min for ACM and CIP. On the other hand, single-component adsorption exhibited a breakthrough time ranging from 48 min to 775 min.

The notable disparity in breakthrough times recorded for single-component and binary-component sorption experiments can be attributed to the suppressive effect of the competition between the pharmaceuticals.

### 4.6.1. Influence of adsorbent loading

The amount of adsorbent packed in a column significantly affects the performance of column and breakthrough curves. The effect of the adsorbent loading was analyzed by comparing experimental runs ($R_2$ versus $R_4$) conducted under identical conditions ($C_o$ = 10 mg/L and Q = 1.5 mL/min) by varying only the CAC loading amount (run 2 = 50 mg and run 4 = 100 mg). In the binary component sorption experimental run 2, the maximum bed capacity for ACM and CIP was 28.59 mg/g and 15.09 mg/g, respectively. However, in run 4, the maximum bed capacity increased to 172.48 and 147.67 mg/g for ACM and CIP, respectively. This improvement in adsorption capacity is associated with a higher number of active binding sites and longer residence time, which led to sufficient contact between the adsorbate and adsorbent as the loading increased from 50 mg to 100 mg (Maged et al., 2023). The lower adsorption capacity of CAC for CIP under similar operating conditions compared to ACM (small molecule) can be associated with the large molecular size of CIP, which hinders its diffusion into the micro-pores of the CAC. Furthermore, the sorption capacity of CAC for CIP is comparatively low due to the lower hydrophobicity of CIP, characterized by a log $K_{ow}$ value of 0.28. The pharmaceutical removal efficiency was significantly enhanced as the CAC loading increased from 50 to 100 mg.

Moreover, the total column operation time increased from 380 to 1300 min, and the removal efficiency increased from 25% to 44.23% for ACM and from 13.23% to 37.86% for CIP in the binary system (Table 4.9). Also, the ACM and CIP uptake capacity increased from 1.43 mg/g to 17.25 mg/g and from 0.76 mg/g to 14.77 mg/g, respectively. As a result, the ACM and CIP equilibrium concentration ($C_{eq}$) in the effluent was reduced from 7.52 mg/g and 8.69 mg/L to 5.58 mg/g and 6.21 mg/L, respectively. For both single and binary component systems, the column reached faster breakthrough ($C/C_o$: 0.1) for CIP at any given loading amount than ACM, as shown in Figure 4.21. This can be related to the larger molecular weight of CIP, which enables it to reach equilibrium faster. Initially, the ACM and CIP breakthrough curves coincided and broadened with time, which was observed at a lower loading amount (50 mg). The

difference in the breakthrough curve shapes of ACM and CIP in the binary component system (Figure 4.21 (a-b)) may be due to axial dispersion, which leads to a sluggish diffusion of the sorbate from the liquid to the solid phase. As a result, the mass transfer phenomena predominate, and the effect of competition would be plausible. However, the axial dispersion effect becomes less at higher loading amounts, and the gap between ACM and CIP breakthrough curves narrows, as depicted in Figure 4.21 (c-d) (Juela et al., 2021).

In the single-component system, the removal efficiency of ACM and CIP increased from 53.73 to 65.83% for ACM and 38.96 to 42.59% for CIP under experimental conditions given in Figure 4.21 (f and h)). Unlike the binary component system, the improved removal efficiency observed in the single component column adsorption process can be attributed to the absence of competition for active sites between the pollutants.

### 4.6.2. Influence of initial concentration of ACM and CIP

Figure 4.21 (a-b) illustrates the influence of ACM and CIP initial concentrations on the breakthrough curves of CAC in a binary component system. The initial concentration variation from 5 mg/L ($R_1$) to 10 mg/L ($R_2$) in the binary pollutant system resulted in changes in column performance parameters (Table 4.7). However, it should be noted that the residual equilibrium concentration ($C_{eq}$) of both ACM and CIP in the column effluent increased from 3.85 mg/L and 4.61 mg/L to 7.52 mg/L and 8.69 mg/L, respectively. Also, the total mass of pollutants fed into the column increased from 5.45 mg to 5.71 mg. Meanwhile, the breakthrough time decreased to 11 and 5 min from 22 and 17 min for ACM and CIP, respectively. Besides, the total column operation time was reduced from 720 min to 380 min. A plausible reason for this phenomenon could be that a higher concentration gradient of the adsorbate generates a more potent mass transfer driving force, leading to a rapid adsorption rate and quicker saturation attainment. These findings confirm the significant influence of adsorbate initial concentration on the fixed-bed adsorption process (Ye et al., 2020). On the other hand, the higher breakthrough time in the lower concentration ($R_1$) was due to the smoother transport (transport delayed effect). Furthermore, the ACM and CIP removal efficiency (%) increased from 23.75% and 8.62% to 25% and 13.23%, respectively. In this case, improvement in removal efficiency with higher initial concentration could be attributed to the sufficient availability of sorbate molecules, which

enhanced the mass transfer rate into the pores of the CAC at a lower flow rate of 1.5 mL/min. In the single component system (Figure 4.21 (e)) at run ($R_1$), the removal efficiencies were 66.15% (ACM) and 37.73% (CIP), which is remarkably higher than the binary component removal efficiency at the same condition.

Most importantly, the maximum bed capacity of the CAC in the single component systems was 196.86 mg/g (ACM) and 68.59 mg/g (CIP) as opposed to the binary component bed capacity of 34.54 mg/g (ACM) and 9.41 mg/g (CIP). The lower bed capacity in the binary component system was due to the antagonistic nature of ACM and CIP adsorption. The single component system had a long breakthrough time at similar experimental conditions as expected (no interference effect).

### 4.6.3. Influence of inlet flow rate

The column experimental runs ($R_3$ and $R_4$) show the effect of flow rate (1.5 mL/min and 3 mL/min) on ACM and CIP removal in the binary systems (Figure 4.21 (c-d)). Increasing the inlet flow rate from 1.50 mL/min to 3.00 mL/min decreased the bed capacity from 172.48 mg/g and 147.67 mg/g to 67.59 mg/g and 74.91 mg/g for ACM and CIP, respectively. Similarly, the removal efficiency decreased from 44.23% and 37.86% to 31.92% and 28.83%. Accordingly, the untreated equilibrium concentration of the pollutants increased from 5.58 mg/L and 6.21 mg/L to 6.83 mg/L and 7.13 mg/L for ACM and CIP, respectively. Additionally, at a higher flow rate (3 mL/min), the lower amount of effluent water (2340 mL/min) was treated compared to effluent water (3900 mL/min) treated at 1.5 mL/min. At high flow rates, turbulence can occur within the bed interstitial spaces, which increases the likelihood of axial dispersion effects. These effects can limit the mass transfer of sorbate to the adsorbent pores, which may result in lower bed capacity ($q_{bed}$), total adsorbed quantity ($q_{tot}$), removal efficiency, and saturation times. Therefore, turbulence is a possible reason for the faster breakthrough and saturation times at high flow rates (Juela et al., 2021). Likewise, increasing the flow rate in the single component sorption study revealed that the breakthrough time and removal efficiency decreased from 550 min and 68 min to 251 min and 48 min and from 65% and 42.59% to 50.96% and 40.39% for ACM and CIP, respectively. Comparative evaluation of single and binary component column data under similar experimental conditions ($R_3$ and $R_4$) showed a notable difference in the values of the column

performance parameters. Compared to single-component adsorption, the reduced breakthrough time, bed capacity, and removal (%) observed in binary-component adsorption can be ascribed to the antagonistic effect of pollutants during the adsorption process. Based on the plotted breakthrough curve (Figure 4.21 (b)) and calculated column performance parameters (Table 4.7), the inlet flow rate of 1.50 mL/min showed higher performance in the binary pollutant fixed-bed operation.

In sum, the experimental column data and breakthrough curve analysis of single and binary component systems ($R_1$-$R_4$) depicted notable variation in removal efficiency for both pollutants in the following order: adsorbent loading amount > inlet flow rate > feeding (ACM and CIP) concentration. Overall, the binary component column optimal conditions represented by $R_4$ ($C_o$ = 10 mg/L, w = 100 mg, Q = 1.5 mL/min) provided the highest $q_{bed}$ of ACM (172.48 mg/g) and CIP (147.67 mg/g) and highest removal efficiency of 44.23 and 37.86%. Under similar conditions, the single component system exhibited a maximum removal efficiency of 65.83% and 42.59% for ACM and CIP, respectively. Conversely, the lowest column performance was observed.

Table 4.7. Breakthrough parameters at different initial ACM and CIP concentrations ($C_0$), CAC amounts (M), flow rates (Q), breakthrough times ($t_b$), total operation time ($t_{total}$), total adsorbed quantities ($q_{total}$), experimental maximum sorption capacities ($q_{bed}$), total amount of adsorbate delivered to the column system ($m_{total}$), total removal efficiencies of the column (RE%), treated volume of effluent ($V_{eff}$) and unadsorbed adsorbate concentrations at equilibrium ($C_{eq}$).

| Parameters | | $C_o$ | $Q$ | EBCT | $M$ | $V_{eff}$ | $t_b$ | $t_{total}$ | $q_{total}$ | $q_{bed}$ | $m_{total}$ | $RE$ | $C_{eq}$ |
|---|---|---|---|---|---|---|---|---|---|---|---|---|---|
| Experiments | | (mg/L) | (mL/min) | (min) | (mg) | (mL) | (min) | | (mg) | (mg/g) | (mg) | (%) | (mg/L) |
| Binary component system | | | | | | | | | | | | | |
| Run 1 | CIP | 5 | 1.50 | 0.68 | 50 | 1080 | 17 | 720 | 0.47 | 9.41 | 5.45 | 8.62 | 4.61 |
| | ACM | | | | | | 22 | | 1.73 | 34.54 | | 23.75 | 3.85 |
| Run 2 | CIP | 10 | 1.50 | 0.68 | 50 | 570 | 5 | 380 | 0.76 | 15.09 | 5.71 | 13.23 | 8.69 |
| | ACM | | | | | | 11 | | 1.43 | 28.59 | | 25.00 | 7.52 |
| Run 3 | CIP | 10 | 3.00 | 0.34 | 100 | 2340 | 10 | 780 | 6.76 | 67.59 | 23.45 | 28.83 | 7.13 |
| | ACM | | | | | | 16 | | 7.49 | 74.91 | | 31.92 | 6.83 |
| Run 4 | CIP | 10 | 1.50 | 0.68 | 100 | 3900 | 6 | 1300 | 14.77 | 147.67 | 39.00 | 37.86 | 6.21 |
| | ACM | | | | | | 10 | | 17.25 | 172.48 | | 44.23 | 5.58 |
| Single component system | | | | | | | | | | | | | |
| Run 1 | CIP | 5 | 1.50 | 0.68 | 50 | 1800 | 98 | 1200 | 3.43 | 68.59 | 9.09 | 37.73 | 3.15 |
| | ACM | | | | | 2970 | 775 | 1980 | 9.84 | 196.87 | 14.88 | 66.15 | 1.69 |
| Run 2 | CIP | 10 | 1.50 | 0.68 | 50 | 1350 | 65 | 900 | 5.27 | 105.29 | 13.51 | 38.96 | 6.11 |
| | ACM | | | | | 2250 | 287 | 1500 | 12.10 | 242.01 | 22.52 | 53.73 | 4.63 |
| Run 3 | CIP | 10 | 3.00 | 0.34 | 100 | 2700 | 48 | 900 | 10.92 | 109.19 | 27.03 | 40.39 | 5.97 |
| | ACM | | | | | 3960 | 251 | 1320 | 20.18 | 201.82 | 39.60 | 50.96 | 4.90 |
| Run 4 | CIP | 10 | 1.50 | 0.68 | 100 | 1680 | 68 | 1120 | 7.18 | 71.76 | 16.85 | 42.59 | 5.76 |
| | ACM | | | | | 2340 | 550 | 1560 | 15.42 | 154.20 | 23.42 | 65.83 | 3.42 |

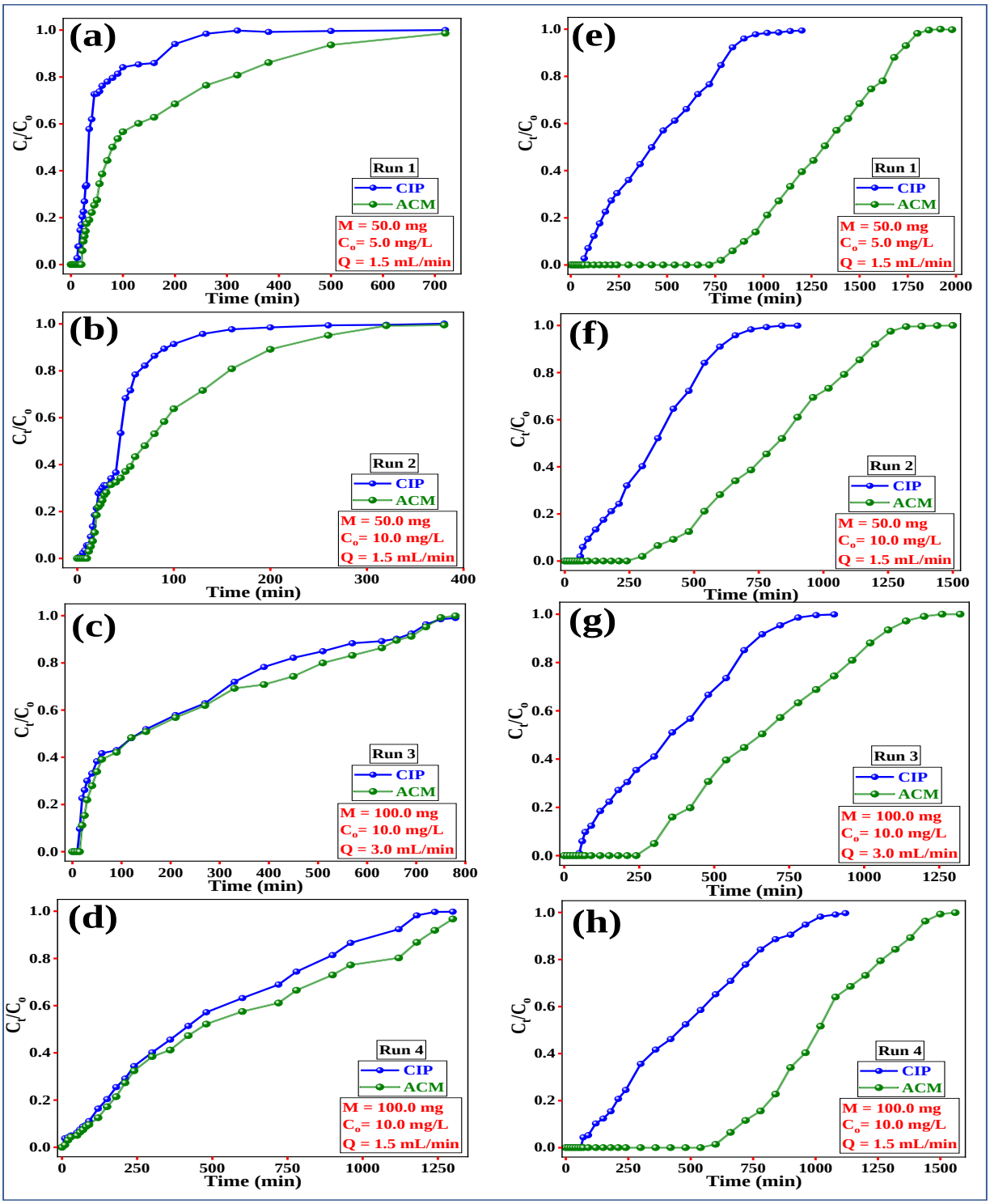


Figure 4.21. Breakthrough curves of CIP and ACM sorption onto CAC in (a-d) Run 1-4 for the binary component solution and (e-h) Run 1-4 for the single component solution.

## 4.7. Electrochemical oxidation results

### 4.7.1. Cyclic voltammetry (CV) analysis

The cyclic voltammetry **(**CV) analysis was employed to understand the electrochemical oxidation behavior of ACM and CIP using $IrO_2$/Ti electrodes. Cyclic voltammograms were recorded using a computer-aided Autolab (PGSTAT12, Netherlands) in a three electrode system. The $IrO_2$/Ti was used as a working electrode, while the platinum wire and Ag/AgCl were used as counter and reference electrodes, respectively. The chromatograms of binary (ACM+CIP) and multiple (ACM+CIP+ATN+AMX) removal using EO is provided in appendix (Figure C.1-Figure C.2). The CV analysis was carried out in the presence and absence of pharmaceuticals (ACM and CIP) at 0.05 M NaCl electrolyte solution. Moreover, the CV analysis was performed for single and binary component aqueous solutions of ACM and CIP for a potential window between +0.2 and -0.2 vs Ag/AgCl at a scan rate of 10 mV/s. Figure 4.22 presents the CV voltammograms of the electrolyte solution (without pharmaceuticals) and with pharmaceuticals (single and binary component aqueous solutions of ACM and CIP). In comparison to the blank electrolyte (0.05 M NaCl), no new oxidation or reduction peaks emerged after adding 20 mg/L of ACM and CIP in binary and single component pharmaceuticals solutions. This implies that the single and simultaneous degradation of ACM and CIP using $IrO_2$/Ti was mainly an indirect oxidation reaction involving hydroxyl radical ($OH^{\bullet}$) (Zhuoyao Chen et al., 2021; Ojo et al., 2023). However, a direct degradation of ACM+CIP is plausible with a chemi-sorbed active oxygen, which is electro-generated by the transition of oxygen from the adsorbed •OH radicals to the lattice of the oxide anode ($IrO_2$), resulting in the formation of higher oxide ($IrO_3$) species, which is generated at the anode surface from water discharge Eqs. (4.6)–(4.8) (Giraldo et al., 2015). This is a well-known route for dimensionally stable electrodes and has been reported in several studies (Körbahti & Alaca, 2021; Onur, 2023; Appia et al., 2021) as shown in Eqs. (4.5-4.11).

$$IrO_2 + H_2O \rightarrow IrO_2(^{\bullet}OH)_{ads} + H^+ + e^- \quad (4.5)$$

$$IrO_2(^{\bullet}OH)_{ads} \rightarrow IrO_3 + H^+ + e^- \quad (4.6)$$

$$IrO_3 + R \rightarrow IrO_2 + RO \quad (4.7)$$

The higher oxide usually gives only selective and partial oxidation with the formation of organic intermediates (RO).

In contrast, the pharmaceuticals (ACM+CIP) reaction with physi-sorbed •OH radicals (electro-generated at the metal oxide anode from the water discharge) is presented in Eqs. (4.8-4.9). This process is heterogeneous and the anode surface absorbs the electro-generated •OH radicals.

$$IrO_2 + H_2O \rightarrow IrO_2(^{\bullet}OH)_{ads} + H^+ + e^- \quad (4.8)$$

$$IrO_2(^{\bullet}OH)_{ads} + R \rightarrow IrO_2 + CO_2 + H_2O \quad (4.9)$$

The physi-sorbed •OH radicals induce non-selective oxidation of pharmaceuticals, leading to their complete combustion.

The reaction of pharmaceuticals (R) with •OH radicals in the bulk solution can be expressed using Eq. (4.10-4.11):

$$2H_2O \rightarrow O_2 + 4H^+ + 4e^- \quad (4.10)$$

$$R + {}^{\bullet}OH \rightarrow RO + CO_2 + H_2O \quad (4.11)$$

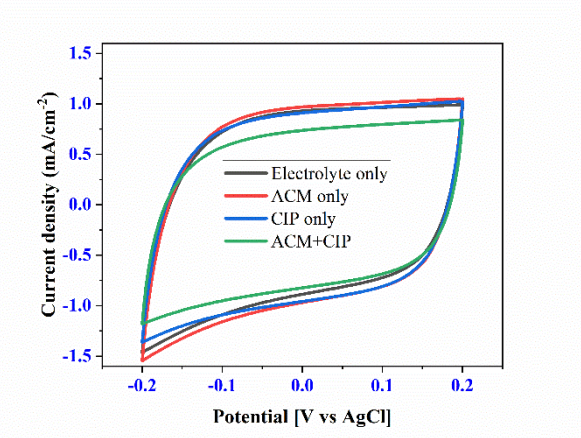


Figure 4.22. Cyclic voltammograms of 0.05 M NaCl solution in the presence/absence of the 20 mg/L of ACM and CIP on I $rO_2$/Ti electrode at 25 ℃ (Scan rate = 10 mV/s and pH = 5.5).

### 4.7.2. EO process optimization using RSM

#### i) Model fitting and analysis of variance (ANOVA) using CCD

The ACM and CIP degradation experiment was optimized using the CCD optimization technique. The EO process CCD experimental design is provided in the appendix (Table C.1). Also, the chromatograms of ACM and CIP recorded during the EO process are provided in appendix (Figures C.1- C.2). The EO degradation of ACM and CIP was best represented by the second-order polynomial model (i.e. quadratic model) with the highest fit statistics ($R^2$ for ACM = 0.992 and $R^2$ for CIP = 0.993). As depicted in Table 4.8, ANOVA was used to assess the validity and adequacy of the model and determine the effect of the main factors and possible interaction factors. The ANOVA indicated that the suggested polynomial model was statistically significant. Based on Table 4.8, the model F- and P-values were 134.47 and less than 0.0001 for ACM and 162.82 and less than 0.0001 for CIP. The chance of an F-value this large could occur due to noise is only 0.01%. The model terms with p-values less than 0.05 affected the EO of ACM+CIP significantly, whereas those with p-values higher than 0.05 did not significantly affect the degradation of ACM+CIP using EO. In this case, A, B, C, D, AB, AD, BC, BD, $A^2$, $B^2$, $C^2$, and $D^2$ are statistically significant model terms. The model terms with p-values greater than 0.05 are not significant. In ACM removal, AC and CD are the model terms that were not significant and were removed from the final model equation for simplicity. On the other hand, the model terms such as AC, CD, and $D^2$ are the model terms that were not significant in CIP removal and, hence, were removed from the final model equation. Relative to pure error, the Lack of Fit is not significant, as indicated by the Lack of Fit F-value of 0.0826 (ACM) and 0.0897 (CIP), which is desirable. There is an 8.26% (ACM) and 8.97% (CIP) chance that a Lack of Fit F-values this large could occur due to noise. The insignificance of lack of fit confirmed that the suggested model represented the EO experimental data well. $Ad_{eq}$ precision measures the signal-to-noise ratio, and a value greater than 4 is desirable. In this CCD design, the ratio of 65.72 indicates an adequate signal. This model can be used to navigate the design space successfully. The model equations for the simultaneous degradation of ACM and CIP involving only the statistically significant terms (at a 95% confidence level) are expressed in Eqs. (4.8-4.11). The adequacy of the suggested quadratic model was evaluated using a coefficient of determination ($R^2$ of 0.992 for ACM and 0.993 for CIP) and adjusted $R^2$ of 0.987 for ACM and 0.984 for CIP. The high $R^2$ values show that the suggested model was suitable for representing

most EO data variations. In this case, the coefficient of determination is close to unity, indicating that the model predictability of experimental data was fair enough. On the other hand, the closeness of adjusted $R^2$ to $R^2$ revealed the significance of the model. The coefficient of variation (CV = 0.77 for ACM and 0.75 for CIP) value of less than 10% indicated that the model was reproducible, whereas the adequate precision value (AP = 35.72 for ACM and 42.98 for CIP) of above 4 confirmed the adequacy of the model (Basturk et al., 2021). The model diagnostic plots for ACM and CIP is provided in appendix (Figure C.5 – Figure C.6). The suggested quadratic model can be applied to navigate the design space. The final equations in terms of coded and actual factors are provided in Eqs. (4.12-4.13).

Table 4.8. ANOVA for ACM and CIP degradation using the EO process.

| Source: ACM | Sum of Squares | df | Mean Square | F-value | p-value | |
|---|---|---|---|---|---|---|
| Model | 885.35 | 14 | 63.24 | 134.47 | < 0.0001 | significant |
| A-EO Time | 165.06 | 1 | 165.06 | 350.97 | < 0.0001 | |
| B-pH | 46.31 | 1 | 46.31 | 98.48 | < 0.0001 | |
| C-Current density | 311.76 | 1 | 311.76 | 662.89 | < 0.0001 | |
| D-Initial concentration | 26.25 | 1 | 26.25 | 55.82 | < 0.0001 | |
| AB | 4.31 | 1 | 4.31 | 9.16 | 0.0085 | |
| AC | 0.0001 | 1 | 0.0001 | 0.0002 | 0.9886 | |
| AD | 5.59 | 1 | 5.59 | 11.89 | 0.0036 | |
| BC | 8.47 | 1 | 8.47 | 18.01 | 0.0007 | |
| BD | 5.27 | 1 | 5.27 | 11.20 | 0.0044 | |
| CD | 0.3721 | 1 | 0.3721 | 0.7912 | 0.3878 | |
| $A^2$ | 66.15 | 1 | 66.15 | 140.64 | < 0.0001 | |
| $B^2$ | 228.76 | 1 | 228.76 | 486.40 | < 0.0001 | |
| $C^2$ | 86.82 | 1 | 86.82 | 184.61 | < 0.0001 | |
| $D^2$ | 2.64 | 1 | 2.64 | 5.62 | 0.0316 | |
| Residual | 7.05 | 15 | 0.4703 | | | |
| Lack of Fit | 6.21 | 10 | 0.6206 | 3.66 | 0.0826 | not significant |

Table 4.8. Continued.

| Source: ACM | Sum of Squares | df | Mean Square | F-value | p-value | |
|---|---|---|---|---|---|---|
| Pure Error | 0.8487 | 5 | 0.1697 | | | |
| Cor Total | 892.41 | 29 | | | | |
| Source: CIP | Sum of Squares | df | Mean Square | F-value | p-value | |
| Model | 951.37 | 14 | 67.95 | 162.82 | < 0.0001 | significant |
| A-EO Time | 164.64 | 1 | 164.64 | 394.47 | < 0.0001 | |
| B-pH | 56.06 | 1 | 56.06 | 134.32 | < 0.0001 | |
| C-Current density | 325.46 | 1 | 325.46 | 779.79 | < 0.0001 | |
| D-Initial concentration | 47.43 | 1 | 47.43 | 113.65 | < 0.0001 | |
| AB | 6.66 | 1 | 6.66 | 15.95 | 0.0012 | |
| AC | 0.7921 | 1 | 0.7921 | 1.90 | 0.1885 | |
| AD | 6.94 | 1 | 6.94 | 16.64 | 0.0010 | |
| Source: ACM | Sum of Squares | df | Mean Square | F-value | p-value | |
| BC | 4.77 | 1 | 4.77 | 11.44 | 0.0041 | |
| BD | 4.24 | 1 | 4.24 | 10.17 | 0.0061 | |
| CD | 1.72 | 1 | 1.72 | 4.11 | 0.0607 | |
| $A^2$ | 36.04 | 1 | 36.04 | 86.35 | < 0.0001 | |
| $B^2$ | 277.59 | 1 | 277.59 | 665.09 | < 0.0001 | |
| $C^2$ | 66.54 | 1 | 66.54 | 159.42 | < 0.0001 | |
| $D^2$ | 0.0000 | 1 | 0.0000 | 0.0001 | 0.9920 | |
| Residual | 6.26 | 15 | 0.4174 | | | |
| Lack of Fit | 5.48 | 10 | 0.5477 | 3.50 | 0.0897 | not significant |
| Pure Error | 0.7831 | 5 | 0.1566 | | | |
| Cor Total | 957.63 | 29 | | | | |

$$\text{ACM removal} = +93.2617 + 2.6225 \times A - 1.38917 \times B + 3.60417 \times C - 1.04583 \times D - 0.51875 \times AB + 0.59125 \times AD + 0.7275 \times BC + 0.57375 \times BD - 1.55292 \times A^2 - 2.88792 \times B^2 - 1.77917 \times C^2 - 0.310417 \times D^2 \quad (4.12)$$

$$\text{CIP removal} = +90.3083 + 2.61917 \times A - 1.52833 \times B + 3.6825 \times C + -1.40583 \times D - 0.645 \times AB + 0.65875 \times AD + 0.54625 \times BC + 0.515 \times BD - 1.14625 \times A^2 - 3.18125 \times B^2 - 1.5575 \times C^2 \quad (4.13)$$

It should be noted from the equation in terms of actual factors that all the main factors have a synergistic effect on the responses (ACM and CIP degradation). However, the initial concentration of ACM/CIP has an antagonistic effect on the responses. The equation in terms of coded factors can be used to make predictions about the response for given levels of each factor. By default, the high levels of the factors are coded as +1, and the low levels are coded as -1. The coded equation is useful for identifying the relative impact of the factors by comparing the factor coefficients.

On the other hand, the equation in terms of actual factors can be used to make predictions about the response for given levels of each factor. Here, the levels should be specified in the original units for each factor. This equation should not be used to determine the relative impact of each factor because the coefficients are scaled to accommodate the units of each factor, and the intercept is not at the center of the design space. Moreover, the Pareto analysis can provide valuable information to interpret the results of the response surface model. This analysis was employed to determine the influence of each variable (main and interaction) on the response as shown in Eq. (4.14) (Ahmadi et al., 2021).

$$P_i = \left(\frac{b_i^2}{\sum b_i^2}\right) \times 100 (i \neq 0) \quad (4.14)$$

In Eq. 4.15, $b_i$ represents the coefficients of the main and interaction factors of the model. Pareto graph analysis of ACM and CIP is depicted in Figure. 4.23 (a-b); the EO reaction time (C) (33.85% for ACM and 33.89% for CIP) had the greatest effect on the degradation of ACM and CIP in the EO process. The interaction factor (BC) showed a relatively higher influence on ACM degradation among the interaction effects of ACM degradation. On the other hand, AD demonstrated a relatively higher impact on CIP degradation.

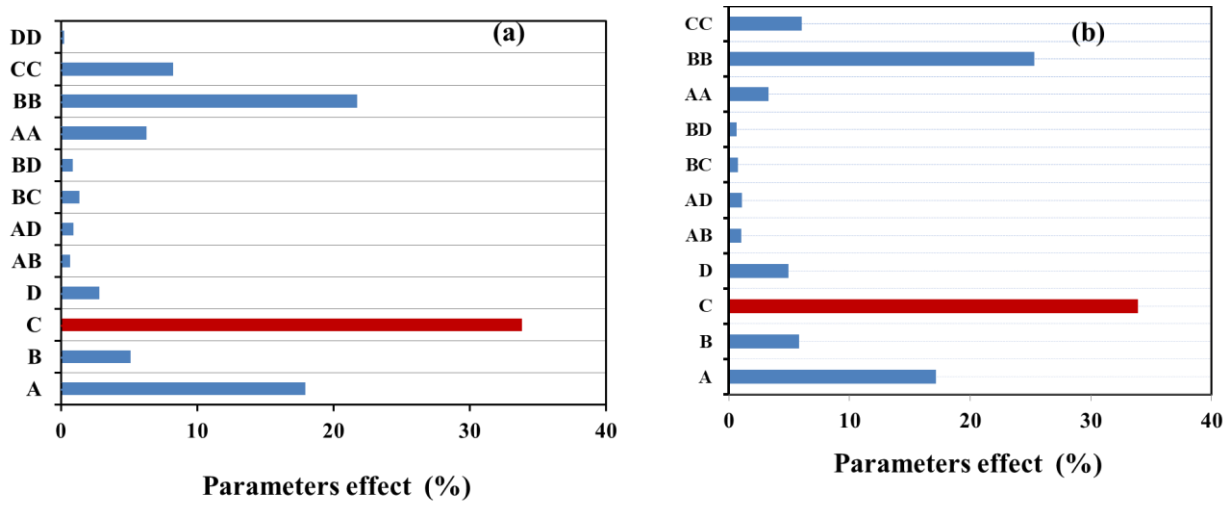


Figure 4.23. Pareto analysis for ACM (a) and CIP (b) degradation using EO.

### ii) Effect of EO operational parameters

The effect of main EO process variables such as EO time, pH, current density and initial pharmaceutical concentration on simultaneous degradation of ACM and CIP was studied using the CCD experimental design. The extents of their influence on the simultaneous degradation of ACM and CIP were identified from the ANOVA statistical analysis of the EO experimental data. The effect of the electrolyte (NaCl) concentration on the simultaneous degradation of ACM and CIP during the EO process was studied before the EO process optimization. The optimized concentration of NaCl (0.05 M) was then used during the EO process optimization. The one factor plot of ACM and CIP for the EO process is presented in appendix (Figures C.3 - C.4). Whereas, the model diagnostic plots of ACM and CIP for EO process are presented in appendix (Figures C.5 – C.6).

#### a) Effect of electrolyte (NaCl)

The concentration of the NaCl is one of the detrimental factors in the EO process operation. It should be noted that the NaCl concentration is strongly associated with the improvement of the conductivity of the aqueous solution, electron transfer rate and generation of the reactive chlorine, such as $Cl_2$, HClO, or $ClO^-$ in the solution (Xia et al., 2023). The effect of NaCl concentration on the simultaneous degradation of ACM and CIP is depicted in Figure 4.24. As

shown in Figure 4.24, the degradation efficiency of ACM and CIP increased across all pH values (3, 6 and 9) as the concentration of NaCl increased from 0.01 to 0.25M. The higher NaCl concentration enhanced solution conductivity and electron transfer and, promoted active chlorine generation in aqueous solutions (Xia et al., 2023). The generated active chlorine leads to a higher degradation efficiency in combination with the electro-generated hydroxyl radical (Rubia et al., 2023). Electro-generated active chlorine species (gaseous chlorine ($Cl_2$), hypochlorous acid (HOCl) and hypochlorite ($OCl^-$)) from oxidation of chloride ions present in water are responsible for indirect oxidation of pharmaceuticals (R: referring to ACM+CIP), as shown in Eqs. (4.15-4.17). The anodic, cathodic and solution reactions that take place during the EO process employing a NaCl electrolyte is provided in Eqs. (4.18-4.26) (Xia et al., 2023).

$$2Cl^- \rightarrow Cl_2 + 2e^- \quad (4.15)$$

$$Cl_2 + H_2O \rightarrow HOCl^- + H^+ + Cl^- \quad (4.16)$$

$$HOCl + R \rightarrow CO_2 + H_2O + H^+ + Cl^- \quad (4.17)$$

Higher electro-active chlorine oxidizing species can be formed at higher NaCl concentrations (Onur, 2023).

Anodic reactions:

$$2Cl^- \rightarrow Cl_2 + 2e^- \quad (4.18)$$

$$6HOCl + 3H_2O \rightarrow 2ClO_3^- + 4Cl^- + 12H^+ + 1.5O_2 + 6e^- \quad (4.19)$$

$$2H_2O \rightarrow O_2 + 4H^+ + 6e^- \quad (4.20)$$

Cathodic reactions:

$$2H_2O + 2e^- \rightarrow 2OH^- + H_2 \quad (4.21)$$

$$OCl^- + 2H_2O + 2e^- \rightarrow Cl^- + 2OH^- + H_2O \quad (4.22)$$

$$6ClO^- + 3H_2O \rightarrow 2ClO_3^- + 4Cl^- + 6H^+ + \frac{3}{2}O_2 + 6e^- \quad (4.23)$$

$$ClO_3^- + H_2O \rightarrow ClO_4^- + 2H + 2e^- \quad (4.24)$$

Solution reactions:

$$Cl_2 + H_2O \rightarrow HOCl + H^+ + Cl^- \quad (4.25)$$

$$HOCl \leftrightarrow H^+ + OCl^- \quad (4.26)$$

Overall, increasing NaCl concentration increased the degradation efficiency of ACM and CIP. Nevertheless, an excessive amount of NaCl can cause significant deposition of chloride ions onto the electrode, causing electrode corrosion and can shorten its service life over prolonged operation. Therefore, a NaCl concentration of 0.05M was found to be an optimal concentration as it balances the beneficial effect (enhanced degradation) and detrimental effect (reduction of electrode lifetime) (Xia et al., 2023).

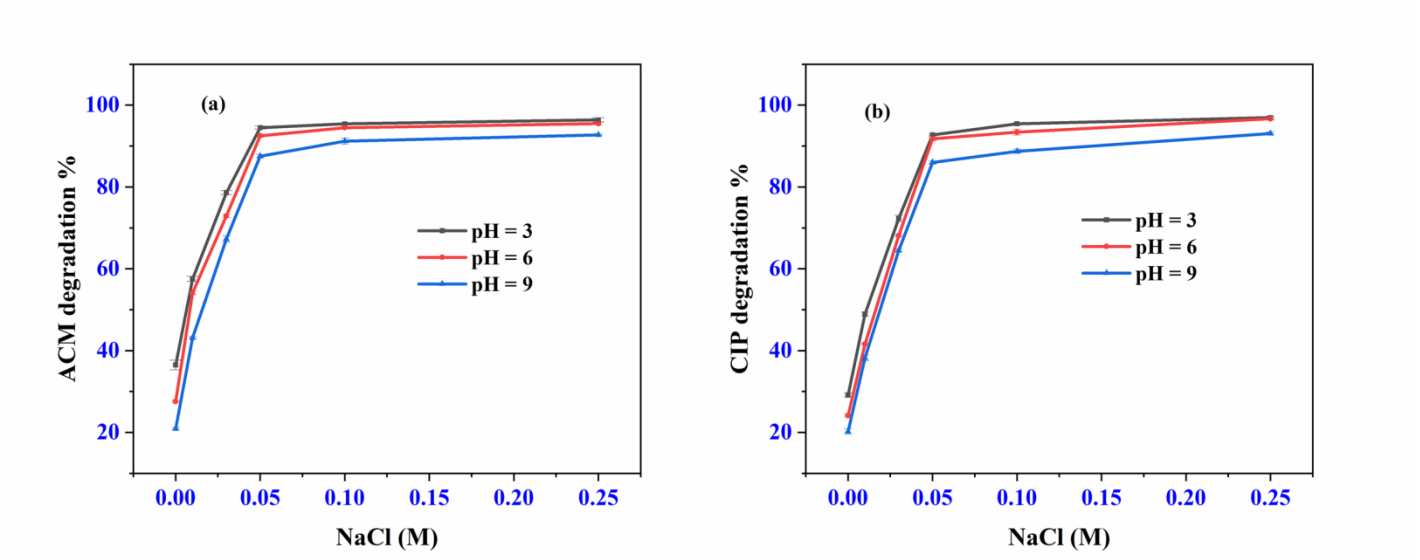


Figure 4.24. Effect of NaCl concentration on simultaneous degradation of (a) ACM and (b) CIP.

**b) Effect of EO time**

The effect of oxidation time is crucial to evaluate the techno-economic feasibility and performance of the oxidation process for practical application (Manjunath et al., 2023). The effect of time on the degradation of ACM and CIP was investigated for an EO time ranging from 40min to 80 min. Under EO process conditions (pH = 5.5, $C_o$ = 20 mg/L and current density = 44 mA/cm$^2$), Figures (4.25-4.26) reveal that the degradation efficiency increased from 86.97% and

84.27% to 93.54% and 90.61% for ACM and CIP, respectively, when the EO time increased from 40 min to 60 min. Increasing the EO time to 80 min increased the degradation efficiency to 94.82% (ACM) and 92.35% (CIP). Therefore, EO time (80 min) is considered as an optimal EO process time to achieve an enhanced degradation of ACM and CIP using the $IrO_2$/Ti mesh electrode. The observed enhanced degradation of ACM and CIP at higher EO time is related to the higher amount of reactive oxygen species generated (mainly •OH radicals) (Moteshaker et al., 2020).

**c) Effect of current density**

The degradation performance of the EO process can be highly influenced by applied current density (Li et al., 2019). In the EO process, active oxidizing species (such as ·OH) are generated depending on the applied current density (Ma et al., 2023). Figures (4.25-4.26) present the effect of the applied current density (23.5-62.5 mA/cm$^2$) on the simultaneous degradation of ACM and CIP in an aqueous solution using an $IrO_2$/Ti mesh electrode. The influence of current density on the simultaneous degradation of ACM and CIP in the EO process was studied while keeping other operational factors such as initial concentrations of pharmaceuticals (20 mg/L), pH (5.5), and time (80 min) constant. As displayed in Figures (4.25-4.26), the degradation efficiency of ACM and CIP increased from 89.53% and 86.89% to 94.82% and 92.35% for ACM and CIP, respectively, when the current density increased from 23.21mA/cm$^2$ to 44 mA/cm$^2$. The recorded increased degradation of ACM and CIP at higher current density could be ascribed to the higher generation of active species such as ·OH and active chlorine species at higher current density (Xia et al., 2023). However, a further increase in current density from 44 mA/cm$^2$ to 62.5 mA/cm$^2$ only increased the simultaneous degradation of ACM and CIP to 96.2% and 94.27%, respectively, less than 2.5% for both pollutants. In this case, the excessive current density might have increased the oxygen evolution on the electrode surface, thus suppressing the ·OH generation (Pinto et al., 2023), and the expected trend of significant degradation was not observed.

Moreover, the increased oxygen evolution might have undergone undesirable side reactions at higher applied current (Xia et al., 2023). It should also be noted that higher current densities are related to higher operational costs. Most importantly, the applied current should be as minimum as possible while not compromising the degradation efficiency. In this study, the current density

of 44 mA/cm$^2$ was recorded as an optimal value for the simultaneous degradation of ACM and CIP in the EO process employing the $IrO_2$/Ti mesh electrode.

**d) Effect of initial solution pH**

The initial solution pH has a significant influence on the electrochemical degradation process because the EO-driven radical chain reactions require the involvement of protons (Xia et al., 2023). As depicted in Figures (4.25-4.26), the degradation efficiencies of ACM and CIP were 93.5% and 90.96%, respectively, at an initial solution pH of 4 and EO process parameters (initial ACM/CIP concentration = 20 mg/L, EO time = 80 min and current density = 44 mA/cm$^2$). The corresponding removal of efficiencies of ACM and CIP increased to 94.82% and 92.35% when the pH increased to 5.5. Further increase in pH to 8 decreased the degradation efficiency to 92.38% (ACM) and 89.57% (CIP). The reason for the reduction in the ACM and CIP degradation with pH can be ascribed to the fact that the ·OH radical was favourably generated in acidic solutions, with its oxidation potential higher in acidic solution (2.85 V) than in the alkaline solution (2.02 V). Moreover, the main active chlorine species under acidic conditions were $Cl_2$ ($E^0$ = 1.36 V vs. SCE) and HClO ($E^0$ = 1.49 V vs. SCE), which have higher oxidation potentials than the active chlorine species (hypochlorite ($E^0$ = 0.89 V vs. SCE)) which forms in the alkaline solutions (Xia et al., 2023). Moreover, the acidic pH reduces oxygen generation, increasing the efficacy of contaminant degradation. In contrast, oxygen production is elevated in an alkaline solution, which results in a reduction of •OH production (Mosur et al., 2023). Herein, a pH value of 5.5 was taken as the optimal value for the simultaneous degradation of ACM and CIP using the $IrO_2$/Ti mesh electrode.

**e) Effect of initial pollutant concentration**

The initial concentration of pharmaceutical contaminants affects the efficiency of the EO process, and it is important to determine to what pollutant load the EO process can be operated at good efficiency. A decreasing trend of the ACM and CIP degradation was observed when the initial pollutant concentration increased, as shown in Figures (4.25-4.26). As depicted in Figures (4.25-4.26), the degradation efficiencies of ACM and CIP were 95.2% and 93.32%, respectively, for an initial concentration of 15 mg/L of ACM+CIP at EO process experimental conditions (pH = 5.5, EO time = 80 min and current density = 44 mA/cm$^2$). Under the same EO parameters,

ACM and CIP degradation efficiencies were reduced to 94.8% and 92.35% when the initial concentration increased to 20 mg/L. However, the observed reduction in degradation efficiency with an increase in initial concentration is insignificant. A relatively significant efficiency reduction was observed when the initial pharmaceutical concentration was increased to 25 mg/L. As the initial concentration (ACM/CIP) increases, the parent compound and the intermediate products produced in the EO will become more competitive with radicals, which reduces the degradation rate of parent compound (Liu et al., 2022). However, increasing the initial concentration enhances the overall reaction rate. Therefore, 20 mg/L is an optimal initial concentration value for the studied EO process.

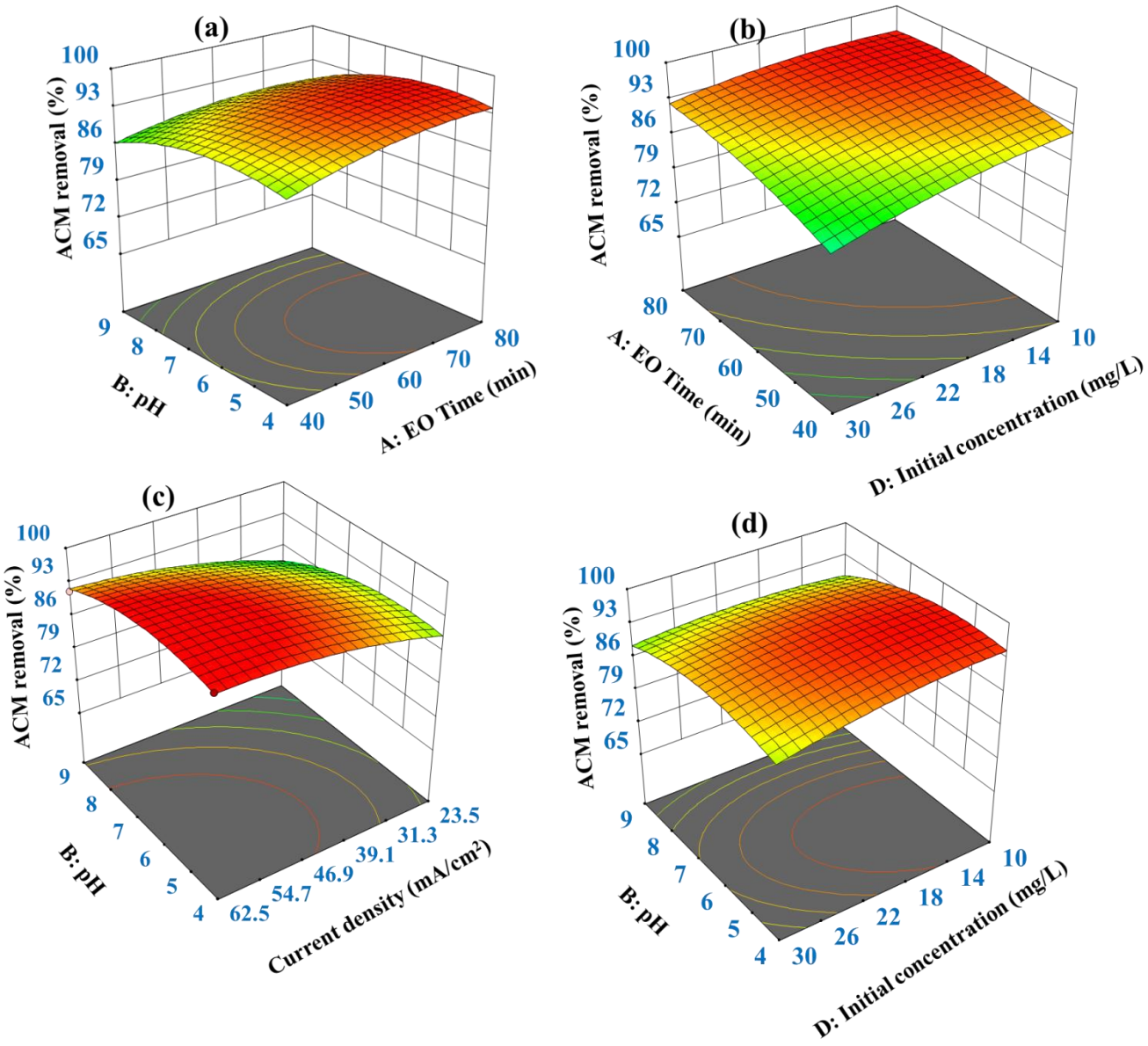


Figure 4.25. The 3D surface plots for the interaction factors of ACM degradation using EO.

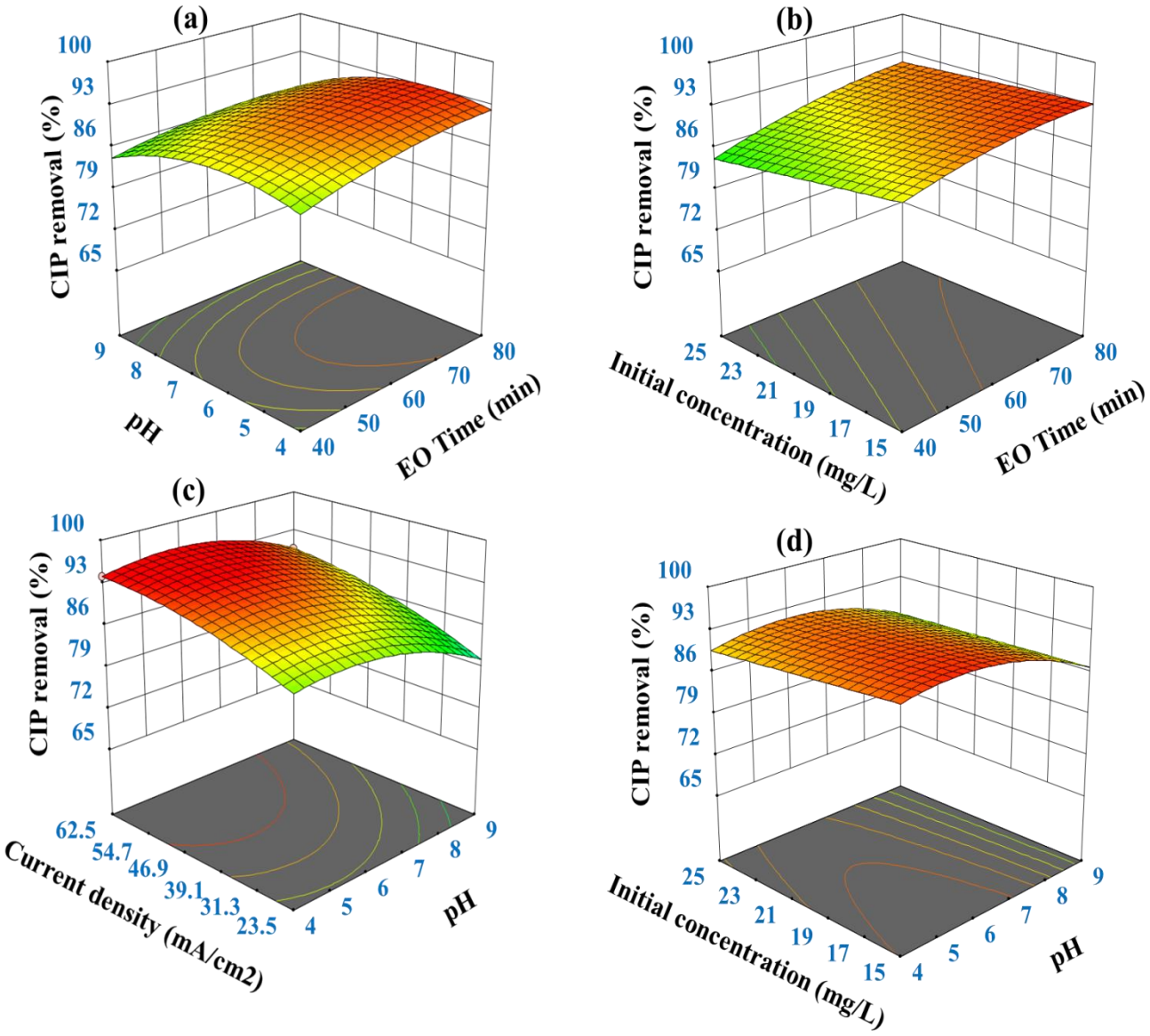


Figure 4.26. The 3D surface plots for the interaction factors of CIP degradation using EO.

**f) Validation of the RSM optimization process**

The simultaneous degradation of ACM and CIP using the EO process was optimized in a way to maximize the degradation efficiency and minimize the energy consumption by the EO process operation. Accordingly, the response variables were set to be maximized, while the current density was set to be minimized. All other parameters were kept in the range of investigation in this study. Consequently, an optimal conditions of the EO process (EO time = 80 min, initial

ACM+CIP concentration = 20 mg/L, pH = 5.5 and current density = 44 mA/cm$^2$) was obtained. Under these conditions, the RSM model predicted the optimal degradation values of 94.5% (ACM) and 92.65% (CIP). These values were further validated in the laboratory by conducting triplicated experiments at these optimal EO conditions, and mean values of 94.22% (ACM) and 92.12% (CIP) were obtained. The closeness of the experimental values to the predicted values shows that the results are valid.

### 4.7.3. Kinetics of EO process

The EO degradation kinetics was conducted under optimal operating conditions determined using RSM. Based on the radical scavenger test, $^{\bullet}$OH radical was found to be the dominant radical species in the EO process. In this regard, the current density and EO time are significantly related to the generation of the hydroxyl radical and its concentration in the solution. The concentration of the hydroxyl radical within the solution affects the rate of the EO reaction. Moreover, the initial ACM/CIP concentration affects the rate of the EO process. The well-known kinetic models, such as pseudo-first-order and pseudo-second-order models were employed to investigate the ACM and CIP reaction kinetics, as depicted in Figure 4.27. It can be seen from Figure 4.27 that the degradation of ACM and CIP followed a pseudo-first-order kinetic process ($R^2$ > 0.97) with reaction constants of 0.034 (1/min) and 0.035 (1/min) for ACM and CIP, respectively. This shows that ACM/CIP reaction rate is directly proportional to the initial concentration of ACM/CIP. Previous research findings indicated that the EO of organic contaminants followed a pseudo-first-order kinetics (Najafinejad et al., 2023).

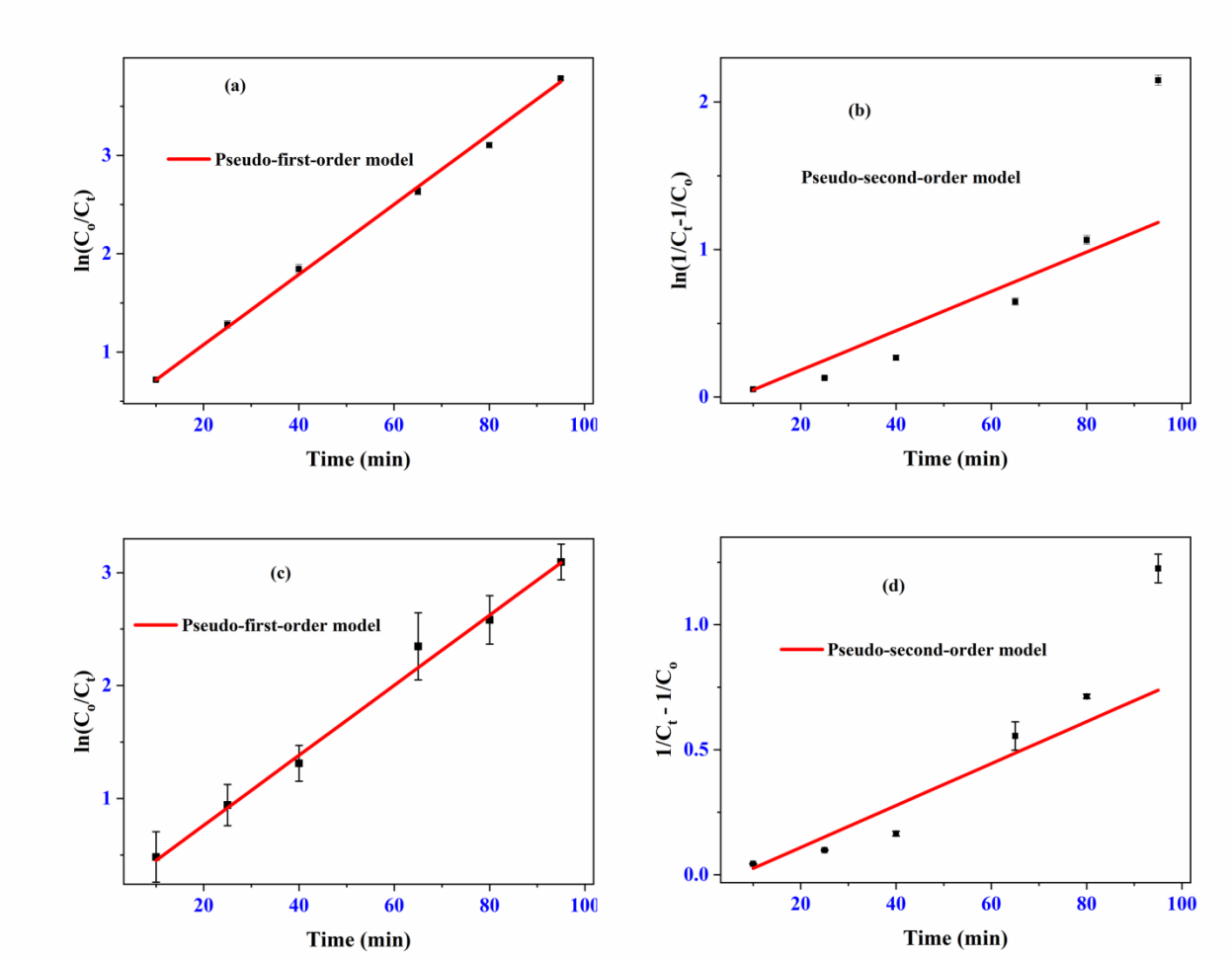


Figure 4.27. Kinetics of EO process (a-b) pseudo-first-order and pseudo-second-order models for ACM and (c-d) pseudo-first-order and pseudo-second-order models for CIP, respectively.

### 4.7.4. Effect of water matrix on EO process

The contaminant removal efficiency of technologies can be significantly affected by the composition of the water matrix. In particular, a real wastewater matrix contains various background substances which either scavenge or compete for the active oxidizing species. In contrast, applying treatment processes like oxidation and adsorption in pure water is helpful for clearly understanding the removal mechanisms in the absence of the background effects. Nevertheless, employing these treatment processes in real wastewater provides insights into the actual scenarios of the treatment processes and real treatment efficiencies. Therefore, various

water matrices such as pure water, tap water and real wastewater were considered to evaluate the degradation efficiency of the EO process on ACM and CIP, as depicted in Figure 4.28. The effect of the water matrix on the EO process was investigated under RSM optimal process conditions. The impact of the water matrix on the EO process was conducted across a range of current densities (10-70 $mA/cm^2$). Water matrices such as pure water, tap water and real wastewater were employed to assess the efficiency of the EO process in the simultaneous degradation of ACM and CIP.

The degradation of ACM from pure water increased from 66.85% to 93.5% when the current density increased from 10 $mA/cm^2$ to 40 $mA/cm^2$. A further increase in current density from 40 $mA/cm^2$ to 70 $mA/cm^2$ increased the ACM degradation from 93.5% to 99.87%. Similarly, the degradation of CIP increased from 63.8 $mA/cm^2$ to 99.75 $mA/cm^2$ in pure water when the current density increased from 10 $mA/cm^2$ to 70 $mA/cm^2$. In the case of tap water, the efficiency of ACM and CIP degradation significantly improved from 61% and 56.35% to 99.25% and 99.65%, respectively, as the current density increased from 10 $mA/cm^2$ to 70 $mA/cm^2$. Compared to the degradation efficiency obtained in pure water, the efficiency of ACM and CIP degradation in tap water showed relatively lower efficiencies at lower current densities. It should be noted that the tap water contains various constituents compared to the pure water. Therefore, the tap water background constituents reduced the EO degradation efficiencies of ACM and CIP. The variation between ACM and CIP degradation efficiencies in pure and tap water becomes pronounced at lower current densities. This can be ascribed to the inadequate supplied current to address all the diverse compositions of the tap water. On the contrary, the discrepancies in the degradation efficiencies between pure and tap water are small at higher current densities, as higher supplied current overcomes the effect of the background matrix.

Moreover, a similar trend was observed for the degradation of ACM and CIP in real wastewater. Real wastewater comprises even more diverse compositions that either scavenge or compete for the active oxidizing species, reducing degradation efficiency. Degradation efficiencies of ACM and CIP showed a notable increase from 54.37% and 50.9% to 99.2% and 99.15%, respectively, for the increment in current density from 10 $mA/cm^2$ to 70 $mA/cm^2$ in real wastewater. The observed variation in the degradation efficiencies between pure water and real wastewater was

due to the background effect, which is more significant at lower current densities. Overall, the water matrix significantly affected the degradation efficiency of ACM and CIP using the EO process.

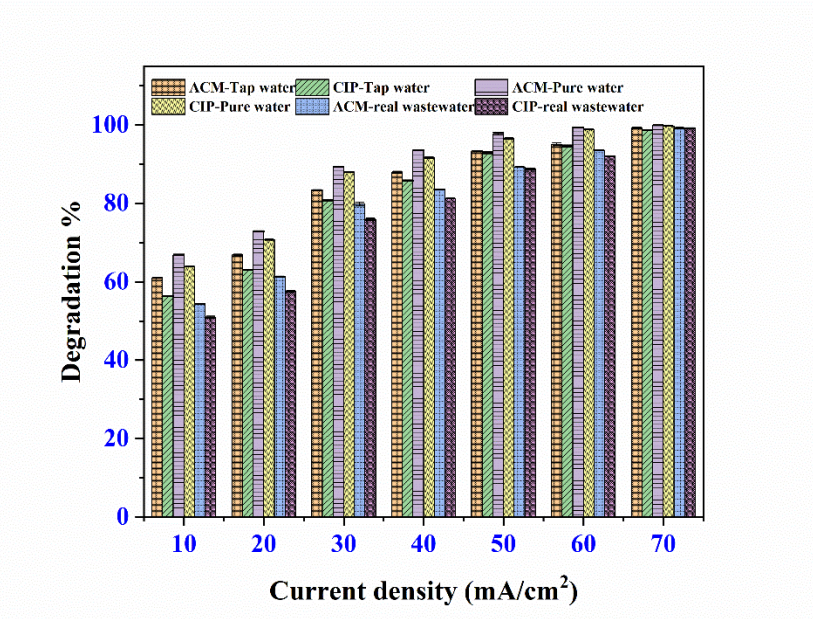


Figure 4.28. Effect of water matrix on the degradation of ACM and CIP using EO (pH = 5.5, EO time = 80 min and initial ACM/CIP = 20 mg/L).

### 4.7.5. Effect of scavenger on EO process

The quenching tests were performed by introducing various radical scavengers to identify the reactive oxygen species (ROS) (Chen et al., 2022) generated during the degradation of ACM and CIP using the EO process. To assess the dominant ROS generated during the EO degradation of ACM and CIP, well-known radical scavengers such as tert-butanol (for hydroxyl radicals) and p-benzoquinone (PBQ, for superoxide ion radicals) were employed (Kermani et al., 2019). Figure 4.29 (a and b) shows a notable reduction of ACM and CIP degradation from 94.92% and 93% to 16% and 15.2%, respectively, when tert-butanol (25 mM) was added to the aqueous solution at 80 min EO time. On the other hand, the addition of PBQ (25 mM) resulted in a relatively small reduction (from 94.92% and 93% to 85.45% and 82.2%) in ACM and CIP degradation efficiencies, respectively. These results suggest that hydroxyl radical reactions primarily dominated the EO degradation of ACM and CIP. In addition, the reduction in the degradation

efficiencies with the addition of PBQ showed that the superoxide radical was also involved in the EO degradation process.

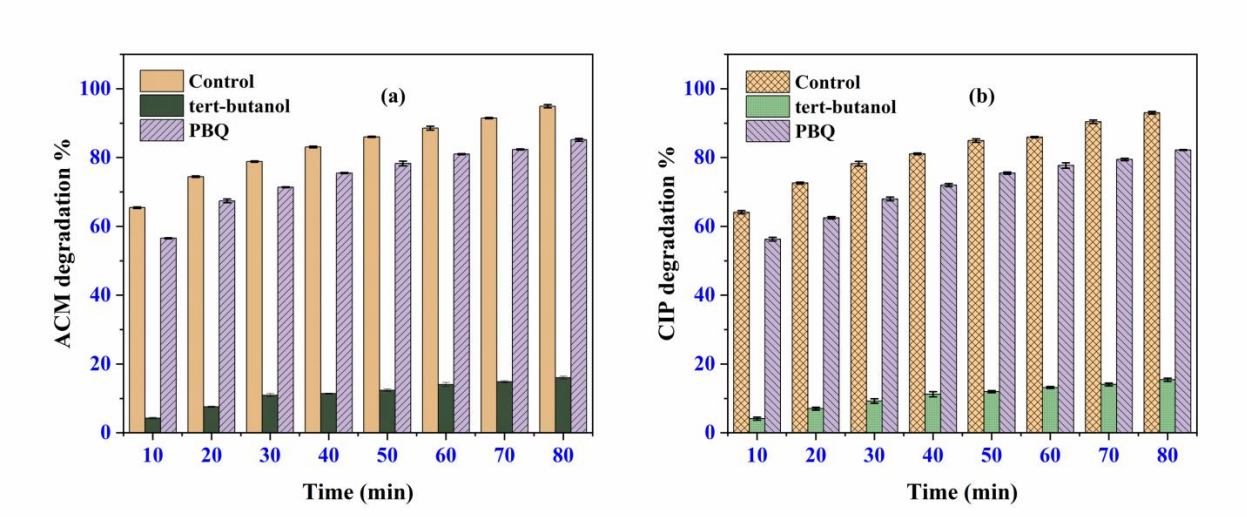


Figure 4.29. Effect of water matrix on the degradation of ACM and CIP using EO (current density = 44 mA/cm$^2$, pH = 5.5, and initial ACM/CIP = 20 mg/L).

### 4.7.6. TOC and COD removal

Mineralization serves as a key efficiency indicator for oxidation-based water treatment technologies. In addition, the TOC removal can be used as indices of the mineralization of organic compounds (Kermani et al., 2019). It can also be used to investigate the current efficiency of the EO process in mineralization. On the other hand, COD removal was also investigated to assess the reduction of pollution levels. The mineralization study (TOC analysis) and COD removal were conducted under optimal conditions of the EO process, and the results are provided in Figure 4.30 (a) and (b). TOC reduction is directly related to the portion of the organic compound converted to compounds like water and carbon dioxide. The initial TOC and COD values of the aqueous solution containing pharmaceuticals (ACM and CIP) were evaluated after spiking ACM and CIP into ultra-pure water. The TOC and COD removal experiments were conducted over a degradation time ranging from 10 min to 300 min and 10 min to 250 min, respectively. Figure 4.30 a and b illustrates the mineralization efficiency of the EO process with the EO time. It can be seen from Figure 4.30 (a) that the mineralization was increased from 13.2% to 72.51% as the oxidation time increased from 10 min to 300 min. On the other hand,

COD removal increased from 39.98% to 90.43% as the EO time increased from 10 min to 240 min. A similar trend of COD reduction with time was observed in the previous study (Montenegro-ayo et al., 2023a). Compared to the degradation efficiency of ACM/CIP, lower TOC and COD removal efficiencies were recorded at lower EO time. This can be attributed to the generation of persistent degradation by-products more resistant to free radical oxidation (Kermani et al., 2019). The TOC removal result obtained in this study is comparable with a previous study which employed a semi-fluid Fe/charcoal micro-electrolysis reactor for treating wastewater containing CIP (75% TOC removal achieved) (Mahdizadeh & Malakootian, 2019).

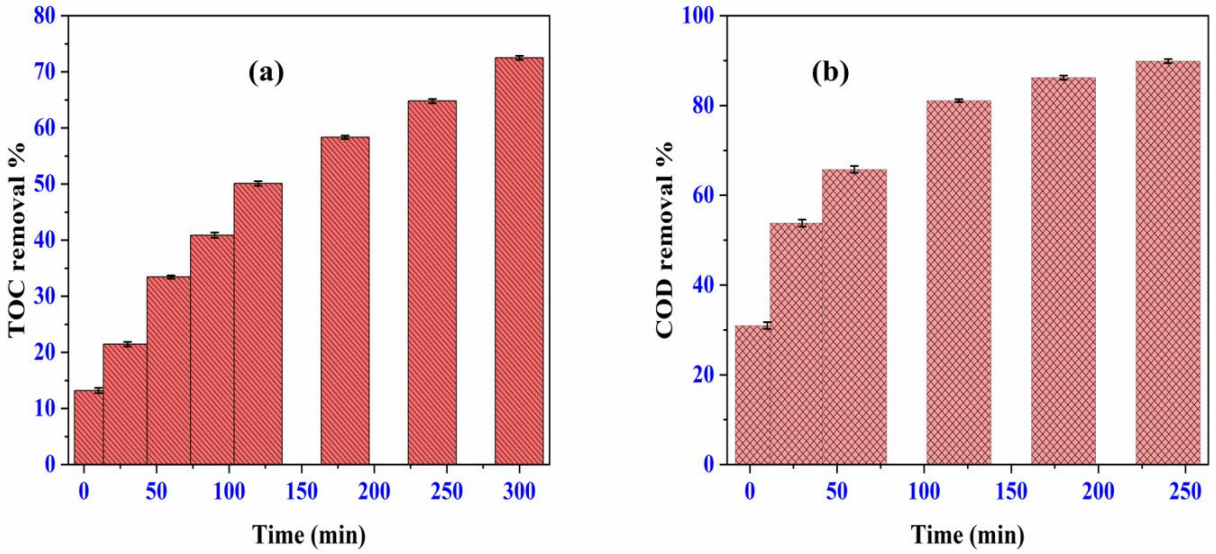


Figure 4.30. The TOC (a) and COD (b) removal efficiencies of the EO process at varying EO times (current density = 44 mA/cm$^2$, pH = 5.5, EO time = 80 min).

### 4.7.7. Application of EO in multiple contaminants removal

The efficiency of the EO process was further tested on the simultaneous degradation of multiple pharmaceutical contaminants under optimal operating conditions. The simultaneous degradation of pharmaceutical contaminants such as ACM, CIP, AMX and ATN was investigated. Figure 4.31 depicts the degradation efficiency of the EO process in removing multiple pharmaceutical contaminants from wastewater. In this study, a pharmaceutical contaminant concentration of 20 mg/L (for each pollutant) was utilized to investigate the simultaneous degradation of multiple

pharmaceutical contaminants. However, it has been reported that these compounds are present in trace amounts in actual environmental water samples.

Degradation efficiencies of 77.5%, 73%, 68.5% and 63% were obtained for ACM, CIP, ATN and AMX, respectively. Under the same conditions, degradation efficiencies of 95.5% (ACM) and 93.55% (CIP) were obtained for binary contaminant mixture (ACM+CIP). The recorded reduction in the degradation efficiency between the multi-component and binary contaminant degradation can be attributed to the shared utilization of the electro-generated ROS among the contaminants. The degradation efficiency would be higher, potentially even complete, under the same operational conditions for environmental concentrations of these compounds. Therefore, testing treatment technologies at higher concentrations helps to understand the extent to which concentrations that the proposed treatment techniques can tolerate.

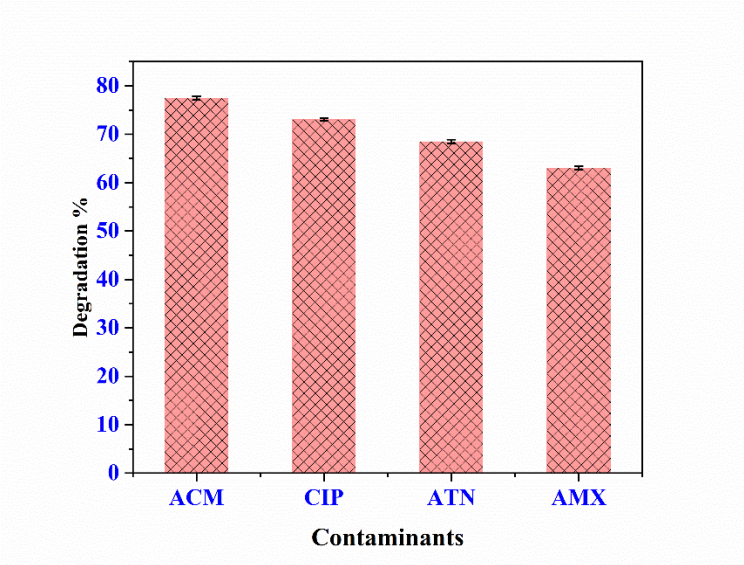


Figure 4.31. Degradation of multiple pharmaceutical contaminants using EO (current density = 44 mA/cm$^2$, pH = 5.5, EO time = 80 min and initial ACM/CIP/ATN/AMX = 20 mg/L).

## 4.8. Coupled process (EO+adsorption) optimization

The coupled process (EO+adsorption) was optimized using a coupled process optimization technique in which the main parameters of the EO and adsorption process were considered. This approach is helpful for understanding the mutual inter-dependence between the EO and the adsorption process parameters. Consequently, coupled optimization determined the best

operating conditions for the integrated process. Moreover, the degradation efficiencies of pharmaceutical compounds were compared and evaluated under optimal conditions of both the coupled and individual processes. The BBD was employed to optimize the removal of ACM and CIP from water in the coupled process. The factorial levels of the EO and adsorption process parameters were set based on the preliminary experimental results. However, among other RSM, the BBD provides reasonably enough experimental design for the coupled process in terms of cost and operational time. The BBD experimental data for ACM and CIP removal is provided in appendix (Table C.2). In the coupled process optimization, the quadratic model (second-order polynomial) well described the experimental data of ACM and CIP removal. The suggested quadratic model's $R^2$ and adjusted $R^2$ were 0.987 and 0.976 for ACM and 0.987 and 0.977 for CIP. ANOVA was employed to investigate the validity and adequacy of the suggested model and evaluated the influence of main and interaction factors on the coupled process. The ANOVA result corroborated that the suggested model was statistically significant, indicating the relevance of the applied model. The ACM and CIP ANOVA results are presented in Table 4.9. As shown in Table 4.9, the F- and p-values of the suggested model were 95.8 and < 0.0001 for ACM and 96.41 and <0.0001 for CIP, respectively.

There is only a 0.01% chance that this large F-value (134.47 (ACM) and 162.82(CIP)) could occur due to noise for both compounds. Based on ANOVA, terms with p-values less than 0.05 were A, B, C, D, E, AC, AE, BD, DE, $A^2$, $B^2$, $C^2$, $D^2$ and $E^2$ showing that these terms were significant model terms. All the main factors and interaction factors (AC, AE, BD and DE) influenced the coupled process during ACM and CIP removal from water. However, terms on the AVONA (Table 4.9) with p-values higher than 0.05 were insignificant and did not affect the coupled process significantly. Another important model parameter is the Lack of Fit (0.0899 for ACM and 0.109 for CIP), which is insignificant for both ACM and CIP, indicating that the suggested model fits the experimental data well. This is further confirmed by noting that there is only 8.99% (ACM) and 10.9% (CIP) chance that Lack of Fit F-values (0.0899 and 0.109) these large could occur due to noise. On top of this, Adeq Precision evaluates the signal-to-noise ratio and a value greater than 4 is desirable. In this BBD design, a ratio of 33.42(ACM) and 33.15 (CIP) indicates an adequate signal, affirming the suitability of the model to successfully navigate the design space.

Table 4.9. ANOVA for ACM and CIP removal using the coupled process (EO+adsorption).

| Source: ACM | Sum of Squares | df | Mean Square | F-value | p-value | |
|---|---|---|---|---|---|---|
| Model | 3566.89 | 20 | 178.34 | 95.80 | < 0.0001 | significant |
| A-EO Time | 134.44 | 1 | 134.44 | 72.22 | < 0.0001 | |
| B-pH | 30.47 | 1 | 30.47 | 16.37 | 0.0004 | |
| C-Current | 1947.90 | 1 | 1947.90 | 1046.37 | < 0.0001 | |
| D-Adsorbent dose | 305.55 | 1 | 305.55 | 164.13 | < 0.0001 | |
| E-Adsorption time | 47.33 | 1 | 47.33 | 25.43 | < 0.0001 | |
| AB | 2.98 | 1 | 2.98 | 1.60 | 0.2178 | |
| AC | 13.10 | 1 | 13.10 | 7.04 | 0.0137 | |
| AD | 1.66 | 1 | 1.66 | 0.8939 | 0.3535 | |
| AE | 44.42 | 1 | 44.42 | 23.86 | < 0.0001 | |
| BC | 1.12 | 1 | 1.12 | 0.6036 | 0.4445 | |
| BD | 29.38 | 1 | 29.38 | 15.78 | 0.0005 | |
| BE | 0.0132 | 1 | 0.0132 | 0.0071 | 0.9335 | |
| CD | 1.59 | 1 | 1.59 | 0.8528 | 0.3646 | |
| CE | 2.37 | 1 | 2.37 | 1.27 | 0.2697 | |
| DE | 5.20 | 1 | 5.20 | 2.79 | 0.1072 | |
| $A^2$ | 159.57 | 1 | 159.57 | 85.72 | < 0.0001 | |
| $B^2$ | 139.13 | 1 | 139.13 | 74.74 | < 0.0001 | |
| $C^2$ | 971.25 | 1 | 971.25 | 521.74 | < 0.0001 | |
| $D^2$ | 127.87 | 1 | 127.87 | 68.69 | < 0.0001 | |
| $E^2$ | 113.49 | 1 | 113.49 | 60.96 | < 0.0001 | |
| Residual | 46.54 | 25 | 1.86 | | | |
| Lack of Fit | 43.34 | 20 | 2.17 | 3.39 | 0.0899 | not significant |
| Pure Error | 3.19 | 5 | 0.6390 | | | |
| Cor Total | 3613.43 | 45 | | | | |

Table 4.9. Continued.

| Source: CIP | Sum of Squares | df | Mean Square | F-value | p-value | |
|---|---|---|---|---|---|---|
| Model | 3878.34 | 20 | 193.92 | 96.41 | < 0.0001 | significant |
| A-EO Time | 148.35 | 1 | 148.35 | 73.76 | < 0.0001 | |
| B-pH | 39.00 | 1 | 39.00 | 19.39 | 0.0002 | |
| C-Current | 2035.81 | 1 | 2035.81 | 1012.16 | < 0.0001 | |
| D-Adsorbent dose | 328.97 | 1 | 328.97 | 163.56 | < 0.0001 | |
| E-Adsorption time | 55.54 | 1 | 55.54 | 27.61 | < 0.0001 | |
| AB | 0.7225 | 1 | 0.7225 | 0.3592 | 0.5543 | |
| AC | 22.28 | 1 | 22.28 | 11.08 | 0.0027 | |
| AD | 0.0006 | 1 | 0.0006 | 0.0003 | 0.9861 | |
| AE | 50.20 | 1 | 50.20 | 24.96 | < 0.0001 | |
| BC | 1.32 | 1 | 1.32 | 0.6575 | 0.4251 | |
| BD | 34.75 | 1 | 34.75 | 17.28 | 0.0003 | |
| BE | 6.38 | 1 | 6.38 | 3.17 | 0.0872 | |
| CD | 1.09 | 1 | 1.09 | 0.5429 | 0.4681 | |
| CE | 6.89 | 1 | 6.89 | 3.43 | 0.0760 | |
| DE | 13.54 | 1 | 13.54 | 6.73 | 0.0156 | |
| $A^2$ | 222.71 | 1 | 222.71 | 110.73 | < 0.0001 | |
| $B^2$ | 188.44 | 1 | 188.44 | 93.69 | < 0.0001 | |
| $C^2$ | 1065.94 | 1 | 1065.94 | 529.96 | < 0.0001 | |
| $D^2$ | 204.79 | 1 | 204.79 | 101.82 | < 0.0001 | |
| $E^2$ | 129.86 | 1 | 129.86 | 64.57 | < 0.0001 | |
| Residual | 50.28 | 25 | 2.01 | | | |
| Lack of Fit | 46.49 | 20 | 2.32 | 3.06 | 0.1090 | not significant |
| Pure Error | 3.79 | 5 | 0.7589 | | | |
| Cor Total | 3928.62 | 45 | | | | |

The final predicted model equations for the removal of ACM and CIP from water using the EO process in terms of coded factors are presented in Eqs. (4.27-4.28). The A, B, C, D, AC, AE, BD, $A^2$, $B^2$, C2, $D^2$ and $E^2$ are the significant model terms for ACM and CIP removal from water.

$$ACM\ removal = +99.23 + 2.90 \times A - 1.38 \times B + 11.03 \times C + 4.37 \times D + 1.72 \times E + 1.81 \times AC + 3.33 \times AE + 2.71 \times BD - 4.28 \times A^2 - 3.99 \times B^2 - 10.55 \times C^2 - 3.83 \times D^2 - 3.61 \times E^2 \quad (4.27)$$

$$CIP\ removal = 99.14 + 3.05 \times A - 1.56 \times B + 11.28 \times C + 4.53 \times D + 1.86 \times E + 2.36 \times AC + 3.54 \times AE + 2.96 \times BD - 5.05 \times A^2 - 4.65 \times B^2 - 11.05 \times C^2 - 4.84 \times D^2 - 3.86 \times E^2 \quad (4.28)$$

The coefficients of the coded equation elucidate how the process factors affect the removal of ACM and CIP through the coupled process treatment. In the coded equation, the antagonistic (negative coefficient) and synergetic effects (positive coefficients) of the process were observed. The positive coefficients of factors in ACM and CIP removal depicted that A, C, D and E were the main factors that positively impacted the ACM and CIP removal. On the other hand, interaction factors such as AC, AE and BD were the factors with a positive influence on the ACM and CIP removal. All other factors (B, $A^2$, $B^2$, $C^2$, $D^2$ and $E^2$) negatively influenced the ACM and CIP removal in the coupled process. The influence of the main factors on the ACM and CIP removal can be ordered as C > D > A > E >B, which agrees with the ANOVA results. These results suggest that current density and adsorbent dose had the most significant impact on the ACM and CIP removal process. It should be noted that the equation in terms of coded factors can be used to make predictions about the response for given levels of each factor. In this context, the high levels of the factors are coded as +1, and the low levels are coded as -1. The coded equation is useful for identifying the relative impact of the factors by comparing the factor coefficients. The one factor plots of the coupled process for ACM and CIP is provided in appendix (Figure D.1– Figure D.2).

Overall, the model fit statistics showed that the suggested ACM and CIP models represented more than 99% of the variation in the ACM and CIP removal responses. The model diagnostic plots, such as externally studentized residuals against predicted, predicted against actual, and the normal probability against externally studentized residuals, were analyzed to evaluate the

adequacy of the model. The model diagnostic plots of ACM and CIP are provided in the appendix (Figure D.3 (a-e)) and appendix (Figure D.4 (a-e)), respectively. The normal probability against externally studentized residual appendix (Figure D.3 (e)) and appendix (Figure D.4 (e)) indicated that all the predicted points are close to the straight line, showing that the error was normally distributed. On the other hand, the plot of predicted against actual shown in appendix (Figure D.3 (a)) and appendix (Figure D.4 (a)) exhibited that the predicted values are well correlated with the actual (experimental) values, and the model predicted data were not significantly different from the experimental results. The highest differences between the actual and predicted values were 1.81 and 1.90 for the predicted values of 89.20% and 90.75% for ACM and CIP, respectively. As can be seen in appendix (Figure D.3 (b)) and appendix (Figure D.4 (b)), the plot of externally studentized residuals against predicted revealed that the residuals were randomly distributed between +3.00 and −3.00, demonstrating that the BBD model successfully established the relationship between the independent variable and the responses (Peng et al., 2021). In sum, the model diagnostic plot results agree with the results of the model fit statistics. Thus, the suggested quadratic model successfully represented the coupled process experimental data of ACM and CIP removal from water.

### 4.8.1. Main process factors affecting the coupled process

#### a) Effect of EO time on coupled process

The ANOVA analysis (Table 4.9) exhibited that the EO time was one of the significant factors that influenced the coupled process operation. The EO time was varied from 10 min to 60 min to evaluate its effect on the coupled process as presented in Figure 4.32 (a and d). Under central conditions (current density = 20 mA/cm$^2$, pH = 6, adsorption time = 50 min and adsorbent dose = 0.1g/L), the removal of ACM and CIP indicated a significant increase from 92.06% and 91.04% to nearly complete removal (> 99.5%) as the EO time extended from 10 min to 40 min. This can be attributed to increased hydroxyl radical production by raising the EO time (Leili et al., 2020). Any further increase in the EO time could not significantly promote the removal efficiency, as complete removal had already been achieved. Therefore, the EO time of 40 min was considered optimal oxidation time for the coupled process. This result can be ascribed to the

generation of enough ROS with increased EO time, which sufficiently degraded ACM and CIP. Also, the one factor analysis of ACM/CIP is provided in the appendix (Figure C.3- Figure C.4).

**b) Effect of initial solution pH**

The initial solution pH has a significant influence on the coupled process. As depicted in Figure 4.32 (c and f), pH varied from 3-9 to investigate the impact of initial solution pH (in the EO step) on the removal of pharmaceuticals. The removal of ACM and CIP increased from 96.62% and 96.05% to 99.35% and 99.26%, respectively, when the initial solution pH of the EO process increased from 3 to 5.5 under central conditions (current density = 20 $mA/cm^2$, EO time = 35 min, adsorption time = 50 min and adsorbent dose = 0.1g/L). However, a further increase in pH from 5.5 to 9 decreased ACM and CIP removal from 99.35% and 99.3% to 93.86% and 92.93%, respectively. These results can be attributed to the combined effect of EO and adsorption process such as: i) EO process is effective in the acidic pH range (pH effect on EO process explained in section 4.8.2 (d)) due to generation of more $^{\bullet}OH$ (inhibiting oxygen evolution) (Hu et al., 2020). ii) In the case of the coupled process, the EO effluent pH affects the subsequent adsorption process as the adsorption process using CAC was highly dependent on the pH of the solution (pH effect on adsorption explained in section 4.4 (i)). In this study, it was observed that pH was elevated after EO. The optimal solution pH value obtained for the coupled process was 5.5 and it became 6.9 in the EO treated water. This pH value (6.9) was suitable for the adsorption of ACM and CIP using CAC. Therefore, the auto adjustment of pH of the EO treated water can be seen as an operational opportunity for the effective application of the coupled process in target pharmaceutical contaminant removal.

**c) Effect of current density**

The effect of current density on the coupled process was investigated for the current density (15-25 $mA/cm^2$) as depicted in the response surface (Figure 4.32) and contour plots (Figure 4.33). In the coupled process, an increasing trend of pharmaceutical contaminant removal was observed with increasing the current density from 15 $mA/cm^2$ to 25 $mA/cm^2$ under central conditions of coupled process parameters. As illustrated in the response surface (Figure 4.30) and contour plots (Figure 4.33), increasing the current density from 15 to 22 $mA/cm^2$ increased ACM and CIP removal from 77.65% and 76.81% to 99.24% and 99.14% for both ACM and CIP,

respectively. This can be attributed to the increased generation of $H_2O_2$, which promoted the generation of $^{\bullet}OH$ and resulted in higher elimination of ACM and CIP from water. However, a decreasing trend of pharmaceutical contaminant removal was observed once the current density exceeded 22 $mA/cm^2$. This phenomenon observed at high current can be ascribed to the formation of side reactions (oxygen evolution and water electrolysis), formation of $HO_2^{\bullet}$ (a weak radical) instead of $^{\bullet}OH$ on the anode surface, less generation of $H_2O_2$ (due to molecules reduction into water), excess electrical energy converted to thermal energy. Moreover high currents are not desirable in terms of cost (Ahmadi et al., 2021).

**d) Effect of adsorbent dose**

The effect of adsorbent dose is one of the significant factors in the coupled process operation. In section 4.4, the influence of the adsorbent dose on the simultaneous removal of ACM and CIP was explained in detail. Under central conditions, Figure (4.32 c and f) revealed that increasing the adsorbent dose from 0.08 to 0.1 g/L increased the ACM and CIP removal efficiency from 91.6% and 89.9% to 100% and 99.9%, respectively. Meanwhile, increasing the adsorbent dose beyond 0.1 g/L has no significant impact on the removal efficiency, as removal higher than 99.9% has already been achieved at 0.1 g/L. Therefore, 0.1 g/L is an optimal adsorbent dose for the coupled process operation (adsorption step).

**e) Effect of adsorption time**

The adsorption time (contact time) has a significant influence on the removal of pharmaceutical contaminants from water in the coupled process (detailed explanation provided in section 4.4). The effect of adsorption time on the removal of ACM and CIP from water employing the coupled process was studied for the contact time ranging from 20 min to 80 min. Under central conditions of the coupled process parameters, Figure 4.32 (e and f) depicted that the removal of ACM and CIP from water was increased from 93.9% and 93.4% to 99.41% and 99.33% when the adsorption time increased from 20 min to 60 min, respectively. This increasing trend of removal efficiency with contact time can be ascribed to the availability of sufficient contact time for the adsorbate and adsorbent during the adsorption process. However, increasing the adsorption time beyond 60 min slightly increased the adsorption of ACM and CIP (insignificant).

Therefore, the adsorption time of 60 min was considered optimal for ACM and CIP removal from water for the coupled process operation.

### 4.8.2. Interaction factors affecting the coupled process

#### a) The effect of interaction factors

The effect of interaction factors such as EO time with current density, EO time with adsorbent dose, and pH with adsorbent dose on ACM and CIP removal from water was provided using the contour plot in Figure 4.33 (a-f). The elliptical contour plots revealed a good interaction between the independent variables (Leili et al., 2020). Moreover, the 3D surface plots also showed interactions between the independent variables (Figure 4.32 (a and d)), which showed the mutual interaction between current density and EO time. Both variables exhibited elliptical structures, indicating that the factors had a quadratic effect on the ACM and CIP removal from water. The removal efficiency of 98-100% was obtained for the current density (20-22 $mA/cm^2$) and EO time (30-60 min) at constant values of other parameters (pH =5.5, adsorbent dose = 0.1 g/L and adsorption time = 60 min). A similar trend of interaction effect was observed in the sugar beet industry wastewater treatment with the EO process (Sharma & Simsek, 2020). Figure 4.32 (b and e) depicts the interaction between adsorption time and EO time. Higher and lower adsorption time did not result in higher removal of ACM and CIP. Again, higher and lower EO time did not result in higher removal of ACM and CIP from water. On the other hand, Figure 4.33 (b and e) indicated the interaction effect of adsorbent dose with pH, and adsorption time with EO time on the ACM and CIP removal, which indicated a quadratic effect on the ACM and CIP removal from water.

### 4.8.3. Validation of the coupled process optimization

The best operating conditions for the coupled process were evaluated using the BBD design of the RSM optimization technique. Maximum removal of pharmaceuticals has been achieved at optimal process conditions. These conditions were as follows: EO time (40 min), current density (22 $mA/cm^2$), initial solution pH (5.5), adsorbent dose (0.1 g/L), and adsorption time (60 min). Under these conditions, experimental results with triplicate removal of ACM (99.92%, 99.96%, and 99.94%) and CIP (99.86%, 99.83%, and 99.84%) were achieved. Accordingly, mean

removal results of 99.94% and 99.85% were obtained for ACM and CIP removal from water, respectively. It can be concluded that the values predicted by the model were close to the actual experimental values, confirming the validity of the predicted results.

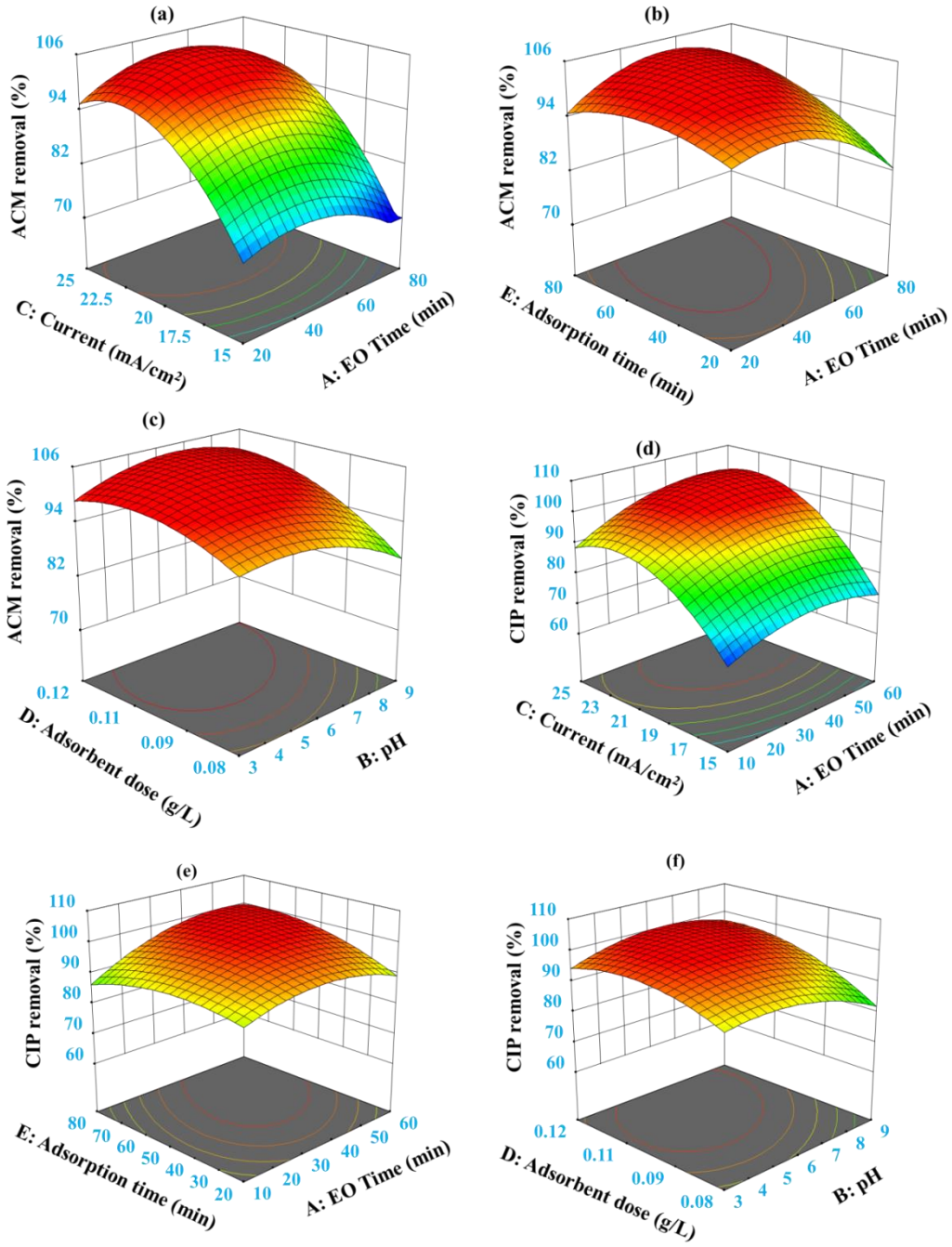


Figure 4.32. The 3D response plots of the coupled process for ACM and CIP removal.

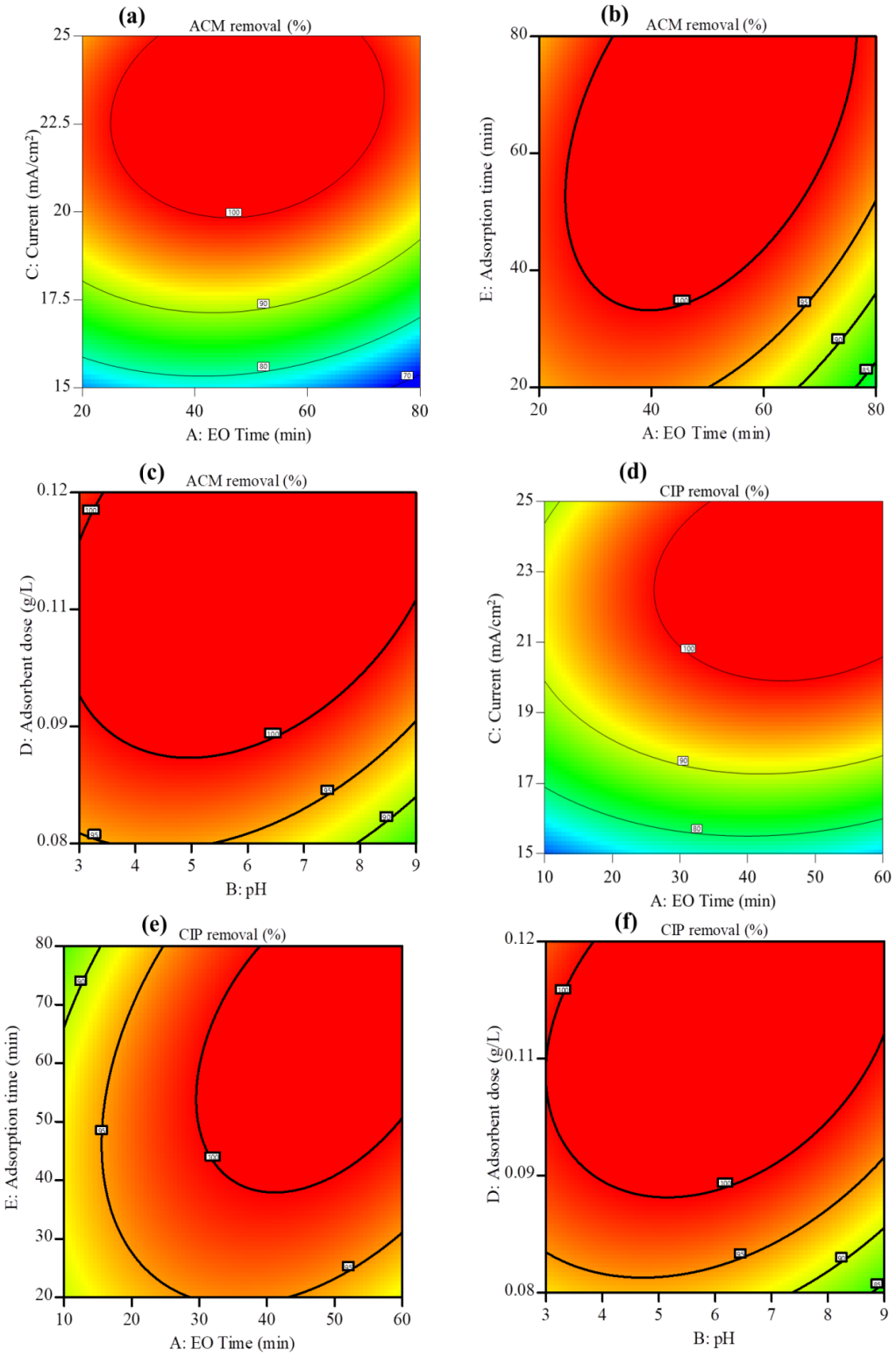


Figure 4.33. The contour plots of the coupled process for ACM and CIP removal.

### 4.8.4. TOC removal by coupled process

The mineralization is the conversion of organic pollutants mainly into $CO_2$ and $H_2O$ (Wohlmuth et al., 2018). TOC analysis is often used to evaluate the degree of mineralization of organic compounds. In advanced oxidation processes (AOPs) like EO, mineralization is frequently associated with the oxidation of organic contaminants. However, the TOC removal in the coupled process represents a combined TOC removal that includes mineralization in the EO step and adsorptive TOC removal. In general, achieving complete mineralization of organic compounds using only EO treatment at economically feasible operation is challenging. This is due to the transformation of pharmaceutical compounds into even more resistant compounds to free radical oxidation (Kermani et al., 2019). Besides, TOC removal depends on the electrode (material type and synthesis conditions) and the effect of the EO process conditions (oxidation time, pH, current density, and contaminant concentration). In the coupled process, as depicted in Figure 4.34, the TOC removal reached 80% only after 80 min of EO followed by 60 min adsorption process. Extending the EO time to 120 min for the same adsorption time resulted in complete removal of TOC from the aqueous solution under optimal conditions of the coupled process. Compared to the EO process alone (Figure 4.30), a notable TOC removal was achieved at relatively lower EO time and lower current density. This result can be ascribed to the combined contribution of EO (mineralization) and adsorption process (removal of target and non-target compounds through binding onto CAC) in TOC removal. Notably, the organic by-products of EO process were effectively eliminated in the subsequent adsorption process, showcasing the synergistic actions of the coupled process in target pharmaceuticals removal from water.

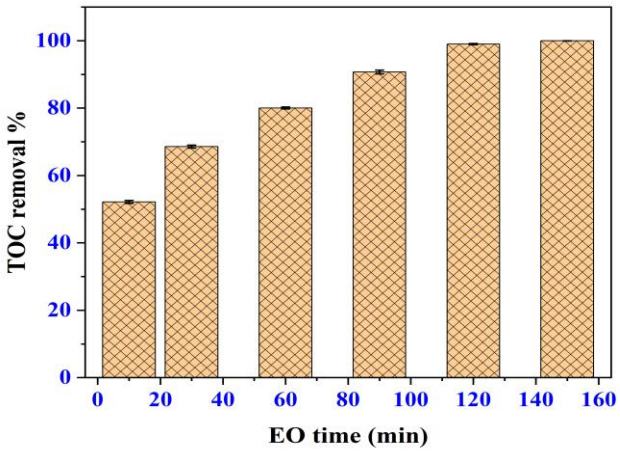


Figure 4.34. TOC removal using the coupled process (current density = 22 mA/cm$^2$, pH = 5.5, adsorbent dose = 0.1 g/L and adsorption time = 60 min).

### 4.8.5. Effect of water matrix on the coupled process

The elimination of organic micro-pollutants (OMPs) from water is greatly affected by the composition of the water matrix (Lado et al., 2019). Unlike the individual processes (EO and adsorption process), the coupled process (EO+adsorption) is very effective on a wide range of water matrices. Individual processes are highly sensitive to the complex water matrices due to either radical scavenging or competition effect of the constituents of the water matrices. However, the coupled process exhibited sufficient tolerance to these effects, resulting in higher contaminant removal. In this study, various water matrices such as pure water, tap water and real wastewater (wastewater treatment effluent) were considered to investigate the potential of the coupled process over different water matrices. As shown in Table 4.10, the current density is the most significant factor among the coupled process parameters. Hence, the variation in current density (5-35 mA/cm$^2$) was considered to study the effect of the water matrix on the simultaneous removal of ACM and CIP from water and wastewater, as shown in Figure 4.35. In the coupled process, as demonstrated in Figure 4.35, the removal of ACM and CIP from water significantly increased from 77.75% and 74.25% to 97.7% and 97.02%, respectively, with an increase in current density from 2 mA/cm² to 20 mA/cm² in pure water, under optimal dosage of adsorbent (0.1 g/L). In the case of tap water, the ACM and CIP removal increased from 69.22%

and 64.25% to 95.82% and 93.85% when the current density increased from 5 mA/cm$^2$ to 20 mA/cm$^2$. In the real wastewater, the ACM and CIP removal raised from 58.15% and 53.87% to 86% and 80.4% when the current density increased from 2 mA/cm$^2$ to 20 mA/cm$^2$. Further, an increase in the current density to 30 mA/cm$^2$ increased the ACM and CIP removal to 94.77% and 93%, respectively.

The order of pharmaceutical removal efficiency in water matrices follows: pure water > tap water > real wastewater. In real wastewater, the removal efficiency is relatively low compared to pure water and tap water, showing that real wastewater comprises diverse constituents that influenced the coupled process removal efficiency. The water matrix compositions have either scavenging or competition effects for the ROS and active sites of the adsorbent in the coupled process. Compared to the individual processes, the coupled process greatly tolerates the effect of the water matrix and provided higher ACM+CIP removal efficiencies with a relatively small current density and adsorbent dose. The benefit of the coupling EO with adsorption is much more evident in a real water matrix, as it shows superior tolerance to these effects compared to the single treatment processes. These results suggest that single processes are susceptible to the water matrix, while the coupled process has shown remarkable tolerance to the effects of various water matrices. Therefore, the application of coupled processes such as EO+adsorption has been demonstrated to be beneficial in actual environmental water matrices.

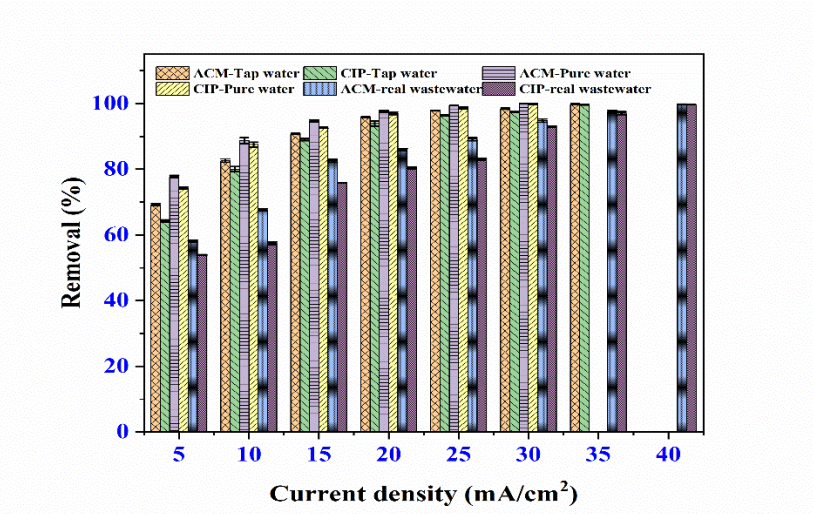


Figure 4.35. Effect of water matrix on simultaneous removal of ACM and CIP from water using the coupled process (pH = 5.5, EO time = 40 min, adsorbent dose = 0.1 g/L and adsorption time = 60 min).

### 4.8.6. COD removal using coupled process

The COD parameter indicates the pollution level of the aqueous solution as it shows the amount of organic matter in the water (Rodríguez-chueca et al., 2018). Therefore, evaluating the COD removal in oxidation-mediated water treatment is worthwhile. In most cases, it is known that the EO process, like other AOPs, cannot fully mineralize organic contaminants from water. The possible factors include the effect of the water matrix, electrode material types, operational parameters, and cost limitations. High COD removal can be achieved at higher current density; however, the cost issues associated with the high current density deter the use of higher current densities. Consequently, evaluating the COD of the aqueous solution provides an alternative way of monitoring the pollution level. The removal of COD by the EO and the coupled process was investigated under their respective optimal conditions. Figure 4.36 indicates the recorded COD removal efficiency for the coupled process varying the EO time (0-120 min) under optimal conditions (current density (22 $mA/cm^2$), adsorbent dose (0.1 g/L) and adsorption time (60 min)). As the EO time increased from 10 to 90 min, the COD reduction rose from 66.5% to 99.5%. Extending the EO time to 120 min resulted in the complete removal of the COD from the aqueous solution. Herein, the COD removal results of the coupled process (EO+adsorption) showed similar findings with another coupled system (air flotation + electrochemical oxidation + adsorption) that depicted 95% COD removal from laundry and food wastewaters (Lee et al., 2020). Overall, these results suggest that the coupled process provided superior COD removal with oxidative+adsorptive removal of target/non-target compounds and EO-generated inorganic compound at a relatively lower EO time compared to the EO process alone.

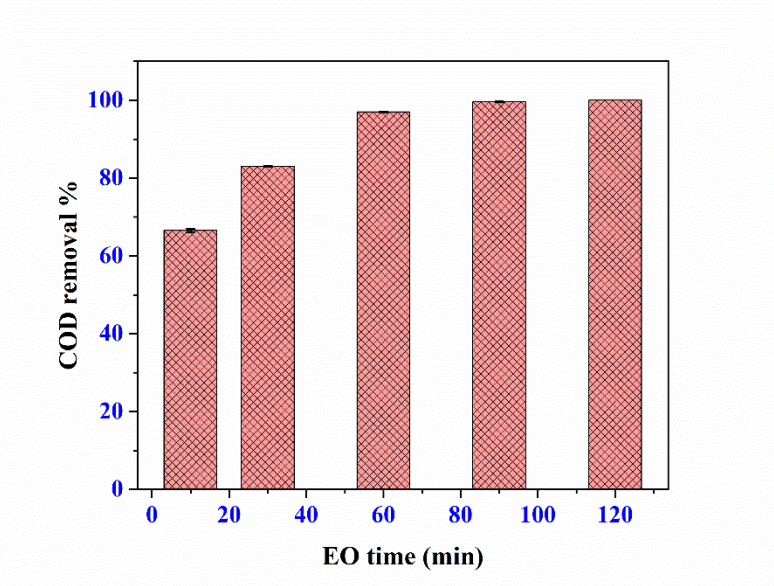


Figure 4.36. The COD removal efficiency of the coupled process (current density = 22 mA/cm$^2$, pH = 5.5, adsorbent dose = 0.1 g/L and adsorption time = 60 min).

### 4.8.7. Application of coupled process in multiple pharmaceuticals removal

The coupled process was employed in the simultaneous removal of pharmaceutical contaminants (ACM+CIP+ATN+AMX) from water. Multiple pharmaceutical removal tests were conducted by spiking the aforementioned pharmaceuticals into ultra-pure water (20 mg/L each) at optimal current density (22 mA/cm$^2$), varying the adsorbent dose (0.01 - 0.2 g/L). The multiple pharmaceutical removal efficiency of the coupled process is provided in Figure 4.37. Figure 4.37 demonstrated that increasing the adsorbent dose from 0.01 to 0.1 g/L resulted in the removal efficiencies of 92.32%, 87.86%, 92.15% and 85.14% for ACM, CIP, ATN and AMX, respectively. Further increase in the adsorbent dose to 0.2 g/L resulted in > 99.7% removal of all the pharmaceuticals from the water. The increase in pharmaceuticals removal with adsorbent dose was due to the availability of more adsorption sites and high surface area (Jasna et al., 2020). A similar trend of contaminant removal with adsorbent dose was reported in a study which considered the integrated electrochemical-adsorption process for nitrate removal from water (Jasna et al., 2020). In this study, other additional pharmaceutical contaminants (ATN and AMX) suppressed the removal efficiencies of ACM and CIP. This result can be attributed to the shared utilization of ROS in the EO process and the active sites of the adsorbent in the adsorption process for the pharmaceuticals. Removal efficiency higher than 85% was achieved in

the coupled process for the removal of ternary component contaminant from the water. Environmental wastewater often contains lower concentrations of pharmaceuticals (ng/L to µg/L). Therefore, the efficiency of the current coupled process is expected to be higher than reported for the lower concentration of pharmaceutical contaminants.

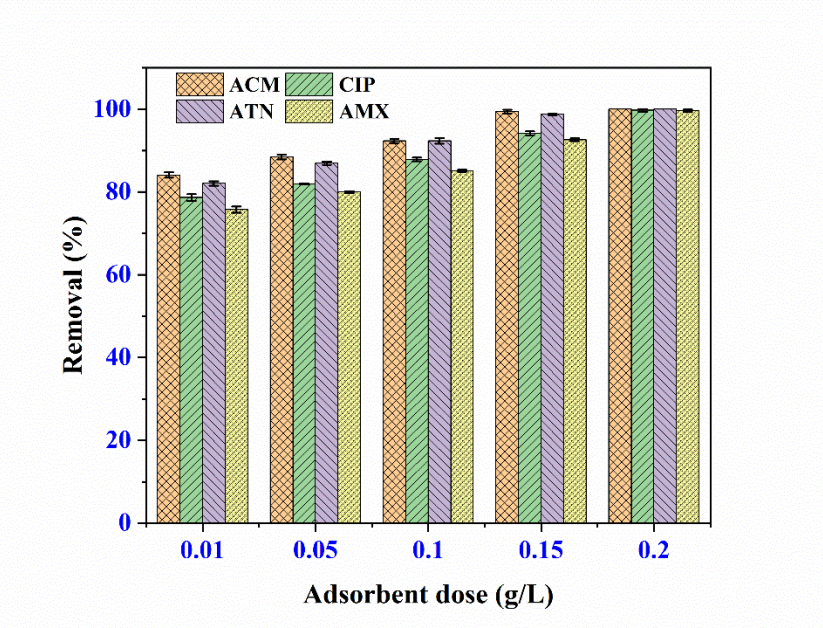


Figure 4.37. The removal of multiple pharmaceuticals from water using the coupled process (current density = 22 mA/cm$^2$, pH = 5.5, EO time = 40 min and adsorption time = 60 min).

## 4.9. Performance evaluation of single and coupled processes

### 4.9.1. COD removal

The removal of COD by the EO process alone and the coupled process was investigated under optimal conditions of the EO and coupled processes. Figure 4.38 demonstrates the increase of COD removal from 30.98% to 90.4% in the EO process alone, as the EO time increased from 10 min to 240 min. On the other hand, COD removal increased from 66.5% to 99.5% in the coupled process as the EO time increased from 10 min to 90 min, indicating a notable removal at only 90 min. The observed increasing trend of COD removal with EO time in single and coupled process is attributed to the sufficient oxidation time provided for the contaminant to be addressed by the generated ROS. The higher COD removal recorded at shorter EO time in the coupled process is due to the combined effect of EO and the adsorption process. The recalcitrant by-products

generated during the EO process (Montenegro-ayo et al., 2023) were removed in the adsorption step. Herein, a complete removal of COD was obtained for EO time exceeding 90 min in the coupled process, showing a distinct advantage of the coupled process over the single process (EO process). In agreement with the results of this study, higher COD removal (93%) was reported for the coupled process (electrochemical oxidation + biodegradation) from Congo Red and textile effluent (Sathishkumar et al., 2019). It can be concluded that the coupled (electrochemical-based) processes provided superior COD removal (oxidative+adsorptive) compared to the individual processes.

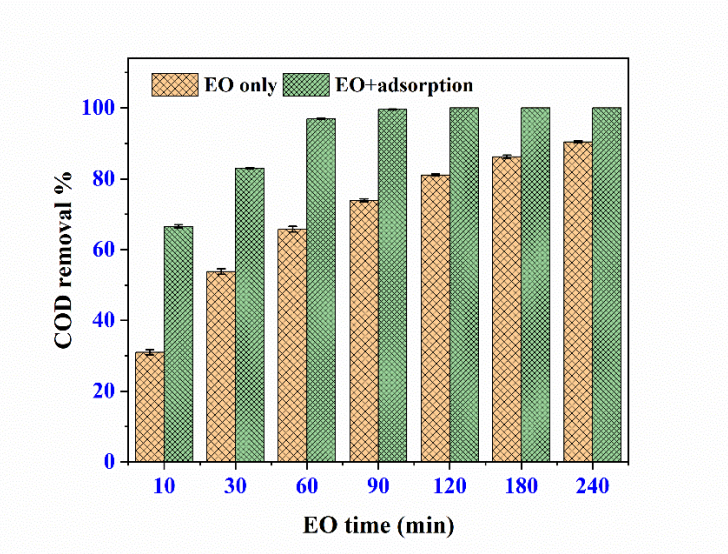


Figure 4.38. Performance evaluation of the single and coupled process in COD removal from water: EO process (current density = 44 mA/cm$^2$, pH = 5.5, $C_o$ = 20 mg/L) and coupled process (current density = 22 mA/cm$^2$, pH = 5.5, adsorption time = 60 min and adsorbent dose = 0.1 g/L) varying the EO process time (10-240 min).

### 4.9.2. TOC removal

The comparative evaluation of EO and coupled process on the elimination of TOC is provided in Figure 4.39. In the single EO process, the TOC removal occurs entirely through the EO process. However, the TOC removal observed in the coupled process is due to the synergistic action of the EO and adsorption process. In the EO process, TOC removal is directly related to the mineralization of the organic compounds present in the treated aqueous solution. Conversely, the

TOC removal through the coupled process signifies a combination of mineralization (contributed by the EO process) and mere physical removal of TOC through adsorption. It should that TOC removal in EO+adsorption is not only due to the mineralization, but due to the combination of mineralization at EO step followed by adsorptive removal of target and non-target compounds from water. Figure 4.39 illustrates the removal of TOC by the single EO process and EO+adsorption process under optimal conditions by varying the EO time in both cases. It can be seen in Figure 4.39 that the TOC removal increased from 13.2% to 72.5% when EO time was increased from 10 min to 300 min. Till now, the permissible level of COD and TOC removal have not been achieved in an economical way for the EO treatment due to the formation of electrochemically non-degradable transformation by-products of organic halogens and toxic ions (Ganesan et al., 2019).

In this regard, coupled processes are required to attain a permissible level of TOC and COD removal economically. As depicted in Figure 4.39, TOC removal increased from 52.16% to > 99% when the EO time improved from 10 min to 120 min in the coupled process. Notably, the coupled process demonstrated superior TOC removal due to the synergistic action, which would otherwise be challenging for the EO process alone. These results unveil the possibility of achieving complete TOC removal with a relatively shorter EO time employing the coupled process. Therefore, the subsequent adsorption process is crucial to remove the chlorinated organic compounds from the electrochemical oxidation effluents (GilPavas et al., 2020).

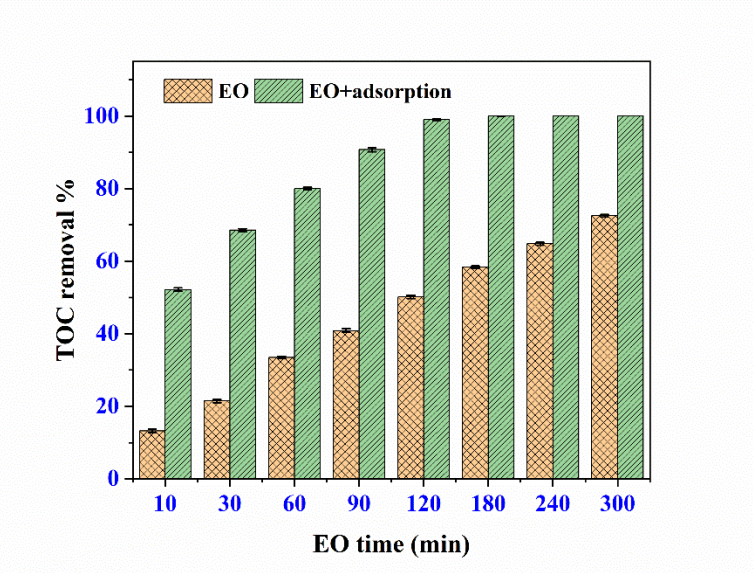


Figure 4.39**.** Performance evaluation of single and coupled process in TOC removal from water (EO process: current density = 44 mA/cm$^2$, pH = 5.5 and coupled process: current density = 22 mA/cm$^2$, pH = 5.5, adsorption time = 60 min and adsorbent dose = 0.1 g/L).

### 4.9.3. Binary contaminant (ACM+CIP) removal

The comparative evaluation of EO, adsorption and coupled process on the simultaneous removal of ACM and CIP (binary contaminant mixture) is provided in Figure 4.40. Under optimal conditions of each process, removal efficiencies of 95.05% for ACM and 93.5% for CIP in EO, 94.07% for ACM and 91.4% for CIP in adsorption, and > 99.8% for both ACM and CIP were achieved in the coupled process. The coupled process provided remarkable removal of the pharmaceutical contaminants (ACM+CIP) from water. On top of this, the coupled process addresses EO oxidation by-products, as evidenced by the higher removal of TOC and COD, as explained earlier. Hence, the coupled process can provide complete removal of pharmaceutical contaminants and associated oxidation by-products under optimal conditions. Higher removal efficiencies were recorded in the binary component contaminant removal systems (ACM and CIP) compared to the multiple component systems. This can be ascribed to the competition among contaminants for the generated ROS and the available adsorbent active sites.

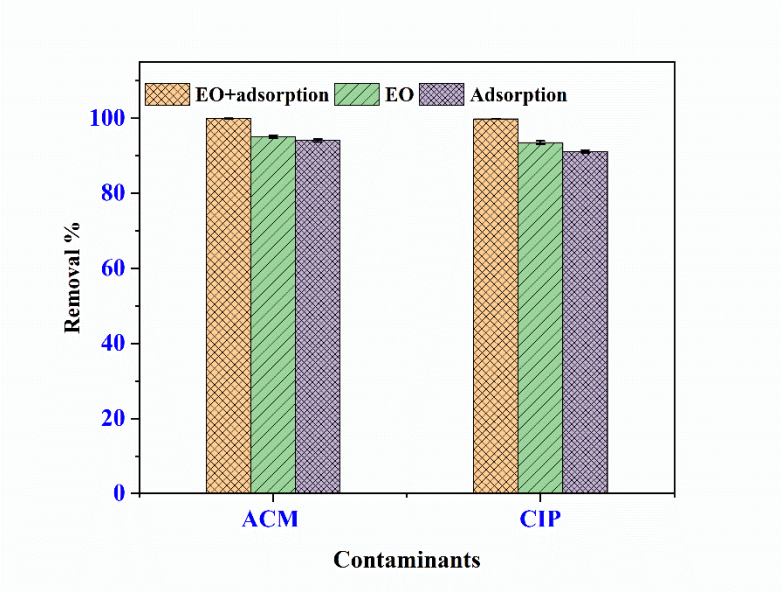


Figure 4.40. Performance evaluation of the single and coupled process in ACM+CIP removal from water (sole EO optimal conditions: pH = 5.5, ACM+CIP initial concentration = 20 mg/L, current density = 44 mA/cm$^2$ and NaCl = 0.05M and oxidation time = 80 min; sole adsorption process optimal conditions: adsorbent dose = 0.5 g/L, pH = 6.8, contact time = 120 min and ACM/CIP concentration = 20 mg/L; coupled process optimal conditions: current density = 22 mA/cm$^2$, EO time = 40 min, NaCl = 0.05 M, adsorbent dose = 0.1 g/L, pH = 5.5, ACM/CIP initial concentration = 20 mg/L and adsorption time = 60 min).

### 4.9.4. Multiple pharmaceuticals removal

The simultaneous removal of multiple contaminants from water demands treatment technologies capable of addressing the diverse nature of pharmaceutical contaminants. In this context, coupled treatment technologies are beneficial in removing contaminants with diverse nature through their synergistic action. Figure 4.41 demonstrates the removal efficiencies of pharmaceutical contaminants (ACM, CIP, ATN and AMX) employing a single EO process, single adsorption process and coupled process (EO+adsorption). Figure 4.41 showed that the removal efficiencies of 83.35% (ACM), 73.1% (CIP), 68.52% (ATN) and 63.05% (AMX) were obtained in the simultaneous removal of multiple contaminants using the EO process. On the other hand, removal efficiencies of 80.37% (ACM), 66.5% (CIP), 73.07% (ATN) and 60.47% (AMX) were

achieved using the adsorption process. Compared to adsorption, the EO process provided the highest removal of ACM, CIP and AMX from water. In contrast, the highest removal of ATN was achieved in the adsorption process. It can be seen in Figure 4.41 that the coupled process provided more than 99% of all the contaminants. Also, it is worth noting that varying efficiencies were obtained between the individual processes, indicating that some contaminants are better removed by the EO process while others are effectively removed by the adsorption process. Therefore, coupling EO with adsorption would offer opportunities to effectively utilize the synergy between the two processes. Unlike the case of single or binary component contaminant removal, the single treatment processes face serious limitations during the simultaneous removal of multiple contaminants from water. This can be ascribed to the diverse nature of the contaminants, the shared utilization of the ROS (EO process) and the limited availability of adsorbent active sites. In this regard, the variation in the removal efficiencies between the coupled and individual processes (EO and adsorption) becomes increasingly pronounced when transitioning from a single to a binary contaminant system and from a binary to the removal of multiple pharmaceuticals. The enhanced removal of multiple pharmaceuticals from water employing the coupled process can be attributed to the systematic utilization of the synergy between EO and the adsorption process. In line with the findings of this study, the integrated process (electrochemical oxidation-adsorption) showed superior performance compared to the individual EO and adsorption process in the removal of nitrate (as a single contaminant) and binary contaminant (nitrate +phosphate and nitrate +sulfate) mixtures from water (Jasna et al., 2020).

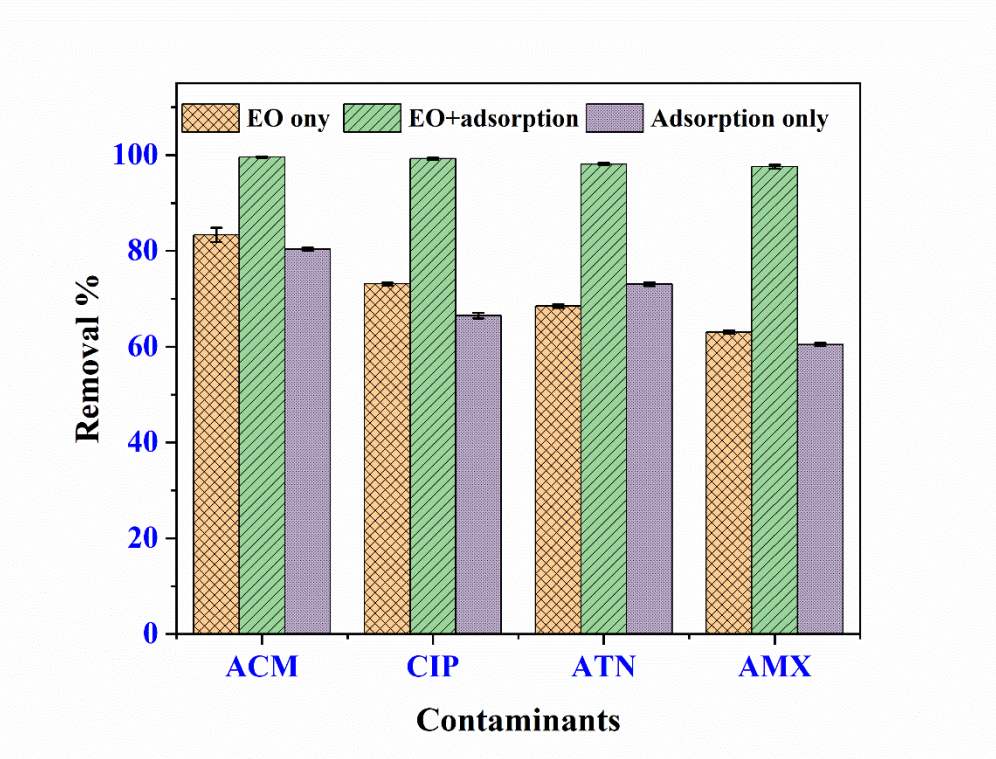


Figure 4.41. Performance evaluation of single and coupled process in multiple pharmaceuticals removal from water (EO optimal conditions: pH = 5.5, ACM/CIP initial concentration = 20 mg/L, current density = 44 mA/cm$^2$ and NaCl = 0.05M and oxidation time = 80 min; adsorption process optimal conditions: adsorbent dose = 0.5 g/L, pH = 6.8, contact time = 120 min and ACM/CIP concentration = 20 mg/L; coupled process optimal conditions: current density = 22 mA/cm$^2$, EO time = 40 min, NaCl = 0.02 M, adsorbent dose = 0.1 g/L, pH = 5.5, ACM/CIP initial concentration = 20 mg/L and adsorption time = 60 min).

### 4.9.5. Effect of water matrix on removal efficiency

The efficiency of the water treatment process is highly dependent on the water matrix. It is thus worthwhile to study the effect of water matrix on the pharmaceutical contaminant removal in EO, adsorption and the coupled process. Figure 4.42 illustrates the effect of the water matrix on the EO, adsorption and coupled process under their respective optimal conditions. It can be seen from Figure 4.42 that removal efficiencies of 95.27%, 94.1% and 99.92% were obtained for ACM in EO, adsorption and coupled processes in pure water matrix, respectively. On the other hand, removal efficiencies of 93.1%, 91.55% and 99.8% were observed for CIP employing an

EO, adsorption and coupled process, respectively, in pure water. In tap water, 76.65%, 70.67% and 94.25% removal efficiencies were obtained for ACM removal through EO, adsorption and the coupled processes, respectively. In contrast, removal efficiencies of 82.65%, 74.1% and 94.55% were achieved for CIP using EO, adsorption and the coupled processes, respectively. Most importantly, ACM removal efficiencies of 66.57%, 63.25% and 93.62% were recorded in EO, adsorption and the coupled processes in real wastewater, respectively. In real wastewater, the EO, adsorption and coupled processes exhibited CIP removal efficiencies of 62.95%, 59.05% and 92.6%, respectively.

The relatively low removal efficiencies recorded in real wastewater indicate that the real wastewater has diverse compositions that influence the removal efficiencies of the EO, adsorption and coupled processes. It implies that the water matrix has minimal effect on the coupled process compared to the individual processes. Conversely, the water matrix significantly impacted the removal of ACM and CIP in individual EO and adsorption processes. The synergistic effects of the coupled processes have been proven to effectively enhance the performance of complex and refractory wastewater treatment (Lin et al., 2022). Therefore, coupling EO and adsorption is an effective strategy for enhancing ACM and CIP removal over diverse water matrices.

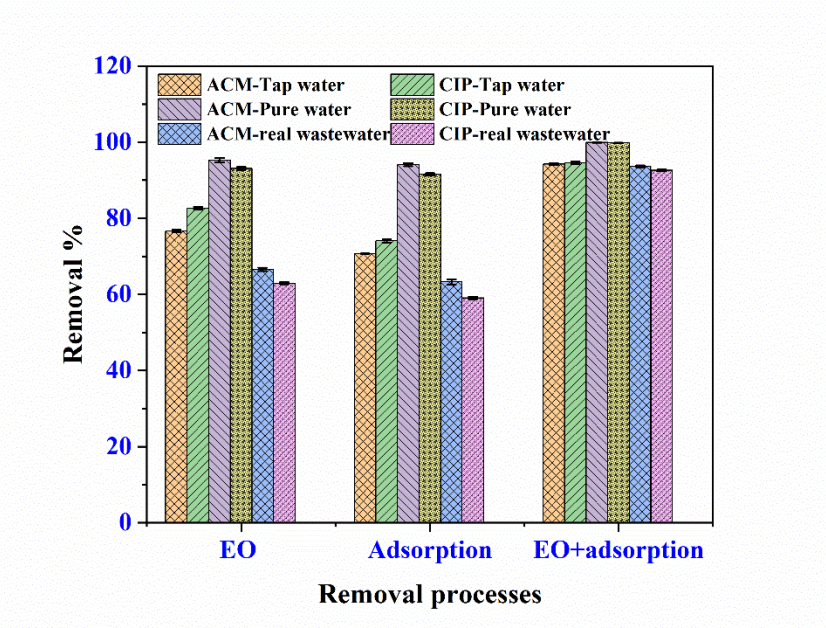


Figure 4.42. Effect of water matrix on ACM and CIP removal using single and coupled process (EO optimal conditions: pH = 5.5, ACM/CIP initial concentration = 20 mg/L, current density = 44 mA/cm$^2$ and NaCl = 0.05M and oxidation time = 80 min; adsorption process optimal conditions: adsorbent dose = 0.5 g/L, pH = 6.8, contact time = 120 min and ACM/CIP concentration = 20 mg/L; coupled process optimal conditions: current density = 22 mA/cm$^2$, EO time = 40 min, NaCl = 0.02 M, adsorbent dose = 0.1 g/L, pH = 5.5, ACM/CIP initial concentration = 20 mg/L and adsorption time = 60 min).

## 4.10. Electrical energy consumption

The energy consumption is an important economic aspect of the EO process operation. In this study, the energy consumption of the EO process is evaluated under optimal conditions of the EO and coupled processes. The energy consumption of the EO for the simultaneous degradation of ACM and CIP was found to be 31.6 kWh/m$^3$. Moreover, the energy consumption of the EO process for simultaneous degradation of ACM and CIP in the EO+adsorption process was 4 kWh/m$^3$. These results indicate that coupling EO with adsorption has significantly reduced the energy consumption of the EO process, enabling even higher removal of ACM and CIP from water compared to the EO process alone.

# 5. Conclusions

In this study, target pharmaceuticals (ACM, CIP, ACM+CIP, ACM+CIP+AMX+ATN) removal efficiencies of the EO process, adsorption and EO+adsorption processes were investigated. The CAC adsorbent was successfully synthesized from bamboo sawdust via carbonation at 700 ºC under a limited oxygen environment. The as-synthesized adsorbent (CAC) was characterized using SEM/EDS, Raman spectroscopy, XRD, FTIR, $pH_{pzc}$, and BET characterization techniques. All these characterization results confirmed that the CAC was suitably modified for enhanced adsorption of the target pharmaceuticals. Among the characterization results, BET analysis has confirmed a two-fold increase in surface area of the CAC (1158.05 $m^2/g$) compared to the raw carbonized bamboo sawdust (565.09 $m^2/g$). Besides, the SEM/EDS analysis showed that the CAC has an interesting surface structure (rich in pores and voids), while the elemental mapping analysis indicated a uniform distribution of the activating agents such as K and Fe on the surface of the CAC.

The single and coupled process studies revealed that target pharmaceuticals removal performances of these processes are highly dependent on the operational parameters. Thus, the effects of all the main operational parameters of the EO, adsorption and the EO+adsorption were rigorously studied using RSM optimization approaches. Moreover, the one-factor-at-a-time optimization approach was utilized when investigating adsorption process parameters across a wide range of levels. In contrast, RSM was used whenever there was a need to investigate many process parameters. These optimization studies revealed that all the studied factors significantly influenced the ACM and CIP removal from water in EO, adsorption and EO+adsorption.

The maximum adsorption capacity obtained in single batch mode sorption was 192.43 mg/g and 70.95 mg/g for ACM and CIP, respectively. In contrast, the maximum adsorption capacity obtained for simultaneous (binary) batch mode sorption was found to be 125.31 mg/g and 65.44 mg/g for ACM and CIP, respectively. These results indicate that the maximum adsorption capacities of ACM and CIP in a binary component adsorption system were lower than the maximum adsorption capacities in the single component adsorption systems, as indicated by the ratio of $q_{m\ binary}/q_{m\ single}$ being less than unity ($q_{m\ binary}/q_{m\ single} < 1$). This implies that when ACM and CIP are both present in water, their removal appears to be hindered by each other, indicating

an antagonistic interaction. Under optimized fixed-bed (column) operational conditions, ACM and CIP removal efficiencies of 44.23% and 37.86%, respectively, with $q_{bed}$ values of 172.48 mg/g and 147.67 mg/g were achieved in binary component pharmaceuticals (ACM+CIP) removal from water. However, higher removal efficiencies of ACM (65.83%) and CIP (42.59%) were achieved in single component column sorption, indicating suppressive adsorption in the binary system. Superior removal of ACM compared to CIP can be attributed to its lower $K_{ow}$ value and lower molecular size which enabled it to diffuse into the micro-pores of CAC. These results indicate that the simultaneous removal of ACM and CIP depends on the unique molecular properties of the ACM/CIP and their interactions with the adsorbent. The comprehensive batch and fixed-bed adsorption experiments demonstrated the promising performance of CAC in diverse water matrices.

The CCD optimization of the EO process provided an optimal EO process conditions, such as current density (44 mA/cm$^2$), pH (5.5), contact time (80 min) and initial pollutant concentration (20 mg/L). Under optimal conditions, efficient simultaneous degradation of ACM (94.5%) and CIP (92.7%) were achieved, with recorded TOC and COD removal efficiencies of 40.88% and 70.56%, respectively. The reason for the relatively lower TOC and COD removal compared to the degradation efficiency is the transformation of ACM and CIP into resistant organic compounds during the EO process. The simultaneous degradation of the ACM and CIP using EO followed a pseudo-first-order kinetic model with a reaction constants of 0.034 (1/min) and 0.035 (1/min) for ACM and CIP, respectively. Moreover, the radical scavenger test revealed that the studied EO process was dominated by the •OH radical reactions. Regardless of the higher degradation of ACM and CIP in the EO process, subsequent treatment process was required to remove the remaining un-oxidized parent pharmaceutical compounds and their degradation by-products.

The BBD optimization of the EO+adsorption process conditions provided optimal conditions such as current density (22 mA/cm$^2$), pH (5.5), contact time (40 min), adsorbent dose (0.1g/L) and adsorption time (60 min). Under these conditions, notable removal (> 99.9%) of pharmaceuticals and (> 99.5%) of TOC and COD removal was obtained (at EO time of 120 min). This result implies that the subsequent adsorption process has effectively eliminated the remaining target pharmaceuticals and the oxidation by-products from EO pre-treated water. The

EO+adsorption showcased superior removal of pharmaceuticals, TOC and COD compared to the individual EO and adsorption processes. The higher removal efficiency observed in the EO+adsorption process was due to the synergistic action of EO and the adsorption process, which combined the advantage of these individual processes. The major drawback of the AOPs, like the EO process, was the generation of degradation products (non-target organic contaminants) during oxidation. On the other hand, the adsorption process is often influenced by the water matrix and is mostly effective in single contaminant removal from simple water matrix. In this regard, the EO+adsorption process effectively removed the target pharmaceutical contaminants and oxidation by-products by addressing the drawbacks of the individual EO and adsorption processes. In addition, the energy consumption analysis of ACM+CIP degradation indicated a significant reduction in energy consumption by the EO step (4 kwh/$m^3$) in the EO+adsorption process compared to the individual EO process (31.6 kwh/$m^3$). Furthermore, the performances of EO, adsorption and EO+adsorption processes were investigated in multiple pharmaceutical removals and various water matrices. The efficiency of the single process is highly influenced in removing multiple pharmaceuticals from complex water matrices. However, the EO+adsorption process showed superior removal of binary pharmaceuticals (ACM+CIP), multiple pharmaceuticals (ACM+CIP+AMX+ATN), COD and TOC from various water matrices. In this regard, it should be noted that the coupled process is much more tolerant to the effect of water matrix compared to the single processes. Therefore, the coupled process is an efficient and environmentally viable technology that can be installed in water treatment systems.

# 6. Recommendations

This study investigated the removal of pharmaceuticals (ACM, CIP, ACM+CIP, ACM+CIP+AMX+ATN) using individual (EO and adsorption) and coupled (EO+adsorption) processes. The CAC adsorbent derived from the bamboo sawdust has been proven effective in removing single and binary component mixtures of these pharmaceuticals (ACM, CIP and ACM+CIP) from water in batch and fixed-bed adsorption processes. Herein, the CAC adsorbent was synthesized from a single precursor, bamboo sawdust. However, it is worthwhile to synthesize an adsorbent from multiple materials through co-carbonation to utilize their advantages, which may address the diverse nature of pharmaceutical compounds.

The EO+adsorption process was found to be highly effective in removing ACM+CIP, ACM+CIP+AMX+ATN, TOC and COD from diverse water matrices. As the coupled process is very interesting and highly effective, further investigation is needed into the detailed mechanism of ACM and CIP degradation pathways in the EO process. In addition to TOC and COD analysis, toxicity analysis is one of the essential studies that indicate the advantage of the coupled process, and thus, it needs to be investigated in the future studies. Most importantly, the solar power system can be employed to supply the required electrical energy for the EO process, thereby reducing the energy expenses.

This study presented that coupling the EO process with adsorption process is effective for pharmaceutical contaminant removal, considering mainly two target compounds (ACM and CIP) with further application in four pharmaceutical compounds (ACM, CIP, AMX and ATN). Further studies can be conducted considering other pharmaceuticals, as the coupled process is highly effective. Herein, a sequential type of the coupled process (EO followed by adsorption) was considered. However, the in-situ coupling of these processes can also be studied for comparative evaluation with the sequential process. In this study, all the experiments were conducted in lab-scale operation. It is, therefore, important to test the coupled process in a pilot-scale operation to simulate the actual scenario of a full-scale operation. The removal of lower concentrations of pharmaceuticals compared to the concentrations used in this work can be investigated in future studies. The process intensification aspect should also be considered for the coupled process. The detailed techno-economic analysis and efficiencies of the various adsorbent

regeneration techniques, such as thermal and electrochemical regeneration, need to be studied in further works. Moreover, the coupled process employed in this study needs to be compared with other coupled processes in terms of cost and safety.

# 7. References


Abdul, A., Shahzad, A., Moztahida, M., Tahir, K., Jeon, H., Kim, B., & Sung, D. (2021). Adsorption and electrochemical regeneration of intercalated $Ti_3C_2Tx$ MXene for the removal of ciprofloxacin from wastewater. Chemical Engineering Journal, 421, 127780. https://doi.org/10.1016/j.cej.2020.127780.

Abidi, J., Clematis, D., Samet, Y., Delucchi, M., Cademartori, D., & Panizza, M. (2022). Influence of anode material and chlorides in the new-gen solid polymer electrolyte cell for electrochemical oxidation–Optimization of Chloroxylenol degradation with response surface methodology. Journal of Electroanalytical Chemistry, 920, 116584.

Aboudalle, A., Djelal, H., Domergue, L., Fourcade, F., Amrane, A., & Unilasalle-ecole, M. (2021). A novel system coupling an electro-Fenton process and an advanced biological process to remove a pharmaceutical compound, metronidazole. Journal of Hazardous Materials, 415, 125705. https://doi.org/10.1016/j.jhazmat.2021.125705.

Acero, J. L., Benitez, F. J., Real, F. J., & Rodriguez, E. (2015). Elimination of selected emerging contaminants by the combination of membrane filtration and chemical oxidation processes. Water, Air, & Soil Pollution, 226, 1-14.

Adeleye, A. S., Xue, J., Zhao, Y., Taylor, A. A., Zenobio, J. E., Sun, Y., Han, Z., Salawu, O. A., & Zhu, Y. (2022). Abundance, fate, and effects of pharmaceuticals and personal care products in aquatic environments. Journal of Hazardous Materials, 424, 127284

Ahmadi, A., Zarei, M., Hassani, A., Ebratkhahan, M., & Olad, A. (2021). Facile synthesis of iron (II) doped carbonaceous aerogel as a three-dimensional cathode and its excellent performance in electro-Fenton degradation of ceftazidime from water solution. Separation and Purification Technology, 278, 119559.

Ahn, Y., Lee, D., Kwon, M., Choi, I. H., Nam, S. N., & Kang, J. W. (2017). Characteristics and fate of natural organic matter during UV oxidation processes. Chemosphere, 184, 960-968.

Ali, M. E., Hoque, M. E., Safdar Hossain, S. K., & Biswas, M. C. (2020). Nanoadsorbents for wastewater treatment: next generation biotechnological solution. International Journal of

Environmental Science and Technology, 17(9), 4095-4132. https://doi.org/10.1007/s13762-020-02755-4.

Al-Sareji, O. J., Grmasha, R. A., Meiczinger, M., Al-Juboori, R. A., Somogyi, V., Stenger-Kovács, C., & Hashim, K. S. (2024). A sustainable and highly efficient fossil-free carbon from olive stones for emerging contaminants removal from different water matrices. Chemosphere, 351, 141189.

Al, T. J., Amir, M., Mahvi, H., Dokht, A., & Davoud, K. (2021). Effective adsorption of ciprofloxacin antibiotic using powdered activated carbon magnetized by iron ( III ) oxide magnetic nanoparticles. Journal of Porous Materials, 28(3), 835–852.

Alexsandro, J., Fortunato, G. V, Kronka, M. S., Vernasqui, L. G., Ferreira, G., & Lanza, M. R. V. (2022). Electrochemical oxidation of ciprofloxacin in different aqueous matrices using synthesized boron-doped micro and nano-diamond anodes. Environmental Research, 204, 112027 Contents. https://doi.org/10.1016/j.envres.2021.112027

Alfonso-muniozguren, P., Serna-galvis, E. A., Bussemaker, M., Torres-palma, A., & Lee, J. (2021). A review on pharmaceuticals removal from waters by single and combined biological , membrane filtration and ultrasound systems. Ultrasonics Sonochemistry, 76, 105656. https://doi.org/10.1016/j.ultsonch.2021.105656

Alqadhi, N., Abdellah, M. H., & Nematulloev, S. (2024). Solution-processable poly (ether-ether-ketone) membranes for organic solvent nanofiltration : from dye separation to pharmaceutical purification. Separation and Purification Technology, 328, 125072. https://doi.org/10.1016/j.seppur.2023.125072.

Alshakhs, F., Rao, D., Islam, A., Akeem, A., & Nazal, K. (2024). A promising palm leaves waste-derived biochar for efficient removal of tetracycline from wastewater. Journal of Molecular Structure, 1296, 136846. https://doi.org/10.1016/j.molstruc.2023.136846.

Amar, A., Khelifa, M., Batonneau-Gener, I., Lecomte-Nana, G. L., Marouf-Khelifa, K., Çoruh, A., & Khelifa, A. (2024). Improved ciprofloxacin removal by a novel organohalloysite obtained by phenylphosphonic acid intercalation. Journal of Environmental Chemical Engineering, 12(1), 111791. https://doi.org/10.1016/j.jece.2023.111791.

Anastopoulos, I., Pashalidis, I., Orfanos, A. G., Manariotis, I. D., Tatarchuk, T., Sellaoui, L., Bonilla-Pertriciolet A., Mital, A. & Núñez-Delgado, A. (2020). Removal of caffeine, nicotine and amoxicillin from (waste) waters by various adsorbents. A review. Journal of Environmental Management, 261, 110236. https://doi.org/10.1016/j.jenvman.2020.110236.

Anjali, R., & Shanthakumar, S. (2022). Simultaneous degradation of amoxicillin , ciprofloxacin and acetaminophen in a mixture by ozonation : Kinetics and mechanisms pathway. Journal of Cleaner Production, 378, 134509. https://doi.org/10.1016/j.jclepro.2022.134509.

Anjali, R., & Shanthakumar, S. (2023). Journal of Water Process Engineering Synergistic effects on the degradation of a mixture of pharmaceutical pollutants in aqueous solution , raw sewage , and hospital wastewater using UV light-assisted Fenton process. Journal of Water Process Engineering, 54, 104025. https://doi.org/10.1016/j.jwpe.2023.104025.

Antonelli, R., Roger, G., Malpass, P., Gurgel, M., Gurgel, M., & Vieira, A. (2022). Photo-assisted electrochemical degradation of ciprofloxacin using DSA ® anode with NaCl electrolyte and simultaneous chlorine photolysis. Journal of Water Process Engineering, 47, 102698. https://doi.org/10.1016/j.jwpe.2022.102698.

Appia, F. T. A., & Ouattara, L. (2021). Electrooxidation of simulated wastewater containing pharmaceutical amoxicillin on thermally prepared $IrO_2$/Ti electrode. Mediterranean Journal of Chemistry, 11(2), 172-184. http://dx.doi.org/10.13171/mjc02104071566ftaa.

Aseman-bashiz, E., Rezaee, A., & Moussavi, G. (2021). Ciprofloxacin removal from aqueous solutions using modi fi ed electrochemical Fenton processes with iron green catalysts. Journal of Molecular Liquids, 324, 114694. https://doi.org/10.1016/j.molliq.2020.114694.

Arias, J. (2019). Pharmaceutical and Personal Hygiene Products (PPcPs): a threat little studied in Colombian waters. Arias, J. (2019). Pharmaceutical and Personal Hygiene Products (PPcPs): a threat little studied in Colombian waters. Agricultural Research Technology, 22, 1-8. https://doi.org/10.19080/ARTOAJ.2019.22.556201.

Atugoda, T., Gunawardane, C., Ahmad, M., & Vithanage, M. (2021). Atugoda, T., Gunawardane, C., Ahmad, M., & Vithanage, M. (2021). Mechanistic interaction of ciprofloxacin on zeolite modified seaweed (Sargassum crassifolium) derived biochar:

Kinetics, isotherm and thermodynamics. Chemosphere, 281, 130676.

Avrami, M. (1939). Kinetics of Phase Change. I General Theory. The Journal of Chemical Physics, 7(12), 1103–1112.

Bagheri, A., Abu-Danso, E., Iqbal, J., & Bhatnagar, A. (2020). Modified biochar from Moringa seed powder for the removal of diclofenac from aqueous solution. Environmental Science and Pollution Research, 27(7), 7318-7327. https://doi.org/10.1007/s11356-019-06844-x.

Bagheri, A., Fallah, A., Karczewski, J., Eslami, A., Asadi, A. M. S., & Boczkaj, G. (2024). Investigating COVID-19 active pharmaceutical ingredients (APIs) degradation using Peroxydisulfate/FeMnOx binary metal oxide/Ultrasound System. Water Resources and Industry, 31, 100232. https://doi.org/10.1016/j.wri.2023.100232.

Balarak, D., Baniasadi, M., Lee, S., & Joon, M. (2021). Ciprofloxacin adsorption onto Azolla filiculoides activated carbon from aqueous solutions Ciprofloxacin adsorption onto Azolla filiculoides activated carbon from aqueous solutions. Desalination and Water Treatment, 218, 444–453. https://doi.org/10.5004/dwt.2021.26986.

Balasubramani, K., Sivarajasekar, N., & Naushad, M. (2020). Effective adsorption of antidiabetic pharmaceutical (metformin) from aqueous medium using graphene oxide nanoparticles : Equilibrium and statistical modelling. Journal of Molecular Liquids, 301, 112426. https://doi.org/10.1016/j.molliq.2019.112426.

Bas, D. (2007). Modeling and optimization I : Usability of response surface methodology. 78, 836–845. https://doi.org/10.1016/j.jfoodeng.2005.11.024.

Baş, D., & Boyacı, İ. H. (2007). Modeling and optimization I: Usability of response surface methodology. Journal of food engineering, 78(3), 836-845.

Basturk, I., Varank, G., Murat-Hocaoglu, S., Yazici-Guvenc, S., Can-Güven, E., Oktem-Olgun, E. E., & Canli, O. (2021). Simultaneous degradation of cephalexin, ciprofloxacin, and clarithromycin from medical laboratory wastewater by electro-Fenton process. Journal of Environmental Chemical Engineering, 9(1), 104666.

Bedia, J., Peñas-Garzón, M., Gómez-Avilés, A., Rodriguez, J. J., & Belver, C. (2020). Review

on Activated Carbons by Chemical Activation with $FeCl_3$. C — Journal of Carbon Research, 6(2), 21. https://doi.org/10.3390/c6020021.

Belhachemi, M., & Djelaila, S. (2017). Removal of Amoxicillin Antibiotic from Aqueous Solutions by Date Pits Activated Carbons. Environmental Pollution, 4, 549–561. https://doi.org/10.1007/s40710-017-0245-8.

Bhattacharya, S., Das, P., Bhowal, A., & Saha, A. (2021). Thermal , Chemical and ultrasonic assisted synthesis of carbonized Biochar and its application for reducing Naproxen : Batch and Fixed bed study and subsequent optimization with response surface methodology (RSM) and artificial neural network (ANN). Surfaces and Interfaces, 26, 101378. https://doi.org/10.1016/j.surfin.2021.101378.

Bose, S., Kumar, P. S., Rangasamy, G., Prasannamedha, G., & Kanmani, S. (2023). A review on the applicability of adsorption techniques for remediation of recalcitrant pesticides. Chemosphere, 313, 137481. https://doi.org/10.1016/j.chemosphere.2022.137481.

Carneiro, J. F., Aquino, M., Silva, B. F., Silva, A. J., & Rocha-filho, R. C. (2020). Comparing the electrochemical degradation of the fluoroquinolone antibiotics norfloxacin and ciprofloxacin using distinct electrolytes and a BDD anode : evolution of main oxidation byproducts and toxicity. Journal of Environmental Chemical Engineering, 8, 104433 Contents. https://doi.org/10.1016/j.jece.2020.104433.

Castaño-Ortiz, J. M., Gil-Solsona, R., Ospina-Álvarez, N., Alcaraz-Hernández, J. D., Farré, M., León, V. M., Barcelo, D., Santos.L.H. & Rodríguez-Mozaz, S. (2024). Fate of pharmaceuticals in the Ebro River Delta region: The combined evaluation of water, sediment, plastic litter, and biomonitoring. Science of The Total Environment, 906, 167467.

Cecone, C., Fiume, V., Bracco, P., & Zanetti, M. (2024). Maltodextrin-Based Cross-Linked Electrospun Mats as Sustainable Sorbents for the Removal of Atenolol from Water. Polymers, 16(6), 752. https://doi.org/10.3390/polym16060752.

Chaabani, A., Ben, T., Noureddine, J., & Tahar, B. (2022). Electrochemical Oxidation of Ciprofloxacin on COOH - Functionalized Multi - Walled Carbon Nanotube – Coated Vitreous Carbon Electrode. Electrocatalysis, 402–413. https://doi.org/10.1007/s12678-022-

00725-7.

Chakhtouna, H., Benzeid, H., Zari, N., & Bouhfid, R. (2021). Functional $CoFe_2O_4$ -modified biochar derived from banana pseudostem as an efficient adsorbent for the removal of amoxicillin from water. Separation and Purification Technology, 266, 118592. https://doi.org/10.1016/j.seppur.2021.118592.

Chandrasekaran, A., Patra, C., Narayanasamy, S., & Subbiah, S. (2020). Adsorptive removal of Ciprofloxacin and Amoxicillin from single and binary aqueous systems using acid-activated carbon from Prosopis juliflora. Environmental Research, 188, 109825.

Chauhan, M., Saini, V. K., & Suthar, S. (2020). Ti-pillared montmorillonite clay for adsorptive removal of amoxicillin, imipramine, diclofenac-sodium, and paracetamol from water. Journal of Hazardous Materials, 399, 122832.

Chen, S., He, P., Zhou, P., Wang, X., Xiao, F., He, Q., ... & Tang, B. (2021). Development of a novel graphitic carbon nitride and multiwall carbon nanotube co-doped $Ti/PbO_2$ anode for electrocatalytic degradation of acetaminophen. Chemosphere, 271, 129830.

Chen, Y., Bai, X., Ji, Y., & Shen, T. (2022). Reduced graphene oxide-supported hollow $Co_3O_4$ @ N-doped porous carbon as peroxymonosulfate activator for sulfamethoxazole degradation. Chemical Engineering Journal, 430, 132951.

Chen, Z., Wu, Y., Huang, Y., Song, L., Chen, H., Zhu, S., & Tang, C. (2022). Enhanced adsorption of phosphate on orange peel-based biochar activated by Ca/Zn composite: Adsorption efficiency and mechanisms. Colloids and Surfaces A: Physicochemical and Engineering Aspects, 651, 129728. https://doi.org/10.1016/j.colsurfa.2022.129728.

Chen, Z., Lai, W., Xu, Y., Xie, G., Hou, W., Zhanchang, P., Kuang, C., & Li, Y. (2021). Anodic oxidation of ciprofloxacin using different graphite felt anodes: kinetics and degradation pathways. Journal of Hazardous Materials, 405, 124262.

Cheng, N., Wang, B., Wu, P., Lee, X., Xing, Y., Chen, M., & Gao, B. (2021). Adsorption of emerging contaminants from water and wastewater by modi fi ed biochar : A review. Environmental Pollution, 273, 116448. https://doi.org/10.1016/j.envpol.2021.116448.

Chinnaiyan, P., Thampi, S. G., Kumar, M., & Mini.K.M. (2018). Pharmaceutical products as emerging contaminant in water : relevance for developing nations and identification of critical compounds for Indian environment. Environmental Monitoring and Assessment, 190:288. https://doi.org/10.1007/s10661-018-6672-9.

De Araújo, T. P., Quesada, H. B., Dos Santos, D. F., da Silva Fonseca, B. C., Barbieri, J. Z., Bergamasco, R., & de Barros, M. A. S. D. (2022). Acetaminophen removal by calcium alginate/activated hydrochar composite beads: Batch and fixed-bed studies. International Journal of Biological Macromolecules, 203, 553-562.

Dehghan, A., Mohammadi, A. A., Yousefi, M., Najafpoor, A. A., Shams, M., & Rezania, S. (2019). Enhanced kinetic removal of ciprofloxacin onto metal-organic frameworks by sonication, process optimization and metal leaching study. Nanomaterials, 9(10), 1–17. https://doi.org/10.3390/nano9101422.

Delgado-Vargas, C. A., Barreneche-Vasquez, J. S., Cógua, N. G., Botero-Coy, A. M., Hernández, F., Martínez-Pachón, D., & Moncayo-Lasso, A. (2023). Optimization and application of a continuous flow photo-electro-Fenton system for the removal of pharmaceutical active compounds detected in irrigation water of Bogotá–Savanna (Colombia) Crops. Journal of Environmental Chemical Engineering, 11(5), 111030.

Demircan, E., Honek, J. F., & Parker, W. J. (2024). Molecular level investigation of interactions between pharmaceuticals and β -cyclodextrin ( β -CD ) functionalized adsorption sites for removal of pharmaceutical contaminants from water. Chemosphere, 347, 140639. https://doi.org/10.1016/j.chemosphere.2023.140639.

Duan, P., Gao, S., Lei, J., Li, X., & Hu, X. (2020). Electrochemical oxidation of ceftazidime with graphite/CNT-Ce/$PbO_2$–Ce anode: Parameter optimization, toxicity analysis and degradation pathway. Environmental pollution, 263, 114436.

Duarte, A. C., Rodrigues, S., Afonso, A., & Coutinho, P. (2022). Antibiotic Resistance in the Drinking Water : Old and New Strategies to Remove Antibiotics , Resistant Bacteria , and Resistance Genes. Pharmaceuticals, 15(4), 393.

Dubey, M., Vellanki, B. P., & Kazmi, A. A. (2023). Removal of emerging contaminants in

conventional and advanced biological wastewater treatment plants in India-a comparison of treatment technologies. Environmental Research, 218, 115012.

Dubinin, M.M. and Radushkevich, L.V. (1947) The Equation of the Characteristic Curve of Activated Charcoal. Proceedings of the Academy of Sciences, Physical Chemistry Section, 55, 331.

El-bendary, N., El-etriby, H. K., & Mahanna, H. (2021). Reuse of adsorption residuals for enhancing removal of ciprofloxacin from wastewater. Environmental Technology, 0(0), 1–17. https://doi.org/10.1080/09593330.2021.1952310

El, H., Beraich, A., Lamsayah, M., Talhaoui, A., & El, A. (2023). The efficiency of carbon modified by phosphoric acid ( $H_3PO_4$) used in the removal of two antibiotics amoxicillin and metronidazole from polluted water : Experimental and theoretical investigation. Journal of Molecular Liquids, 391, 123237. https://doi.org/10.1016/j.molliq.2023.123237.

Elovich, S. Y., & Larionov, O. G. (1962). Theory of adsorption from nonelectrolyte solutions on solid adsorbents: 2. Experimental verification of the equation for the adsorption isotherm from solutions. Bulletin of the Academy of Sciences of the USSR, Division of Chemical Science, 11, 198-203.

Falyouna, O., Maamoun, I., Bensaida, K., Tahara, A., Sugihara, Y., & Eljamal, O. (2022). Encapsulation of iron nanoparticles with magnesium hydroxide shell for remarkable removal of ciprofloxacin from contaminated water. Journal of Colloid and Interface Science, 605, 813-827. https://doi.org/10.1016/j.jcis.2021.07.154.

Feng, D., Guo, D., Zhang, Y., Sun, S., Zhao, Y., Shang, Q., Sun, H., Wu, J. & Tan, H. (2021). Functionalized construction of biochar with hierarchical pore structures and surface O-/N-containing groups for phenol adsorption. Chemical Engineering Journal, 410, 127707.

Feng, Y., Yang, L., Liu, J., & Logan, B. E. (2016). Electrochemical technologies for wastewater treatment and resource reclamation. Environmental Science: Water Research and Technology, 2(5), 800–831. https://doi.org/10.1039/c5ew00289c.

Firdaus, M., Yusop, M., Abdullah, A. Z., & Ahmad, M. A. (2024). Amoxicillin adsorption from

aqueous solution by Cu (II) modified lemon peel based activated carbon : Mass transfer simulation , surface area prediction and F-test on isotherm and kinetic models. Powder Technology, 438(February), 119589. https://doi.org/10.1016/j.powtec.2024.119589.

França, D. B., Trigueiro, P., Silva Filho, E. C., Fonseca, M. G., & Jaber, M. (2020). Monitoring diclofenac adsorption by organophilic alkylpyridinium bentonites. Chemosphere, 242, 125109.

Freundlich, H. (1924). Kolloidchemie und Biologie. Die Naturwissenschaften, 12(13), 233–239. https://doi.org/10.1007/BF01505512.

Fu, R., Zhang, P. S., Jiang, Y. X., Sun, L., & Sun, X. H. (2023). Wastewater treatment by anodic oxidation in electrochemical advanced oxidation process: Advance in mechanism, direct and indirect oxidation detection methods. Chemosphere, 311, 136993.

Wakuma, G., Yaya, E. E., Getachew, N., & Megersa, N. (2024). A selective dispersive liquid-liquid micro-extraction technique for trace level pollutants enrichment of pharmaceutical residues from hospital wastewaters followed by liquid chromatographic analysis. Bulletin of the Chemical Society of Ethiopia, 38(1), 27-42.

Gallouze, H., Akretche, D. E., Daniel, C., Coelhoso, I., & Crespo, J. G. (2021). Removal of synthetic estrogen from water by adsorption on modified bentonites. Environmental Engineering Science, 38(1), 4-14. https://doi.org/10.1089/ees.2020.0048.

Ganesan, S., Amirthalingam, M., & Arivalagan, P. (2019). Absolute removal of ciprofloxacin and its degraded byproducts in aqueous solution using an efficient electrochemical oxidation process coupled with adsorption treatment technique. Journal of Environmental Management, 245(100), 409–417. https://doi.org/10.1016/j.jenvman.2019.05.092.

Ganiyu, S. O., Van Hullebusch, E. D., Cretin, M., Esposito, G., & Oturan, M. A. (2015). Coupling of membrane filtration and advanced oxidation processes for removal of pharmaceutical residues: A critical review. Separation and Purification Technology, 156, 891-914. https://doi.org/10.1016/j.seppur.2015.09.059.

Ganthavee, V., & Trzcinski, A. P. (2023). Removal of pharmaceutically active compounds from

wastewater using adsorption coupled with electrochemical oxidation technology: A critical review. Journal of Industrial and Engineering Chemistry, 126, 20–35.

Garcia-Rosero, H., Romero-Cano, L. A., Aguilar-Aguilar, A., Bailon-Garcia, E., Carvalho, A. P., Perez-Cadenas, A. F., & Carrasco-Marin, F. (2022). Adsorption and thermal degradation of Atenolol using carbon materials: Towards an advanced and sustainable drinking water treatment. Journal of Water Process Engineering, 49, 102987.

García, L., Leyva-Díaz, J. C., Díaz, E., & Ordóñez, S. (2021). A review of the adsorption-biological hybrid processes for the abatement of emerging pollutants: Removal efficiencies, physicochemical analysis, and economic evaluation. Science of the Total Environment, 780. https://doi.org/10.1016/j.scitotenv.2021.146554

Garrido-cardenas, J. A., & Agüera, A. (2020). Wastewater Treatment by Advanced Oxidation Process and Their Worldwide Research Trends. International Journal of Environmental Research and Public Health, 17(1), 170.

Gasmi, I., Hamdaoui, O., Ferkous, H., & Alghyamah, A. (2023). Sonochemical advanced oxidation process for the degradation of furosemide in water: Effects of sonication's conditions and scavengers. Ultrasonics Sonochemistry, 95, 106361.

Georgin, J., Yamil, Y. L., Franco, D. S. P., Netto, M. S., Piccilli, D. G. A., Perondi, D., Silva, L. F. O., Foletto, E. L., & Dotto, G. L. (2021). Development of highly porous activated carbon from Jacaranda mimosifolia seed pods for remarkable removal of aqueous-phase ketoprofen. Journal of Environmental Chemical Engineering, 9(4).

Gezahegn, T., Tegegne, B., Zewge, F., & Chandravanshi, B. S. (2019). Salting-out assisted liquid–liquid extraction for the determination of ciprofloxacin residues in water samples by high performance liquid chromatography–diode array detector. BMC chemistry, 13, 1-10.

Ghadiri, S. K., Alidadi, H., Nezhad, N. T., Javid, A., Roudbari, A., Talebi, S. S., Akbar, A., & Id, M. (2020). Valorization of biomass into amine- functionalized bio graphene for efficient ciprofloxacin adsorption in water-modeling and optimization study. PLOS ONE, 15(4), 1–19. https://doi.org/10.1371/journal.pone.0231045

Ghanbari, F., Yaghoot-nezhad, A., Lin, K. A., Rodríguez-chueca, J., & Mehdipour, F. (2021). Comparative investigation of acetaminophen degradation in aqueous solution by UV/Chlorine and UV/$H_2O_2$ processes : Kinetics and toxicity assessment, process feasibility and products identification. Chemosphere, 285, 131455.

Ghazal, H., Koumaki, E., Hoslett, J., Malamis, S., Katsou, E., Barcelo, D., & Jouhara, H. (2022). Insights into current physical, chemical and hybrid technologies used for the treatment of wastewater contaminated with pharmaceuticals. Journal of Cleaner Production, 361, 132079. https://doi.org/10.1016/j.jclepro.2022.132079.

Gholami, M., Tyagi, R. D., Vanrolleghem, P. A., & Drogui, P. (2022). Modelling and optimization of psychoactive pharmaceutical caffeine removal by electrochemical oxidation process : A comparative study between response surface methodology ( RSM ) and adaptive neuro fuzzy inference system (ANFIS). Separation and Purification Technology, 290, 120902. https://doi.org/10.1016/j.seppur.2022.120902

GilPavas, E., Dobrosz-Gómez, I., & Gómez-García, M. Á. (2020). Efficient treatment for textile wastewater through sequential electrocoagulation, electrochemical oxidation and adsorption processes: Optimization and toxicity assessment. Journal of Electroanalytical Chemistry, 878, 114578. https://doi.org/10.1016/j.jelechem.2020.114578

Giraldo, A. L., Erazo-erazo, E. D., Flórez-acosta, O. A., Serna-galvis, E. A., & Torres-palma, R. A. (2015). Degradation of the antibiotic oxacillin in water by anodic oxidation with Ti/$IrO_2$ anodes : Evaluation of degradation routes, organic by-products and effects of water matrix components. Chemical Engineering Journal, 279, 103–114.

Glaze, W. H., Kang, J., & Douglas, H. (1998). The Chemistry of Water Treatment Processes Involving Ozone, Hydrogen Peroxide and Ultraviolet Radiation. Ozone: Science & Engineering: The Journal of the International Ozone Association, 9(4), 335–352.

Gogoi, A., Mazumder, P., Kumar, V., Chaminda, G. G. T., Kyoungjin, A., & Kumar, M. (2018). Groundwater for Sustainable Development Occurrence and fate of emerging contaminants in water environment : A review. Groundwater for Sustainable Development, 6, 169–180.

Goh, W. J. L. P. S., & Ismail, W. J. L. A. F. (2020). Removal of Pharmaceutical Contaminants

from Aqueous Medium : A State-of-the-Art Review Based on Paracetamol. Arabian Journal for Science and Engineering. https://doi.org/10.1007/s13369-020-04446-1.

Gomes, J., Costa, R., Quinta-Ferreira, R. M., & Martins, R. C. (2017). Application of ozonation for pharmaceuticals and personal care products removal from water. Science of the Total Environment, 586, 265-283. https://doi.org/10.1016/j.scitotenv.2017.01.216.

Gong, C., Han, J., He, C., Shi, L., Shan, Y., & Zhang, Z. (2023). Insights into degradation of pharmaceutical pollutant atenolol via electrochemical advanced oxidation processes with modified $Ti_4O_7$ electrode : Efficiency, stability and mechanism. Environmental Research, 228, 115920. https://doi.org/10.1016/j.envres.2023.115920.

Gong, Y., Wang, L., Liu, J., Tang, J., & Zhao, D. (2016). Removal of aqueous perfluorooctanoic acid (PFOA) using starch-stabilized magnetite nanoparticles. Science of the Total Environment, 562, 191–200. https://doi.org/10.1016/j.scitotenv.2016.03.100.

Gouveia, T. I. A., Garcia-Costa, A. L., Alves, A., & Santos, M. S. F. (2022). Current knowledge on the application of membrane-based technologies for the removal of cytostatics from water. Journal of Water Process Engineering, 47.

Gracia-Lor, E., Sancho, J. V., Serrano, R., & Hernández, F. (2012). Occurrence and removal of pharmaceuticals in wastewater treatment plants at the Spanish Mediterranean area of Valencia. Chemosphere, 87(5), 453-462.

Grandclément, C., Seyssiecq, I., Piram, A., Wong-Wah-Chung, P., Vanot, G., Tiliacos, N., Roche, N., & Doumenq, P. (2017). From the conventional biological wastewater treatment to hybrid processes, the evaluation of organic micropollutant removal: A review. Water Research, 111, 297–317. https://doi.org/10.1016/j.watres.2017.01.005.

Grimm, A., dos Reis, G. S., Dinh, V. M., Larsson, S. H., Mikkola, J. P., Lima, E. C., & Xiong, S. (2024). Hardwood spent mushroom substrate–based activated biochar as a sustainable bioresource for removal of emerging pollutants from wastewater. Biomass Conversion and Biorefinery, 14(2), 2293-2309. https://doi.org/10.1007/s13399-022-02618-7.

Grisales-Cifuentes, C. M., Serna Galvis, E. A., Porras, J., Flórez, E., Torres-Palma, R. A., &

Acelas, N. (2021). Kinetics, isotherms, effect of structure, and computational analysis during the removal of three representative pharmaceuticals from water by adsorption using a biochar obtained from oil palm fiber. Bioresource Technology, 326.

Guillossou, R., Roux, J. Le, Brosillon, S., Mailler, R., Vulliet, E., Morlay, C., Nauleau, F., Rocher, V., & Gasperi, J. (2020). Benefits of ozonation before activated carbon adsorption for the removal of organic micropollutants from wastewater effluents. Chemosphere, 245, 125530. https://doi.org/10.1016/j.chemosphere.2019.125530.

Gulen, B., & Demircivi, P. (2020). Adsorption properties of flouroquinolone type antibiotic ciprofloxacin into 2 : 1 dioctahedral clay structure : Box-Behnken experimental design. Journal of Molecular Structure, 1206, 127659.

Guo, K., Wu, Z., & Fang, J. (2020). UV-based advanced oxidation process for the treatment of pharmaceuticals and personal care products. In Contaminants of emerging concern in water and wastewater (pp. 367-408). Butterworth-Heinemann. https://doi.org/10.1016/B978-0-12-813561-7.00010-9.

Guo, Y., Zhu, S., Wang, B., Huang, J., Deng, S., Yu, G., & Wang, Y. (2019). Modelling of emerging contaminant removal during heterogeneous catalytic ozonation using chemical kinetic approaches. Journal of Hazardous Materials, 380, 120888.

Haenni, M., Dagot, C., Chesneau, O., Bibbal, D., Bachelot, M., Topp, E., & Hocquet, D. (2022). Environmental contamination in a high-income country (France) by antibiotics, antibiotic-resistant bacteria, and antibiotic resistance genes : Status and possible causes. Environment International Journal, 159, 107047. https://doi.org/10.1016/j.envint.2021.107047.

Hamadeen, H. M., & Elkhatib, E. A. (2022). New nanostructured activated biochar for effective removal of antibiotic ciprofloxacin from wastewater : Adsorption dynamics and mechanisms. Environmental Research, 210, 112929.

Han, L., Khalil, A. M. E., Wang, J., Chen, Y., Li, F., Chang, H., Zhang, H., Liu, X., Li, G., Jia, Q., & Zhang, S. (2022). Graphene-boron nitride composite aerogel : A high efficiency adsorbent for ciprofloxacin removal from water. Separation and Purification Technology, 278, 119605. https://doi.org/10.1016/j.seppur.2021.119605

Han, N., Reinhard, M., & Gin, K. Y. (2018). Occurrence and fate of emerging contaminants in municipal wastewater treatment plants from different geographical regions-a review. Water Research, 133, 182–207. https://doi.org/10.1016/j.watres.2017.12.029.

Hawash, H. B., Moneer, A. A., Galhoum, A. A., Elgarahy, A. M., Mohamed, W. A. A., Samy, M., El-seedi, H. R., Gaballah, M. S., Mubarak, M. F., & Attia, N. F. (2023). Occurrence and spatial distribution of pharmaceuticals and personal care products (PPCPs) in the aquatic environment, their characteristics, and adopted legislations. Journal of Water Process Engineering, 52, 103490. https://doi.org/10.1016/j.jwpe.2023.103490.

He, C., Wang, J., Wang, C., Zhang, C., Hou, P., & Xu, X. (2020). Catalytic ozonation of bio-treated coking wastewater in continuous pilot- and full-scale system: Efficiency, catalyst deactivation and in-situ regeneration. Water Research, 116090.

He, H., Huang, B., Fu, G., Du, Y., Xiong, D., Lai, C., & Pan, X. (2017). Coupling electrochemical and biological methods for 17α-ethinylestradiol removal from water by different microorganisms. Journal of hazardous materials, 340, 120-129.

He, R., Peng, Z., Lyu, H., Huang, H., Nan, Q., & Tang, J. (2018). Synthesis and characterization of an iron-impregnated biochar for aqueous arsenic removal. Science of the Total Environment, 612, 1177–1186. https://doi.org/10.1016/j.scitotenv.2017.09.016.

Ho, Y. ., & McKay, G. (1999). Pseudo-second order model for sorption processes. Process Biochemistry, 34(5), 451–465. https://doi.org/10.1016/S0032-9592(98)00112-5.

Hong, M., Wang, Y., & Lu, G. (2020). UV-Fenton degradation of diclofenac , sulpiride , sulfamethoxazole and sul fi somidine : Degradation mechanisms, transformation products, toxicity evolution and effect of real water matrix. Chemosphere, 258, 127351. https://doi.org/10.1016/j.chemosphere.2020.127351.

Hu, J., Bian, X., Xia, Y., Weng, M., Zhou, W., & Dai, Q. (2020). Application of response surface methodology in electrochemical degradation of amoxicillin with Cu-$PbO_2$ electrode: optimization and mechanism. Separation and Purification Technology, 250, 117109. https://doi.org/10.1016/j.seppur.2020.117109.

Hu, X., Hu, X., Peng, Q., Zhou, L., Tan, X., Jiang, L., Tang, C., Wang, H., Liu, S., Wang, Y., & Ning, Z. (2020). Mechanisms underlying the photocatalytic degradation pathway of ciprofloxacin with heterogeneous $TiO_2$. Chemical Engineering Journal, 380, 122366. https://doi.org/10.1016/j.cej.2019.122366.

Huang, W., Huang, Y., Tang, B., Fu, Y., Guo, C., & Zhang, J. (2023). Electrochemical oxidation of carbamazepine in water using enhanced blue $TiO_2$ nanotube arrays anode on porous titanium substrate. Chemosphere, 322, 138193.

Hyun, S., Seung, Y., Lee, C., & Bae, S. (2023). Acetaminophen adsorption to spherical carbons hydrothermally synthesized from sucrose : experimental, molecular, and mathematical modeling studies. Environmental Science and Pollution Research, 49703–49719. https://doi.org/10.1007/s11356-023-25815-x.

Iancu, V., Puiu, D., & Radu, G. L. (2020). Determination of some beta-blockers in surface water samples. University Politehnica of Bucharest Bucharest Science Bulletin Series B, 82(2).

Igwegbe, C. A., Aniagor, C. O., Oba, S. N., Yap, P. S., Iwuchukwu, F. U., Liu, T., de Souza, E. C., & Ighalo, J. O. (2021). Environmental protection by the adsorptive elimination of acetaminophen from water: a comprehensive review. Journal of Industrial and Engineering Chemistry, 104, 117-135. https://doi.org/10.1016/j.jiec.2021.08.015.

Islam, T., Golam, A. H. M., Saenz-arana, R., Hernandez, C., Guinto, T., Ahsan, A., Alvarado-tenorio, B., & Noveron, J. C. (2019). Removal of methylene blue and tetracycline from water using peanut shell derived adsorbent prepared by sulfuric acid reflux. Journal of Environmental Chemical Engineering, 7(1), 102816.

Jaén-gil, A., Buttiglieri, G., Benito, A., Mir-tutusaus, J. A., Gonzalez-olmos, R., Caminal, G., & Barceló, D. (2021). Combining biological processes with UV/$H_2O_2$ for metoprolol and metoprolol acid removal in hospital wastewater. Chemical Engineering Journal, 404, 126482. https://doi.org/10.1016/j.cej.2020.126482.

Jakóbczyk, P., Skowierzak, G., Kaczmarzyk, I., Nadolska, M., Wcisło, A., Lota, K., Bogdanowicz, R., Ossowski, T., Paweł Rostkowski, P., Lota, G., & Ryl, J. (2022). Electrocatalytic performance of oxygen-activated carbon fibre felt anodes mediating

degradation mechanism of acetaminophen in aqueous environments. Chemosphere, 304, 135381. https://doi.org/10.1016/j.chemosphere.2022.135381.

Jameel, Y., Valle, D., & Kay, P. (2020). Spatial variation in the detection rates of frequently studied pharmaceuticals in Asian, European and North American rivers. Science of The Total Environment, 724, 137947. https://doi.org/10.1016/j.scitotenv.2020.137947.

Jasna, R. S., Gandhimathi, R., Lavanya, A., & Ramesh, S. T. (2020). An integrated electrochemical-adsorption system for removal of nitrate from water. Journal of Environmental Chemical Engineering, 8(5), 104387.

Jawad, A. H., & Abdulhameed, A. S. (2020). Statistical modeling of methylene blue dye adsorption by high surface area mesoporous activated carbon from bamboo chip using KOH-assisted thermal activation. Energy, Ecology and Environment, 5(6), 456-469. https://doi.org/10.1007/s40974-020-00177-z.

Jennifer, A., Abdallah, M. A., & Harrad, S. (2017). Pharmaceuticals and personal care products ( PPCPs ) in the freshwater aquatic environment. Emerging Contaminants, 3(1), 1–16. https://doi.org/10.1016/j.emcon.2016.12.004.

Ji, H., Wang, T., Huang, T., Lai, B., & Liu, W. (2021). Adsorptive removal of cipro fl oxacin with different dissociated species onto titanate nanotubes. Journal of Cleaner Production, 278, 123924. https://doi.org/10.1016/j.jclepro.2020.123924.

Jiang, X., Fan, D., Yao, X., Dong, Z., Li, X., Ma, S., Liu, J., Zhang, D., Li, H., Pu, X., & Cai, P. (2023). Highly efficient flower-like ZnIn2S4/$CoFe_2O_4$ photocatalyst with pn type heterojunction for enhanced hydrogen evolution under visible light irradiation. Journal of Colloid and Interface Science, 641, 26-35. https://doi.org/10.1016/j.jcis.2023.03.055.

Juela, D. M. (2020). Comparison of the adsorption capacity of acetaminophen on sugarcane bagasse and corn cob by dynamic simulation. Sustainable Environment Research, 30(1), 23.

Juela, D., Vera, M., Cruzat, C., Alvarez, X., & Vanegas, E. (2021). Adsorption properties of sugarcane bagasse and corn cob for the sulfamethoxazole removal in a fixed-bed column. Sustainable Environment Research, 31(1). https://doi.org/10.1186/s42834-021-00102-x

Jung, C., Boateng, L. K., Flora, J. R., Oh, J., Braswell, M. C., Son, A., & Yoon, Y. (2015). Competitive adsorption of selected non-steroidal anti-inflammatory drugs on activated biochars: experimental and molecular modeling study. Chemical Engineering Journal, 264, 1-9. https://doi.org/10.1016/j.cej.2014.11.076.

Kah, M., Sigmund, G., Xiao, F., & Hofmann, T. (2017). Sorption of ionizable and ionic organic compounds to biochar , activated carbon and other carbonaceous materials. Water Research, 124, 673–692. https://doi.org/10.1016/j.watres.2017.07.070.

Kamal, N., Krishna, A., Singh, E., Pandey, A., & Chaturvedi, P. (2024). Biodegradation of ciprofloxacin using machine learning tools : Kinetics and modelling. Journal of Hazardous Materials, 470, 134076. https://doi.org/10.1016/j.jhazmat.2024.134076.

Kamyab, H., Ali, M., Azizah, F., Ostadrahimi, A., Khademi, T., Ghfar, A. A., & Kirpichnikova, I. (2022). Electrochemical oxidation of palm oil mill effluent using platinum as anode : Optimization using response surface methodology. Environmental Research, 214, 113993. https://doi.org/10.1016/j.envres.2022.113993.

Kanakaraju, D., Glass, B. D., & Oelgem, M. (2018). Advanced oxidation process-mediated removal of pharmaceuticals from water : A review. Journal of Environmental Management, 219, 189–207. https://doi.org/10.1016/j.jenvman.2018.04.103.

Karimi-Maleh, H., Ayati, A., Davoodi, R., Tanhaei, B., Karimi, F., Malekmohammadi, S., Orooji, Y., & Sillanpää, M. (2021). Recent advances in using of chitosan-based adsorbents for removal of pharmaceutical contaminants: A review. Journal of Cleaner Production, 291, 125880. https://doi.org/10.1016/j.jclepro.2021.125880.

Kasprzyk-hordern, B., Dinsdale, R. M., & Guwy, A. J. (2009). The removal of pharmaceuticals , personal care products , endocrine disruptors and illicit drugs during wastewater treatment and its impact on the quality of receiving waters. Water Research, 43(2), 363–380. https://doi.org/10.1016/j.watres.2008.10.047.

Kaur, H., Hippargi, G., Pophali, G. R., & Bansiwal, A. K. (2019). 6. Treatment methods for removal of pharmaceuticals and personal care products from domestic wastewater. In Pharmaceuticals and Personal Care Products: Waste Management and Treatment

Technology. https://doi.org/10.1016/B978-0-12-816189-0.00006-8.

Kermani, M., Mehralipour, J., & Kakavandi, B. (2019). Photo-assisted electroperoxone of 2, 4-dichlorophenoxy acetic acid herbicide: Kinetic, synergistic and optimization by response surface methodology. Journal of Water Process Engineering, 32, 100971.

Khoshnamvand, N., Ahmadi, S., & Mostafapour, F. K. (2017). Kinetic and Isotherm Studies on Ciprofloxacin an Adsorption using Magnesium Oxide Nanopartices. Journal of Applied Pharmaceutical Science, 7(11), 79–83. https://doi.org/10.7324/JAPS.2017.71112.

Kim, M. K., & Zoh, K. D. (2016). Occurrence and removals of micropollutants in water environment. Environmental engineering research, 21(4), 319-332.

Kim, S., Tang, C., Park, Y., Du, A., & Hwang, Y. (2024). Unveiling the adsorption mechanism of beta-blockers and sulfonamides in aqueous environment using disulfide-linked polymer. Separation and Purification Technology, 333, 125897.

Klavarioti, M., Mantzavinos, D., & Kassinos, D. (2009). Removal of residual pharmaceuticals from aqueous systems by advanced oxidation processes. Environment International, 35(2), 402–417. https://doi.org/10.1016/j.envint.2008.07.009.

Kock, A., Glanville, H. C., Law, A. C., Stanton, T., Carter, L. J., & Taylor, J. C. (2023). Emerging challenges of the impacts of pharmaceuticals on aquatic ecosystems: A diatom perspective. Science of the Total Environment, 878, 162939.

Körbahti, B. K., & Alaca, S. (2021). Electrochemical degradation of tetracycline antibiotic with boron-doped diamond electrodes and effect of parameters on removal of reaction intermediates. methods, 2, 5. https://doi.org/10.5004/dwt.2021.27716.

Kovalakova, P., Cizmas, L., McDonald, T. J., Marsalek, B., Feng, M., & Sharma, V. K. (2020). Occurrence and toxicity of antibiotics in the aquatic environment: A review. Chemosphere, 251, 126351.

Kumar, C. S. P., Sylas, V. P., Cyril, N., Ambily, V., Sunila, C. T., Sreekanth, N. P., & Rayaroth, M. P. (2021). Acetaminophen removal using green synthesized iron nanoparticles with a fresh water microalga, Planktochlorella nurekis. Nano-Structures & Nano-Objects, 26,

100700. https://doi.org/10.1016/j.nanoso.2021.100700.

Kumar, M., Sridharan, S., Sawarkar, A. D., Shakeel, A., & Anerao, P. (2023). Current research trends on emerging contaminants pharmaceutical and personal care products ( PPCPs ): A comprehensive review. Science of the Total Environment, 859, 160031.

Kwon, M., Kim, S., Jung, Y., Hwang, T. M., Stefan, M. I., & Kang, J. W. (2019). The impact of natural variation of OH radical demand of drinking water sources on the optimum operation of the UV/H2O2 process. Environmental science & technology, 53(6), 3177-3186. https://doi.org/10.1021/acs.est.8b05686.

Kwon, M., Yoon, Y., Kim, S., Jung, Y., Hwang, T. M., & Kang, J. W. (2018). Removal of sulfamethoxazole, ibuprofen and nitrobenzene by UV and UV/chlorine processes: A comparative evaluation of 275 nm LED-UV and 254 nm LP-UV. Science of the total environment, 637, 1351-1357. https://doi.org/10.1016/j.scitotenv.2018.05.080.

Lado, A. R., Moreira, N. F. F., Li, G., & Silva, A. M. T. (2019). Impact of water matrix on the removal of micropollutants by advanced oxidation technologies. Chemical Engineering Journal, 363, 155–173. https://doi.org/10.1016/j.cej.2019.01.080.

Lagergren, S. K. K. (1898). About the Theory of So-called Adsorption of Soluble Substances. Sven. Vetenskapsakad. Handingarl, 24, 1–39.

Laksaci, H., Belhamdi, B., Khelifi, O., & Khelifi, A. (2023). Elimination of amoxicillin by adsorption on coffee waste based activated carbon. Journal of Molecular Structure, 1274, 134500. https://doi.org/10.1016/j.molstruc.2022.134500.

Lan, Y., Coetsier, C., Causserand, C., & Serrano, K. G. (2017). On the role of salts for the treatment of wastewaters containing pharmaceuticals by electrochemical oxidation using a boron doped diamond anode. Electrochimica Acta, 231, 309–318.

Langmuir, I. (1918). The adsorption of gases on plane surfaces of glass, mica and platinum. Journal of the American Chemical Society, 40(9), 1361–1403.

Lee, J., Cho, W., Poo, K., Choi, S., Kim, T., Son, E., Choi, Y., Mo, Y., & Chae, K. (2020). Refractory oil wastewater treatment by dissolved air flotation, electrochemical advanced

oxidation process, and magnetic biochar integrated system. Journal of Water Process Engineering, 36, 101358. https://doi.org/10.1016/j.jwpe.2020.101358.

Leili, M., Shirmohammadi, N., Godini, K., Azarian, G., Moussavi, R., & Peykhoshian, A. (2020). Application of central composite design (CCD) for optimization of cephalexin antibiotic removal using electro-oxidation process. Journal of Molecular Liquids, 313, 113556. https://doi.org/10.1016/j.molliq.2020.113556.

Lengauer, C. L., Viglašová, E., Galamboš, M., Danková, Z., Krivosudsky, L., Hood-nowotny, R., Soja, G., Rompel, A., Matík, M., & Brianc, J. (2018). Production , characterization and adsorption studies of bamboo-based biochar / montmorillonite composite for nitrate removal. 79, 385–394. https://doi.org/10.1016/j.wasman.2018.08.005.

Li, B., Xu, D., Zhou, X., Yin, Y., Feng, L., Liu, Y., & Zhang, L. (2023). Environmental behaviors of emerging contaminants in freshwater ecosystem dominated by submerged plants : A review. Environmental Research, 227, 115709.

Li, G., Zhou, S., Shi, Z., Meng, X., Li, L., & Liu, B. (2019). Electrochemical degradation of ciprofloxacin on BDD anode using a differential column batch reactor: mechanisms, kinetics and pathways. Environmental Science and Pollution Research, 26(17), 17740–17750. https://doi.org/10.1007/s11356-019-04900-0.

Li, J., Pan, L., Yu, G., Li, C., Xie, S., & Wang, Y. (2021). Synthesis of an easily recyclable and safe adsorbent from sludge pyrochar for ciprofloxacin adsorption. Environmental Research, 192, 110258. https://doi.org/10.1016/j.envres.2020.110258.

Li, J., Yu, G., Pan, L., Li, C., You, F., Xie, S., Wang, Y., Ma, J., & Shang, X. (2018). Study of ciprofloxacin removal by biochar obtained from used tea leaves. Journal of Environmental Sciences, 73, 20–30. https://doi.org/10.1016/j.jes.2017.12.024.

Li, K., Chen, M., Chen, L., Zhao, S., Pan, W., Li, P., & Han, Y. (2024). Adsorption of tetracycline from aqueous solution by ZIF-8: Isotherms, kinetics and thermodynamics. Environmental Research, 241, 117588. https://doi.org/10.1016/j.envres.2023.117588.

Li, Z., Xing, B., Ding, Y., Li, Y., & Wang, S. (2020). A high-performance biochar produced

from bamboo pyrolysis with in-situ nitrogen doping and activation for adsorption of phenol and methylene blue. Chinese Journal of Chemical Engineering, 28(11), 2872-2880.

Lin, R., Li, Y., Yong, T., Cao, W., Wu, J., & Shen, Y. (2022). Synergistic effects of oxidation , coagulation and adsorption in the integrated fenton-based process for wastewater treatment : A review. Journal of Environmental Management, 306, 114460.

Liu, Z., Wan, J., Yan, Z., Wang, Y., & Ma, Y. (2022). Efficient removal of ciprofloxacin by heterogeneous electro-Fenton using natural air – cathode. Chemical Engineering Journal, 433, 133767. https://doi.org/10.1016/j.cej.2021.133767.

Loc, T. T., Dat, N. D., & Tran, H. N. (2023). Nano-sized hematite-assembled carbon spheres for effectively adsorbing paracetamol in water : Important role of iron. Korean Journal of Chemical Engineering, 40(12), 3029–3038. https://doi.org/10.1007/s11814-021-1013-z.

Lu, X., & Zhao, J. (2024). Chinese Journal of Analytical Chemistry Adsorption of ciprofloxacin on co-pyrolyzed biochar from fish scale and pine needle. Chinese Journal of Analytical Chemistry, 52(1), 100350. https://doi.org/10.1016/j.cjac.2023.100350

Luiz, A., Neto, S., Pimentel-almeida, W., Niero, G., Wanderlind, E. H., & Radetski, C. M. (2023). Application of a biochar produced from malt bagasse as a residue of brewery industry in fixed-bed column adsorption of paracetamol. Chemical Engineering Research and Design, 194, 779–786. https://doi.org/10.1016/j.cherd.2023.05.009.

Luo, Q., Liu, P., Bi, L., Shi, L., Zhou, J., Fang, F., & Lv, Q. (2024). Selective and efficient removal of ciprofloxacin from water by bimetallic MOF beads : Mechanism quantitative analysis and dynamic adsorption. Separation and Purification Technology, 332, 125832. https://doi.org/10.1016/j.seppur.2023.125832.

Ma, X., He, C., Yan, Y., Chen, J., Feng, H., Hu, J., Zhu, H. & Xia, Y. (2023). Energy-efficient electrochemical degradation of ciprofloxacin by a Ti-foam/$PbO_2$-GN composite electrode: Electrode characteristics, parameter optimization, and reaction mechanism. Chemosphere, 315, 137739. https://doi.org/10.1016/j.chemosphere.2023.137739.

Ma, Yanan, Wang, Z., Li, J., Song, B., & Liu, S. (2022). Chemosphere Electrochemical-assisted

ultraviolet light coupled peroxodisulfate system to degrade ciprofloxacin in water : Kinetics , mechanism and pathways. Chemosphere, 295, 133838.

Ma, Yongfei, Yao, Y., Qian, S., Deng, Z., Liu, Y., & Ma, J. (2024). Ball milling boosted hydrothermal N-doped sludge-derived biochar towards efficiently adsorptive removal of sulfamethoxazole from waters : Behavior , mechanism and DFT study. Separation and Purification Technology, 338, 126453. https://doi.org/10.1016/j.seppur.2024.126453.

Maged, A., Kharbish, S., Ismael, I. S., & Bhatnagar, A. (2020). Characterization of activated bentonite clay mineral and the mechanisms underlying its sorption for ciprofloxacin from aqueous solution. Environmental Science and Pollution Research, 27, 32980-32997.

Maged, A., Dissanayake, P. D., Yang, X., Pathirannahalage, C., Bhatnagar, A., & Ok, Y. S. (2021). New mechanistic insight into rapid adsorption of pharmaceuticals from water utilizing activated biochar. Environmental Research, 202, 111693.

Maged, A., Elgarahy, A. M., Haneklaus, N. H., Kumar, A., Show, P., & Bhatnagar, A. (2023). Sustainable functionalized smectitic clay-based nano hydrated zirconium oxides for enhanced levofloxacin sorption from aqueous medium. Journal of Hazardous Materials, 452, 131325. https://doi.org/10.1016/j.jhazmat.2023.131325.

Mahdizadeh, H., & Malakootian, M. (2019). Optimization of ciprofloxacin removal from aqueous solutions by a novel semi-fluid Fe/charcoal micro-electrolysis reactor using response surface methodology. Process Safety and Environmental Protection, 123, 299–308. https://doi.org/10.1016/j.psep.2019.01.024.

Malesic-eleftheriadou, N., Evgenidou, E., Lazaridou, M., Bikiaris, D. N., Yang, X., Kyzas, G. Z., & Lambropoulou, D. A. (2021). Simultaneous removal of anti-inflammatory pharmaceutical compounds from an aqueous mixture with adsorption onto chitosan zwitterionic derivative. Colloids and Surfaces A: Physicochemical and Engineering Aspects, 619, 126498. https://doi.org/10.1016/j.colsurfa.2021.126498.

Manjunath, S. V., Biradar, U. S., & Sanjeev, N. O. (2023). Evaluation of peroxide assisted multi-oxidation systems for simultaneous removal of pharmaceutical active compounds from aqueous environment. Journal of Environmental Chemical Engineering, 11(5), 110601.

https://doi.org/10.1016/j.jece.2023.110601.

Manjunath, S. V, & Kumar, M. (2018). Evaluation of single-component and multi-component adsorption of metronidazole, phosphate and nitrate on activated carbon from Prosopıs julıflora. Chemical Engineering Journal, 346, 525–534.

Mantovani, M., Rossi, S., Ficara, E., Collina, E., Marazzi, F., Lasagni, M., & Mezzanotte, V. (2024). Science of the Total Environment Removal of pharmaceutical compounds from the liquid phase of anaerobic sludge in a pilot-scale high-rate algae-bacteria pond. Science of the Total Environment, 908, 167881. https://doi.org/10.1016/j.scitotenv.2023.167881.

Marqués, M. D., Cotoruelo, L. M., & Cordero, T. (2015). Removal of paracetamol on biomass-derived activated carbon : Modeling the fixed bed breakthrough curves using batch adsorption experiments. Chemical Engineering Journal Journal, 279, 18–30. https://doi.org/10.1016/j.cej.2015.04.144.

Mary, G. S., Niveditha, P. S. S., & Mary, G. S. (2016). Production , characterization and evaluation of biochar from pod ( Pisum sativum ) , leaf (Brassica oleracea) and peel (Citrus sinensis) wastes. International Journal of Recycling of Organic Waste in Agriculture, 5(1), 43–53. https://doi.org/10.1007/s40093-016-0116-8.

Mehmood, S., Ahmed, W., Rizwan, M., Bundschuh, J., Elnahal, A. S. M., & Li, W. (2024). Green synthesized zinc oxide nanoparticles for removal of carbamazepine in water and soil systems. Separation and Purification Technology, 334, 125988.

Menya, E., Jjagwe, J., & Mpagi, H. (2023). Progress in deployment of biomass-based activated carbon in point-of-use filters for removal of emerging contaminants from water : A review. Chemical Engineering Research and Design, 192, 412–440.

Mheidli, N., Malli, A., Mansour, F., & Al-Hindi, M. (2022). Occurrence and risk assessment of pharmaceuticals in surface waters of the Middle East and North Africa: A review. Science of The Total Environment, 851, 158302. https://doi.org/10.1016/j.scitotenv.2022.158302.

Mian, M., Liu, G., Yousaf, B., Fu, B., Ullah, H., Ubaid, M., Abbas, Q., Ahmed, M., Munir, M., & Ruijia, L. (2018). Simultaneous functionalization and magnetization of biochar via $NH_3$

ambiance pyrolysis for ef fi cient removal of Cr (VI). Chemosphere, 208, 712–721. https://doi.org/10.1016/j.chemosphere.2018.06.021.

Miarov, O., Tal, A., & Avisar, D. (2020). A critical evaluation of comparative regulatory strategies for monitoring pharmaceuticals in recycled wastewater. Journal of Environmental Management, 254, 109794. https://doi.org/10.1016/j.jenvman.2019.109794.

Minaei, S., Benis, K. Z., McPhedran, K. N., & Soltan, J. (2023). Evaluation of a $ZnCl_2$-modified biochar derived from activated sludge biomass for adsorption of sulfamethoxazole. Chemical Engineering Research and Design, 190, 407-420.

Mondal, S., Aikat, K., & Halder, G. (2016). Biosorptive uptake of ibuprofen by chemically modified Parthenium hysterophorus derived biochar : Equilibrium , kinetics , thermodynamics and modeling. Ecological Engineering, 92, 158–172.

Montenegro-ayo, R., Tzayam, P., Lanza, M. R. V, & Brillas, E. (2023). New electrochemical reactor design for emergent pollutants removal by electrochemical oxidation. Electrochimica Acta, 458, 142551. https://doi.org/10.1016/j.electacta.2023.142551.

Mosur, A., Subramanian, A., Prasad, K., Mohanakrishna, G., & Sivagami, K. (2023). Electrochemical-based approaches for the treatment of pharmaceuticals and personal care products in wastewater. Journal of Environmental Management, 344, 118385. https://doi.org/10.1016/j.jenvman.2023.118385.

Moteshaker, P. M., Rokni, S. E., Farnoodian, N., Akhlaghi, N. M., Saadi, S., Ahmadidoust, G., & Yousefi, A. (2020). Application of response surface methodology for optimization of electrochemical process in metronidazole (MNZ) removal from aqueous solutions using stainless steel 316 (SS316) and lead (Pb) anodes. International Journal of Chemical Reactor Engineering, 18(8). https://doi.org/10.1515/ijcre-2020-0055.

Moussavi, G., Hossaini, Z., & Pourakbar, M. (2016). High-rate adsorption of acetaminophen from the contaminated water onto double-oxidized graphene oxide. Chemical Engineering Journal, 287, 665–673. https://doi.org/10.1016/j.cej.2015.11.025.

Mzukisi, L., Ncube, S., & Chimuka, L. (2020). Analysis, occurrence and removal of

pharmaceuticals in African water resources : A current status. Journal of Environmental Management, 253, 109741. https://doi.org/10.1016/j.jenvman.2019.109741.

Nafisur, R., & Nasir, M. (2020). Effective removal of acetaminophen from aqueous solution using Ca (II)-doped chitosan / β -cyclodextrin composite. Journal of Molecular Liquids, 301, 112454. https://doi.org/10.1016/j.molliq.2020.112454.

Najafinejad, M. S., Chianese, S., Fenti, A., Iovino, P., & Musmarra, D. (2023). Application of electrochemical oxidation for water and wastewater treatment: an overview. Molecules, 28(10), 4208.

Najafpoor, A. A., Sani, O. N., Alidadi, H., Yazdani, M., Fezabady, A. A. N., & Taghavi, M. (2019). Optimization of ciprofloxacin adsorption from synthetic wastewaters using γ-Al2O3 nanoparticles: An experimental design based on response surface methodology. Colloid and Interface Science Communications, 33, 100212.

Natarajan, R., Anil Kumar, M., & Vaidyanathan, V. K. (2022). Synthesis and characterization of rhamnolipid based chitosan magnetic nanosorbents for the removal of acetaminophen from aqueous solution. Chemosphere, 288(P2), 132532.

Natarajan, R., Banerjee, K., Kumar, P. S., Somanna, T., Tannani, D., Arvind, V., Raj, R. I., Vo, D. V. N., Saikia, K., & Vaidyanathan, V. K. (2021). Performance study on adsorptive removal of acetaminophen from wastewater using silica microspheres: Kinetic and isotherm studies. Chemosphere, 272, 129896. https://doi.org/10.1016/j.chemosphere.2021.129896.

Nesßeli, S., Yaldız, S., & Erol, T. (2011). Optimization of tool geometry parameters for turning operations based on the response surface methodology Süleyman Nes. Measurement, 44, 580–587. https://doi.org/10.1016/j.measurement.2010.11.018.

Nguyen, M., Lin, C., Nguyen, H., Tri, N., & Hung, Q. (2023). Occurrence , fate , and potential risk of pharmaceutical pollutants in agriculture : Challenges and environmentally friendly solutions. Science of the Total Environment, 899, 165323.

Nie, J., Zhi, D., & Zhou, Y. (2021). Magnetic biochar-based composites for removal of recalcitrant pollutants in water. In Sorbents Materials for Controlling Environmental

Pollution (pp. 163-187). Elsevier. https://doi.org/10.1016/B978-0-12-820042-1.00015-8.

Nuguse, R., Kebede, S., Wun, J., Lee, I., Verma, M., & Kim, H. (2023). Performance evaluation of Fe 3 O 4 @ ACF-supported bio-electro Fenton system for simultaneous sewage treatment and methyl orange degradation. Materials Today Communications, 35, 106331.

Nyankson, E., & Kumar, R. V. (2019). Removal of water-soluble dyes and pharmaceutical wastes by combining the photocatalytic properties of $Ag_3PO_4$ with the adsorption properties of halloysite nanotubes. Materials Today Advances, 4, 100025.

Ogundele, O. D., Oyegoke, D. A., & Anaun, T. E. (2023). Exploring the Potential and Challenges of Electrochemical Processes for Sustainable Waste Water Remediation and Treatment Acadlore Transactions on Geosciences Exploring the Potential and Challenges of Electrochemical Processes for Sustainable Waste Water. Acadlore Transactions on Geosciences, 2, 80–93. https://doi.org/10.56578/atg020203.

Ojo, B. O., Arotiba, O. A., & Mabuba, N. (2023). Coupling piezo-polarization effect on Ti/$BaZrTiO_3$ anode with sonoelectro-Fenton oxidation for the removal of aspirin in wastewater. Electrochimica Acta, 459, 142501.

Oluwole, A. O., Omotola, E. O., & Olatunji, O. S. (2020). Pharmaceuticals and personal care products in water and wastewater : a review of treatment processes and use of photocatalyst immobilized on functionalized carbon in AOP degradation. BMC Chemistry, 14, 62. https://doi.org/10.1186/s13065-020-00714-1.

Onur, S. (2023). Electrochemical Oxidation of Wastewater Contaminated with Astrazon Red Electrochemical Oxidation of Wastewater Contaminated with Astrazon Red Violet 3RN Dye on Ti/$IrO_2$/$RuO_2$ : Evaluation of Process Parameters, Kinetics, and Energy Consumption. Inranian Journal of Chemistry and Chemical Engineering, 42(11). https://doi.org/10.30492/IJCCE.2023.1973975.5729.

Orimolade, B. O., Zwane, B. N., Koiki, B. A., Rivallin, M., & Arotiba, A. (2020). Coupling cathodic electro-fenton with anodic photo-electrochemical oxidation : A feasibility study on the mineralization of paracetamol. Journal of Environmental Chemical Engineering, 8(5), 104394. https://doi.org/10.1016/j.jece.2020.104394.

Ortiz, I., San-rom, M., & Schr, S. (2024). Electrochemical degradation of key drugs to treat COVID-19 : Experimental analysis of the toxic by-products formation (PCDD/Fs). Science of the Total Environment, 906, 167660. https://doi.org/10.1016/j.scitotenv.2023.167660.

Östman, M., Björlenius, B., Fick, J., & Tysklind, M. (2019). Effect of full-scale ozonation and pilot-scale granular activated carbon on the removal of biocides , antimycotics and antibiotics in a sewage treatment plant. Science of the Total Environment, 649, 1117–1123. https://doi.org/10.1016/j.scitotenv.2018.08.382.

Ouyang, J., Zhou, L., Liu, Z., Heng, J. Y., & Chen, W. (2020). Biomass-derived activated carbons for the removal of pharmaceutical mircopollutants from wastewater: A review. Separation and Purification Technology, 253, 117536.

Pai, C., & Wang, G. (2022). Treatment of PPCPs and disinfection by-product formation in drinking water through advanced oxidation processes : Comparison of UV, UV/Chlorine, and UV/$H_2O_2$. Chemosphere, 287, 132171.

Pal, B., Singh, S., & Bansal, M. (2024). Superior adsorptive removal of ciprofloxacin by graphene oxide modified Ni-Al layered double hydroxide composites. Journal of Alloys and Compounds, 976, 173220. https://doi.org/10.1016/j.jallcom.2023.173220.

Palomares-reyna, D., Carrera-crespo, J. E., Sosa-rodríguez, F. S., García-p, U. M., Fuentes-camargo, I., Lartundo-rojas, L., & Vazquez-, J. (2022). Photo-electrochemical and ozonation process to degrade ciprofloxacin in synthetic municipal wastewater, using C, N-codoped $TiO_2$ with high visible-light absorption. Journal of Environmental Chemical Engineering, 10, 107380. https://doi.org/10.1016/j.jece.2022.107380.

Panizza, M., & Martinez-huitle, C. A. (2013). Role of electrode materials for the anodic oxidation of a real landfill leachate – Comparison between Ti–Ru–Sn ternary oxide , $PbO_2$ and boron-doped diamond anode. Chemosphere, 90(4), 1455–1460.

Papac Zjačić, J., Morović, S., Košutić, K., & Ašperger, D. (2022). Combined Application of Membrane and Advanced Oxidation Processes for Removal of Pharmaceuticals from Water. Kemija u Industriji, 71(11–12), 719–727. https://doi.org/10.15255/kui.2022.008.

Patel, M., Kumar, R., Pittman, C. U., & Mohan, D. (2021). Ciprofloxacin and acetaminophen sorption onto banana peel biochars: Environmental and process parameter influences. Environmental Research, 201, 111218. https://doi.org/10.1016/j.envres.2021.111218.

Pauletto, Paola S, Lütke, S. F., Dotto, G. L., & Salau, N. P. G. (2021a). Adsorption mechanisms of single and simultaneous removal of pharmaceutical compounds onto activated carbon : Isotherm and thermodynamic modeling. Journal of Molecular Liquids, 336, 116203. https://doi.org/10.1016/j.molliq.2021.116203.

Pauletto, P S, Lütke, S. F., Dotto, G. L., & Salau, N. P. G. (2024). Exploring the simultaneous mass transport of nimesulide and paracetamol adsorption on activated carbon : A PVSDM approach. Separation and Purification Technology, 329, 125148..

Peng, H., Guo, J., Qiu, H., Wang, C., Zhang, C., Hao, Z., Rao, Y., & Gong, Y. (2021). Efficient removal of Cr(Vi) with biochar and optimized parameters by response surface methodology. Processes, 9(5). https://doi.org/10.3390/pr9050889.

Peng, X., Hu, F., Zhang, T., Qiu, F., & Dai, H. (2018). Amine-functionalized magnetic bamboo-based activated carbon adsorptive removal of cipro fl oxacin and nor fl oxacin : A batch and fi xed-bed column study. Bioresource Technology, 249, 924–934.

Pham, T. (2018). Occurrence of pharmaceutical residues in water and treatment solutions. Thesis Submitted to Metropolia University of Applied Sciences, Helsinki, Finland.

Rosal, R., Rodríguez, A., Perdigón-Melón, J. A., Petre, A., García-Calvo, E., Gómez, M. J., Agüera, A., & Fernández-Alba, A. R. (2010). Occurrence of emerging pollutants in urban wastewater and their removal through biological treatment followed by ozonation. Water research, 44(2), 578-588.

Pereira, A., De Morais, E. G., Silva, L., Pena, A., Freitas, A., Teixeira, M. R., Varela, J., & Barreira, L. (2023). Pharmaceuticals removal from wastewater with microalgae: a pilot study. Applied Sciences, 13(11), 6414.

Peres, J. A., Ovejero, G., & García, J. (2017). Effective adsorption of non-biodegradable pharmaceuticals from hospital wastewater with different carbon materials. Chemical

Engineering Journal. https://doi.org/10.1016/j.cej.2017.03.077.

Periyasamy, S., & Muthuchamy, M. (2018). Electrochemical oxidation of paracetamol in water by graphite anode : E ff ect of pH, electrolyte concentration and current density. Journal of Environmental Chemical Engineering, 6(6), 7358–7367.

Petromelidou, S., Anagnostopoulou, K., Koronaiou, L., Kalaronis, D., Maria, N., Evgenidou, E., Papageorgiou, M., Christodoulou, A., Lioumbas, I., Kyzas, G. Z., Mitropoulos, A., Bikiaris, D. N., & Lambropoulou, D. A. (2024). Exploring patterns of antibiotics during and after COVID-19 pandemic in wastewaters of northern Greece: Potential adverse effects on aquatic environment. Science of The Total Environment, 914, 169832.

Pinto, V. L., Cervantes, T. N., Soto, P. C., Sarto, G., Bessegato, G. G., & de Almeida, L. C. (2023). Multivariate optimization of methylene blue dye degradation using electro-Fenton process with self-doped $TiO_2$ nanotube anode. Chemosphere, 344, 140336.

Poelmans, S., Nagels, M., Mignot, M., Dewil, R., Cabooter, D., & Dries, J. (2020). Effect of ozonation as pre-treatment and polishing step on removal of ecotoxicity and alkylphenol ethoxylates from tank truck cleaning wastewater. Journal of Water Process Engineering, 37, 101441. https://doi.org/10.1016/j.jwpe.2020.101441.

Prada-Vásquez, M. A., Estrada-Flórez, S. E., Serna-Galvis, E. A., & Torres-Palma, R. A. (2021). Developments in the intensification of photo-Fenton and ozonation-based processes for the removal of contaminants of emerging concern in Ibero-American countries. Science of The Total Environment, 765, 142699. https://doi.org/10.1016/j.scitotenv.2020.142699.

Puri, M., Gandhi, K., & Kumar, M. S. (2023). Emerging environmental contaminants : A global perspective on policies and regulations. Journal of Environmental Management, 332, 117344. https://doi.org/10.1016/j.jenvman.2023.117344.

Qian, J., Mi, X., Chen, Z., Xu, W., Liu, W., Ma, R., Zhang, Y., Du, Y., & Ni, B. (2023). Efficient emerging contaminants (EM) decomposition via peroxymonosulfate (PMS) activation by $Co_3O_4$/carbonized polyaniline (CPANI) composite : Characterization of tetracycline (TC) degradation property and application for the remediation of EM-polluted water body. Journal of Cleaner Production, 405, 137023.

Qiu, B., Shao, Q., Shi, J., Yang, C., & Chu, H. (2022). Application of biochar for the adsorption of organic pollutants from wastewater : Modification strategies, mechanisms and challenges. Separation and Purification Technology, 300, 121925.

Rajapaksha, A. U., Premarathna, K. S. D., Gunarathne, V., Ahmed, A., & Vithanage, M. (2019). Sorptive removal of pharmaceutical and personal care products from water and wastewater. In Pharmaceuticals and personal care products: Waste management and treatment technology (pp. 213-238). https://doi.org/10.1016/B978-0-12-816189-0.00009-3.

Rao, A., Kumar, A., Dhodapkar, R., & Pal, S. (2021). Adsorption of five emerging contaminants on activated carbon from aqueous medium: kinetic characteristics and computational modeling for plausible mechanism. Environmental Science and Pollution Research, 28(17), 21347–21358. https://doi.org/10.1007/s11356-020-12014-1.

Ripanda, A., Rwiza, M. J., Charles, E., Numph, L., Hossein, M., Bakari, R., Kumar, S., Reddy, G., Ravikumar, C. R., Murthy, H. C. A., Njau, K. N., Ali, S., Vuai, H., & Machunda, R. L. (2024). HydroResearch Optimizing ciprofloxacin removal from water using jamun seed (Syzygium cumini) biochar : A sustainable approach for ecological protection. HydroResearch, 7, 164–180. https://doi.org/10.1016/j.hydres.2024.03.001.

Rocha, L. S., Pereira, D., Sousa, É., Otero, M., Esteves, V. I., & Calisto, V. (2020). Recent advances on the development and application of magnetic activated carbon and char for the removal of pharmaceutical compounds from waters : A review. Science of the Total Environment, 718, 137272. https://doi.org/10.1016/j.scitotenv.2020.137272.

Rodríguez-Chueca, J., Laski, E., García-Cañibano, C., De Vidales, M. M., Encinas, Á., Kuch, B., & Marugán, J. (2018). Micropollutants removal by full-scale UV-C/sulfate radical based Advanced Oxidation Processes. Science of the Total Environment, 630, 1216-1225.

Rodríguez-rodríguez, C. E., Ramírez-morales, D., Masis-mora, M., Montiel-mora, R., Soto-garita, C., Araya-valverde, E., Brice, S., Cambronero-heinrichs, J. C., Alexandre, S., Mendez-rivera, M., & Balc, L. (2023). Chemosphere Occurrence and risk assessment of pharmaceuticals in hospital wastewater in Costa Rica. 339.

Rosas-ramírez, J. R., Raldua, D., Elizalde-vel, G. A., P, K. R.-, García-medina, S., Orozco-hern,

M., Islas-flores, H., Galar-martínez, M., & Guzm, X. (2022). Low concentrations of ciprofloxacin alone and in combination with paracetamol induce oxidative stress, upregulation of apoptotic-related genes, histological alterations in the liver, and genotoxicity in Danio rerio. Chemosphere, 294, 133667.

Rout, P. R., Zhang, T. C., Bhunia, P., & Surampalli, R. Y. (2021). Treatment technologies for emerging contaminants in wastewater treatment plants: A review. Science of the Total Environment, 753, 141990. https://doi.org/10.1016/j.scitotenv.2020.141990.

Roy, N., Kannabiran, K., & Mukherjee, A. (2023). Integrated adsorption and photocatalytic degradation based removal of ciprofloxacin and sulfamethoxazole antibiotics using Fc @ rGO-ZnO nanocomposite in aqueous systems. Chemosphere, 333, 138912.

Santhosh, R., Govindan, K., & Ramakrishnan, S. (2021). $Fe_3O_4$ nanorods decorated on polypyrrole / reduced graphene oxide for electrochemical detection of dopamine and photocatalytic degradation of acetaminophen. Applied Surface Science, 556, 149765. https://doi.org/10.1016/j.apsusc.2021.149765.

Sathishkumar, K., AlSalhi, M. S., Sanganyado, E., Devanesan, S., Arulprakash, A., & Rajasekar, A. (2019). Sequential electrochemical oxidation and bio-treatment of the azo dye congo red and textile effluent. Journal of Photochemistry and Photobiology B: Biology, 200, 111655. https://doi.org/10.1016/j.jphotobiol.2019.111655.

Serna-Galvis, E. A., Silva-Agredo, J., Botero-Coy, A. M., Moncayo-Lasso, A., Hernández, F., & Torres-Palma, R. A. (2019). Effective elimination of fifteen relevant pharmaceuticals in hospital wastewater from Colombia by combination of a biological system with a sonochemical process. Science of the total environment, 670, 623-632.

Shang, J. G., He, X. R. K. L. L., & Liao, W. H. L. Q. J. H. (2016). Low-cost biochar derived from herbal residue : characterization and application for ciprofloxacin adsorption. Internal Journal of Environmental Science and Technology, 13, 2449–2458.

Sharma, P., Sharma, M., Laddha, H., Gupta, R., & Agarwal, M. (2023). Non-toxic and biodegradable κ-carrageenan/ZnO hydrogel for adsorptive removal of norfloxacin: Optimization using response surface methodology. International Journal of Biological

Macromolecules, 238, 124145.

Sharma, S., & Simsek, H. (2020). Sugar beet industry process wastewater treatment using electrochemical methods and optimization of parameters using response surface methodology. Chemosphere, 238, 124669.

Shi, H., Wang, Q., Ni, J., Xu, Y., Song, N., & Gao, M. (2020). Highly efficient removal of amoxicillin from water by three-dimensional electrode system within granular activated carbon as particle electrode. Journal of Water Process Engineering, 38, 101656. https://doi.org/10.1016/j.jwpe.2020.101656.

Shi, W., Chu, Y., Xia, M., Wang, F., & Fu, C. (2021). The adsorption performance and micro-mechanism of MoS2/montmorillonite composite to atenolol and acebutolol: Adsorption experiments and a novel visual study of interaction. Ecotoxicology and Environmental Safety, 213, 111993. https://doi.org/10.1016/j.ecoenv.2021.111993.

Shi, Y., Zhang, Y., Cui, Y., Shi, J., Meng, X., Zhang, J., & He, H. (2019). Magnetite nanoparticles modi fi ed β -cyclodextrin PolymerCoupled with KMnO 4 oxidation for adsorption and degradation of acetaminophen. Carbohydrate Polymers, 222, 114972. https://doi.org/10.1016/j.carbpol.2019.114972.

Shin, J., Kwak, J., Lee, Y. G., Kim, S., Choi, M., Bae, S., Lee, S. H., Park, Y., & Chon, K. (2021). Competitive adsorption of pharmaceuticals in lake water and wastewater effluent by pristine and NaOH-activated biochars from spent coffee wastes: Contribution of hydrophobic and π-π interactions. Environmental Pollution, 270, 116244.

Shin, J., Lee, Y. G., Lee, S. H., Kim, S., Ochir, D., Park, Y., Kim, J., & Chon, K. (2020). Single and competitive adsorptions of micropollutants using pristine and alkali-modified biochars from spent coffee grounds. Journal of Hazardous Materials, 400, 123102.

Shirani, Z., Song, H., & Bhatnagar, A. (2020). Efficient removal of diclofenac and cephalexin from aqueous solution using Anthriscus sylvestris-derived activated biochar. Science of the total environment, 745, 140789.

Singh, V., & Suthar, S. (2021). Occurrence, seasonal variations, and ecological risk of

pharmaceuticals and personal care products in River Ganges at two holy cities of India. Chemosphere, 268, 129331. https://doi.org/10.1016/j.chemosphere.2020.129331.

Sipma, J., Osuna, B., Collado, N., Monclús, H., Ferrero, G., Comas, J., & Rodriguez-Roda, I. (2010). Comparison of removal of pharmaceuticals in MBR and activated sludge systems. Desalination, 250(2), 653-659. https://doi.org/10.1016/j.desal.2009.06.073.

Sips, R. (1948). On the Structure of a Catalyst Surface. The Journal of Chemical Physics, 16(5), 490–495. https://doi.org/10.1063/1.1746922.

Skwarczynska-Wojsa, A., & Puszkarewicz, A. (2024). Removal of Acetaminophen from Aqueous Solutions in an Adsorption Process. Materials, 17(2), 431.

Sohn, S., Kim, M. K., Lee, Y. M., Sohn, E. J., Choi, G. Y., Chae, S. H., & Zoh, K. D. (2024). Removal characteristics of 53 micropollutants during ozonation, chlorination, and UV/$H_2O_2$ processes used in drinking water treatment plant. Chemosphere, 141360.

Son, D. J., Kim, C. S., Lee, J. H., Yoon, J. K., Lee, S. H., & Jeong, D. H. (2023). Occurrence Assessment of Pharmaceuticals in Various Sewage Treatment Plants and Effluent-Receiving Streams in Korea. Water, 15(22), 3897.

Sözüdoğru, O., Seda, E., Alper, K., Ylmaz, E., Bakirdere, S., & Tarık, O. (2023). The experimental design approach to removal of endocrine disrupting compounds from domestic wastewater by electrooxidation process. Journal of Applied Electrochemistry, 53(10), 1971–1990. https://doi.org/10.1007/s10800-023-01903-1.

Stylianou, M., Christou, A., Michael, C., Agapiou, A., Papanastasiou, P., & Fatta-kassinos, D. (2021). Adsorption and removal of seven antibiotic compounds present in water with the use of biochar derived from the pyrolysis of organic waste feedstocks. Journal of Environmental Chemical Engineering, 9(5), 105868.

Stucchi, M. G., Rigamonti, D., Carnevali, D. C., & Boffito. (2020). A Kinetic Study on the Degradation of Acetaminophen and Amoxicillin in Water by Ultrasound. ChemistrySelect, 5(47), 14986–14992. https://doi.org/10.1002/slct.202004147.

Sulyman, M., Namiesnik, J., & Gierak, A. (2017). Low-cost Adsorbents Derived from

Agricultural By-products/Wastes for Enhancing Contaminant Uptakes from Wastewater: A Review. Polish Journal of Environmental Studies, 26(3).

Szabová, P., Hencelová, K., Sameliaková, Z., Marcová, T., Vojs, A., Grabicová, K., & Bodík, I. (2020). Ozonation : effective way for removal of pharmaceuticals from wastewater. Monatshefte Für Chemie -Chemical Monthly, 0123456789. https://doi.org/10.1007/s00706-020-02600-x.

Tan, C., Gao, N., Fu, D., Deng, J., & Deng, L. (2017). Efficient degradation of paracetamol with nanoscaled magnetic $CoFe_2O_4$ and $MnFe_2O_4$ as a heterogeneous catalyst of peroxymonosulfate. Separation and Purification Technology, 175, 47–57.

Tang, K., Spiliotopoulou, A., Chhetri, R. K., Ooi, G. T. H., Kaarsholm, K. M. S., Sundmark, K., Florian, B., Kragelund, C., Bester, K., & Andersen, H. R. (2019). Removal of pharmaceuticals, toxicity and natural fluorescence through the ozonation of biologically-treated hospital wastewater, with further polishing via a suspended biofilm. Chemical Engineering Journal, 359, 321–330. https://doi.org/10.1016/j.cej.2018.11.112.

Tang, L., Ma, X. Y., Wang, Y., Zhang, S., Zheng, K., Wang, X. C., & Lin, Y. (2020). Removal of trace organic pollutants (pharmaceuticals and pesticides) and reduction of biological effects from secondary effluent by typical granular activated carbon. Science of the Total Environment, 749, 141611. https://doi.org/10.1016/j.scitotenv.2020.141611.

Temkin, M. and Pyzhev, V. (1940) Kinetics of Ammonia Synthesis on Promoted Iron Catalysts. Acta Physicochimica URSS, 12, 217-222.

Taylor, P., Mashayekh-salehi, A., & Moussavi, G. (2015). Removal of acetaminophen from the contaminated water using adsorption onto carbon activated with $NH_4Cl$. Desalination and Water Treatment, June, 37–41. https://doi.org/10.1080/19443994.2015.1051588.

Thanh, D., Nguyen, H., Juang, R., Duy, N., Nguyen, V. P., & Chao, H. (2020). Adsorption process and mechanism of acetaminophen onto commercial activated carbon. Journal of Environmental Chemical Engineering, 8(6), 104408.

Thiebault, T. (2020). Raw and modified clays and clay minerals for the removal of

pharmaceutical products from aqueous solutions: State of the art and future perspectives. Critical Reviews in Environmental Science and Technology, 50(14), 1451-1514. https://doi.org/10.1080/10643389.2019.1663065.

Tiwari, B., Sellamuthu, B., Ouarda, Y., Drogui, P., Tyagi, R. D., & Buelna, G. (2016). Review on Fate and Mechanism of removal of pharmaceutical pollutants from wastewater using biological approach. Bioresource Technology.

Tong, F., Liu, D., Zhang, Z., Chen, W., Fan, G., & Gao, Y. (2023). Heavy metal-mediated adsorption of antibiotic tetracycline and ciprofloxacin on two microplastics : Insights into the role of complexation. Environmental Research, 216, 114716.

Tovar-Gómez, R., del Rosario Moreno-Virgen, M., Moreno-Pérez, J., Bonilla-Petriciolet, A., Hernández-Montoya, V., & Durán-Valle, C. J. (2015). Analysis of synergistic and antagonistic adsorption of heavy metals and acid blue 25 on activated carbon from ternary systems. Chemical Engineering Research and Design, 93, 755-772.

Tunç, M. S., Yıldız, B., & Taşar, Ş. (2022). Removal of paracetamol from aqueous solution by wood sawdust-derived activated carbon: Process optimization using response surface methodology. Chemical Engineering Communications, 209(8), 1130–1150.

Tzabar, N., & Brake, H. J. M. (2016). Adsorption isotherms and Sips models of nitrogen , methane, ethane, and propane on commercial activated carbons and polyvinylidene chloride. Adsorption, 22(7), 901–914. https://doi.org/10.1007/s10450-016-9794-9.

Vieira, D. S., Rom, L. P. C., Sim, A. J. A., & Eguiluz, K. I. B. (2023). Electrochemical degradation of ciprofloxacin using a coupled 3D anode to a microfluidic flow-through reactor. Journal of Water Process Engineering, 51, 103443.

Waleng, N. J., & Nomngongo, P. N. (2022). Occurrence of pharmaceuticals in the environmental waters: African and Asian perspectives. Environmental Chemistry and Ecotoxicology, 4, 50-66. https://doi.org/10.1016/j.enceco.2021.11.002.

Wang, C., Zhang, T., Luo, J., Wu, M., Niu, J., Shang, E., Ni, C., & Ni, J. (2022). Synergistic enhancement of piezocatalysis and electrochemical oxidation for the degradation of

ciprofloxacin by $PbO_2$ intercalation material. Separation and Purification Technology, 297, 121528. https://doi.org/10.1016/j.seppur.2022.121528

Wang, Y., Gupta, K., Li, J., Yuan, B., & Yang, J. E. (2018). Novel chalcogenide based magnetic adsorbent KMS-1 / L-Cystein / Fe 3 O 4 for the facile removal of cipro fl oxacin from aqueous solution. Colloids and Surfaces A, 538, 378–386.

Weber Jr, W. J., & Morris, J. C. (1963). Kinetics of adsorption on carbon from solution. Journal of the sanitary engineering division, 89(2), 31-59.

Wei, K., Cui, T., Huang, F., Zhang, Y., & Han, W. (2020). Membrane separation coupled with electrochemical advanced oxidation processes for organic wastewater treatment: A short review. Membranes, 10(11), 1–29. https://doi.org/10.3390/membranes10110337.

Wei, X., Wang, Y., Chen, J., Xu, F., Liu, Z., He, X., & Li, H. (2020). Adsorption of pharmaceuticals and personal care products by deep eutectic solvents-regulated magnetic metal-organic framework adsorbents : Performance and mechanism. Chemical Engineering Journal, 392, 124808. https://doi.org/10.1016/j.cej.2020.124808.

Weng, M., & Yu, X. (2019). Electrochemical Oxidation of Para-Aminophenol With Rare Earth Doped Lead Dioxide Electrodes : Kinetics Modeling and Mechanism. Frontiers in Chemistry, 7, 1–6. https://doi.org/10.3389/fchem.2019.00382.

Wilt, A. De, Gijn, K. Van, Verhoek, T., Vergnes, A., Hoek, M., & Rijnaarts, H. (2018). Enhanced pharmaceutical removal from water in a three step bio-ozone-bio process. Water Research, 138, 97–105. https://doi.org/10.1016/j.watres.2018.03.028

Wohlmuth, S., Nelson, A., Heberle, A., Pereira, A., Antônio, M., Rodrigues, S., & Pérez-herranz, V. (2018). Antibiotics mineralization by electrochemical and UV-based hybrid processes : evaluation of the synergistic effect. Environmental Technology, 3330, 3456–3466. https://doi.org/10.1080/09593330.2018.1478453.

Wong, S., Lim, Y., Ngadi, N., Mat, R., Hassan, O., & Inuwa, I. M. (2018). Removal of acetaminophen by activated carbon synthesized from spent tea leaves : equilibrium , kinetics and thermodynamics studies. Powder Technology, 338, 878–886.

Wu, L., Zhang, X., & Si, Y. (2022). Polydopamine functionalized superhydrophilic coconut shells biomass carbon for selective cationic dye methylene blue adsorption. Materials Chemistry and Physics, 279, 125767. https://doi.org/10.1016/j.matchemphys.2022.125767.

Xia, Y., Dai, J., Yan, Y., Ma, X., Feng, H., & Ding, Y. (2023). Energy-efficient electrochemical treatment of paracetamol using a $PbO_2$ anode based on pulse electrodeposition strategy : Kinetics, energy consumption and mechanism. Environmental Research, 216, 114673. https://doi.org/10.1016/j.envres.2022.114673.

Xu, Z., Sun, Z., Zhou, Y., Chen, W., Zhang, T., Huang, Y., & Zhang, D. (2019). Insights into the pyrolysis behavior and adsorption properties of activated carbon from waste cotton textiles by $FeCl_3$-activation. Colloids and Surfaces A, 582, 123934.

Yadav, M. S. P., Sanjeev, N. O., Vallabha, M. S., Sekar, A., Valsan, A. E., & Varghese, G. K. (2022). Competitive adsorption analysis of antibiotics removal from multi-component systems using chemically activated spent tea waste: effect of operational parameters, kinetics, and equilibrium study. Environmental Science and Pollution Research, 0123456789. https://doi.org/10.1007/s11356-022-22323-2.

Yaghmaeian, K., Moussavi, G., & Alahabadi, A. (2014). Removal of amoxicillin from contaminated water using NH 4 Cl-activated carbon : Continuous flow fixed-bed adsorption and catalytic ozonation regeneration. Chemical Engineering Journal, 236, 538–544. https://doi.org/10.1016/j.cej.2013.08.118.

Yang, C., Li, R., Wang, Q., Wang, W., Gao, P., & Hu, B. (2021). Synthesis of alkyl-functionalized magnetic for fluoroquinolones removal: Adsorption performance and mechanism studies in single and binary systems. Colloids and Surfaces A: Physicochemical and Engineering Aspects, 608, 125549. https://doi.org/10.1016/j.colsurfa.2020.125549.

Yang, H., Kang, J., Jeong, S., Park, S., & Lee, C. (2022). Removal of perfluorooctanoic acid from water using peroxydisulfate / layered double hydroxide system : Optimization using response surface methodology and artificial neural network. Process Safety and Environmental Protection, 167, 368–377. https://doi.org/10.1016/j.psep.2022.09.032.

Yang, X., Wang, B., & Cheng, F. (2024). Adsorption performance on tetracycline by novel

magnetic adsorbent derived from hydrochar of low-rank coal and sewage sludge. Separation and Purification Technology, 330, 125482. https://doi.org/10.1016/j.seppur.2023.125482.

Yang, Y., Luo, X., Zhang, J., Ma, X., Sun, P., & Zhao, L. (2022). Sewage sludge–coconut fiber co-pyrolysis biochar: Mechanisms underlying synergistic heavy metal stabilization and ciprofloxacin adsorption. Journal of Cleaner Production, 375, 134149.

Yanyan, L., Kurniawan, T. A., Albadarin, A. B., & Walker, G. (2018). Enhanced removal of acetaminophen from synthetic wastewater using multi-walled carbon nanotubes (MWCNTs) chemically modified with NaOH, $HNO_3/H_2SO_4$, ozone, and/or chitosan. Journal of Molecular Liquids, 251, 369-377. https://doi.org/10.1016/j.molliq.2017.12.051.

Ye, Y., Wei, Y., Gu, Y., Kang, D., Jiang, W., & Kang, J. (2020). Simultaneous removal of fl uoride and phosphate in a continuous fixed-bed column filled with magnesia-pullulan composite. Journal of Alloys and Compounds, 838, 155528.

Yin, R., & Shang, C. (2020). Removal of micropollutants in drinking water using UV-LED/chlorine advanced oxidation process followed by activated carbon adsorption. Water Research, 185, 116297. https://doi.org/10.1016/j.watres.2020.116297.

Yılmaz, Ş., Zengin, A., & Şahan, T. (2021). Effective utilization of Fe(III)-based metal organic framework-coated cellulose paper for highly efficient elimination from the liquid phase of paracetamol as a pharmaceutical pollutant. Environmental Technology and Innovation, 24, 101799. https://doi.org/10.1016/j.eti.2021.101799.

Yoon, Y., Cho, E., Jung, Y., Kwon, M., Yoon, J., & Kang, J. W. (2015). Evaluation of the formation of oxidants and by-products using Pt/Ti, $RuO_2$/Ti, and $IrO_2$/Ti electrodes in the electrochemical process. Environmental technology, 36(3), 317-326.

Yousefi, M., Gholami, M., Oskoei, V., & Akbar, A. (2021). Comparison of LSSVM and RSM in simulating the removal of ciprofloxacin from aqueous solutions using magnetization of functionalized multi-walled carbon nanotubes : Process optimization using GA and RSM techniques. Journal of Environmental Chemical Engineering, 9(4), 105677.

Yu, Y., Wang, S., Yu, P., Wang, D., Hu, B., Zheng, P., & Zhang, M. (2024). A bibliometric

analysis of emerging contaminants (ECs)(2001− 2021): Evolution of hotspots and research trends. Science of The Total Environment, 907, 168116.

Yun, W., Lin, K. A., Tong, W., Lin, Y., & Du, Y. (2019). Enhanced degradation of paracetamol in water using sulfate radical-based advanced oxidation processes catalyzed by 3-dimensional $Co_3O_4$ nanoflower. Chemical Engineering Journal, 373, 1329–1337.

Zafar, R., Nabi, D., Al-huqail, A. A., Jamil, U., Jamal, S., Ahmed, Z., & Arshad, M. (2023). Efficient and simultaneous removal of four antibiotics with silicone polymer adsorbent from aqueous solution. Emerging Contaminants, 9(4), 100258.

Zhang, B., Han, X., Gu, P., Fang, S., & Bai, J. (2017). Response surface methodology approach for optimization of cipro fl oxacin adsorption using activated carbon derived from the residue of desilicated rice husk. Journal of Molecular Liquids, 238, 316–325. https://doi.org/10.1016/j.molliq.2017.04.022.

Zhang, Q., Xin, B., Bo, Y., Chen, B., & Hong, J. (2020). Science of the Total Environment Sulfur doped-graphene for enhanced acetaminophen degradation via electro-catalytic activation : Efficiency and mechanism. Science of the Total Environment, 715, 136730. https://doi.org/10.1016/j.scitotenv.2020.136730.

Zhang, R., Li, Y., Wang, Z., Tong, Y., & Sun, P. (2020). Biochar-activated peroxydisulfate as an effective process to eliminate pharmaceutical and metabolite in hydrolyzed urine. Water Research, 177, 115809. https://doi.org/10.1016/j.watres.2020.115809.

Zhang, Y., Wang, H., Li, Y., Wang, B., Huang, J., Deng, S., Yu, G., & Wang, Y. (2020). Removal of micropollutants by an electrochemically driven UV/chlorine process for decentralizedwater treatment. Water Research, 183, 116115.

Zhao, H., Liu, X., Cao, Z., Zhan, Y., Shi, X., Yang, Y., & Zhou, J. (2016). Adsorption behavior and mechanism of chloramphenicols, sulfonamides, and non-antibiotic pharmaceuticals on multi-walled carbon nanotubes. Journal of Hazardous Materials, 310, 235–245.

Zheng, Z., & Duan, X. (2022). Mitigating the Health Effects of Aqueous Cr(VI) with Iron-Modified Biochar. International Journal of Environmental Research and Public Health,

19(3). https://doi.org/10.3390/ijerph19031481

Ziylan-Yavaş, A., & Ince, N. H. (2018). Catalytic ozonation of paracetamol using commercial and Pt-supported nanocomposites of $Al_2O_3$: the impact of ultrasound. Ultrasonics Sonochemistry, 40, 175-182. https://doi.org/10.1016/j.ultsonch.2017.02.017.

# Appendices

## Appendix A: Characterization

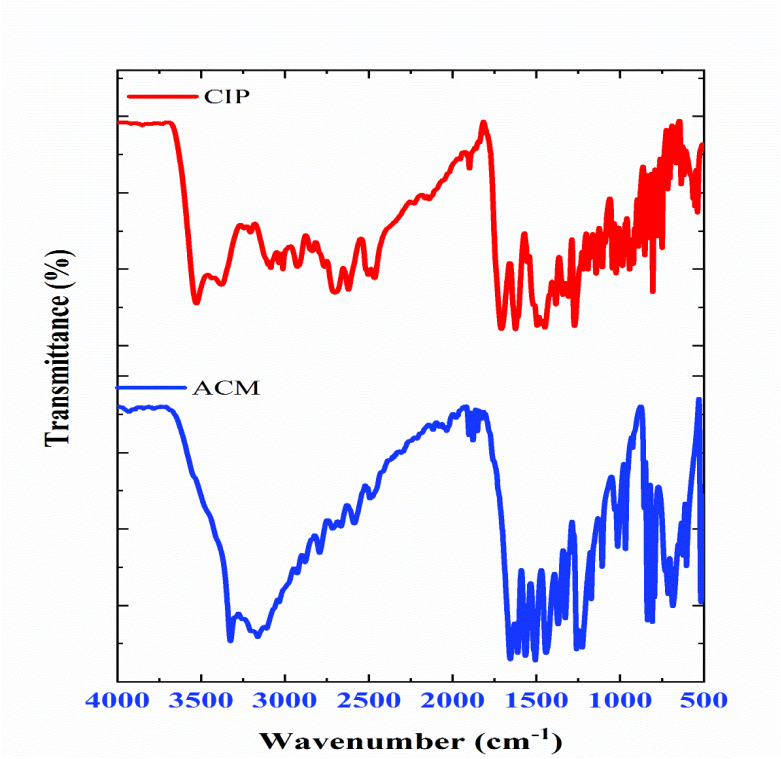


Figure A.1. FTIR spectra of ACM and CIP compounds.

Table A.1. The secondary WWTPs effluent characteristics.

| Parameters | Akaki kality WWTP effluent (values) | Mikkeli WWTPs effluent (values) |
|---|---|---|
| pH | 7.20 | 7.05 |
| Conductivity | 919.50 | 495 |
| COD (mg/L) | 52.83 | 26 |
| BOD5 (mg/L) | 7.33 | 4.5 |
| COD/BOD5 | 7.95 | 5.78 |
| Total suspended solid (TSS) (mg/L) | 12.16 | 8.5 |

Table A.1. Continued.

| Parameters | Akaki kality WWTPs effluent (parameters value) | Mikkeli WWTPs effluent (parameters value) |
|---|---|---|
| Volatile suspended solid (VSS) (mg/L) | 7.50 | 5.2 |
| VSS/TSS | 0.63 | 0.61 |
| $SO_4$ (mg/L) | 46.58 | 44.25 |
| $NH_4$ (mg/L) | 18.45 | 16.28 |
| Total nitrogen (TN) (mg/L) | 57.00 | 40.54 |
| $NO_3$ (mg/L) | 39.1 | 20.33 |
| Total phosphorus (TP) (mg/L) | 8.65 | 7.55 |

Table A.2. Molecular properties of ACM and CIP (Rao et al., 2021).

| Compound | Molecular volume ($Å^3$) | Molecular area ($Å^2$) | Molecular length (nm) | Molecular width (nm) |
|---|---|---|---|---|
| CIP | 133.04 | 104.36 | 1.50 | 1.01 |
| ACM | 72.25 | 58.75 | 1.15 | 0.69 |

# Appendix B: Adsorption (single process)

Table B.1. CCD experimental design of CIP adsorption using CAC.

| Run | A: Initial CIP con (mg/L) | B: Adsorbent dose (g/L | C: pH | D: Contact time (min) | CIP removal % | Predicted Value | Residual |
|---|---|---|---|---|---|---|---|
| 1 | 30 | 0.75 | 7.5 | 32.5 | 87.94 | 89.42 | -1.48 |
| *2* | *30* | 0.75 | *12* | *32.5* | *75.66* | *75.66* | *-2.50* |
| 3 | 30 | 0.75 | 7.5 | 32.5 | 90.24 | 89.42 | 0.8152 |
| 4 | 30 | 0.75 | 7.5 | 32.5 | 87.54 | 89.42 | -1.88 |
| 5 | 30 | 0.75 | 7.5 | 32.5 | 88.24 | 89.42 | -1.18 |
| 6 | 50 | 0.75 | 7.5 | 32.5 | 77.85 | 78.30 | -0.4490 |
| 7 | 10 | 0.75 | 7.5 | 32.5 | 99.57 | 100.55 | -2.96 |
| 8 | 20 | 0.5 | 9.75 | 46.25 | 95.52 | 94.07 | 1.45 |
| 9 | 20 | 1 | 9.75 | 18.75 | 89.24 | 87.66 | 1.58 |
| 10 | 40 | 0.5 | 9.75 | 46.25 | 76.21 | 73.90 | 2.31 |
| 11 | 40 | 0.5 | 5.25 | 46.25 | 71.99 | 73.34 | -1.35 |
| 12 | 30 | 0.75 | 3 | 32.5 | 86.12 | 86.29 | -0.1703 |
| 13 | 40 | 1 | 9.75 | 46.25 | 97.51 | 96.50 | 1.01 |
| 14 | 20 | 0.5 | 5.25 | 18.75 | 82.35 | 82.95 | -0.6003 |
| 15 | 20 | 1 | 5.25 | 46.25 | 99.56 | 98.02 | 1.54 |
| 16 | 20 | 1 | 9.75 | 46.25 | 99.1 | 98.59 | 0.5127 |
| 17 | 40 | 0.5 | 5.25 | 18.75 | 61.64 | 62.79 | -1.15 |
| 18 | 20 | 0.5 | 9.75 | 18.75 | 73.12 | 71.75 | 1.37 |
| 19 | 30 | 0.75 | 7.5 | 32.5 | 90.23 | 89.42 | 0.8052 |
| 20 | 40 | 1 | 9.75 | 18.75 | 83.51 | 85.58 | -2.07 |
| 21 | 30 | 1.25 | 7.5 | 32.5 | 98.45 | 99.88 | -1.43 |
| 22 | 40 | 1 | 5.25 | 46.25 | 97.08 | 95.93 | 1.15 |
| 23 | 40 | 1 | 5.25 | 18.75 | 98.19 | 96.77 | 1.42 |
| 24 | 30 | 0.75 | 7.5 | 60 | 99.12 | 100.16 | -1.04 |
| 25 | 20 | 0.5 | 5.25 | 46.25 | 95.11 | 93.50 | 1.61 |
| 26 | 30 | 0.75 | 7.5 | 32.5 | 89.62 | 89.42 | 0.1952 |
| 27 | 30 | 0.25 | 7.5 | 32.5 | 60.13 | 61.37 | -1.24 |
| 28 | 30 | 0.75 | 7.5 | 5 | 80.54 | 78.69 | 1.85 |
| 29 | 20 | 1 | 5.25 | 18.75 | 99.25 | 98.86 | 0.3881 |
| 30 | 40 | 0.5 | 9.75 | 18.75 | 53.09 | 51.59 | 1.50 |

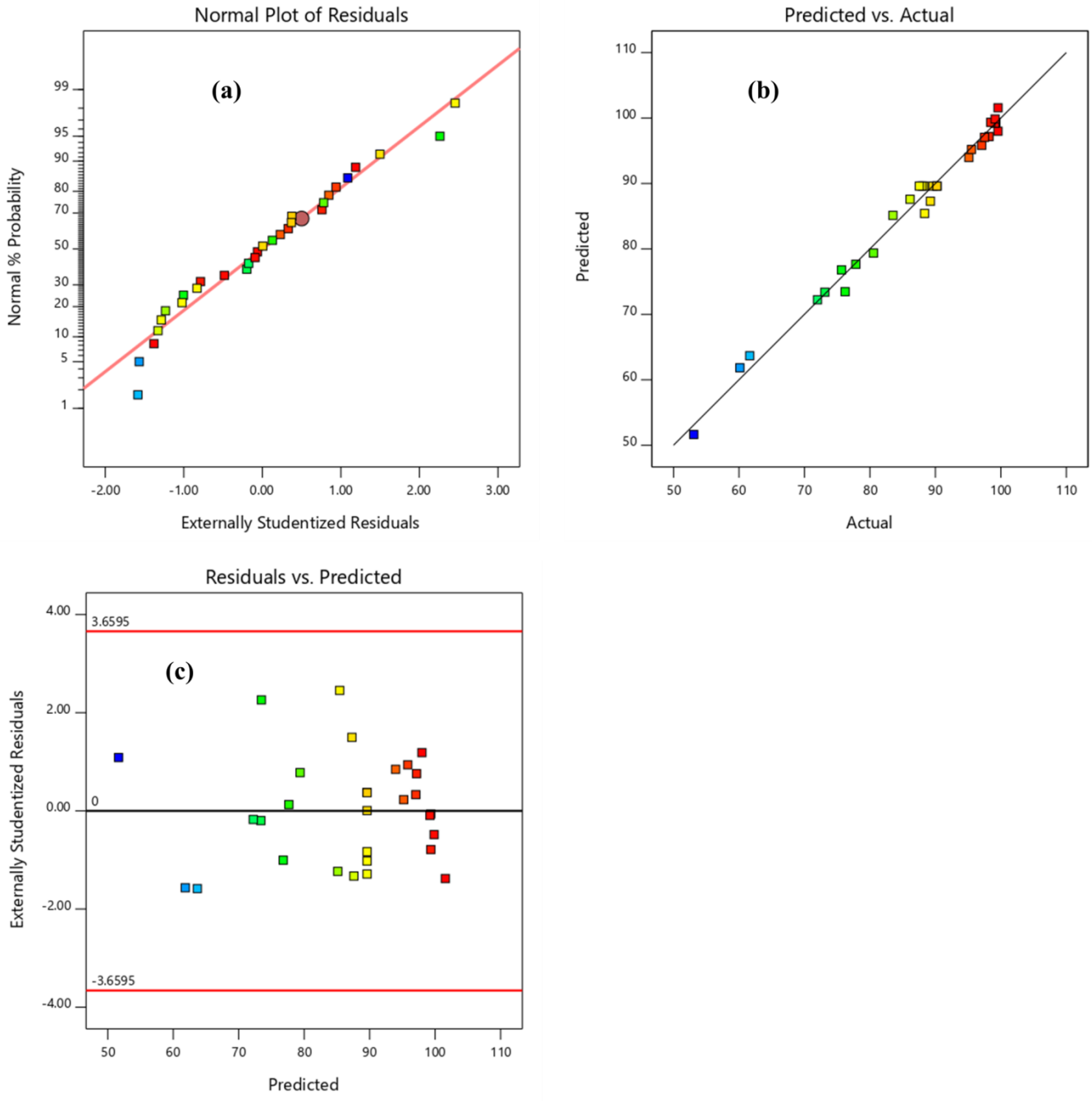


Figure B.1. Diagnostic plots of the quadratic model for CIP removal: a) Normal probability versus externally studentized residuals; (b) externally studentized residuals againist predicted (c) predicted againist actulal.

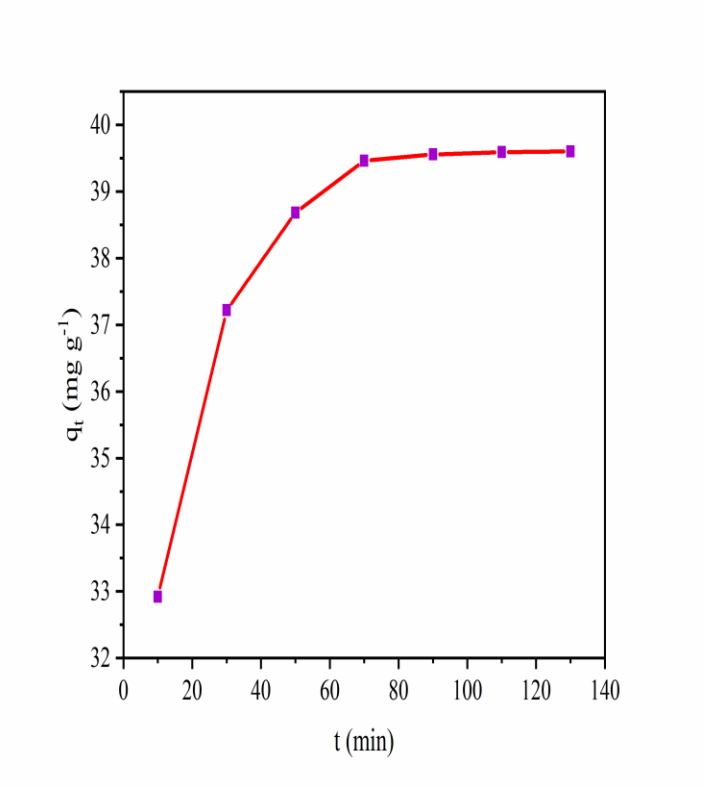


Figure B.3. The plot of CAC adsorbent capacity for single sorption of CIP with time.

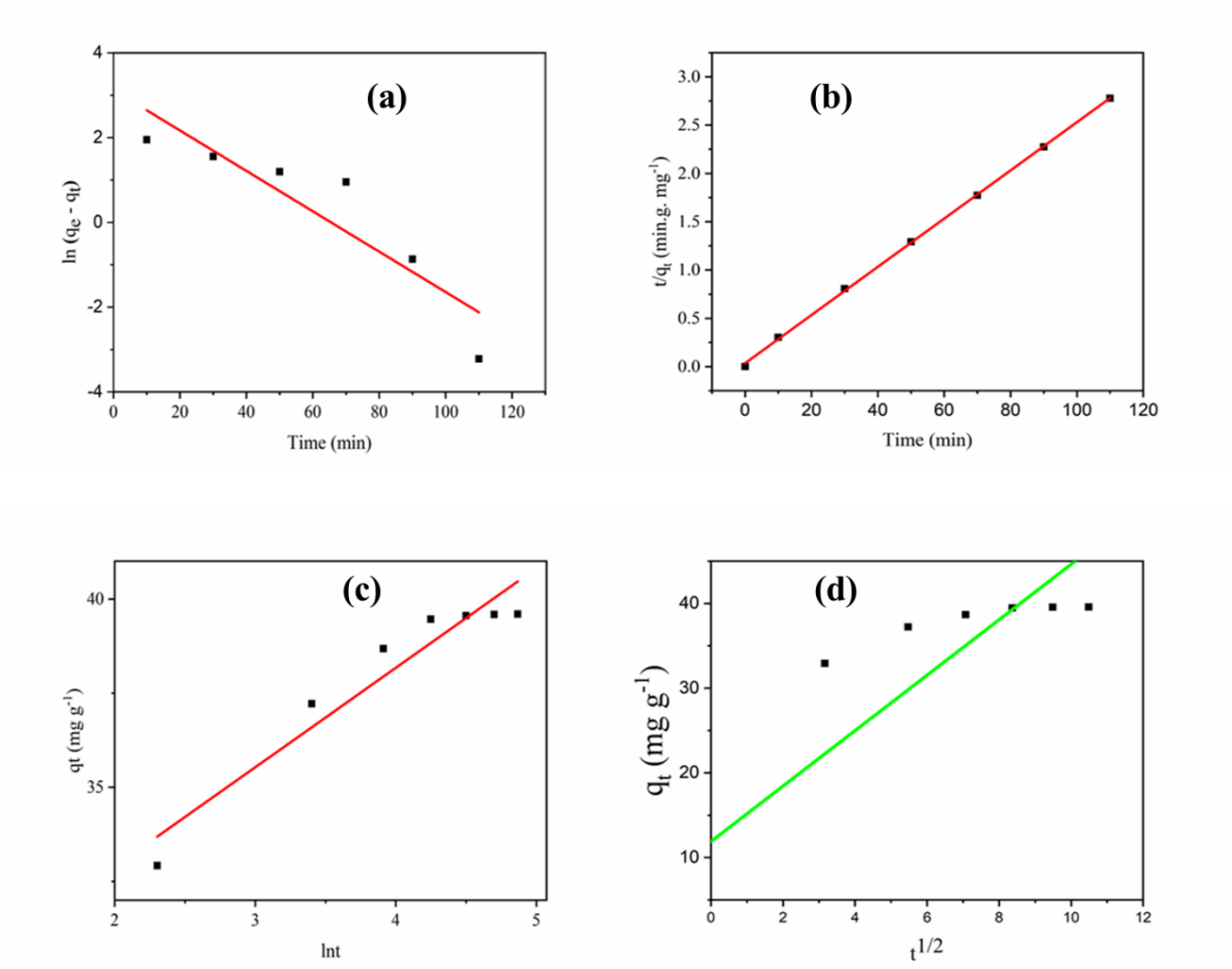


Figure B.4. Linear kinetic models employed for CIP single sorption onto CAC (a) Pseudo-first-order model, (b) Pseudo-second-order model, (c) Elovich and (d) intra-particle models.

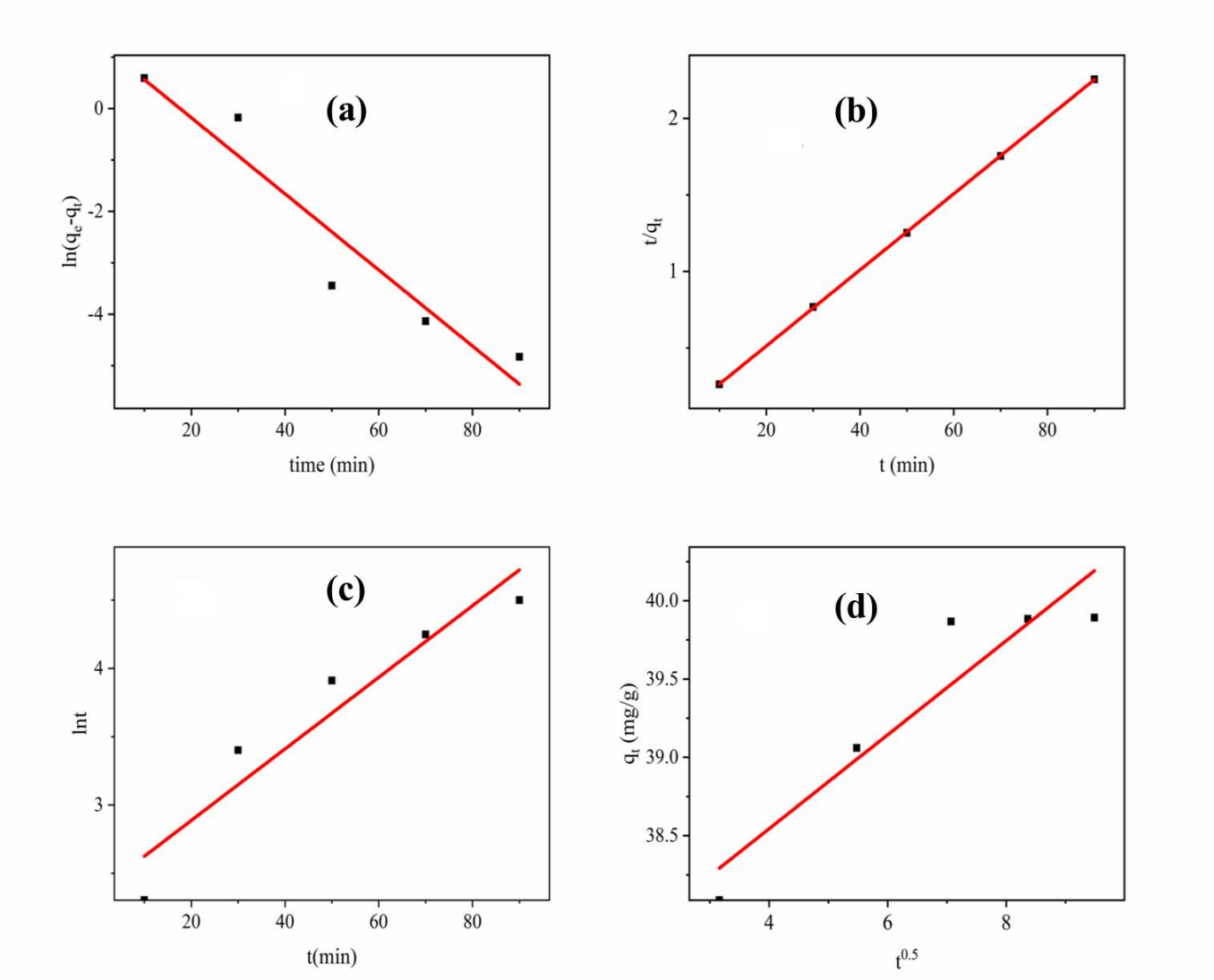


Figure B.5. Linear kinetic models of ACM single sorption onto CAC (a) Pseudo-first-order, (b) Pseudo-second-order, (c) Elovich and (d) intra-particle model.

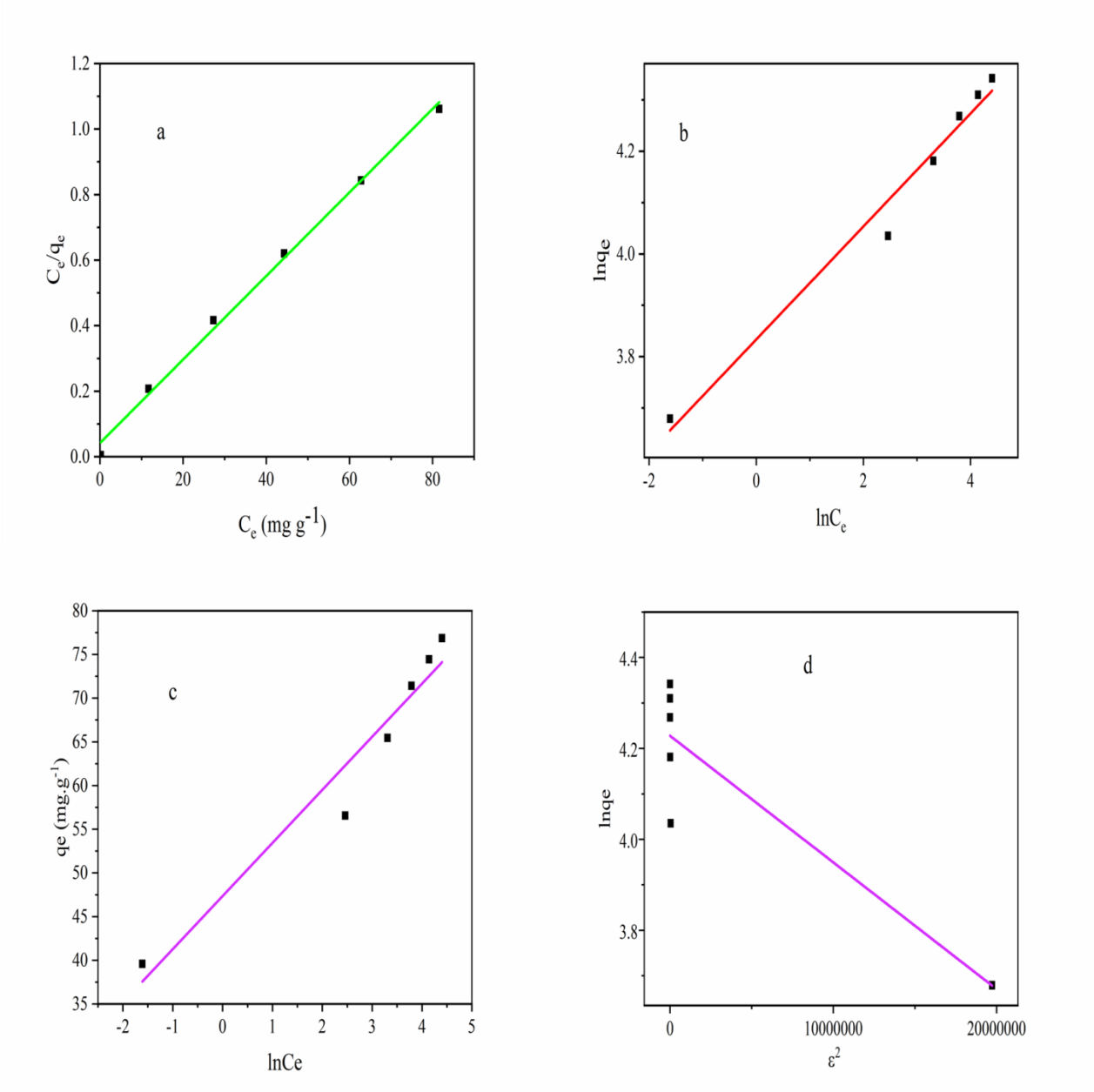


Figure B.6. Linear isotherm model plots for CIP single sorption onto CAC (a) Langmuir, (b) Freundlich, (c) Temkin and (d) Dubinin-Radushkevich.

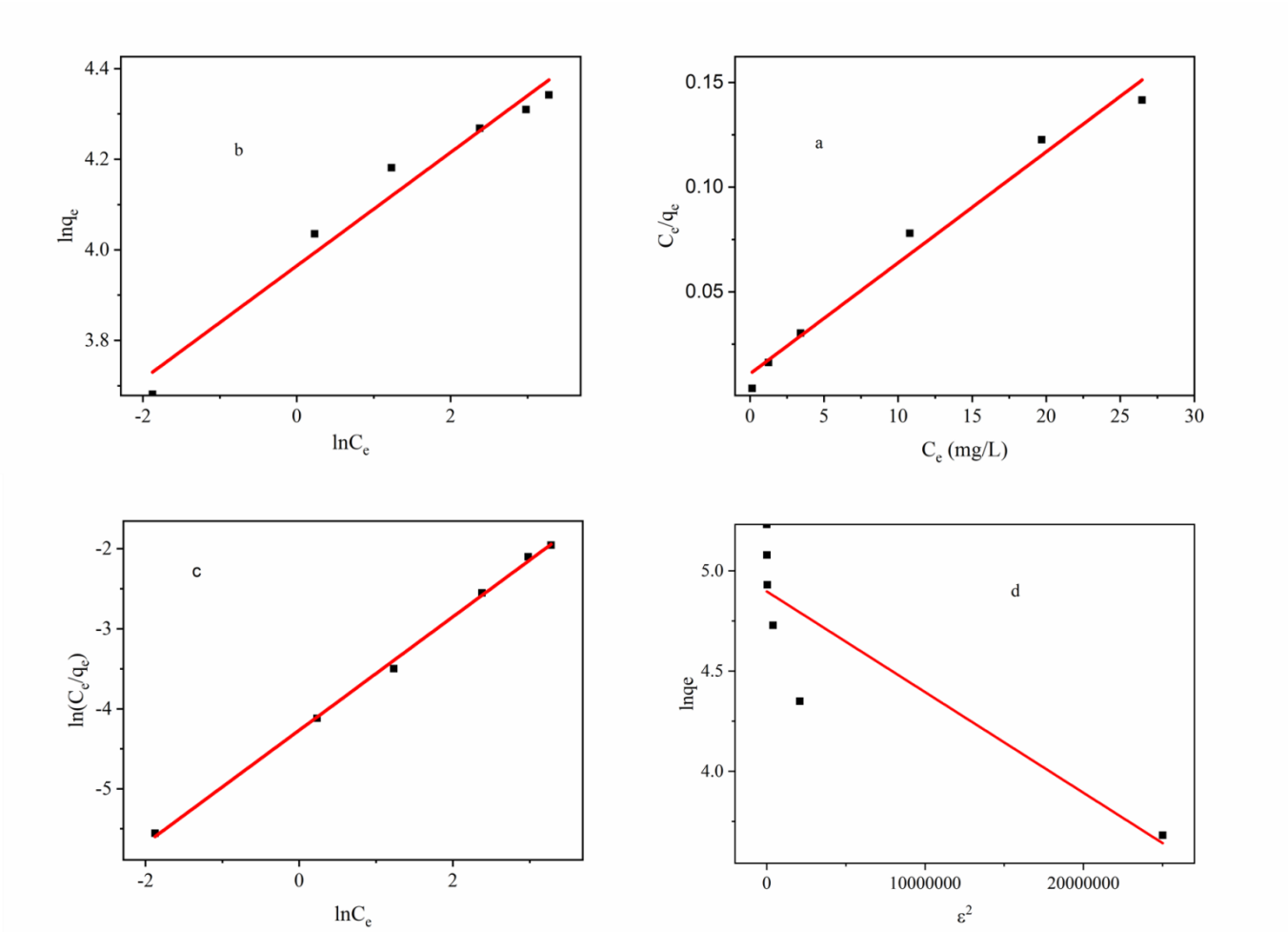


Figure B.7. Linear isotherm model plots for ACM single sorption onto CAC (a) Langmuir, (b) Freundlich, (c) Redlich-Peterson, (d) Dubinin-Radushkevich.

Table B.2. Linear kinetic and isotherm model parameters for single sorption of ACM and CIP onto CAC.

| Kinetics analysis | | | | Isotherm analysis | | | |
|---|---|---|---|---|---|---|---|
| Model | Model parameters | Single component | | Model | Model parameters | Single component | |
| | | ACM | CIP | | | ACM | CIP |
| PFO | $q_{e,cal}$ (mg/g) | 39.90 | 39.60 | Langmuir | $K_L$ (L/mg) | 0.49 | 0.306 |
| | $q_{e,exp}$ (mg/g) | 3.685 | 5.029 | | $q_m$ (mg/g) | 188.67 | 78.43 |
| | $k_1$(1/min) | 0.074 | 0.05 | | $R^2$ | 0.98 | 0.994 |
| | $R^2$ | 0.916 | 0.81 | | | | |
| | RMSE | | 2.02 | | | | |
| | SSE | | 32.79 | Freundlich | $K_F$ (mg/g)(L/mg)$^{1/n}$ | 52.70 | 5.28 |
| PSO | $q_{e,exp}$ (mg/g) | 40.02 | 40.38 | | n | 7.98 | 46.22 |
| | $q_{e,cal}$ (mg/g) | 39.90 | 39.60 | | $R^2$ | 0.96 | 0.972 |
| | $k_2$ (g/mg.min) | 0.999 | 0.011 | | | | |
| | $R^2$ | 0.198 | 0.994 | | | | |
| | RMSE | | 0.67 | Temkin | β | | 0.97 |
| | SSE | | 3.57 | | $K_T$ (L mg$^{-1}$) | | 2765.56 |
| Intra-particle model | $K_{id}$ (mg/g. min$^{1/2}$) | 0.30 | 3.27 | | $R^2$ | | 0.93 |
| | $K_o$ | 37.34 | 11.89 | Redlich-Peterson | B (L/mg) | 0.71 | |
| | $R^2$ | 0.88 | 0.64 | | A (L/g) | 71.37 | |

Table B.2. Continued.

| Kinetics analysis | | | | Isotherm analysis | | | |
|---|---|---|---|---|---|---|---|
| Intra-particle model | RMSE | | | | $R^2$ | 0.99 | |
| | SSE | | | | | | |
| Elovich | α (mg/g.min) | 3.65 | 0.12 | Dubinin-Radushkevich (D-R) | $q_m$ | 133.96 | 68.56 |
| | β (g/mg) | 38.15 | 15.90 | | $K_D$ | $1.34 \times 10^{-8}$ | $2.784 \times 10^{-8}$ |
| | $R^2$ | 0.908 | 0.859 | | $R^2$ | 0.77 | 0.859 |

Table B.3. Calibration curve equations and $R^2$ values for the quantification of pharmaceuticals using UV-Vis spectrophotometer in single and simultaneous adsorption systems.

| Adsorption system | Pharmaceutical | Equation | $R^2$ |
|---|---|---|---|
| Single | CIP | Y = 0.0912X+0.02133 | 0.998 |
| Single | ACM | Y = 0.067X + 0.00051 | 0.997 |
| Binary (simultaneous) | ACM | Y = 0.053X+0.04514 | 0.982 |
| | CIP | Y = 0.099X+0.0001 | 0.986 |

## Appendix C: Electrochemical oxidation (EO) (single process)

Table C.1. The CCD experimental design of the EO process in ACM/CIP degradation.

| Run | EO Time(min) | pH | Current density ($mA/cm^2$) | Initial concentration (mg/l) | ACM removal (%) | CIP removal (%) |
|---|---|---|---|---|---|---|
| 1 | 60 | 6.5 | 42.855 | 10 | 93.55 | 92.54 |
| 2 | 60 | 6.5 | 42.855 | 30 | 90.52 | 88.14 |
| 3 | 80 | 4 | 23.21 | 15 | 88.95 | 86.85 |
| 4 | 60 | 6.5 | 42.855 | 20 | 93.06 | 90.25 |
| 5 | 60 | 6.5 | 42.855 | 20 | 93.66 | 90.56 |
| 6 | 20 | 6.5 | 42.855 | 20 | 81.28 | 80 |
| 7 | 100 | 6.5 | 42.855 | 20 | 92.85 | 91.52 |
| 8 | 40 | 9 | 23.21 | 15 | 80.24 | 78.68 |
| 9 | 80 | 4 | 23.21 | 25 | 86.94 | 84.28 |
| 10 | 80 | 9 | 62.5 | 15 | 91.25 | 89.82 |
| 11 | 40 | 4 | 23.21 | 25 | 80.51 | 77.52 |
| 12 | 40 | 4 | 62.5 | 15 | 89.85 | 87.88 |
| 13 | 60 | 6.5 | 42.855 | 20 | 93.15 | 89.99 |
| 14 | 60 | 6.5 | 42.855 | 20 | 92.85 | 89.95 |
| 15 | 60 | 11.5 | 42.855 | 20 | 78.3 | 73.97 |
| 16 | 60 | 1.5 | 42.855 | 20 | 85.15 | 81.27 |
| 17 | 40 | 4 | 23.21 | 15 | 84.56 | 82.54 |
| 18 | 60 | 6.5 | 42.855 | 20 | 92.97 | 90.98 |
| 19 | 80 | 9 | 23.21 | 25 | 83.65 | 81.08 |
| 20 | 60 | 6.5 | 3.565 | 20 | 78.29 | 76.15 |
| 21 | 80 | 4 | 62.5 | 15 | 95.5 | 94.16 |
| 22 | 80 | 9 | 62.5 | 25 | 91.42 | 88.23 |
| 23 | 60 | 6.5 | 42.855 | 20 | 93.88 | 90.12 |
| 24 | 40 | 9 | 62.5 | 25 | 86.56 | 82.93 |
| 25 | 80 | 9 | 23.21 | 15 | 83.54 | 80.34 |
| 26 | 80 | 4 | 62.5 | 25 | 92.44 | 90.38 |
| 27 | 40 | 4 | 62.5 | 25 | 84.86 | 82.66 |
| 28 | 40 | 9 | 62.5 | 15 | 89.42 | 87.43 |
| 29 | 40 | 9 | 23.21 | 25 | 77.89 | 75.68 |
| 30 | 60 | 6.5 | 82.145 | 20 | 94.03 | 92.08 |

Table C. 2. Experimental results of BBD for the coupled process.

| | Factor 1 | Factor 2 | Factor 3 | Factor 4 | Factor 5 | Response 1 | Response 2 |
|---|---|---|---|---|---|---|---|
| Run | A: EO Time (min) | B: pH | C: Current ($mA/cm^2$) | D: Adsorbent dose (g/L) | E: Adsorption time (min) | ACM removal (%) | CIP removal (%) |
| 1 | 60 | 6 | 20 | 0.12 | 50 | 96.66 | 95.27 |
| 2 | 10 | 6 | 20 | 0.08 | 50 | 83.88 | 82.76 |
| 3 | 10 | 3 | 20 | 0.10 | 50 | 90.45 | 88.82 |
| 4 | 35 | 6 | 20 | 0.08 | 20 | 85.57 | 84.71 |
| 5 | 35 | 6 | 20 | 0.10 | 50 | 98.52 | 98.04 |
| 6 | 60 | 6 | 20 | 0.10 | 80 | 99.85 | 98.85 |
| 7 | 35 | 6 | 20 | 0.10 | 50 | 99.95 | 99.67 |
| 8 | 10 | 6 | 20 | 0.10 | 20 | 91.18 | 90.46 |
| 9 | 60 | 6 | 25 | 0.10 | 50 | 100 | 100 |
| 10 | 35 | 9 | 20 | 0.08 | 50 | 82.26 | 80.83 |
| 11 | 35 | 9 | 20 | 0.10 | 80 | 93.08 | 92.17 |
| 12 | 35 | 3 | 20 | 0.10 | 20 | 89.96 | 90.76 |
| 13 | 35 | 9 | 20 | 0.12 | 50 | 98.85 | 97.29 |
| 14 | 10 | 6 | 20 | 0.12 | 50 | 91.81 | 88.85 |
| 15 | 35 | 6 | 25 | 0.12 | 50 | 100 | 100 |
| 16 | 35 | 6 | 15 | 0.10 | 20 | 73.65 | 72.84 |
| 17 | 10 | 6 | 15 | 0.10 | 50 | 72.54 | 70.66 |
| 18 | 35 | 6 | 15 | 0.08 | 50 | 70.96 | 67.24 |
| 19 | 35 | 3 | 20 | 0.12 | 50 | 95.91 | 93.16 |
| 20 | 60 | 6 | 15 | 0.10 | 50 | 75.24 | 73.36 |
| 21 | 35 | 6 | 15 | 0.10 | 80 | 74.41 | 73.75 |
| 22 | 35 | 6 | 20 | 0.08 | 80 | 86.88 | 84.91 |
| 23 | 35 | 6 | 25 | 0.10 | 80 | 97.05 | 97.21 |
| 24 | 35 | 6 | 25 | 0.10 | 20 | 93.21 | 91.05 |
| 25 | 35 | 6 | 20 | 0.12 | 20 | 94.13 | 92.44 |
| 26 | 60 | 6 | 20 | 0.08 | 50 | 91.31 | 89.23 |
| 27 | 35 | 6 | 20 | 0.10 | 50 | 98.21 | 98.09 |
| 28 | 60 | 3 | 20 | 0.10 | 50 | 92.96 | 92.28 |
| 29 | 35 | 9 | 25 | 0.10 | 50 | 94.68 | 93.36 |
| 30 | 60 | 6 | 20 | 0.10 | 20 | 91.01 | 89.56 |
| 31 | 35 | 9 | 20 | 0.10 | 20 | 87.27 | 84.36 |
| 32 | 35 | 6 | 15 | 0.12 | 50 | 76.01 | 74.43 |
| 33 | 35 | 6 | 20 | 0.10 | 50 | 99.91 | 99.97 |
| 34 | 10 | 6 | 25 | 0.10 | 50 | 90.06 | 87.86 |
| 35 | 35 | 6 | 20 | 0.10 | 50 | 98.86 | 99.23 |
| 36 | 35 | 3 | 20 | 0.08 | 50 | 90.16 | 88.49 |
| 37 | 60 | 9 | 20 | 0.10 | 50 | 91.88 | 89.73 |
| 38 | 35 | 3 | 15 | 0.10 | 50 | 74.56 | 73.85 |
| 39 | 10 | 9 | 20 | 0.10 | 50 | 85.92 | 84.57 |
| 40 | 35 | 3 | 20 | 0.10 | 80 | 95.54 | 93.52 |

Table C.2. Continued.

| | | | | | | | |
|---|---|---|---|---|---|---|---|
| 41 | 35 | 6 | 20 | 0.10 | 50 | 99.96 | 99.85 |
| 42 | 35 | 3 | 25 | 0.10 | 50 | 98.92 | 97.96 |
| 43 | 35 | 6 | 25 | 0.08 | 50 | 92.43 | 90.72 |
| 44 | 35 | 6 | 20 | 0.12 | 80 | 100 | 100 |
| 45 | 35 | 9 | 15 | 0.10 | 50 | 72.44 | 71.55 |
| 46 | 10 | 6 | 20 | 0.10 | 80 | 86.69 | 85.58 |

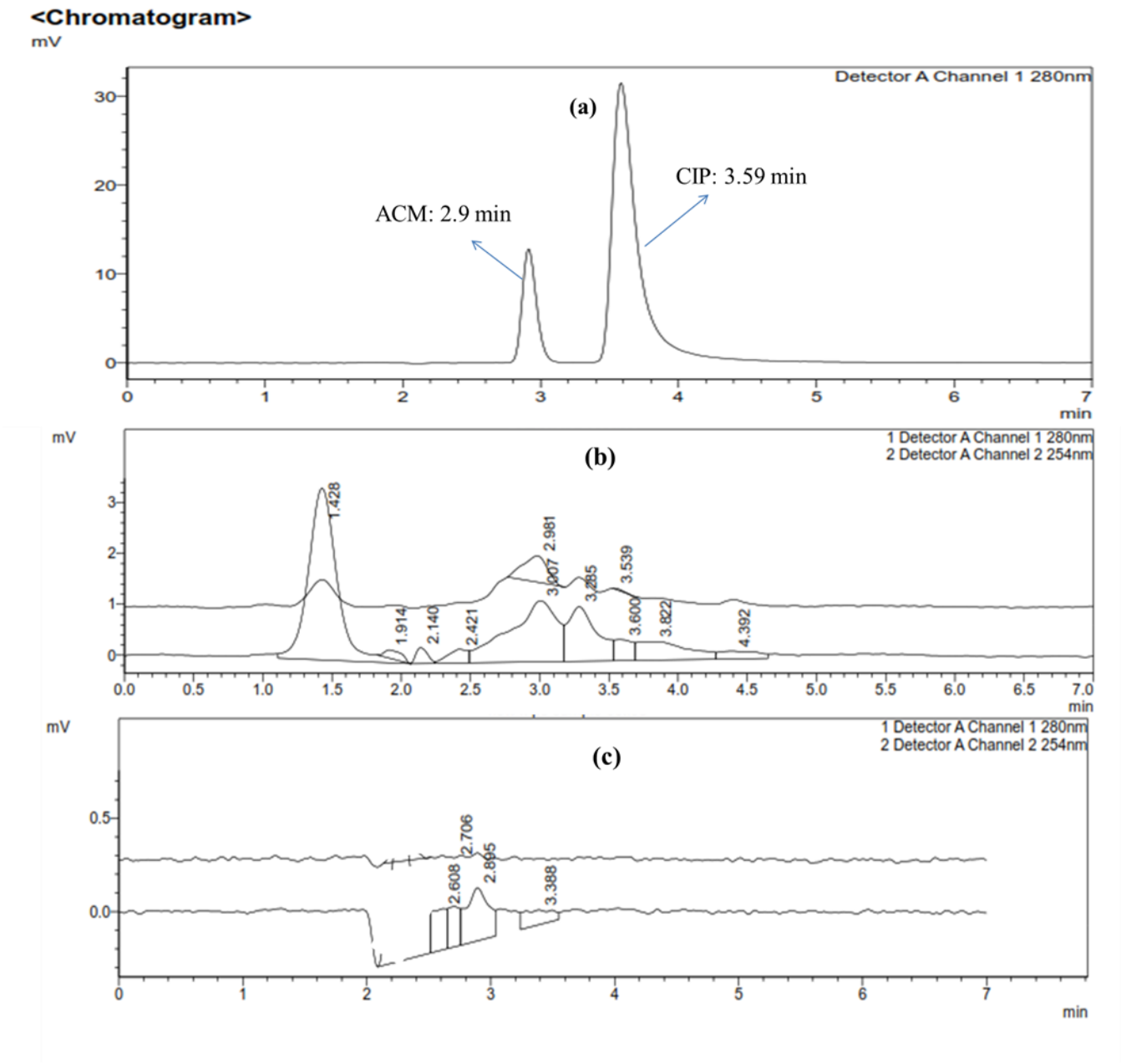


Figure C.1. Chromatograms of ACM and CIP for binary contaminant system (a) before EO and (b) after EO (EO time = 80 min, pH = 5, current density = 44 mA/cm$^2$) and (c) after EO+adsorption (EO time = 40 min, current density = 22 mA/cm$^2$, adsorbent dose = 0.1 g/L and adsorption time = 60 min*).*

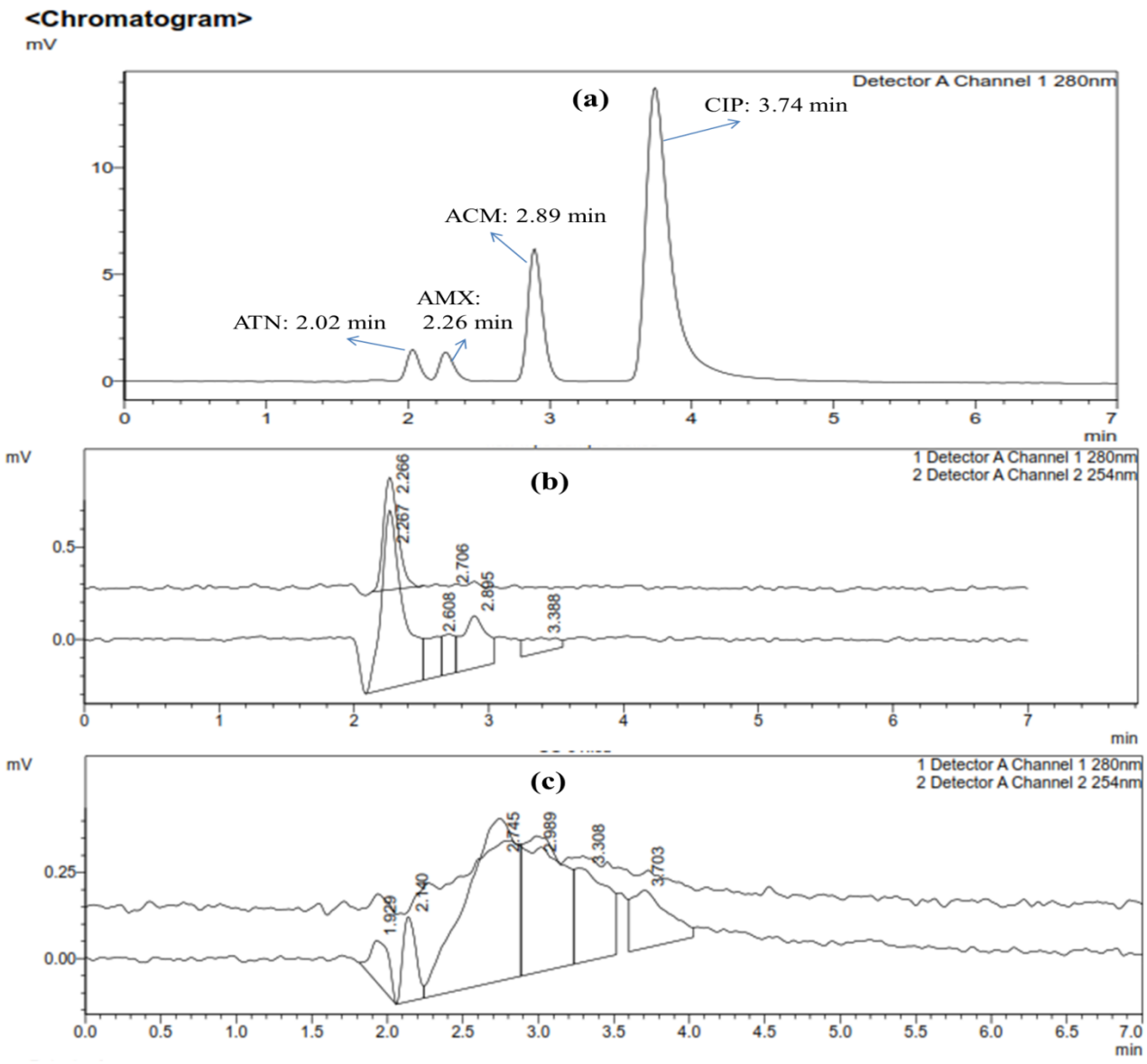


Figure C.2. Chromatograms of ACM, CIP, AMX and ATN (a) before EO and (b) after EO (EO time = 80 min, pH = 5, current density = 44 mA/cm$^2$) and (c) after EO+adsorption (EO time = 40 min, current density = 22 mA/cm$^2$, adsorbent dose = 0.1 g/L and adsorption time = 60 min).

Table C.3. The HPLC method employed for the quantification of the pharmaceuticals for the performance evaluation of adsorption, EO and EO+adsorption processes.

| Pharmaceutical | $R^2$ | Recovery | LOD (µg/L) | LOQ (µg/L) | Detected in real wastewater (Mikkeli, Finland) (µg/L) |
|---|---|---|---|---|---|
| ACM | 0.999 | 100.02 | 0.13 | 0.38 | 0.68 |
| CIP | 0.997 | 100.01 | 0.24 | 0.47 | <LOQ |
| AMX | 0.998 | 99.86 | 0.25 | 0.45 | 0.55 |
| ATN | 0.996 | 99.92 | 0.11 | 0.32 | <LOQ |

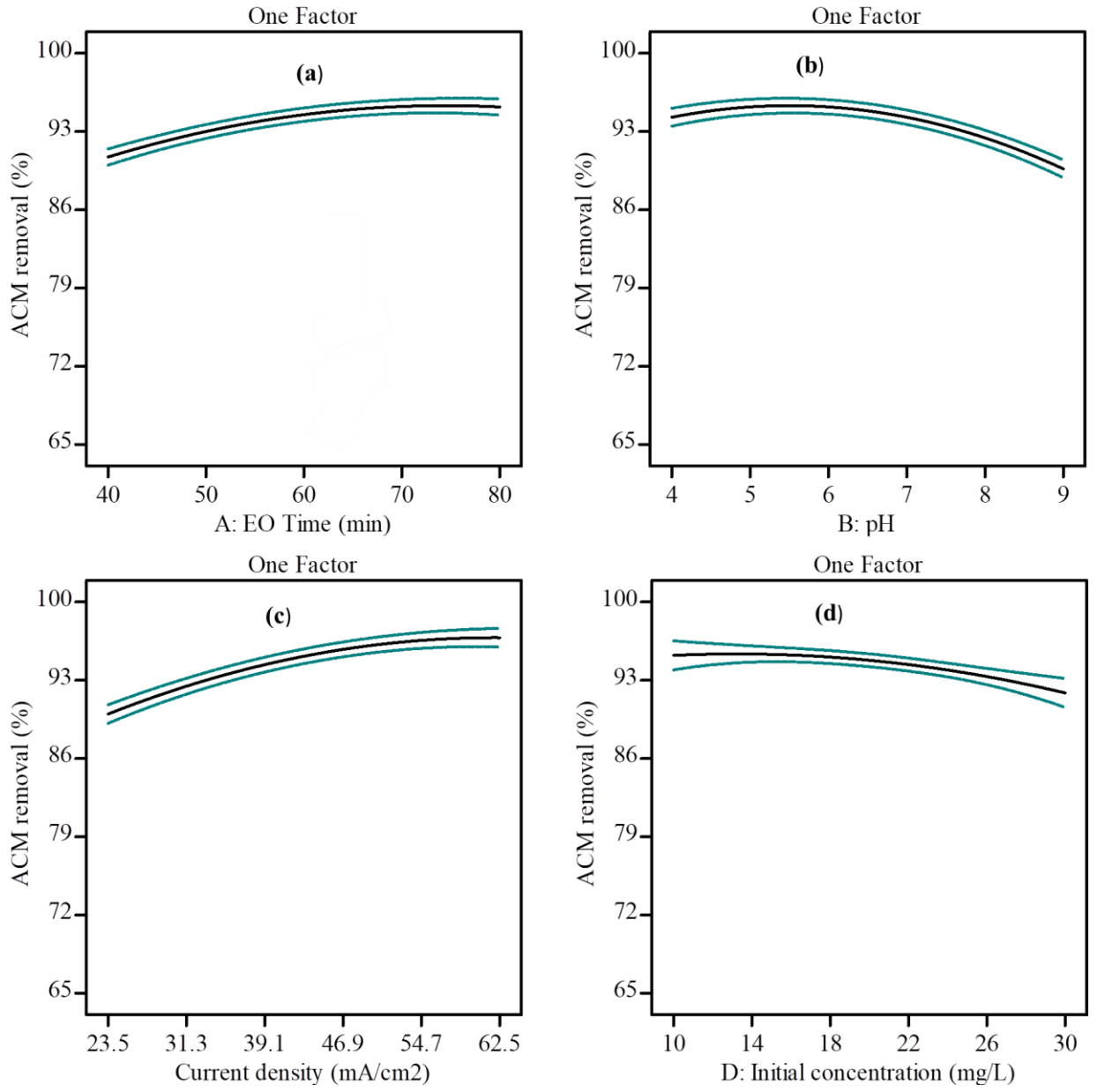


Figure C.3. The influence of main EO process factors on ACM degradation (a) EO time (min), (b) pH, (c) Current density (mA/cm$^2$), (d) Initial pollutant concentration (mg/L).

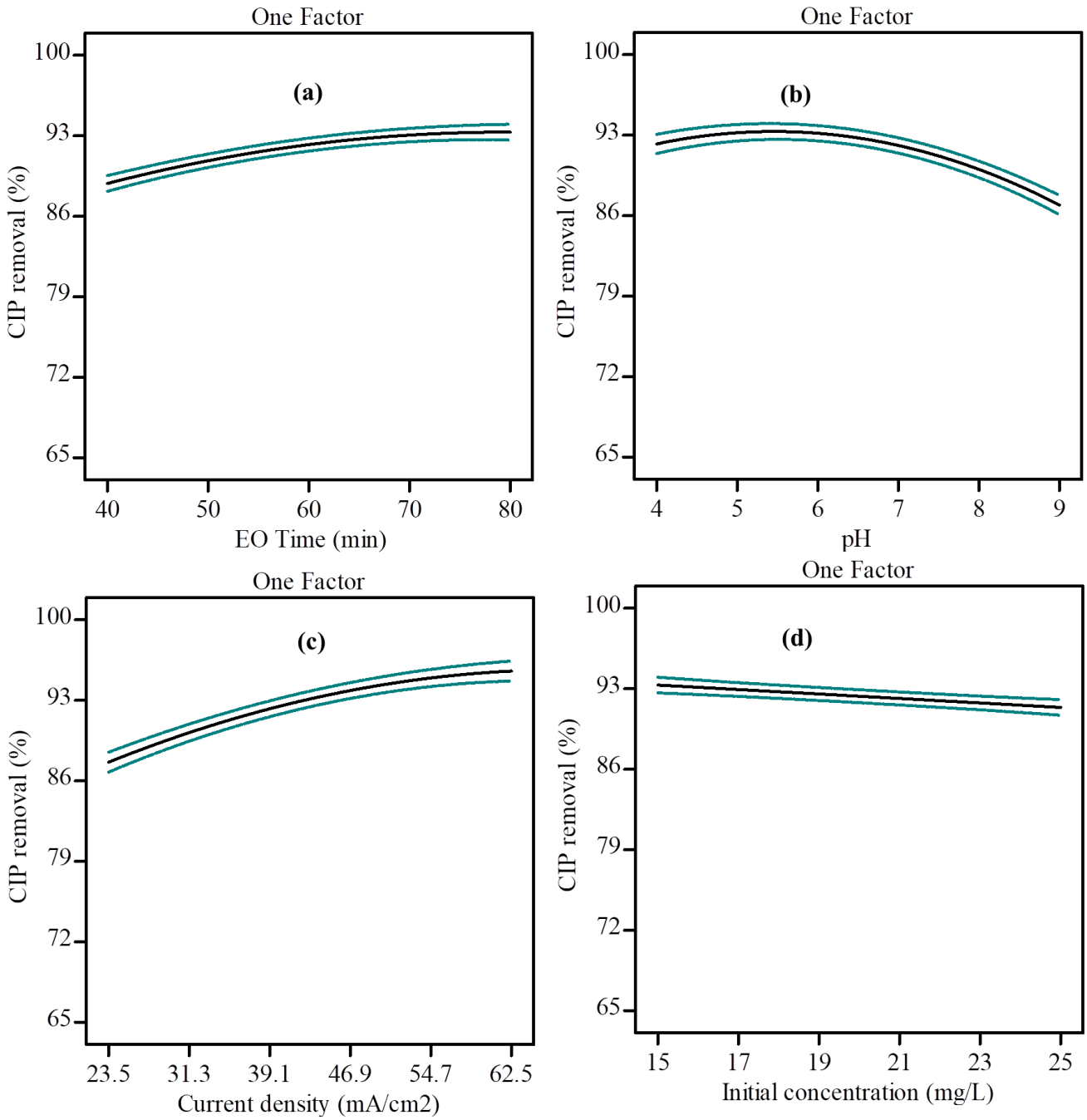


Figure C.4. The influence of main EO process factors on CIP degradation (a) EO time (min), (b) pH, (c) Current density (mA/cm$^2$), (d) Initial pollutant concentration (mg/L).

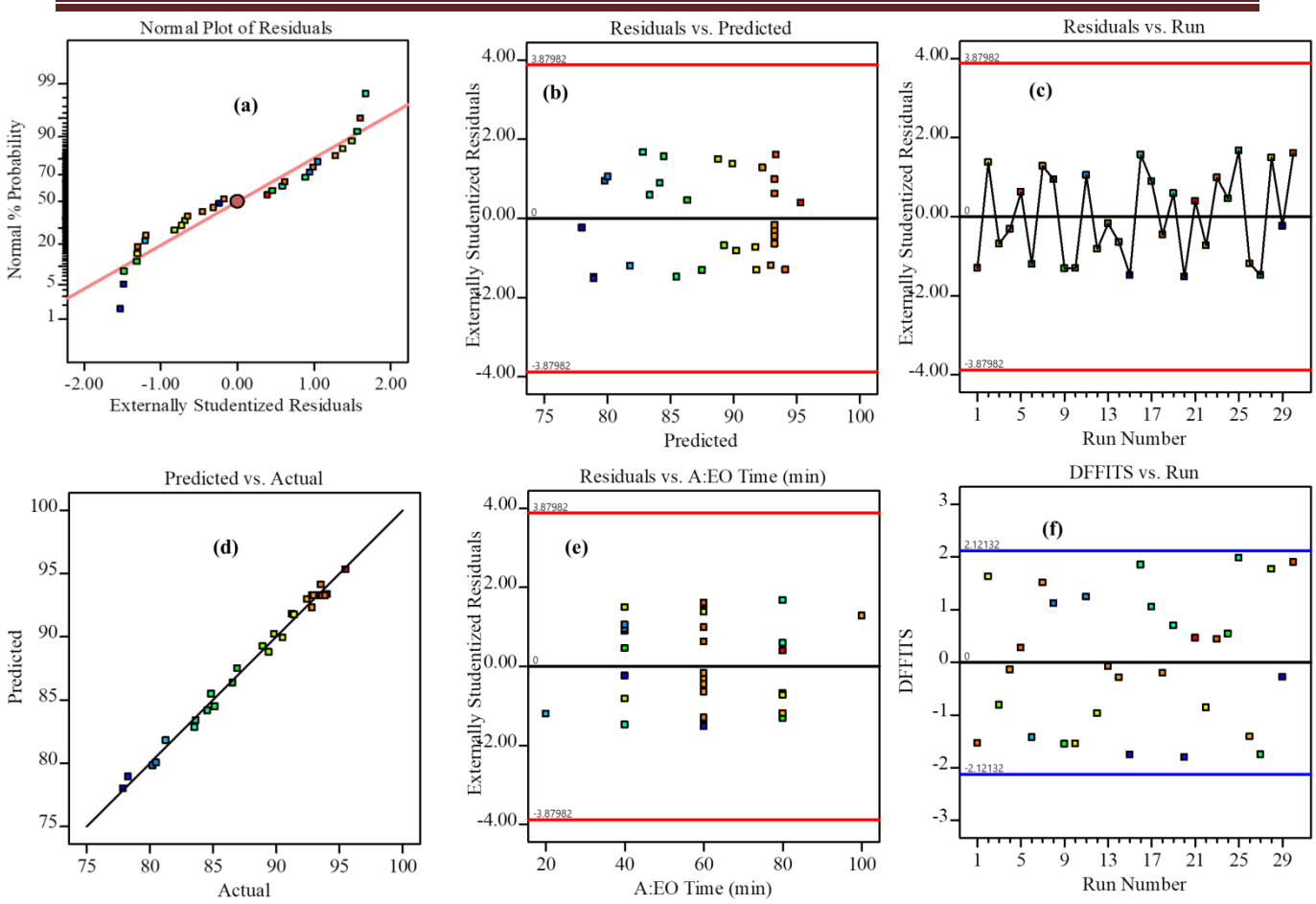


Figure C.5. Diagnostic plots for the ACM degradation quadratic model: a) Normal probability versus externally studentized residuals; (b) Residual vs. Predicted (c) residual vs. Run (d) Predicted vs. Actual (e) Residual vs. EO time (min) (f) DFFITS vs. Run.

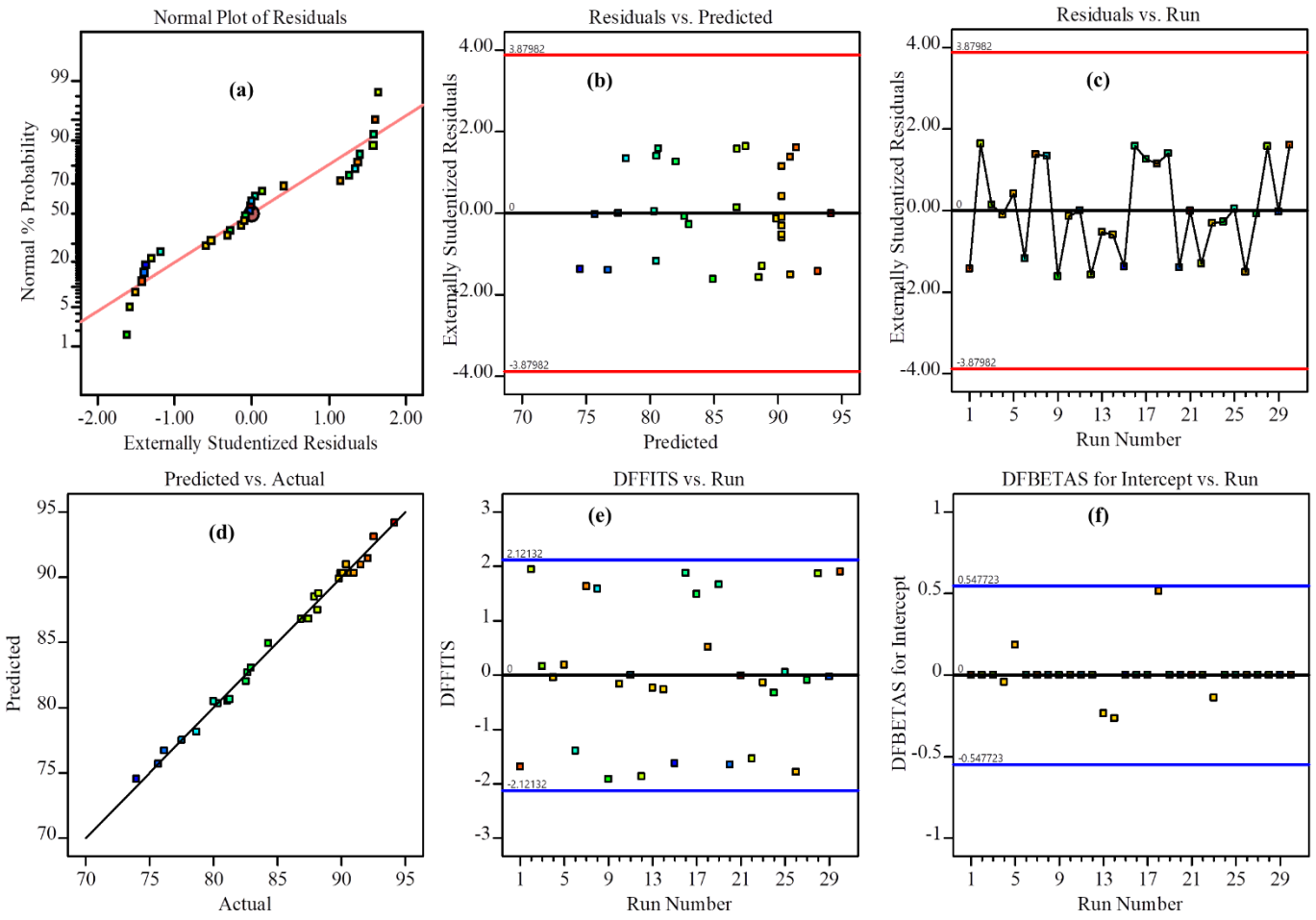


Figure C.6. Diagnostic plots for the CIP degradation quadratic model: a) Normal probability versus externally studentized residuals; (b) Residual vs. Predicted (c) residual vs. Run (d) Predicted vs. Actual (e) Residual vs. EO time (min) (f) DFFITS vs. Run.

# Appendix D: Coupled process (EO+adsorption)

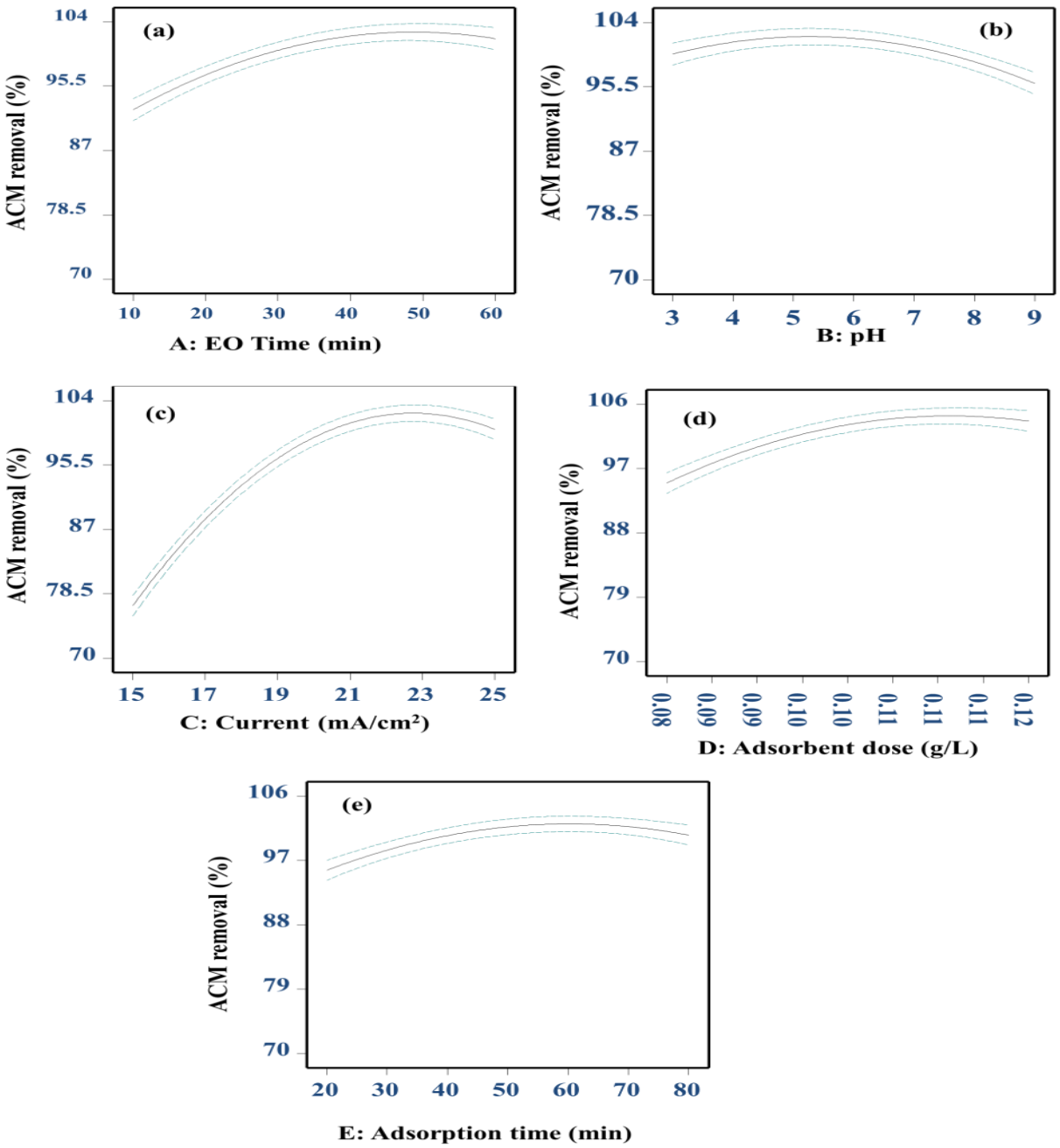


Figure D.1. One factor effect analysis for ACM removal using the coupled process.

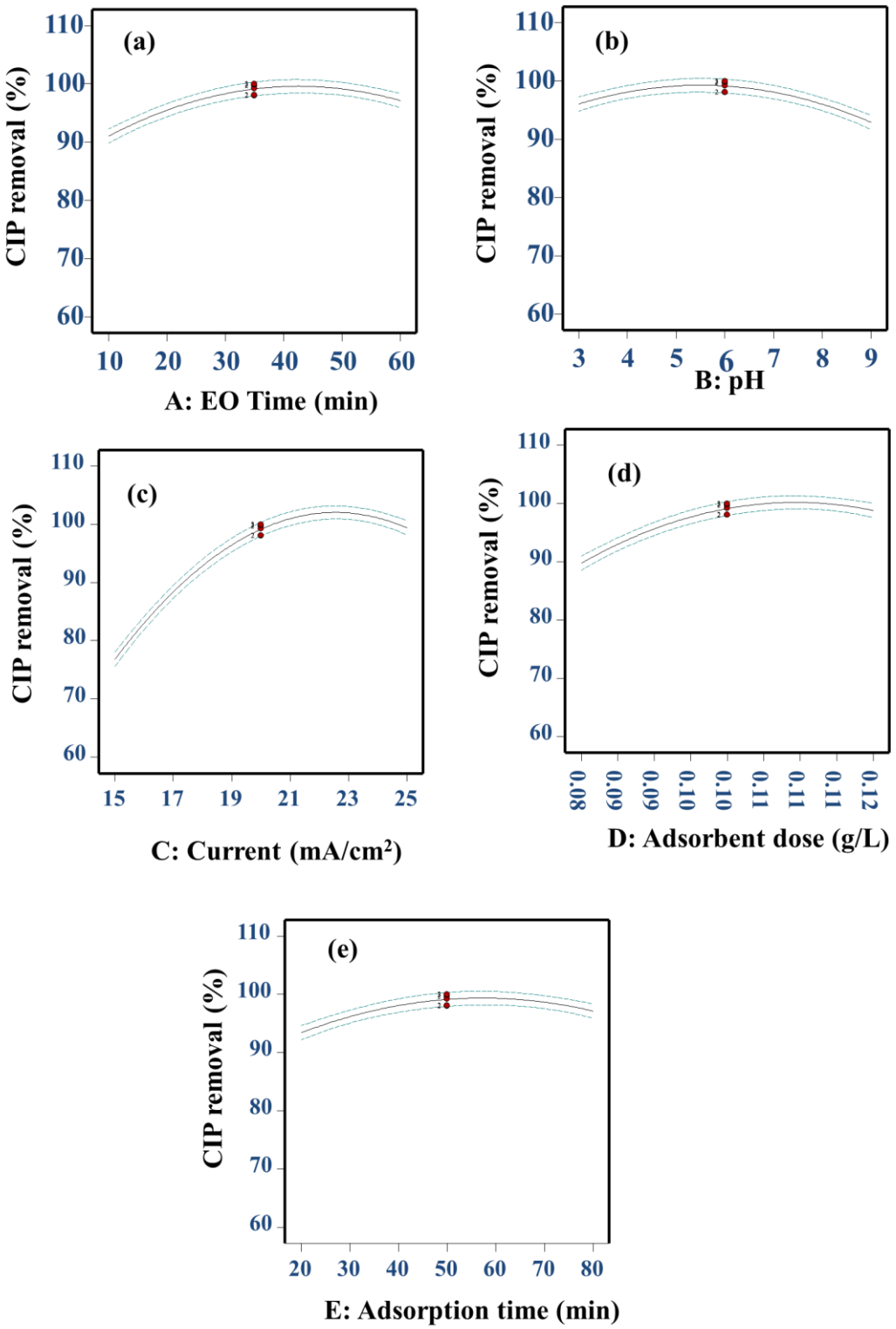


Figure D.2. One factor effect analysis for CIP removal using the coupled process.

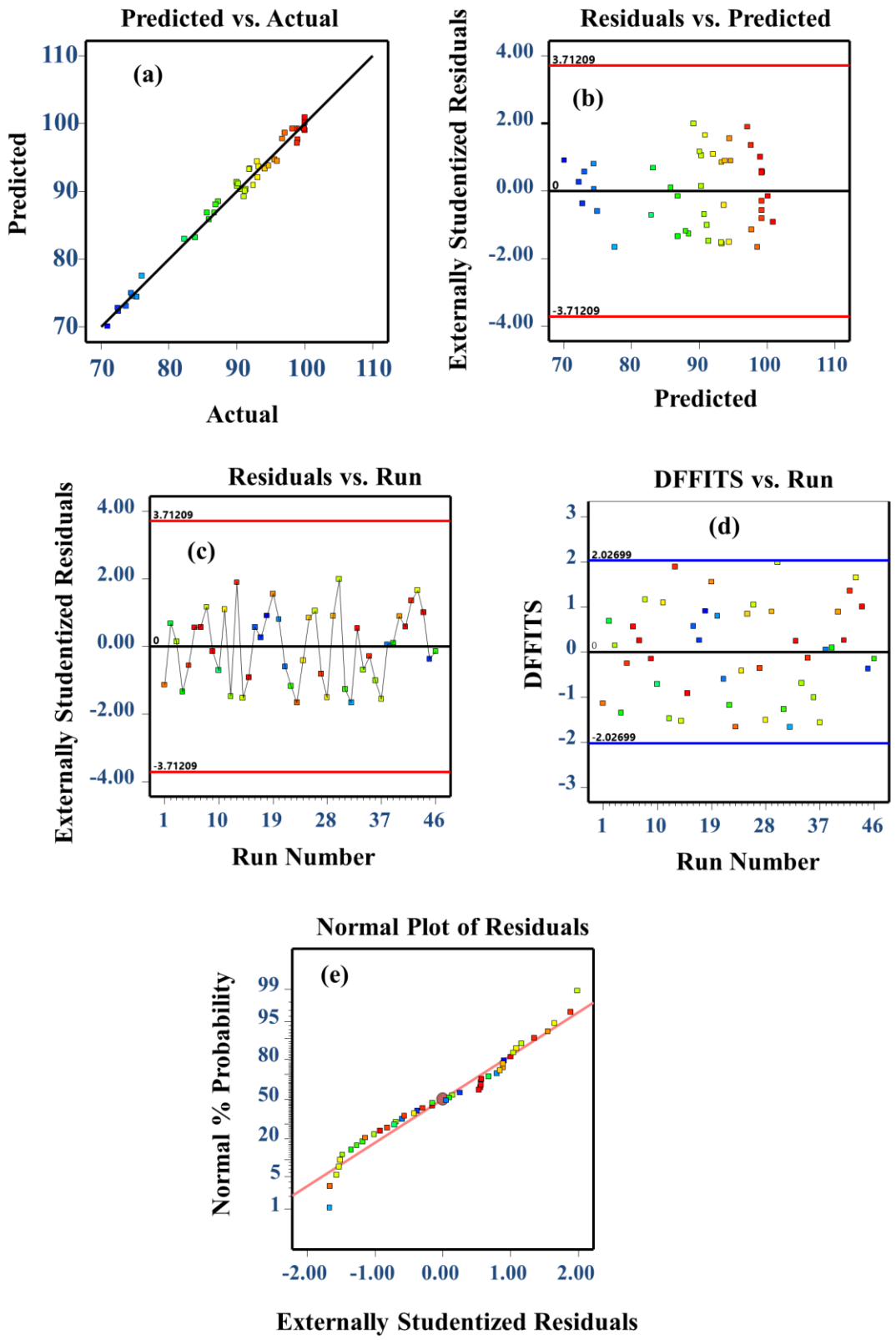


Figure D.3. Diagnostic analysis for ACM removal using the coupled process.

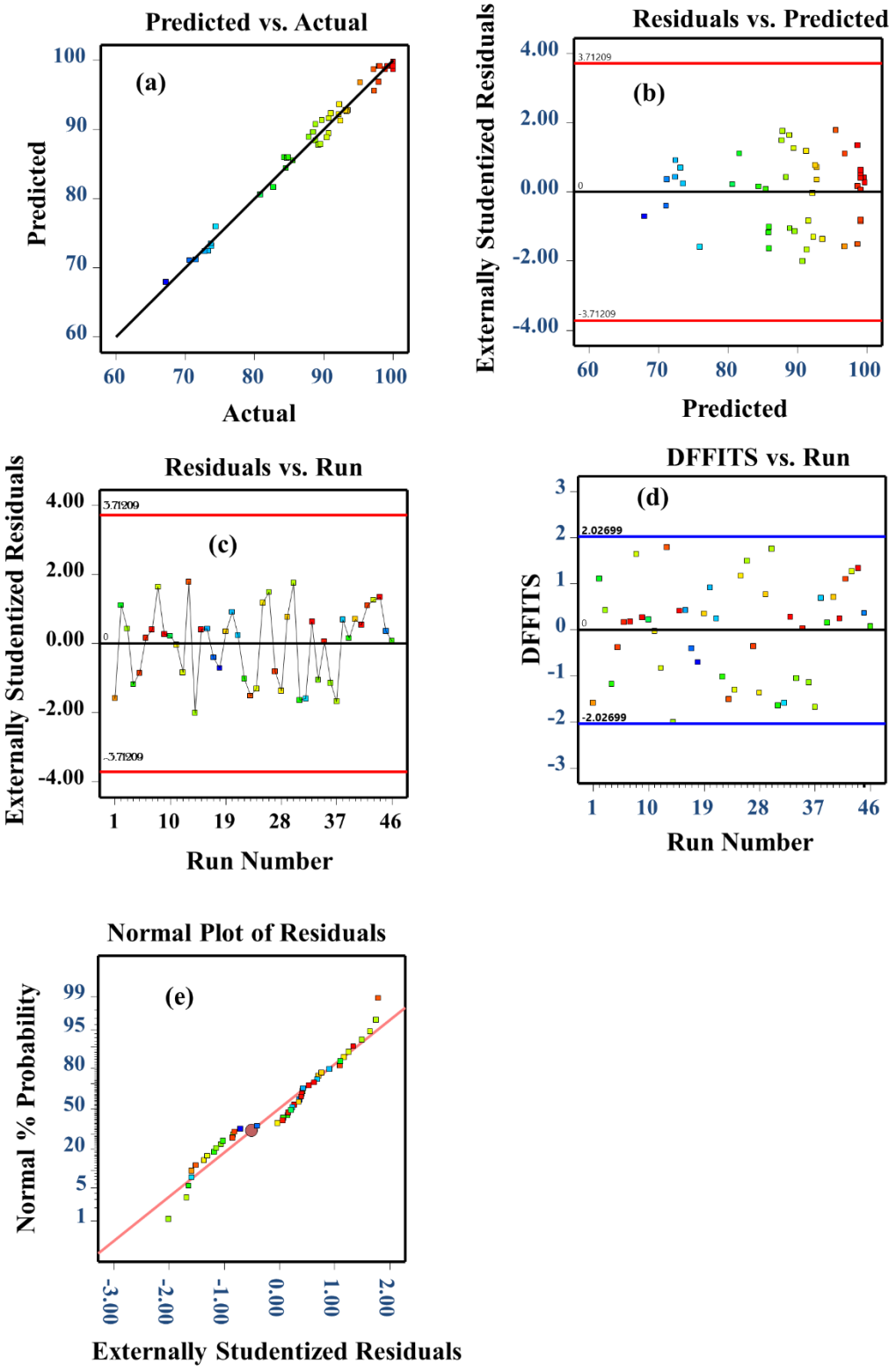


Figure D.4. Diagnostic analysis for CIP removal using the coupled process.

# Appendix E: Publications

Colloids and Surfaces A: Physicochemical and Engineering Aspects 681 (2024) 132718

Contents lists available at ScienceDirect

Colloids and Surfaces A: Physicochemical and Engineering Aspects

journal homepage: www.elsevier.com/locate/colsurfa

## Tuneable functionalized biochar for simultaneous removal of pharmaceuticals from binary mixture

Wondimu K. Wakejo [a,b,c,*], Ali Maged [a,j], Beteley T. Meshesha [b,d], Joon W. Kang [e], Abayneh G. Demesa [f], Sandip Chakrabarti [g], Thallada Bhaskar [h], Ashok Kumar Gupta [i], Amit Bhatnagar [a]

[a] Department of Separation Science, LUT School of Engineering Science, LUT University, Sammonkatu 12, FI-50130 Mikkeli, Finland
[b] Africa Center of Excellence for Water Management, Addis Ababa University, P.O. Box.1176, Addis Ababa, Ethiopia
[c] Department of Chemical Engineering, Wachemo University, P.O. Box 667, Hosaena, Ethiopia
[d] School of Chemical and Bioengineering, Addis Ababa Institute of Technology, Addis Ababa, Ethiopia
[e] Division of the Department of Environment and Energy, Yonsei University, South Korea
[f] Department of Separation Science, LUT School of Engineering Science, LUT University, FI-53850 Lappeenranta, Finland
[g] Amity Institute of Nanotechnology, Amity University Uttar Pradesh, Noida 201313, India
[h] Thermo Catalytic Process Area (TPA), Material Resource Efficiency Division (MRED) CSIR-Indian Institute of Petroleum (IIP), Dehradun 248005, Uttarakhand, India
[i] Environmental Engineering Division, Department of Civil Engineering, Indian Institute of Technology Kharagpur, Kharagpur 721302, India
[j] Institute of Process Engineering, Johannes Kepler University Linz, Altenberger Straße 69, 4040 Linz, Austria

### HIGHLIGHTS

- Highly functionalized biochar (FBC) was prepared via dual chemical modification.
- Rigorous batch and fixed-bed studies were provided for single and binary sorption.
- Simultaneous sorption of ACM and CIP has antagonistic nature.
- FBC exhibited uptake of 125.31 mg/g (ACM) and 65.44 mg/g (CIP) in binary sorption.
- The synthesized biochar adsorbent was found to be effective on real water matrix.

### GRAPHICAL ABSTRACT

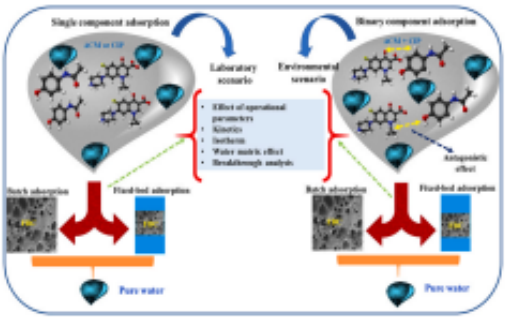

Hindawi
Adsorption Science & Technology
Volume 2022, Article ID 2699530, 23 pages
https://doi.org/10.1155/2022/2699530

*Research Article*

# Enhanced Ciprofloxacin Removal from Aqueous Solution Using a Chemically Modified Biochar Derived from Bamboo Sawdust: Adsorption Process Optimization with Response Surface Methodology

**Wondimu K. Wakejo**,[1,2] **Beteley T. Meshasha**,[1,3] **Joon W. Kang**,[3] **and Yonas Chebude**[1,4]

[1]*Africa Center of Excellence for Water Management, Addis Ababa University, Addis Ababa, Ethiopia P.O. Box 1176*
[2]*Department of Chemical Engineering, Wachemo University, Hossana, Ethiopia P.O. Box 667*
[3]*School of Chemical and Bio Engineering, Addis Ababa Institute of Technology, Addis Ababa, Ethiopia*
[4]*Department of Chemistry, College of Natural and Computational Science, Addis Ababa University, Addis Ababa, Ethiopia*

Correspondence should be addressed to Wondimu K. Wakejo; wondimu.kebede@aau.edu.et

Received 25 April 2022; Revised 29 June 2022; Accepted 8 July 2022; Published 31 July 2022

Academic Editor: Ming Hua



Contamination of water by ciprofloxacin has become a significant concern due to its adverse health effects and growing evidence of antimicrobial-resistant gene evolution. To this end, a chemically modified bamboo biochar was prepared from bamboo sawdust to effectively remove ciprofloxacin (CIP) from an aqueous solution. Under similar adsorption conditions, the modified bamboo biochar (MBC) has an excellent CIP removal efficiency (96%) compared to unmodified bamboo biochar (UBC) efficiency (45%). Thus, MBC was used in batch adsorption experiments, and the process was optimized with the central composite design (CCD) framework of response surface methodology (RSM). Sorption process parameters such as initial CIP concentration, pH, adsorbent dose, and contact time were studied and found to have a significant effect on CIP removal. The optimal CIP removal (96%) was obtained at MBC dose (0.5 g $L^{-1}$), CIP initial concentration (20 mg $L^{-1}$), pH (7.5), and contact time (46 min). The adsorption kinetic data were well described by the pseudo-second-order model ($R^2 = 0.999$), and both Langmuir ($R^2 = 0.994$) and Freundlich ($R^2 = 0.972$) models gave the best fit in CIP adsorption isotherm analysis. The maximum monolayer adsorption capacity of the MBC was 78.43 mg $g^{-1}$ based on the Langmuir isotherm model. These results suggest that CIP adsorption was mainly controlled by chemisorption. Moreover, the CIP adsorption process was endothermic and spontaneous. Overall, MBC is a low-cost, efficient, and recyclable adsorbent for eliminating emerging contaminants such as ciprofloxacin from an aqueous solution.

Water Practice & Technology

© 2023 The Authors

Water Practice & Technology Vol 18 No 6, 1366 doi: 10.2166/wpt.2023.094

# Bamboo sawdust-derived high surface area activated carbon for remarkable removal of paracetamol from aqueous solution: sorption kinetics, isotherm, thermodynamics, and regeneration studies

Wondimu Kebede Wakejo[a,b,*], Beteley Tekola Meshesha[a,c], Joon Wun Kang[d] and Abayneh Getachew Demesa[e]

[a] Africa Center of Excellence for Water Management, Addis Ababa University, Addis Ababa, P.O. Box 1176, Ethiopia
[b] Department of Chemical Engineering, Wachemo University, Hossana, P.O. Box 667, Ethiopia
[c] School of Chemical and Bioengineering, Addis Ababa Institute of Technology, Addis Ababa, Ethiopia
[d] Division of the Department of Environment and Energy, Yonsei University, Seoul, South Korea
[e] School of Engineering Science, Department of Separation Science, LUT University, Lappeenranta, Finland
*Corresponding author. E-mail: wondimu.kebede@aau.edu.et

## ABSTRACT

Due to its widespread consumption, paracetamol (PCT) has emerged as one of the leading contaminants that pollute water. Herein, a PCT removal of 99.6% was achieved using chemically activated carbon (CAC), derived from bamboo sawdust using KOH/$FeCl_3$ as an activating agent, at optimal conditions of PCT (20 mg/L), CAC (0.5 g/L), contact time (90 min), and pH (8). Kinetic study revealed that the PCT adsorption process followed the pseudo-second-order kinetic model ($R^2 = 0.99$), indicating that chemical adsorption dominated the adsorption mechanism. On the other hand, isotherm experimental data were best described by the Langmuir ($R^2 = 0.98$) and Freundlich ($R^2 = 0.96$) models. CAC had a maximum Langmuir monolayer capacity of 188.67 mg/g at a PCT concentration of 120 mg/L. Moreover, the Redlich–Peterson model gave the best fit ($R^2 = 0.99$) to the experimental data, confirming that PCT adsorption was monolayer adsorption onto the heterogeneous surface. Thermodynamically, the PCT adsorption was exothermic, spontaneous, and favorable. The reusability study depicted that CAC can be successfully reused for five consecutive adsorption–desorption cycles. Furthermore, the application of CAC to environmental samples showed interesting results. The overall adsorption study indicated that CAC could serve as a promising adsorbent for eliminating PCT from water.

GRAPHICAL ABSTRACT

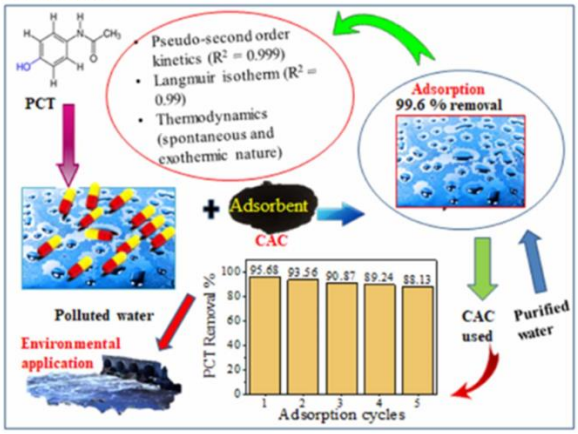

Water Supply



IWA PUBLISHING



Water Supply Vol 22 No 11, 8157 doi: 10.2166/ws.2022.377

# Anthropogenic nitrate contamination of water resources in Ethiopia: an overview

Wondimu Kebede Wakejo[a,b,*], Beteley Tekola Meshesha[a,c], Nigus Gabbiye Habtu[d] and Yilkal Gebeyehu Mekonnen[a,e]

[a] Africa Center of Excellence for Water Management, Addis Ababa University, P. O. Box 1176, Addis Ababa, Ethiopia
[b] Chemical Engineering Department, Wachemo University, P. O. Box 667, Hossana, Ethiopia
[c] Addis Ababa institute of Technology, Addis Ababa, Ethiopia
[d] Bahir Dar institute of Technology, Bahir Dar, Ethiopia
[e] Department of Natural Resource Management, Debre Markos University, Debre Markos, Ethiopia
*Corresponding author. E-mail: wondimkebed@yahoo.com

WKW, 0000-0002-4408-394X

## ABSTRACT

Nitrate is one of the water contaminants that mainly results from anthropogenic activities. The major causes of nitrate contamination of water resources are anthropogenic activities such as animal or human waste, septic or sewage systems, fertilizer application, concentrated animal farming, industrial waste, and landfill leachates. These man-made activities are the primary sources of nitrate contamination in water resources. Nitrate contamination of water is a global issue that has been increasing over time. According to previous research, exposure to nitrate in water above the World Health Organization (WHO) guideline limit (50 mg of $NO_3$/L) has been found to induce major health effects such as methemoglobinemia in humans, with the severity depending on the amount consumed. This problem has become a major threat to humans and the environment. Thus, this article presented an overview of nitrate contamination of water resources in Ethiopia, emphasizing anthropogenic activities to indicate the current nitrate water contamination status for the necessary remedial actions.

GRAPHICAL ABSTRACT

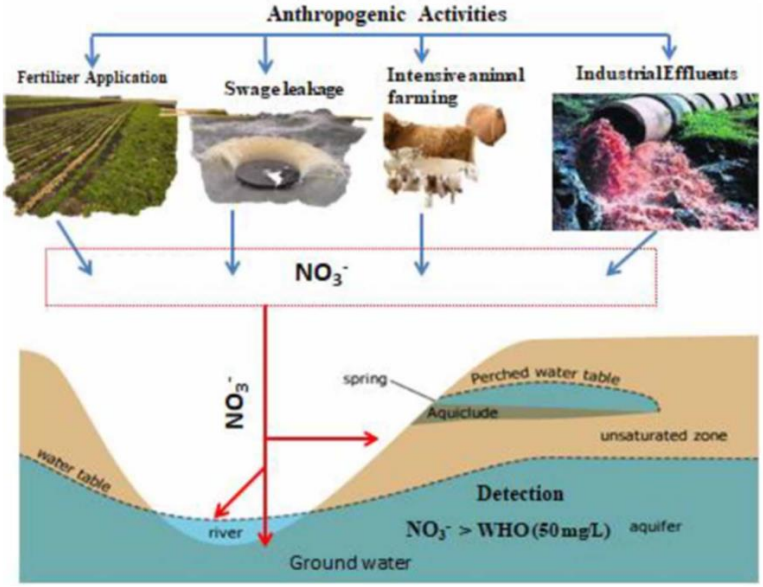

# Appendix F: Conference presentations

The UNIVERSITY of OKLAHOMA
College of Professional and Continuing Studies

certifies that

Wondimu Kebede Wakejo

has participated in

The Water Conference

Africa Center of Excellence for Water Management

9/26/22 - 9/27/22
DATE

Norman, OK
LOCATION

PRESIDENT, THE UNIVERSITY OF OKLAHOMA

Kristin Trammell
PROGRAM DIRECTOR

INTERIM DEAN, COLLEGE OF PROFESSIONAL AND CONTINUING STUDIES


unesco
Intergovernmental Hydrological Programme
IWRA ONLINE CONFERENCE
17-19 JANUARY 2023
3rd IN THE IWRA ONLINE CONFERENCE SERIES
International Water Resources Association
IWRA
CERTIFICATE OF PARTICIPATION
This is to certify that
WONDIMU KEBEDE
20, January 2023
IWRA Executive Office
Served as a Panelist
at the UNESCO-IWRA Online Conference on
« EMERGING POLLUTANTS: PROTECTING WATER QUALITY FOR
THE HEALTH OF PEOPLE AND THE ENVIRONMENT »
www.iwraonlineconference.org